

Department of Electrical and Computer Engineering

**Stable Overload Management Schemes for Isolated
Coupled Microgrids**

Ehsan Pashajavid

**This thesis is presented for the Degree of
Doctor of Philosophy
of
Curtin University**

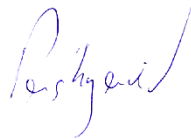
August 2017

DECLARATION

To the best of my knowledge and belief this thesis contains no material previously published by any other person except where due acknowledgment has been made.

This thesis contains no material which has been accepted for the award of any other degree or diploma in any university.

Signature:

A handwritten signature in blue ink, appearing to read 'R. S. H. G. A. I.', written in a cursive style.

Date: 28/08/2017

ABSTRACT

Enhancing the self-healing capability of isolated AC microgrids (MGs) through mutual support of neighbouring MGs is the main aim of this thesis. Power deficiency is one of the main challenges with isolated MGs due to their limited power generation capacities. To address this issue, the coupling of neighbouring MGs is considered as an economically promising alternative to the traditional methods of grid interconnection, since it imposes almost no extra capital investment of installing power lines. Instead of a back-to-back power converter, an instantaneous static switch (ISS) is employed in this thesis to form a coupled MG (CMG) system in order to avoid the power loss incurred by the converters.

Firstly, a self-healing scheme is developed to facilitate the interconnection as well as isolation of the neighbouring AC MGs. The criteria required for detecting the overloading are accurately formulated for the CMG system. It can operate employing either a decentralized approach or a centralized approach, depending on the availability of a data communication system. However, the focus is mainly on decreasing the dependency on the communication infrastructures. The detailed small signal model of the MGs and the CMG under study is also formulated. The stability of the CMG is investigated before the interconnection to prevent any instability problems.

Moreover, a two-level power exchange strategy is proposed under which the lighter power deficiencies in the isolated MGs can be addressed by small-scale battery energy storages (BESes) locally while the CMG formation can be limited to severe deficiencies only. The conditions and constraints for BES connection along with the ones for coupling of two neighbouring MGs are accurately formulated. Also, the associated small signal model is developed based on which the stability of the system after any modification can be evaluated. An MG with this strategy offers more resilience and flexibility when overloaded, leading to a reduced necessity and rate of load-shedding.

Although the aforementioned methods are presented to handle the overloading, still there may be some occasions when the load demand is higher than the total generation capacity of a system, resulting in drastic frequency drops. In such occasions, implementing an under frequency load shedding (UFLS) procedure is inevitable; otherwise, the MG would experience a black out. For this, a hierarchical cooperative strategy is proposed to support frequency of isolated MGs during power shortfalls. At the primary level, a multi-layer droop-based UFLS technique is presented for proper dispatching of the required load to be shed. At the secondary level, a decentralized scheme is developed for forming the CMG after evaluating the relevant conditions. The coordination between these two levels is fulfilled such that their cooperative operation can facilitate the overloading management.

Developing the decentralized methods for conducting the interconnection as well as the isolation actions of the MGs is highly desirable. However, some challenges are still posed with the communication-free ISS-based coupling of isolated droop-regulated MGs. The supporting power supplied by the neighbouring MG is probably larger than the actual requirement of the MG experiencing the power shortfall. Also, the isolation of the coupled MGs can cause destructive transients. Therefore, a supervisory strategy is developed in this thesis that can effectively address these challenges under three operating modes. By applying the strategy on the CMG, the power output of the overloaded MG can be maintained close to its maximum. Also, a successful isolation of the MGs is fulfilled when the interconnection is not required anymore. The latter can be performed based on the defined load to capacity factors.

The effectiveness of the proposed strategies is validated through the results obtained from PSCAD/EMTDC simulations. Also, the small signal stability of the system is examined using the developed models in MATLAB.

To my love forever, my wife,

Marie

for her constant support, sacrifices and unconditional love

ACKNOWLEDGMENT

I would like to express my sincere appreciation to my supervisor Prof. Arindam Ghosh for the support and guidance he gave me, as well as, for his always valuable scientific and personal advice throughout this thesis. Likewise, I am really grateful to my thesis committee Dr. Yee-Hong Leung and Prof. Firuz Zare for their invaluable support at all times. Also, I would like to show my gratitude to all my friends at Curtin University who provided me with a warm and encouraging environment during my research.

Last but certainly not least, I would like to express my sincere gratitude to my parents, for their continuous support and prayers. My deepest gratitude is to my lovely wife Mari, who has been with me all these years and has made them the best years of my life. Thank you so much for inspiring me and providing me with the encouragement whenever I needed it.

TABLE OF CONTENTS

| | | |
|------------|--|----|
| Chapter 1. | Introduction | 1 |
| 1.1 | Background | 1 |
| 1.2 | Literature review | 4 |
| 1.2.1. | Control architecture of MG clusters | 5 |
| 1.2.2. | Power and energy trade | 7 |
| 1.2.3. | Reliability improvement | 8 |
| 1.2.4. | Resilience enhancement | 8 |
| 1.2.5. | Stability analysis | 9 |
| 1.3 | Thesis objectives and contributions | 10 |
| 1.3.1. | Objectives of the thesis | 10 |
| 1.3.2. | Specific contributions | 11 |
| 1.4 | Thesis outline..... | 12 |
| Chapter 2. | AC Microgrids: general concepts..... | 15 |
| 2.1 | The notion of Microgrid..... | 15 |
| 2.2 | Control architecture of microgrids | 18 |
| 2.3 | Clusters of MGs..... | 22 |
| 2.4 | Droop regulator..... | 24 |
| 2.4.1 | DER to MG power flow | 25 |
| 2.4.2 | Droop equations | 26 |
| 2.4.3 | Power sharing among DERs | 27 |
| 2.5 | Converter interfaced DERs | 29 |
| 2.5.1 | Voltage source converter | 29 |
| 2.5.2 | Modelling of dispatchable DERs | 30 |
| 2.5.3 | Modelling of non-dispatchable DERs | 31 |
| 2.6 | Switching controllers | 32 |
| 2.6.1 | Single-step prediction horizon | 32 |
| 2.6.2 | State feedback control | 34 |
| 2.7 | Conclusion..... | 36 |
| Chapter 3. | Enhancing overloading resilience of isolated microgrids..... | 37 |
| 3.1 | The network under consideration | 38 |
| 3.2 | The centralized self-healing strategy | 40 |
| 3.2.1. | Interconnection of the MGs | 41 |
| 3.2.2. | Isolation of the interconnected MGs | 43 |
| 3.3 | The decentralized self-healing strategy | 44 |
| 3.3.1 | Interconnection of the MGs | 44 |

| | | |
|------------|--|-----|
| 3.3.2 | Isolation of the interconnected MGs | 46 |
| 3.4 | Discussion on the Self-Healing Parameters | 47 |
| 3.5 | Required Time for MGs Interconnection | 48 |
| 3.6 | Reduced load-shedding level | 49 |
| 3.6.1. | Under the centralized approach | 49 |
| 3.6.2. | Under the decentralized approach | 52 |
| 3.7 | Small signal stability analysis of CMG | 53 |
| 3.7.1. | Model derivation | 53 |
| 3.7.2. | Modal analysis | 58 |
| 3.8 | Performance evaluation | 60 |
| 3.8.1. | Dynamic response | 61 |
| 3.8.2. | Stability analysis | 75 |
| 3.9 | Conclusion | 79 |
| Chapter 4. | Internal/external power exchange for supporting isolated MGs | 81 |
| 4. 1 | Network under consideration | 83 |
| 4. 2 | Power exchange strategy | 84 |
| 4.2.1. | The centralized approach | 86 |
| 4.2.2. | The decentralized approach | 90 |
| 4. 3 | Operation Flowchart of the PExS Agents | 95 |
| 4. 4 | Impact of the Power Exchange Strategy | 97 |
| 4.4.1. | The centralized approach | 97 |
| 4.4.2. | The decentralized approach | 98 |
| 4. 5 | Impact of the PExS Parameters | 99 |
| 4. 6 | Performance Evaluation | 101 |
| 4.6.1. | Dynamic performance of the centralized approach | 101 |
| 4.6.2. | Dynamic performance of the decentralized approach | 108 |
| 4. 7 | Small Signal Stability Analysis | 114 |
| 4.7.1. | Model derivation | 114 |
| 4.7.2. | Stability evaluation | 117 |
| 4. 8 | Conclusion | 122 |
| Chapter 5. | A hierarchical strategy to support frequency in isolated MGs | 124 |
| 5. 1 | Basic structure of the considered MG | 125 |
| 5. 2 | Primary level of the proposed strategy | 127 |
| 5.2.1 | Load shedding criteria | 127 |
| 5.2.2 | Demand prioritizing | 129 |
| 5.2.3 | Shed load dispatch | 130 |
| 5.2.4 | Demand restoration | 131 |
| 5.2.5 | Execution of the primary level | 133 |

| | | |
|-------------------------------|---|-----|
| 5.3 | Secondary level of the proposed strategy | 134 |
| 5.3.1 | Operating modes of the CLs | 135 |
| 5.3.2 | Coupling algorithm | 136 |
| 5.3.3 | Fulfilling the primary level scheme in the CMG | 139 |
| 5.4 | Performance evaluation..... | 141 |
| 5.5 | Conclusion..... | 150 |
| Chapter 6. | A supervisory scheme for coupling isolated microgrids | 151 |
| 6.1 | The network under consideration | 152 |
| 6.2 | Problem statement..... | 154 |
| 6.2.1 | Coupling and isolation conditions..... | 154 |
| 6.2.2 | Challenges with the communication-free CMG | 156 |
| 6.3 | Improved fully decentralized isolation..... | 158 |
| 6.3.1 | Load-to-capacity ratio | 158 |
| 6.3.2 | The proposed method | 160 |
| 6.4 | The proposed supervisory scheme | 163 |
| 6.4.1 | Mode 1: Coupling | 163 |
| 6.4.2 | Mode 2: Cancelling the tie-line power | 167 |
| 6.4.3 | Mode 3: Isolation | 169 |
| 6.4.4 | Overall description | 170 |
| 6.5 | Small signal stability analysis..... | 171 |
| 6.6 | Performance evaluation..... | 173 |
| 6.6.1 | Improved fully decentralized isolation..... | 173 |
| 6.6.2 | The supervisory scheme | 179 |
| 6.6.3 | Eigenvalue studies..... | 188 |
| 6.7 | Conclusion..... | 190 |
| Chapter 7. | Conclusions and scope of future research | 191 |
| 7.1 | General conclusions | 191 |
| 7.2 | Scope of future research..... | 193 |
| Appendix | | 194 |
| Appendix A. | Synchronization Process | 194 |
| Appendix B. | Charging Control of the BESes | 196 |
| References | | 198 |
| Publications from this thesis | | 208 |

LIST OF FIGURES

| | |
|--|----|
| Fig. 2.1: General structure of (a) centralized control, (b) distributed control, and (c) fully decentralized control modes. | 19 |
| Fig. 2.2: Hierarchical control of the MGs. | 21 |
| Fig. 2.3: Power flow from the DER to the MG..... | 25 |
| Fig. 2.4(a) angle droop curve, (b), voltage droop curve and (c) frequency droop curve...26 | |
| Fig. 2.5: Power sharing between the DERs. | 27 |
| Fig. 2.6: Structure of the utilized voltage source converter. | 29 |
| Fig. 2.7: (a) General structure and (b) single-line diagram of the associated VSC, and (c) droop-based control scheme of the dispatchable DERs. | 30 |
| Fig. 2.8: (a) General structure and (b) single-line diagram of the associated VSC, and (c) PQ control scheme of the non-dispatchable DERs. | 31 |
| Fig. 2.9: Diagram of the switching technique based on single-step prediction horizon method..... | 34 |
| Fig. 2.10: Diagram of the switching technique based on the LQR state feedback control. | 35 |
| Fig. 3.1: Single line diagram of the network of two isolated MGs with an interconnecting line..... | 38 |
| Fig. 3.2 The schematic of the MG interconnecting devices: (a) a back-to-back converter and (b) the adopted structure for the ISS..... | 39 |
| Fig. 3.3: The centralized self-healing agent for interconnecting two neighbouring MGs. | 42 |
| Fig. 3.4: Operation flowchart for the developed self-healing strategy. | 42 |
| Fig. 3.5: The decentralized self-healing agent for interconnecting two neighbouring MGs. | 45 |
| Fig. 3.6: UPC margins of (a) islanded MGs, (b) CMG depending on the variations of the self-healing parameters..... | 48 |
| Fig. 3.7: Required time for interconnection of MGs for different $\Delta\theta$ and Δf | 50 |
| Fig. 3.8: Required load-shedding level for MG-1 in: (a) islanded mode, (b) interconnected mode under the centralized approach. | 51 |
| Fig. 3.9: Required load-shedding level for MG-1 in: (a) islanded mode, (b) interconnected mode under the decentralized approach. | 52 |
| Fig. 3.10: Single-line diagram of the CMG including its DERs along with their controllers..... | 61 |
| Fig. 3.11: Simulation results for the developed self-healing agent under the centralized approach: Case-1..... | 65 |
| Fig. 3.12: Simulation results for the developed self-healing agent under the centralized approach: Case-2..... | 66 |
| Fig. 3.13: Simulation results for the developed self-healing agent under the centralized approach: Case-3..... | 67 |

| | |
|---|-----|
| Fig. 3.14: Simulation results for the developed self-healing agent under the decentralized approach: Case-1. | 71 |
| Fig. 3.15: Simulation results for the developed self-healing agent under the decentralized approach: Case-2. | 72 |
| Fig. 3.16: Simulation results for the developed self-healing agent under the decentralized approach: Case-3. | 73 |
| Fig. 3.17: Eigenvalues of the considered system of CMG, with the dynamic performance investigated in Section 3.8.1..... | 76 |
| Fig. 3.18: Eigenvalues of the considered CMG..... | 77 |
| Fig. 4.1: A large remote area supplied by multiple isolated MGs. | 81 |
| Fig. 4.2: Single line diagram of the network of two isolated MGs..... | 83 |
| Fig. 4.3: Steps of the operation of the PExS on a two-MG system..... | 85 |
| Fig. 4.4: Loading level of the DERs in the MG operating under the proposed PExS..... | 86 |
| Fig. 4.5: Structure of the centralized approach to realize the PExS on a two-MG system. | 87 |
| Fig. 4.6: Structure of the decentralized approach to realize the PExS on a two-MG system. | 91 |
| Fig. 4.7: Operation flowchart of the PExS agents under centralized and decentralized approaches..... | 96 |
| Fig. 4.8: Level of load-shedding for MG-1 under the decentralized and centralized approaches: (a) without and with the BES support, (b) after forming the CMG (SoC = 100%)..... | 98 |
| Fig. 4.9: (a) UAPC thresholds of MG-1 as a function of various values for α_1 and β in the C&Cs, (b) Frequency thresholds of CMG as a function of various values for α_2 and β in the C&Cs..... | 100 |
| Fig. 4.10: Dynamic performance of the system with the centralized approach, Case 1. | 103 |
| Fig. 4.11: Dynamic performance of the system with the centralized approach, Case 2. | 104 |
| Fig. 4.12: Dynamic performance of the system with the centralized approach, Case 3. | 105 |
| Fig. 4.13: Dynamic performance of the system with the centralized approach, Case 4. | 106 |
| Fig. 4.14: Dynamic performance of the system with the centralized approach, Case 5. | 107 |
| Fig. 4.15: Dynamic performance of the system with the decentralized approach, Case 1. | 109 |
| Fig. 4.16: Dynamic performance of the system with the decentralized approach, Case 2. | 110 |
| Fig. 4.17: Dynamic performance of the system with the decentralized approach, Case 3. | 111 |
| Fig. 4.18: Dynamic performance of the system with the decentralized approach, Case 4. | 112 |
| Fig. 4.19: Dynamic performance of the system with the decentralized approach, Case 5. | 113 |
| Fig. 4.20: Eigenvalue trajectory for the considered BCMG for variation of m | 117 |

| | |
|--|-----|
| Fig. 4.21: Eigenvalue trajectory for the considered BCMG for variation of n . | 118 |
| Fig. 4.22: Eigenvalue trajectory for the considered BCMG for variation of the tie-line impedance. | 118 |
| Fig. 4.23: Eigenvalue trajectory for the considered BCMG for SoC variation. | 119 |
| Fig. 4.24: Marginal frequency deviations of the BCMG. | 120 |
| Fig. 4.25: Marginal voltage deviations of the BCMG. | 120 |
| Fig. 4.26: Participation factor of each state on BCMG eigenvalues. | 121 |
| Fig. 5.1: An isolated microgrid consisting of the dispatchable and non-dispatchable DGs along with the controllable and uncontrollable loads. | 126 |
| Fig. 5.2: (a) Power sharing droop curves of DDGs, (b) multi-layer shed load sharing curves of CLs. | 129 |
| Fig. 5.3: Load shedding and restoring curves of layer k . | 132 |
| Fig. 5.4: Flowchart of the proposed shed load dispatching scheme. | 134 |
| Fig. 5.5: Distribution network of a remote area consisting of two isolated MGs. | 135 |
| Fig. 5.6: Transition of the operating modes by receiving a notification signal. | 136 |
| Fig. 5.7: (a) Control scheme, and (b) single-line diagram of a load PEI. | 142 |
| Fig. 5.8: Simulation results of Case 1. | 144 |
| Fig. 5.9: Simulation results of Case 2. | 146 |
| Fig. 5.10: Simulation results of Case 3. | 148 |
| Fig. 5.11: Simulation results of Case 4. | 149 |
| Fig. 6.1: Equivalent droop curve of an MG along with droop curves of its DGs. | 155 |
| Fig. 6.2: The Thevenin equivalent of the considered CMG. | 157 |
| Fig. 6.3: The network of two isolated neighbouring microgrids with ACLs. | 158 |
| Fig. 6.4: Flowchart of the developed communication-free approach for isolation. | 162 |
| Fig. 6.5: The power transitions at the ISS by applying the developed approach when (a) $L2C_{MG-1} \geq L2C_{MG-2}$ and (b) $L2C_{MG-1} \leq L2C_{MG-2}$. | 162 |
| Fig. 6.6: Operating modes of the developed supervisory scheme. | 164 |
| Fig. 6.7: Operation flowchart of the supervisory scheme. | 164 |
| Fig. 6.8: The network of two isolated neighbouring microgrids with the supervisory controller. | 166 |
| Fig. 6.9: Performance of the developed supervisory scheme under Mode 1. | 166 |
| Fig. 6.10: Simulation results of Case 1. | 175 |
| Fig. 6.11: Voltages at two sides of the ISS at the isolation moment (a) without applying the developed approach, (b) with applying the developed approach. | 175 |
| Fig. 6.12: Simulation results of Case 2. | 176 |
| Fig. 6.13: Simulation results of Case 3. | 177 |
| Fig. 6.14: Simulation results of Case 4. | 177 |
| Fig. 6.15: Simulation results of Case 5. | 178 |
| Fig. 6.16: Simulation results of Case 6. | 179 |

| | |
|---|-----|
| Fig. 6.17: Simulation results of Case 1. | 181 |
| Fig. 6.18: Simulation results of Case 2. | 182 |
| Fig. 6.19: Simulation results of Case 3. | 184 |
| Fig. 6.20: Simulation results of Case 4. | 186 |
| Fig. 6.21: Simulation results of Case 5. | 187 |
| Fig. 6.22: Trace of dominant modes of the CMG when the SMF decreases from 1.6 to 0.5. | 189 |
| Fig. 6.23: Marginal droop coefficients of the sample DGs when the ratio of the coupling reactance of the DGs to line impedances varies from 1 to 10. | 189 |

LIST OF TABLES

| | |
|--|-----|
| Table 3.1: Comparison between the ISS and B2B converters used for coupling the MGs. | 40 |
| Table 3.2: Parameters of MGs, Self-healing agent and VSCs of DERs..... | 60 |
| Table 3.3: Time sequence of the events in a network controlled with the centralized approach. | 64 |
| Table 3.4: Time sequence of the events in a network controlled with the decentralized approach. | 70 |
| Table 3.5: Required level of load-shedding [pu] in MG-1 in simulation studies cases 1-3 of the centralized approach..... | 74 |
| Table 3.6: Required level of load-shedding [pu] in MG-1 in simulation studies cases 1-3 of the decentralized approach. | 74 |
| Table 3.7: Dominant modes of CMG and their characteristics..... | 78 |
| Table 3.8: Marginal voltage and frequency deviations of MGs and CMG. | 79 |
| Table 4.1: Summary of the different steps of the proposed PExS. | 84 |
| Table 4.2: Parameters of MGs, DERs and BESeS, Synchronization, and the PExS | 101 |
| Table 4.3: Time sequence of the events in the system with the centralized approach, Case 1. | 103 |
| Table 4.4: Time sequence of the events in the system with the centralized approach, Case 2. | 104 |
| Table 4.5: Time sequence of the events in the system with the centralized approach, Case 3. | 105 |
| Table 4.6: Time sequence of the events in the system with the centralized approach, Case 4. | 106 |
| Table 4.7: Time sequence of the events in the system with the centralized approach, Case 5. | 107 |
| Table 4.8: Time sequence of the events in the system with the decentralized approach, Case 1..... | 109 |
| Table 4.9: Time sequence of the events in the system with the decentralized approach, Case 2..... | 110 |
| Table 4.10: Time sequence of the events in the system with the decentralized approach, Case 3..... | 111 |
| Table 4.11: Time sequence of the events in the system with the decentralized approach, Case 4..... | 112 |
| Table 4.12: Time sequence of the events in the system with the decentralized approach, Case 5..... | 113 |
| Table 4.13: Dominant modes of the considered BCMG and their characteristics. | 122 |
| Table 5.1: Parameters of the MGs and the proposed strategy. | 143 |
| Table 6.1: Technical parameters of the MGs considered in Section 6.6.1. | 174 |
| Table 6.2: Technical parameters of the MGs and the CMG..... | 180 |

ABBREVIATIONS

| | |
|------|--|
| ACL | Auxiliary controllable load |
| AUPC | Available unused power capacity |
| B2B | Back-to-back |
| BES | Battery energy storages |
| BSS | BES static switch |
| C&C | Conditions and constraints |
| CL | Controllable loads |
| CMG | Coupled microgrids |
| DDG | Dispatchable distributed generator |
| DER | Distributed energy resources |
| DG | Distributed generators |
| ESS | Energy storage systems |
| IGBT | Insulated gate bipolar transistors |
| ISS | Instantaneous static switches |
| L2C | Load-to-capacity |
| LQR | Linear quadratic regulator |
| MG | Microgrid |
| MGCC | Microgrid central controller |
| MMG | Multi-microgrid |
| MPPT | Maximum power point tracking |
| N/A | Not allowed |
| NDDG | Non-dispatchable distributed generator |
| PEI | Power electronics interface |
| PExS | Power exchange strategy |
| SMF | Slope modification factor |
| SoC | State of charge |
| SSS | Small signal stability |
| UAPC | Unused active power capacity |
| UCL | Uncontrollable loads |
| UFLS | Under frequency load shedding |
| UPC | Unused power capacity |
| VSC | Voltage source converters |
| WG | Wind generator |

LIST OF SYMBOLS

Converter interface VSC

| | |
|----------------|---|
| L_f | Leakage reactance of transformer |
| R_f | Copper losses |
| L_T | Coupling inductance |
| C_f | Filter capacitance |
| v_c | Voltage across C_f |
| i_f | Current through L_f |
| i_T | Current through L_T |
| V^{com} | References for v_c magnitude |
| δ^{com} | References for v_c angle |
| f^{com} | References for frequency |
| V_T | Magnitude of voltage on MG side of the coupling inductor |
| δ_T | Angle of voltage on MG side of the coupling inductor |
| ω | Angular frequency |
| V_{DC} | DC side voltage |
| u | Switching function |
| u_c | Continuous-time approximation of u |
| T_s | Sampling time |
| h | Hysteresis band |
| λ_i | Control coefficients of single-step prediction horizon method |

Isolated MGs

| | |
|------------|-------------------------------------|
| f_{max} | Maximum of frequency in MG |
| f_{min} | Minimum of frequency in MG |
| V_{max} | Maximum of voltage magnitude in MG |
| V_{min} | Minimum of voltage magnitude in MG |
| V_{base} | Base voltage of MG |
| S_{base} | Base power of MG |
| m | Slope of the frequency droop curves |
| m_δ | Slope of the angle droop curves |
| n | Slope of voltage droop curves |
| δ_r | Rated angle of DER |

| | |
|------------|---|
| V_D | Magnitude of the voltage at DER side of coupling inductor |
| δ_D | Angle of the voltage at DER side of coupling inductor |
| V_G | Magnitude of the voltage at MG side of coupling inductor |
| δ_G | Angle of the voltage at MG side of coupling inductor |
| Z | Magnitude of impedance |
| θ | Angle of impedance |
| R | Real term of impedance |
| X | Imaginary term of impedance |
| V_r | Rated voltage magnitudes of DER |

CMG systems

| | |
|----------------------------------|--|
| $Z_{\text{tie-line}}$ | Impedance of the tie line |
| $f_{\text{MG-}i}$ | Frequency of MG- i |
| f_{CMG} | Frequency of CMG |
| m_{ij} | Frequency droop gain of j^{th} DER in MG- i |
| $\Delta\theta$ | Voltage angle difference across ISS |
| $\alpha, \beta, \psi, \kappa$ | Self-healing parameters |
| $S_{\text{MG-}i}^{\text{cap}}$ | Sum of the maximum capacities of all the DERs in MG- i |
| $/S_{\text{MG-}i}/$ | Sum of the apparent powers of all the DERs in MG- i |
| $S_{\text{BMG-}i}^{\text{cap}}$ | Sum of the maximum capacities of all the DERs in BMG- i |
| $/S_{\text{BMG-}i}/$ | Sum of the apparent powers of all the DERs in BMG- i |
| $S_{\text{CMG}}^{\text{cap}}$ | Sum of the maximum capacities of all the DERs in CMG |
| $/S_{\text{CMG}}/$ | Sum of the apparent powers of all the DERs in CMG |
| $S_{\text{BCMG}}^{\text{cap}}$ | Sum of the maximum capacities of all the DERs in BCMG |
| $/S_{\text{BCMG}}/$ | Sum of the apparent powers of all the DERs in BCMG |
| $S_{\text{DER-}ij}^{\text{cap}}$ | Maximum capacity of the j^{th} DER in MG- i |
| $S_{\text{DER-}ij}$ | Apparent power of the j^{th} DER in MG- i |
| $S_{\text{BES-}i}^{\text{cap}}$ | Maximum capacity of the i^{th} BES |
| $/S_{\text{BES-}i}/$ | Apparent power magnitude of BES- i |
| $S_{\text{Tie-line}}$ | Apparent power flowing through tie-line |
| $S_{\text{MG-}i}^{\text{shed}}$ | Required load-shedding level from MG- i |
| $ML_{\text{ZLS}}^{\text{MG-}i}$ | The maximum loading of MG- i for zero load-shedding in the neighbouring MG |
| $P_{\text{MG-}i}^{\text{cap}}$ | Total maximum active power capacity of all the DERs in MG- i |
| $P_{\text{MG-}i}$ | Total active power output of all DERs in MG- i |
| $P_{\text{BMG-}i}^{\text{cap}}$ | Total maximum active power capacity of all the DERs in BMG- i |

| | |
|------------------------------------|--|
| $P_{\text{BMG-}i}$ | Total active power output of all DERs in BMG- i |
| $P_{\text{CMG}}^{\text{cap}}$ | Total maximum active power capacity of all the DERs in CMG |
| P_{CMG} | Total active power output of all DERs in CMG |
| $P_{\text{BCMG}}^{\text{cap}}$ | Total maximum active power capacity of all the DERs in BCMG |
| P_{BCMG} | Total active power output of all DERs in BCMG |
| $P_{\text{DER-}ij}^{\text{cap}}$ | Maximum active power capacity of j^{th} DER in MG- i |
| $P_{\text{DER-}ij}$ | Active power of j^{th} DER in MG- i |
| $P_{\text{BES-}i}^{\text{cap}}$ | Maximum active power capacity of BES- i |
| $P_{\text{BES-}i}$ | Active power of i^{th} BES |
| $P_{\text{Tie-line}}$ | Active power flowing through tie-line |
| $P_{\text{CL-}i}^{\text{org}}$ | Original value of CL- i |
| $P_{\text{CL-}i}^{\text{Dshd}}$ | Shed dispatch of CL- i |
| $P_{\text{CL-}i}^{\text{com}}$ | Load command sent by CL controller |
| $P_{\text{CL-}i}^{\text{shd}}$ | Shed part of CL- i |
| $P_{\text{CL-}i}^{\text{Drest}}$ | portion of $P_{\text{CL-}i}^{\text{shd}}$ to be restored |
| $P_{\text{CMG}}^{\text{Load}}$ | Total load of CMG |
| $P_{\text{MG-}i}^{\text{Load}}$ | Total load of MG- i |
| $P_{\text{ACL-}i}$ | Active power demanded by ACL- i |
| $P_{\text{MG-}i}^{\text{DSR}}$ | Desired value of $P_{\text{MG-}i}$ |
| $P_{\text{Tie-line}}^{\text{DSR}}$ | Desired value of $P_{\text{Tie-line}}$ |
| $P_{\text{MG-}i}^{\text{Vcap}}$ | Virtual power capacity of MG- i |
| $P_{\text{MG-}i}^{\text{shed}}$ | Required active load-shedding level from MG- i |
| $mF_{\text{ZLS}}^{\text{MG-}i}$ | The minimum frequency of MG- i for zero load-shedding in the neighbouring MG |
| $m_{\text{CL}}^{\text{Type-}k}$ | Equivalent droop coefficient of all CLs of Type- k |
| $\gamma_{\text{MG-}i}$ | Slope modification factor (SMF) of MG- i |

Small signal models

| | |
|-------|-------------------------------------|
| N_c | Number of converter-interfaced DERs |
| N_d | Number of loads |
| N_e | Number of lines |

| | |
|-----------------------|---|
| N_b | Number of buses |
| $x(t), z(t)$ | State vector in continues-time domain |
| $x(k), z(k)$ | State vector in discrete-time domain |
| $z^{\text{com}}(k)$ | Desired state vector in discrete-time domain |
| $J(\cdot)$ | Objective function for switching methods |
| K_i | Gain vector of state-feedback control law for the i^{th} converter |
| Q | State weighting matrix of LQR controller |
| R | Control cost matrix of LQR controller |
| x_{load}^j | State vector of j^{th} load |
| x_{line}^k | State vector of k^{th} line |
| x_{conv}^i | State vector of the i^{th} converter in direct-quadrature domain |
| x_{MG} | State vector of MG |
| x_{CMG} | State vector of CMG |
| i_d, i_q | dq currents |
| v_{Td}, v_{Tq} | dq terminal volatges |
| v_{cd}, v_{cq} | dq capacitor volatges |
| ω_c | Cut-off frequency of low pass filter |
| ω_{com} | common angular frequency in the MG |
| ω_n | Undamped natural frequency of the modes |
| ζ | Damping ratio of modes |
| $NoC_{50\%}$ | Number of cycles for a mode to damp by 50% |
| A_{CMG}^H | State matrix of CMG in its homogeneous form |
| $Pf(u, w)$ | Participation factor, contribution of state u on mode w |

Chapter 1. INTRODUCTION

In this chapter, the main objectives of this thesis are presented. First the motivations of the concept of microgrids are introduced. Then, the necessity of clustering of microgrids along with different associated targets is reviewed. Afterwards, the research gaps in this new field are identified through an in-depth literature survey. The main objectives and contributions of this research are then presented in accordance with the identified gaps. Eventually, the outline of the thesis is presented.

1.1 Background

With the aim of addressing various environmental concerns which are mainly caused by fossil fuel-based electric power generation, the tendency to use renewable energy resources such as the wind and solar systems has been gaining considerable attention throughout the world [1, 2]. The recent advancements in the field of renewable energy technologies have further increased penetration level of renewable distributed energy resources (DER) [3, 4]. Such distributed generators (DG) can play an important role in decreasing the air pollution along with attaining numerous technical merits such as power loss reductions and reliability enhancement in electric distribution systems [5, 6].

Various technical and operational challenges nevertheless are imposed on the distribution networks when the DGs are scattered in a large number across the network with no coordination [7, 8]. In such cases, the DGs can deteriorate the performance of the system in terms of power quality and reliability. Voltage fluctuation, frequency drop, increasing power losses and inverse power flow can be mentioned as a few side effects. Consequently, the non-coordinated DGs can

cause further concerns for the main grid, rather than alleviating the problem of reliability and power losses [9, 10].

The concept of microgrid (MG) was originally introduced to facilitate reliable integrations of different types of DERs [11, 12]. Generally, each MG can be considered as a cluster of DGs, storage systems, and loads which can operate as a single entity. In such an approach, different components of an MG can be internally controlled to reduce their negative impacts on the distribution networks. Consequently, the main grid can consider MGs as controllable components which are capable of responding appropriately to different control signals.

The MGs can be operated in either grid-connected mode or islanded mode [13, 14]. In the grid-connected mode, the MG load demands should be mainly met by the power generated in the MG and the deficit can be supplied by the main grid. If the DGs can satisfy the MG demand, however, the surplus power, if any, can be transferred to the main grid. Such power exchanges can provide more flexible and reliable operation of the entire system. In the islanded mode, the DERs are responsible for regulating the frequency and bus voltages in the MG since there is no connection to the main grid. Thus, the MG operation should be managed such that the generation-demand balance can always be maintained.

In the MGs with grid availability, fulfilling a successful transition between the grid-connected and islanded modes is critical and should be done in accordance with the system conditions and the operational objectives. The associated control mechanisms should be designed such that the transition can be performed with the minimum disruption [15, 16]. This can include several measurement and synchronization procedures [17].

Generally, control architectures for the MGs can be categorized as centralized, distributed and decentralized methods [18, 19]. In the centralized control systems, a central controller is responsible for regulating all the operations within the MGs and determines the power outputs of the DERs based on the information it receives from all components and devices of the MGs [20, 21]. The distributed control methods operate based on the limited amount of communications that should be established between each DER and its immediate

neighbours so that the concerns with a single point of failure can be removed [22]. In the decentralized control systems, which are mostly based on droop regulators, all DERs should operate using the local measurements only [23, 24]. Although the structure of MGs with decentralized control methods is simple, successful operation of such systems can be compromised due to lack of the sufficient information.

Further to aforementioned three control architectures, the supervisory schemes can also be considered. This mainly is a combination of the centralized and decentralized control systems [25, 26, 27]. The lower level of this hierarchy is composed of the local controllers of the DERs that can operate independently using the droop regulators. At the higher level control, a central controller coordinates the operation of the devices by preparing the updated set points as well as the other supervisory commands. The data and information are transferred within such systems by taking advantage of low bandwidth communication systems [28, 29].

The hierarchical control structures consisting of primary, secondary, and tertiary levels can be employed in order to facilitate the desirable operation of the MGs [30]. The primary level control is responsible for regulating the frequency and voltage of the DERs along with adjusting the power outputs. The secondary level control attempts to compensate the deviation of the output frequency and voltage of the DERs from the MG set points. At the tertiary level control, the power flow among the MGs is regulated with the aim of achieving various pre-specified technical and economic objectives.

Although the MGs were originally introduced to handle the desirable integration of the renewable DERs, the growing number of MGs can pose new challenges to distribution networks since the interactions among such subsystems should be controlled properly [12]. Therefore, the new concept of multi-MG (MMG) systems has been proposed [31, 32, 33]. Such systems consist of a number of neighbouring MGs that can be operated in either interconnected or isolated modes based on the associated control approaches. The main idea of CMGs is to facilitate control of the distribution networks with high penetration of

renewable DERs, where the entire network is split into a number of locally controlled interconnected MGs [34]. In this way, both the control and communication complexity can be considerably reduced. However, the desired operation of such systems is subjected to the proper control of the interactions amongst the MGs.

Clustering of the MGs can be done for achieving various objectives such as enhancing the reliability of the network [35, 36], power and energy trade [37, 38], improving dynamic performance and stability of the system [39, 40], and enhancing the resilience of the system [41, 42]. Based on the applied control architecture, the appropriate regulating schemes should be designed and implemented for attaining the considered targets. Furthermore, the MGs can be normally interconnected whereas they should carry on the operation in islanded mode during the contingencies [43] or vice versa [36]. Thus, the interconnection architecture of the MGs within the cluster should be taken into account in selecting the appropriate management scheme as well.

Recently, assessment of different aspects of MG clusters is more attractive to researchers in the MG area. As a new field in MG research, many further studies should be conducted in order to investigate various facets of this concept. A literature survey on MG clusters is presented in the next section in order to identify the associated research gaps.

1.2 Literature review

Control mechanism and structure of the devices employed for realizing the interconnection amongst the MGs depend on the nature of the MGs and the operation goals [44]. For a cluster of AC MGs, the interconnection can be implemented by using different types of AC/AC power converters (e.g., back-to-back (B2B) converters [45, 46, 47]). Considering the DC MG clusters, the MGs coupling and the power flow control should be carried out using appropriate types of DC/DC converters [48, 49]. For hybrid AC/DC clusters in which both DC and AC MGs can be included, different types of AC/DC interlinking converters along with aforementioned devices suitable for AC/AC and DC/DC interconnections

can be used [50, 51]. Selection of the types, topology and ratings of the devices should be performed based on the MG ratings at the point of common coupling and also, the performance which is expected from the devices.

1.2.1. Control architecture of MG clusters

CENTRALIZED CONTROL: The communication requirements of CMG systems depend highly on the selected control architecture. The operation of CMGs with central controllers can involve a considerable data transferring actions via a high bandwidth communication system. A fully centralized control system is presented in [52] to coordinate the power transactions among the MGs for a future distribution network. With the aim of minimizing the power exchange among the MGs, a central controller is developed in [53] that can optimally regulate the power generation of the MGs. A communication system is required to send the DG power outputs and battery storages to the controller and then, to carry the generation reference signals to the DERs. A model predictive control is employed in [54] in order to derive the optimal amount of power that should be exchanged amongst the MGs of a distribution network in order to maximize the global benefits. In [55], a two-level coordinated energy management approach based on an interactive game matrix is presented for a distribution system with MG clusters. The lower level scheme coordinates the interactions among the MGs whereas the upper level controls the operation of the entire system. Various types of centralized control-based approaches are presented in [56, 57, 58] that utilize bi-level optimal algorithms in order to regulate optimally the operation of the total network. In such strategies, the lower level is responsible for managing an individual MG while the upper level deals with coordinating the operation of the MG clusters and the distribution network.

DISTRIBUTED CONTROL: Distributed control schemes can be used in CMG systems in order to alleviate the concerns with a single point failure. With the aim of controlling the system frequency, a distributed strategy based on multi-agent systems is developed in [59] that can operate utilizing the optimized average consensus algorithm. A distributed hierarchical technique is presented in [60, 61]

in order to perform power sharing among the MGs of a cluster. In [62], an optimization-based energy management strategy is presented for MG communities. This method, which is designed based on multi-agent systems, uses the available power capacity of the MGs as a decision parameter in performing the regulation.

DECENTRALIZED CONTROL: In a fully decentralized control system, the interaction amongst the MGs should be managed based only on the local information. Such control strategies are usually implemented by using droop regulators [63]. A fully decentralized scheme is developed in [64] to implement the power exchanged between two adjacent MGs which are interconnected via a B2B power converter. The power transfer is done based on the normalized droop curves. A normalized droop curves-based decentralized method is presented in [65, 66] to address the power exchange between AC and DC MGs and the charging/discharging actions of the storages. Combined droop regulator of each MG is employed to obtain the normalized one. Likewise, the active and reactive power sharing between two AC MGs interconnected through a B2B converter is demonstrated in [67]. The combined droop curves are used for managing the exchange power when a deviation from the voltage and frequency set points is detected.

SUPERVISORY CONTROL: Supervisory control methods are employed to maintain the reliability and simplicity of the network by avoiding complex communication systems [68]. In [69], the B2B-based interconnection of multiple MGs to the distribution network is implemented using a supervisory control technique. Angle droop regulation is used for the primary level control while the central controller coordinates the angle reference for the droop regulators. Power management of a hybrid MG system comprising an AC and a DC MGs is presented in [70]. The interconnection is done through a bi-directional voltage source converter operating based on droop regulation. The considered supervisory controller improves the power sharing performance of the droop regulators, causing a more desirable power exchange between the MGs. In [39], dynamic operation and stability control of a distribution network composed of interconnected microgrids are presented. In this system, the MG generators are

regulated using a modified angle droop controller including a transient term to adjust the angle at the reference value. The supervisory coordinator can request the DGs to modify their droop coefficients if the evaluated stability criteria are not satisfied. In [40], a hierarchical supervisory scheme is developed in order to guarantee the stability of a CMG system. For this, the supervisory controller should calculate an interaction coefficient to be sent to the secondary level controller of the MGs for updating the droop coefficients of the associated DGs.

1.2.2. Power and energy trade

In a CMG system, the power and energy trade among the MGs, as well as, between the MGs and the main grid, should be implemented based on a proper mechanism. In [71], the interaction between an energy services provider representing several MGs and the electricity market is evaluated. For this, the bilateral agreement is set between the entities for maximizing the net profits taking into account the impact of demand response. In [72], likewise, the competitive negotiations between the energy agents of the coupled MGs and the network aggregator are enabled through adopting a reverse auction model. The aggregated energy in this paper is employed for the energy support. In [73], the Nash bargaining theory is utilized for investigating the energy trading problem among the interconnected MGs.

The framework of an energy market suitable for power exchange among isolated MGs with various interconnection topologies is developed in [37]. In this regard, the local energy bid of each MG should be derived at first to be revealed to the sellers. Then, the law of demand is employed to adjust the energy prices within the market clearing procedure. An agent based transactive energy framework is presented in [74] for distribution networks with multiple MGs. The transactive market is actually an inter-MG auction based electricity market in which the MGs can contribute as either sellers or buyers with the aim of coping with the excess supply or residual demand.

1.2.3. Reliability improvement

MG clusters can effectively improve the reliability of the system due to the capability of power exchange among the MGs under a coordinated management of energy [75]. In [35, 76], the optimal planning of the distribution network is done based on the concept of the CMG systems in order to achieve the self-healing capability in the networks. This is fulfilled by allocating a combination of different types of the DERs in the system. Further, an optimum self-healing scheme is developed for the system in [77] includes control actions such as power output regulation of DERs, system reconfiguration and load shedding for addressing all possible fault scenarios.

With the aim of facilitating the aforementioned clustering of distribution networks during the faults, the method for designing the associated communication and control infrastructure is presented in [78] that can decrease the sensitivity of the network to the variations in the load and DGs. Likewise, an optimal stochastic sectionalizing technique is discussed in [43] for transforming the on-outage portions of the distribution network into the interconnected self-adequate MGs. Consequently, the reliability of the system can be considerably increased since the affected customers can be provided with the power. In [36], a transformative architecture is presented with the aim of enhancing reliability in the system of autonomous MGs. It is assumed that the MGs can operate independently during the normal conditions. When a contingency occurs, the on-emergency section of the system should be supplied by the surplus capacity of the other MGs under a consensus algorithm.

1.2.4. Resilience enhancement

The MGs can be employed to restore the distribution systems after natural disasters such as hurricanes, floods, blizzard storms, and earthquakes [79, 80]. For this, the network can be assumed as a cluster of MGs including various types of DERs capable of supplying the local loads. Also, proper interconnections amongst the MGs should be organized in order to perform the required power exchanges

[42, 81, 82]. In [83], a sequence of control actions is designed for service restoration in distribution networks after a general black out. For this, a central controller is responsible to perform the control procedure which includes dividing the network into some isolated MGs, connection/disconnection of loads and DGs, and fulfilling the synchronization amongst the MGs before the interconnection.

In [84], the service restoration is done using a decentralized method for performing the required reconfigurations amongst the involved MGs. This is performed through formulating a mixed-integer quadratic program for managing the network components. Spanning tree search algorithm is incorporated in [85] in order to fulfil an optimal restoration for distribution networks via finding the most suitable topologies. This can minimize the number of switching operations required for performing the MGs interconnections.

1.2.5. Stability analysis

Stability of MGs can be examined by taking advantage of small and large signal analysis. However, most of the reported studies on the stability of the interconnected MGs are based on the small signal stability analysis [86, 87]. In [69], small signal stability analysis is done for a system of multiple MGs which are connected to the distribution network via B2B converters. The derived model is employed to demonstrate stable operation of the system under various operating conditions. The impact of the tie-line impedances, as well as their connection points on the stability of the whole CMG system, is investigated in [88] through considering the critical clusters.

In [39], a small signal model based strategy is employed for online evaluating the stable operation of a distribution network composed of interconnected droop-regulated MGs. The required stability criteria in the sense of Lyapunov are formulated in detail. Then, the DGs are requested to modify their droop coefficients when the criteria are not satisfied. Likewise, a hierarchical control scheme based on the small signal stability model is developed in [40] in order to guarantee the stable interactions within a CMG system. In this system, an interaction coefficient is taken into account to be sent to the secondary level

controller of the MGs for updating the droop coefficients of the associated DGs. In [89], a small signal model-based criterion is derived for evaluating the transient stability within a CMG system.

1.3 Thesis objectives and contributions

An in-depth literature review of the CMG systems is conducted in the previous section. Some research gaps are identified which are based on both the dynamic operation and stability analysis of the CMG systems during overloading. The objectives of this thesis along with the specific contributions are as follows.

1.3.1. Objectives of the thesis

Enhancing the self-healing capability of the isolated AC MGs through mutual support of neighbouring MGs is the main aim of this thesis. To achieve this, the following objectives are established for the thesis:

- Developing the criteria required for interconnecting the two neighbouring isolated AC MGs to cope with the overloading conditions.
- Employing the instantaneous static switches (ISS) for coupling instead of using the conventional VSCs or B2B power converters.
- Handling a synergy between the local energy storages in the MG and the external support from a neighbouring MG.
- Developing the small signal model of the MGs and the CMG system for ensuring the stability of the system under different structures.
- Maintaining the reliability and simplicity of the network by avoiding complex communication systems.
- Coordinating the load-shedding actions required within the overloaded MGs when the supporting power is insufficient.
- Implementing disturbance-free isolation of the CMG based on the developed criteria when power shortfall is removed.

1.3.2. Specific contributions

Regarding the objectives mentioned above, the specific contributions of this thesis are as follows.

- 1- A self-healing agent is developed to facilitate the interconnection as well as isolation of the neighbouring AC MGs. The considered coupling interface is an ISS that is located between the two MGs. The criteria required for detecting the overloading are accurately formulated for the CMG system. It can operate as either a decentralized approach or a centralized approach, depending on the availability of a data communication system.
- 2- A two-level power exchange strategy is proposed under which the lighter power deficiencies can be addressed by small-scale battery energy storages (BESes) locally while the CMG formation can be limited to severe deficiencies only. The conditions and constraints for BES connection or the coupling of two neighbouring MGs are derived. The strategy can operate as either a decentralized approach or a centralized approach.
- 3- Small signal model of the MGs and the CMG under study is accurately formulated. The detail models of the all components such as DERs, BESes, loads, lines and the tie line are included in the small signal model, which is then eventually expressed in a homogeneous form with the aim of performing the eigenvalue analysis. This model is required to assess the stability of the CMG before the interconnection to prevent any instability problems. The results of this analysis are used as a decision-making criterion for the BESes connection and the CMG interconnection.
- 4- With the aim of reducing the dependency of the system to the communication infrastructures, the control schemes are mainly designed for operating based on the local measurements only. Consequently, they can be easily applied to isolated MGs (off-grid MGs). This is done through developing the appropriate control schemes by utilizing the droop regulators.

- 5- When the power shortfall is removed, the coupled MGs should be isolated to carry on the operations independently. The criteria required for detecting such conditions is precisely developed and formulated based on the local measurements only.
- 6- A hierarchical cooperative strategy is proposed to support frequency of isolated MGs during power shortfalls. At the primary level, a multi-layer droop-based under frequency load shedding strategy is developed for proper dispatching of the required load to be shed among the participating controllable loads. At the secondary level, a decentralized CMG forming scheme is conducted after evaluating the relevant conditions. The coordination between these two levels is performed such that their cooperative operation can facilitate the power deficiency management in isolated MGs.
- 7- An accurate supervisory control scheme is designed in order to operate under three different modes for facilitating the ISS-based coupling of the neighbouring MGs, as well as, a proper disturbance-free isolation strategy for the coupled MGs. The ISS controller is responsible for implementing the developed scheme by appropriately modifying the droop coefficients of the DGs located within the overloaded MG.

1.4 Thesis outline

The remainder of this thesis is organized as follows.

In **Chapter 2**, the definitions along with the consisting components and control structure of the MGs are discussed. The switching techniques employed for converter interface DERs are also explained. Further, the concept of the system of coupled MGs (CMG) is presented and some related aspects including the main objectives of such systems are described.

In **Chapter 3**, the development of a self-healing agent for interconnection as well as isolation of the neighbouring MGs is presented. This agent can implement using either centralized or decentralized methods. When the communication system is available to transmit the power generation data of the DERs in real-time

(centralized approach), the self-healing agent appears as a module of the tertiary controller. Alternatively, when data communication system does not exist or is temporarily unavailable (decentralized approach), the self-healing agent appears as a local controller.

Further, a detailed small signal stability model is derived for the MGs and the CMG system under study as a decision-making criterion for interconnecting the neighbouring MGs.

In **Chapter 4**, a two-level power exchange strategy is developed to support an overloaded isolated sustainable MG. The strategy is a synergy of local support from the BES in the MG and external support from a coupled neighbouring MG. It can operate under either a decentralized approach or a centralized approach, depending on the availability of a data communication system. The conditions and constraints for BES connection or the coupling of two neighbouring MGs are formulated. Likewise, the conditions and constraints under which a BES should be disconnected or the interconnected MGs need to be isolated are established. A isolated sustainable MG with the developed strategy offers more resilience and flexibility when overloaded, since all, or a portion of the demand of the MG is supported by the local BES or is imported from the neighbouring MG, leading to a reduced necessity and rate of load-shedding.

The SSS analysis is also performed, and its results are used as a decision-making criterion for connecting the BESEs and coupling the MGs. Alternatively, if instability is observed, the SSS analysis defines a range of droop control coefficients for the DERs to enable power exchanges.

In **Chapter 5**, a two-level hierarchical cooperative strategy in order to support frequency of isolated MGs during power shortfalls is presented. The primary level organizes proper dispatch of the required load to be shed among the participating CLs. For this, a multi-layer droop-based algorithm is developed to be embedded in controllers of the CLs. The secondary level of the strategy is responsible for forming a CMG system after evaluating the relevant conditions. A set of frequency-based criteria essential to guarantee the success of interconnection of two neighbouring isolated MGs in coping with the power

deficiencies is defined and then, their accurate formulation is derived. The coordination between the two levels of the strategy is fulfilled such that their cooperative operation can facilitate the power deficiency management in isolated areas.

In **Chapter 6**, a supervisory control scheme is developed in order to facilitate ISS-based coupling of the neighbouring MGs, as well as, a proper isolation strategy for the coupled MGs. This is to handle the major concerns with the ISS-based coupling of the neighbouring MGs under a fully decentralized system. The operation of the developed strategy is conducted under three different modes – namely, Mode 1: that is initiated by forming the CMG to sustain the power output of the overloaded MG close to its maximum, Mode 2: that aims to fulfil a successful isolation when the interconnection is not required anymore and Mode 3: that starts by opening the ISS to reset default values of the DG primary controllers. The ISS controller is responsible for implementing the developed scheme by appropriately modifying the droop coefficients of the DGs located within the overloaded MG.

Chapter 7 concludes the thesis and discusses the scope for the future works.

In **Appendix**, the synchronization process required for transient-free closing of the ISS is presented and the employed algorithm to compute the synchronization time is presented. Furthermore, performance of the proposed charging control of the BESEs which is based on the droop regulators is studied under various operating regions

Chapter 2. AC MICROGRIDS:

GENERAL CONCEPTS

General configuration of MGs is actually dependent on the structure of their components as well as the level of performance expected from such systems. Also, it is possible to have various control options in order to achieve a desirable performance in the MGs. At the first step, therefore, it is essential to introduce the main objectives of utilizing the MGs, the control architecture of such systems and the components available to enhance their performance. This chapter begins with presenting the general definitions of MGs along with introducing different levels of a hierarchical control structure. Then, the concept of CMG is presented and a number of main aims for clustering of MGs are described. It is expected that each MG will have several converter interface DERs. Therefore, the switching controllers for these converters are integral parts of an MG operation. These are also discussed in this chapter.

2.1 The notion of Microgrid

Although numerous studies have been conducted throughout the world on various aspects of MGs, proposing a generally accepted definition for this concept is still an issue to be addressed. Various MG characterizations can be found in the literature depending on the interpretations by the researchers. Below a number of these definitions are reviewed and the common points are summarized.

The concept of MG is proposed in [11] as “a cluster of micro-sources, storage systems, and loads which presents itself to the grid as a single entity that can respond to the central control signals”. A flexible and controllable interface between the MG and the grid is considered as the heart of this concept. The U.S Department of Energy has presented the definition of MGs as [90]: “A microgrid

is a group of interconnected loads and distributed energy resources within clearly defined electrical boundaries that acts as a single controllable entity with respect to the grid. A microgrid can connect and disconnect from the grid to enable it to operate in both grid-connected or island-mode”. CIGRÉ C6.22 Working Group defined MGs as “electricity distribution systems containing loads and distributed energy resources, (such as distributed generators, storage devices, or controllable loads) that can operate in a controlled, coordinated way either in grid-connected or islanded modes” [91].

These definitions are only a few samples already presented in the literature. Despite the diversity in details, some common features of the definitions can clearly be identified as follows:

- An MG is a cluster of interconnected DGs, energy storage systems (ESS) and loads.
- An MG is a distinct electrical unit.
- There is coordination amongst the components of an MG to provide flexibility against different contingencies.
- An MG can operate in either grid-connected or islanded mode.

The DGs of an MG can be either dispatchable or non-dispatchable. The dispatchable DGs such as diesel generators and microturbines can be easily controlled by the associated controllers to follow the desired generation patterns [19]. On the other hand, the non-dispatchable ones, which are mainly the renewable DGs such as wind and solar, cannot be properly controlled due to the fluctuation of their input power. Intermittency and volatility are the main characteristics of this type of DGs that can deteriorate the power quality indices, if their penetration level is high. Usually, these effects can be avoided by installing a proper capacity of ESS [92]. Actually, the ESS can smooth fluctuations of the output power of the DGs by absorbing or injecting the appropriate amount of power. Therefore, the combination of ESS and the non-dispatchable DGs can yield dispatchable energy sources that, beside other dispatchable DGs, can be employed to control both frequency and voltage of an MG [93].

An MG consisting of the aforementioned components and controllers can be considered as a single entity [94]. From the main grid point of view, an MG is capable of representing itself as a distinct unit that can operate either as a load demanding power from the grid or as a source delivering power to the grid. Thus, the grid-connected MGs are actually controllable units that can be actively involved in improving both dynamic response and stability issues of the grid [95].

MGs can operate in either grid-connected or islanded mode [96]. In the grid-connected mode, the renewable DGs are mainly operated as current sources injecting power to the grid as much as they can. This is because the frequency is regulated by generation units of the grid and the DGs of the MG probably have minor impacts on it. In the islanded mode, however, most of the DERs should be capable of operating as voltage sources since they are responsible for regulating both frequency and bus voltages of the MG [97]. As has been mentioned before, this can be fulfilled via using dispatchable DGs as well as the combination of the renewable DGs and ESS. The renewable DGs with no ESS nevertheless should carry on the operation as current sources. Proper coordination of different types of DGs within an islanded MG is a critical matter to maintain the stability of the system.

The interconnection of most of renewable DGs as well as ESS is fulfilled through power electronic interfaces [63]. This is also the case for the interconnection of MGs and the grid [97]. Most of the control issues such as voltage and frequency regulation and power flow control can be carried out in MGs by properly operating the interfacing converters. Different levels of control should be applied in order to achieve a successful operation of the MGs. This covers a wide range of control from the inner level of each DG to coordination amongst MGs as well as between the MGs and the grid. The control levels are defined based on the control modes selected to manage the entire operation, as discussed in the next section.

2.2 Control architecture of microgrids

Generally, three control modes can be considered for management of the MGs, namely centralized, distributed and decentralized. The structures of these control modes and their main features are summarized below.

CENTRALIZED CONTROL: In this mode, an MG central controller (MGCC) is the main regulator of the system [98, 99], as can be seen from Fig. 2.1a. The MGCC is responsible for taking appropriate decisions to organize all the control actions within the MG. As the main objective, the MGCC should maintain generation-demand balance in the MG, satisfying some pre-defined technical and economic constraints. All information and measurements related to both DERs and loads should be regularly transmitted to the MGCC via a suitable communication infrastructure. The MGCC derives appropriate control commands required by the components. In this mechanism, the MGCC operations can involve a lot of computations along with considerable data transfer via a high bandwidth communication system that can compromise the outcome, especially in case a communication failure. Furthermore, there is a potential for single point of failure in this centralized control mode. This means a failure in the MGCC operation can cause a failure of the entire system.

DISTRIBUTED CONTROL: The structure of an MG with distributed controllers is shown in Fig. 2.1b. In this mode, each DG is considered as an agent that should exchange information with its immediate neighbors only [22, 100]. Although the successful operation of this control mode is dependent on the availability of communication system, the concerns with a single point failure are removed. Much more complex control techniques nevertheless are required to guarantee desirable operations of an MG under this control mode.

DECENTRALIZED CONTROL: A fully decentralized control mode is actually a communication-free scheme, as can be seen from Fig. 2.1c. In this mode, each DER operates based only on the local information [101]. The structure of the system is much simpler since there is no dependency on communication systems. Thus, this mode is preferred when either there is no access to any communication infrastructure or communication systems are not reliable. Controller of each DER

determines the output power according to local measurements such as frequency and voltage at the connection point. Dynamic responses along with the stability of the MG under a fully decentralized control mode nevertheless can be vulnerable to different contingencies if appropriate supportive measures are not applied.

The control actions within an MG can be realized through the application of a hierarchical structure consisting of three stages, namely the primary level, the secondary level, and the tertiary level [22, 12, 30], as shown in

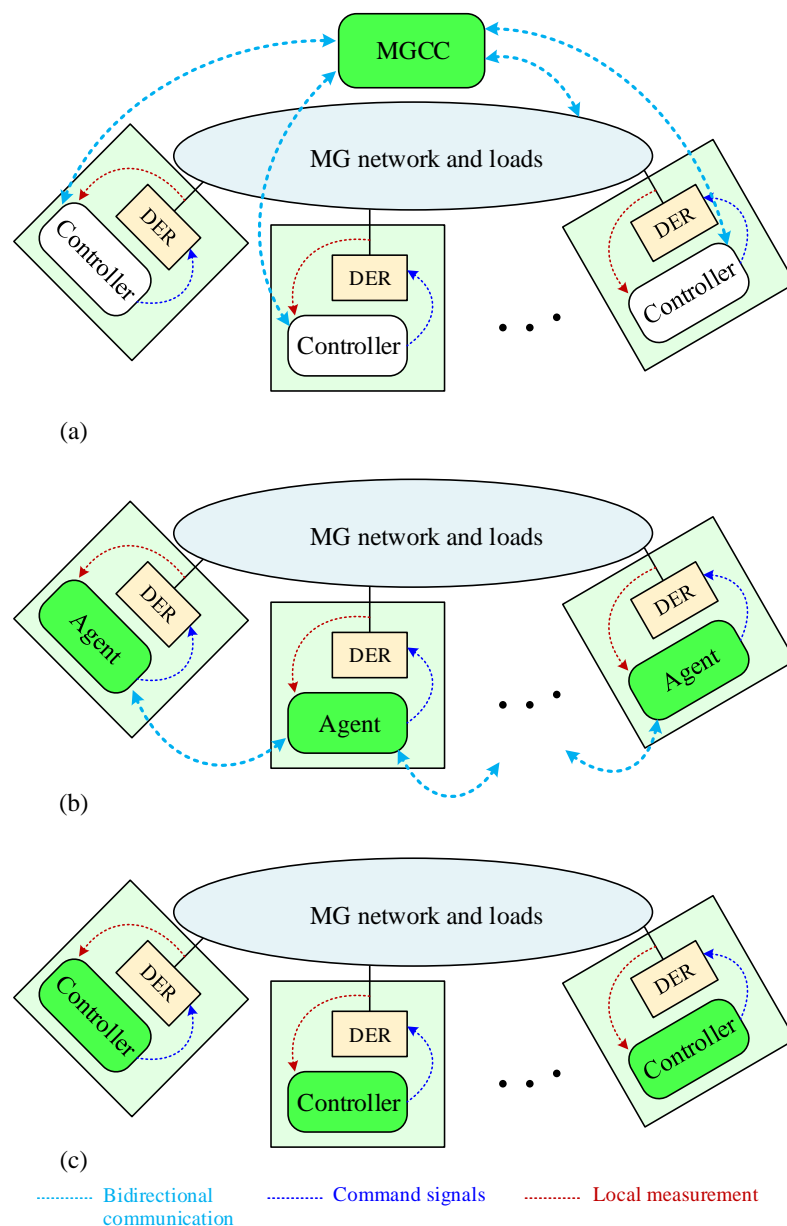


Fig. 2.1: General structure of (a) centralized control, (b) distributed control, and (c) fully decentralized control modes.

Fig. 2.2. These levels can be characterized according to their required time frames, which are briefly described below.

PRIMARY LEVEL: At this level, the local controller of each DER fulfills control of the output frequency and voltage of the device along with its output power. In this, the local controller can either follow the associated set points provided by the higher stages of the control structure or operate independently using a decentralized scheme. Typically, droop regulators are employed to implement the primary level controls for the converter-interfaced DERs operating as voltage source converters (VSC). Usually, the primary control has the fastest response.

SECONDARY LEVEL: This control is mainly responsible for compensating the deviation of the output voltage and frequency of the DERs from their respective set points. In fact, the coordination amongst the local controllers of the MGs can be realized at this level. A communication system is required to implement this level of control since the information and commands should be regularly transferred between the local regulators and the secondary controller. Usually, the operation time frame of this control is slower than that of the primary level. In accordance with the detected deviations, the appropriate corrective terms should be calculated by the secondary controller to be sent to the local regulators. Further, power quality improvements of the MGs along with loss minimizations can be carried out by using this level of control. Handling seamless transitions between the grid-connected and islanded modes of the MGs can be also performed by the secondary controllers.

TERTIARY LEVEL: At this level, the interactions and power exchanges amongst the MGs as well as between the MGs and the main grid is of concern. Generally, these actions are organized in order to achieve various technical, economic and environmental objectives within the whole system, while satisfying some pre-specified constraints. According to the objectives under consideration, the tertiary controller should determine the amount of power to be exchanged amongst the subsystems along with the associated timings. In fact, the tertiary controller, which has the highest level of control within the system, is responsible

for coordinating the operation of the MGs through sending appropriate commands to the secondary controllers. If the secondary controller is not included in an MG, the tertiary controller should be capable of adjusting the set points for the local controllers of that MG. Overload relieving, reliability improvement, resilience enhancement, and loss minimization within the system are some sample technical objectives for the tertiary controllers.

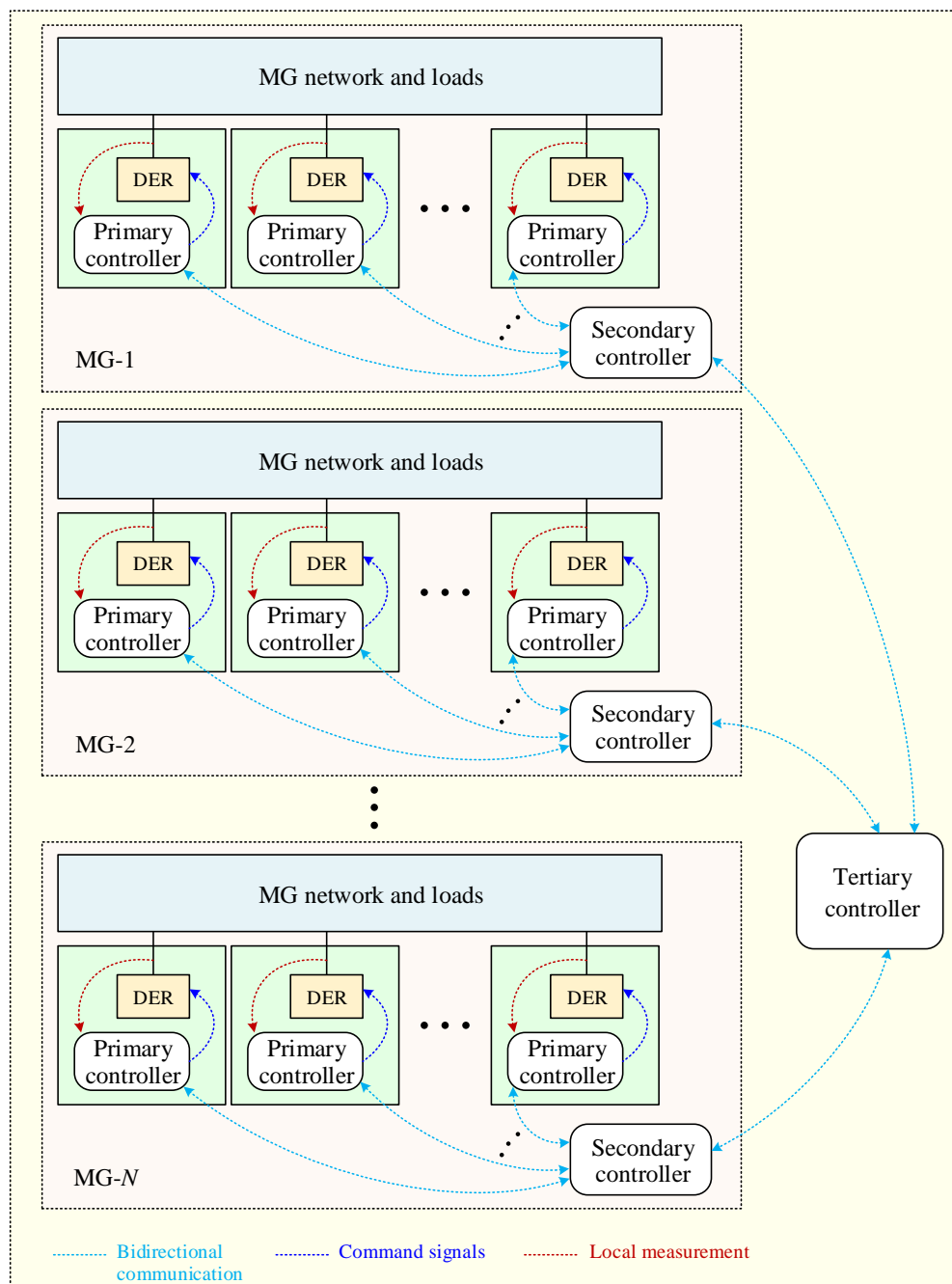


Fig. 2.2: Hierarchical control of the MGs.

2.3 Clusters of MGs

The increasing number of renewable DERs within distribution networks can impose an extensive computational burden on central energy management units. The handling of such networks also requires complex communication infrastructures to perform the associated bidirectional data transfer. The idea of coupled MGs has been actually presented to facilitate control of the distribution networks with high penetration of renewable DERs [34]. Through splitting the whole network into a number of locally controlled interconnected MGs, both the control and communication complexity can be significantly reduced. With the opportunities, nevertheless come the associated challenges to be addressed. Successful operation of such networks highly depends on the proper control of the interactions amongst the MGs.

The interconnection, as well as the isolating of MGs, can be an interesting issue to be investigated for the MGs in a remote area. Supplying electric energy to rural and remote areas has always been a challenging task mainly due to the distance involved with their connections to the existing electric power grids. Isolated MGs is a promising solution to handle this problem [102]. Such MGs normally operate independently since they probably have different owners or jurisdictions. However, remote MGs are highly vulnerable to power shortfalls since they are of comparatively smaller sizes. Therefore, it is preferred for such MGs to couple with the neighbouring MGs in order to get some supporting power during the deficiencies.

The MGs of a cluster can have either the same owners such as utility-owned MGs or different owners. For the former, the network operator should manage the operation of the MGs such that the overall system can attain the best outcomes. In such clusters, the MGs should be considered as the subsystems that should be organized in order to achieve the optimum values for the main system. For the latter, however, the efforts of each MG should be fulfilled in such a way that it can primarily satisfy its own targets. Usually, there is no interconnection or power exchange among such MGs during normal conditions. The MG coupling should be conducted during contingencies or for some power and energy trades.

A number of main aims for clustering of MGs are briefly described below.

POWER AND ENERGY TRADE: the DERs within the isolated MGs should adjust their power outputs such that the generation-demand balanced can always be met. For this, the controllers can perform the loads sharing in accordance with the economic dispatch algorithms in order to minimize the generation cost. When such MGs are interconnected, they can trade power and energy with each other and also with the main grid. This issue can be done within a market framework to increase the profits of the owners [103]. Each MG should carefully implement the associated bidding and generation scheduling steps. Recently, design of the transactive energy frameworks has been gaining considerable attention that can address these issues [74]. Also, the MGs can decrease their dependency on the main grid through forming a cluster of cooperative MGs [104, 54]. In this way, the power exchange among the MGs is amplified with the aim of raising the penetration level of renewable DERs along with the revenue maximization.

OVERLOAD MANAGEMENT: it is highly likely for isolated MGs to experience various types of power shortfalls. This can be mainly due to either variation in the input power of the DERs or short term rises in load demands. Typically, the MGs can employ ESS or oversized diesel generators to cope with these concerns [105, 106]. As a less expensive alternative, the overloaded MG can be interconnected to a neighbouring MG with surplus generation capacity to get the required supports. The coupling mechanism along with the level of power exchange between the MGs is the issue to be addressed.

RELIABILITY IMPROVEMENT: Various reliability indices should be satisfied during both planning and operation stages of electrical networks in order to ensure a desirable performance of the system. Accurately sizing and siting of the system components, installing the required communication systems, and establishing proper control structures are some well-known actions to take in order to achieve a reliable network. Besides, clustering of the distribution networks into a set of interconnected MGs can be a promising technique for improving the reliability aspects [78]. This idea can considerably strengthen the robustness of the network against various uncertainties mainly caused by renewable DERs. Also, the

network can be designed as a cluster of MGs that operate autonomously during normal conditions [107, 108]. If any contingency occurs in an MG, the supportive MGs can rearrange their generation levels along with reconfiguring the connection patterns in order to remedy the problem.

RESILIENCE ENHANCEMENT: natural disasters such as hurricanes, floods, blizzard storms, and earthquakes can cause extreme power outages. This is also the case for deliberate attacks and accidents. Resiliency is defined as “the ability to prepare for and adapt to changing conditions and withstand and recover rapidly from disruptions” [109]. Accordingly, developing the efficient methods for restoring the distribution system quickly after disasters is of great importance to achieve resilient power grids [110]. One idea is to use MGs to supply the critical loads when the utility power is unavailable as a result of the disasters [111]. Appropriate MG forming schemes should be prepared to reconfigure interconnection pattern of the DERs such that more critical loads can be restored. It is to be noted that defining suitable indices to quantify the grid resilience in extreme conditions is an essential prerequisite to tackle such concerns [112].

2.4 Droop regulator

Droop regulators are widely used as controllers of the DERs at the primary level [113, 114]. These schemes are often employed for regulating frequency and voltage of MGs along with proper load sharing amongst the dispatchable DERs. This is because droop regulators show superior capabilities in operating based only on the local measurements [115]. As a result, costly and complicated communication infrastructures can be avoided, increasing reliability and avoiding the single point of failure. Various types of droop regulators are presented in the literature [63]. Traditionally, voltage droop scheme, $Q - V$, is utilized for reactive power sharing and output voltage regulation while frequency droop scheme, $P - f$, is employed for active power sharing as well as frequency control. Alternatively, angle droop scheme, $P - \delta$, can be applied for active power sharing in an MG consisting of converter interface DERs [97]. These regulators are described in this section.

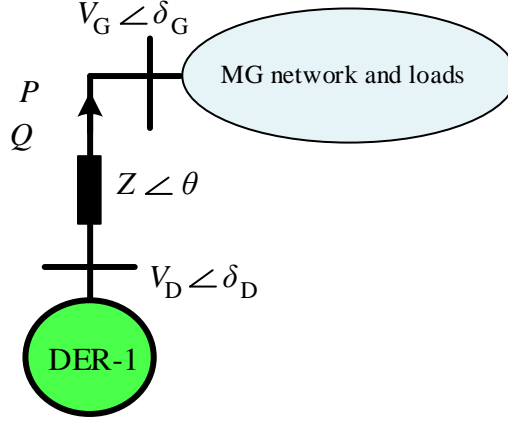


Fig. 2.3: Power flow from the DER to the MG.

2.4.1 DER to MG power flow

Let us consider the MG of Fig. 2.3. A sample DER (i.e., DER-1) injects an average active power of P and reactive power of Q to the MG. These powers can be obtained by passing the instantaneous powers through low pass filters. The power delivered by the DER can be calculated as

$$P + jQ = V_D \angle \delta_D \left(\frac{V_D \angle \delta_D - V_G \angle \delta_G}{Z \angle \theta} \right)^* \quad (2.1)$$

where V_D and δ_D are respectively magnitude and angle of the voltage at the DER side, V_G and δ_G are respectively magnitude and angle of the voltage at MG side, and Z and θ are respectively magnitude and angle of the impedance in between. From (2.1), P and Q can be obtained as

$$P = \frac{V_D}{R^2 + X^2} (R[V_D - V_G \cos(\delta_D - \delta_G)] + XV_G \sin(\delta_D - \delta_G)) \quad (2.2)$$

$$Q = \frac{V_D}{R^2 + X^2} (-RV_G \sin(\delta_D - \delta_G) + X[V_D - V_G \cos(\delta_D - \delta_G)]) \quad (2.3)$$

where R and X are respectively real and imaginary terms of the impedance. These equations can be rewritten as [116]

$$V_G \sin(\delta_D - \delta_G) = \frac{XP - RQ}{V_D} \quad (2.4)$$

$$V_D - V_G \cos(\delta_D - \delta_G) = \frac{RP + XQ}{V_D} \quad (2.5)$$

Assuming $X \gg R$ and the angle difference is small, (2.4) and (2.5) can be further simplified as

$$(\delta_D - \delta_G) = \frac{X}{V_D V_G} P \quad (2.6)$$

$$V_D - V_G = \frac{X}{V_D} Q \quad (2.7)$$

2.4.2 Droop equations

From (2.6) and (2.7), it can be seen that δ_D and V_D are predominantly dependant on P and Q , respectively. Thus, δ_D can be controlled by regulating P . Also, V_D can be adjusted by regulating Q . Based on these results, the angle and voltage droop regulators can be characterized as

$$\delta_D = \delta_r - m_\delta (P - P_r) \quad (2.8)$$

$$V_D = V_r - n(Q - Q_r) \quad (2.9)$$

where δ_r and V_r are respectively the rated angle and voltage magnitudes of DER when it is supplying rated powers of P_r and Q_r , and m_δ and n are slopes of the angle and voltage droop curves, respectively. Fig. 2.4a-b show sample curves for the angle and voltage droop regulators. Likewise, frequency droop regulator can be defined from (2.6) as

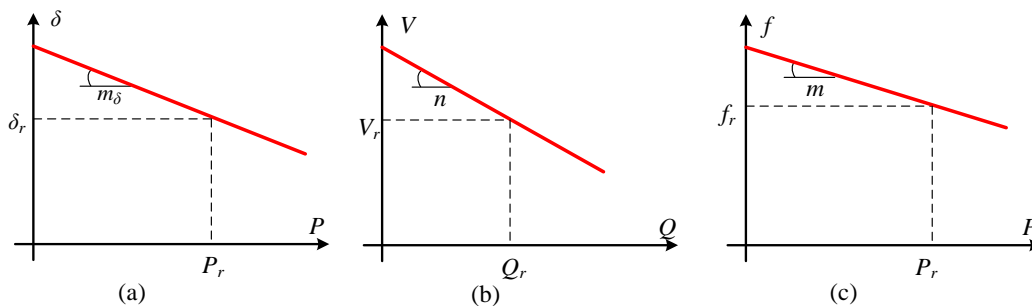


Fig. 2.4(a) angle droop curve, (b), voltage droop curve and (c) frequency droop curve.

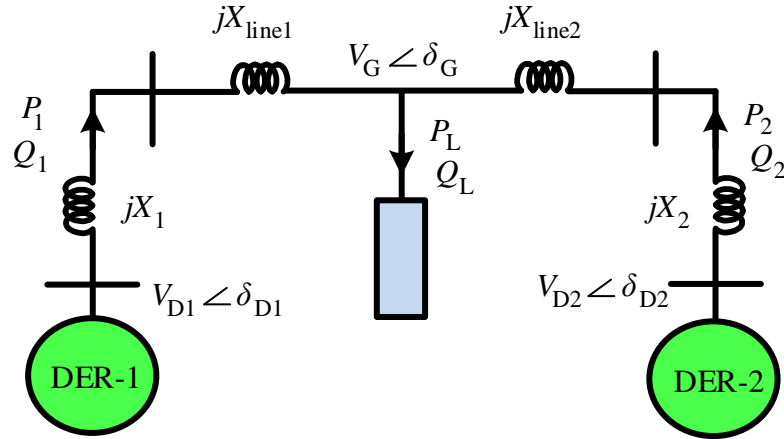


Fig. 2.5: Power sharing between the DERs.

$$f = f_r - m(P - P_r) \quad (2.10)$$

where f is the frequency, f_r is the rated frequency at which the DER delivers the rated power of P_r , and m is the droop gain. Fig. 2.4c illustrates a sample curve for the frequency droop regulators.

2.4.3 Power sharing among DERs

The traditional droop regulators are often used to apply the local control on the DERs. However, the accuracy of the outcomes can be compromised if the gain adjustments are not fulfilled properly. Let us consider the MG of Fig. 2.5 with two DERs (i.e., DER-1 and DER-2) supplying a load. Applying the angle droop of (2.8) and taking the rated values as $\delta_r = m_\delta P_r$, the angles difference can be obtained as

$$\delta_{D1} - \delta_{D2} = -m_{\delta 1} P_1 + m_{\delta 2} P_2 \quad (2.11)$$

From (2.6), likewise, the angles difference is

$$\delta_{D1} - \delta_{D2} = \left(\frac{X_1 + X_{line1}}{V_{D1} V_G} \right) P_1 + \left(\frac{X_2 + X_{line2}}{V_{D2} V_G} \right) P_2 \quad (2.12)$$

where X and X_{line} are the DER output reactance and the line reactance, respectively. Since $P_1 + P_2 = P_L$, it can be shown that [97]

$$\frac{P_1}{P_2} = \frac{\frac{X_2 + X_{line2}}{V_{D2}V_G} + m_{\delta 2}}{\frac{X_1 + X_{line1}}{V_{D1}V_G} + m_{\delta 1}} \quad (2.13)$$

In order to achieve an ideal power sharing, therefore, a constraint as

$$m_{\delta 1} \gg \frac{X_1 + X_{line1}}{V_{D1}V_G}, m_{\delta 2} \gg \frac{X_2 + X_{line2}}{V_{D2}V_G} \quad (2.14)$$

should be ensured during the design procedure. Then, the power sharing can be desirably performed as

$$\frac{P_1}{P_2} = \frac{m_{\delta 2}}{m_{\delta 1}} \quad (2.15)$$

This is also the case for the frequency droop regulators.

Let us rewrite the droop equations of (2.9) and (2.10) as [66]

$$\begin{aligned} f &= f_{\max} - mP \\ V &= V_{\max} - nQ \end{aligned} \quad (2.16)$$

where f_{\max} and V_{\max} are respectively the rated frequency and voltage magnitude. In order to share the total load among the DERs as per their capacity within an MG consisting of N DERs, the droop gains should be selected as

$$\begin{aligned} m &= \frac{f_{\max} - f_{\min}}{P^{cap}} \\ n &= \frac{V_{\max} - V_{\min}}{Q^{cap}} \end{aligned} \quad (2.17)$$

where superscript cap indicates power capacity of each DER and f_{\min} and V_{\min} are respectively the minimum of frequency and voltage magnitude in the MG. Consequently, the load sharing between any two DERs, e.g., i^{th} and j^{th} , can be presented according to their droop coefficients as

$$\begin{aligned} \frac{P_i}{P_j} &= \frac{m_j}{m_i} \rightarrow \frac{P_i}{P_j} = \frac{P_i^{cap}}{P_j^{cap}} \\ \frac{Q_i}{Q_j} &= \frac{n_j}{n_i} \rightarrow \frac{Q_i}{Q_j} = \frac{Q_i^{cap}}{Q_j^{cap}} \end{aligned} \quad (2.18)$$

2.5 Converter interfaced DERs

Renewable DERs are normally connected to the MG through converter interfaces. Configuration of the interfaces should be selected in accordance with the characteristics of the DERs. The interfaces considered for modelling the dispatchable and non-dispatchable DERs are explained in this section.

2.5.1 Voltage source converter

Structure of the employed VSC is shown in Fig. 2.6 [117]. The VSC consists of three single-phase H-bridges where each H-bridge is composed of insulated gate bipolar transistors (IGBT) with anti-parallel diodes. In this structure, each phase can be controlled individually, enhancing both dynamic performance and controllability of the device. A single-phase transformer is used to boost the input voltage along with providing galvanic isolation. The inverters are connected to the MG via LCL filters in which L_f represents the leakage reactance of the transformers, R_f represents copper losses, C_f indicates the filter capacitance and L_T indicates the coupling inductance. It is to be noted that the voltage across C_f , v_c , is actually considered as the output voltage of the VSC.

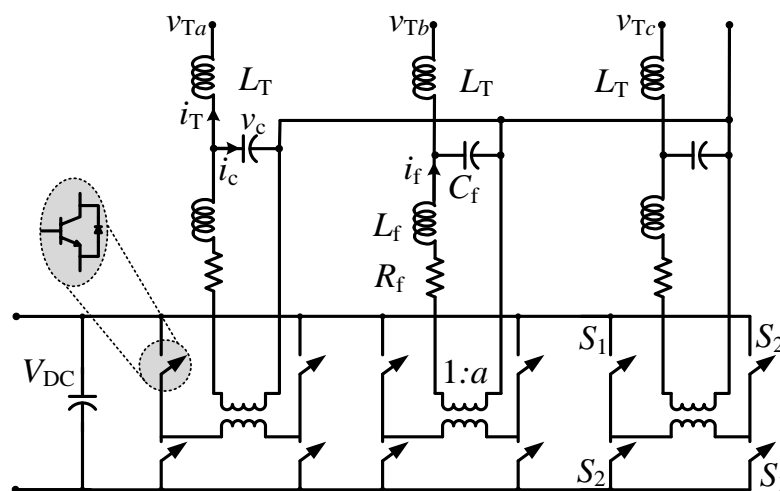


Fig. 2.6: Structure of the utilized voltage source converter.

2.5.2 Modelling of dispatchable DERs

As can be seen from Fig. 2.7, the combination of a DG and its local smoothing BES is considered as a general model for the dispatchable DERs [118]. Rectification and battery management details can be excluded by modelling their combination as a VSC. The dispatchable DERs can involve in frequency and voltage regulation of the MG. For this, the reference output voltage of the DER v_c^{com} should be adjusted by its droop controller according to the local measurements (e.g., v_c and f) along with the power outputs P and Q . Let us assume v^{com} and f^{com} are respectively the references for v_c magnitude and frequency obtained through taking advantage of (2.16). Then, the three phase reference voltages for v_c can be calculated as

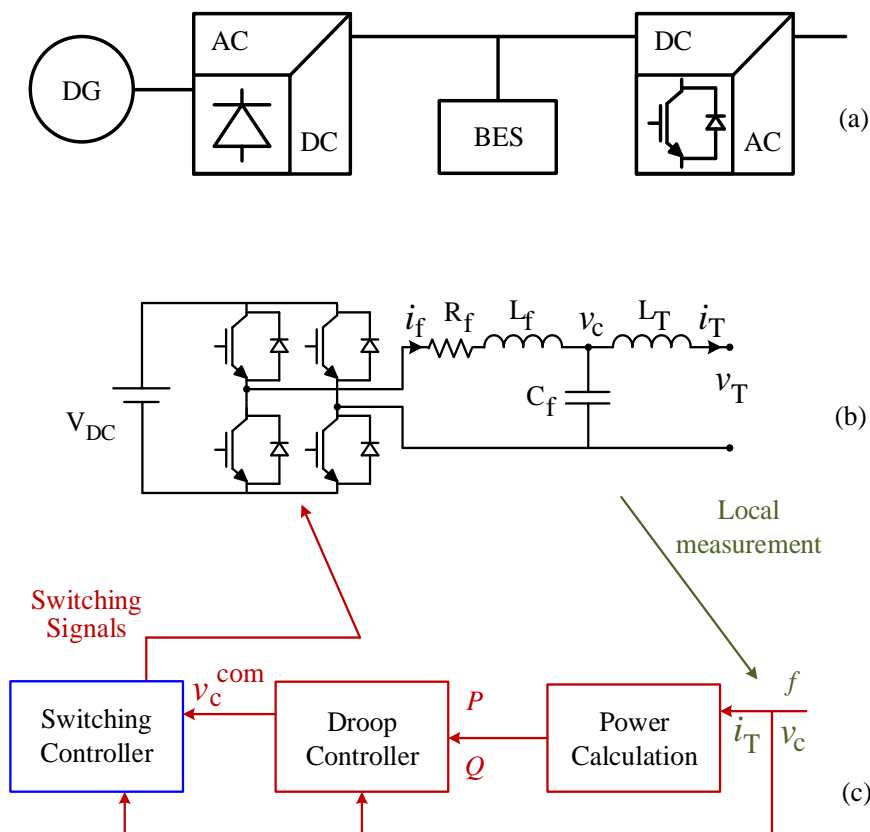


Fig. 2.7: (a) General structure and (b) single-line diagram of the associated VSC, and (c) droop-based control scheme of the dispatchable DERs.

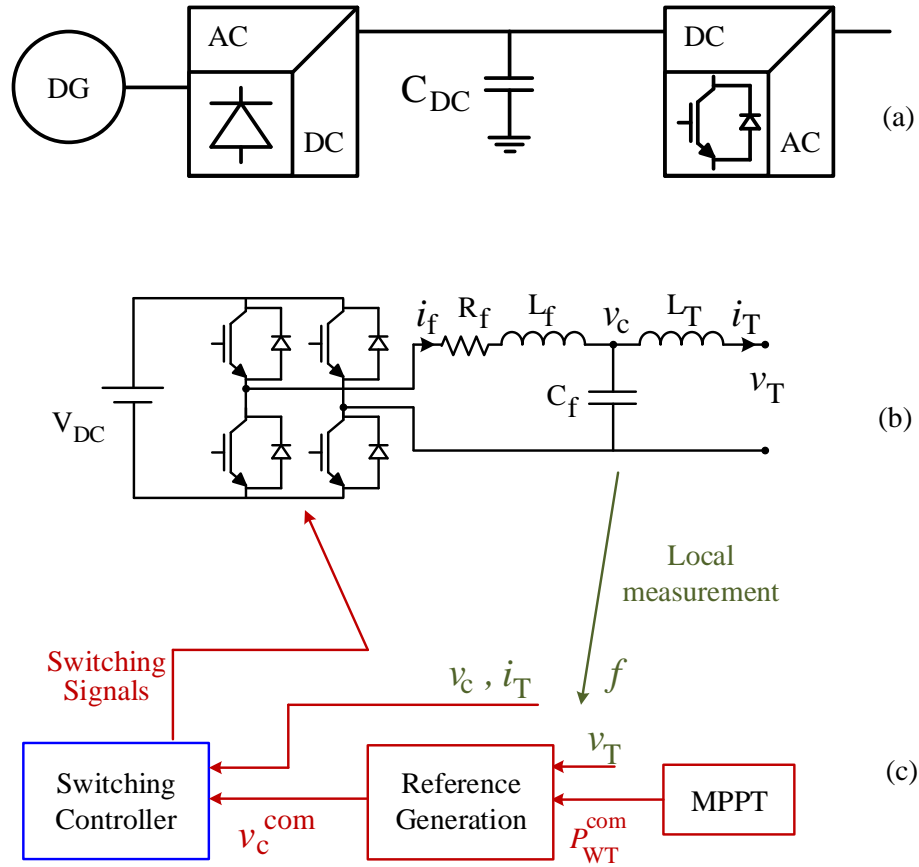


Fig. 2.8: (a) General structure and (b) single-line diagram of the associated VSC, and (c) PQ control scheme of the non-dispatchable DERs.

$$\begin{aligned}
 v_{ca}^{com} &= \sqrt{2}V^{com} \sin(2\pi f^{com} t) \\
 v_{cb}^{com} &= \sqrt{2}V^{com} \sin(2\pi f^{com} t - \frac{2\pi}{3}) \\
 v_{cc}^{com} &= \sqrt{2}V^{com} \sin(2\pi f^{com} t + \frac{2\pi}{3})
 \end{aligned} \tag{2.19}$$

These calculated reference voltages should be sent to a switching controller. Then, the controller can generate the corresponding switching signals for each phase.

2.5.3 Modelling of non-dispatchable DERs

By using a smoothing capacitor instead of the BES, the DGs can be assumed as non-dispatchable DERs [118]. In this case, the VSC is responsible for injecting the powers dictated by the maximum power point tracking (MPPT) block. As shown in Fig. 2.8, the DER is modelled by a PQ-controlled VSC. Let us assume

that the active and reactive power references for each phase are P^{com} and Q^{com} , respectively. In order to deliver the powers to the MG, the reference voltage across the filtering capacitor, $V^{\text{com}} \angle \delta^{\text{com}}$, are expressed as [97]

$$\begin{aligned} \delta^{\text{com}} &= \tan^{-1} \left(\frac{P^{\text{com}} L_T \omega}{V_T^2 + Q^{\text{com}} L_T \omega} \right) + \delta_T \\ V^{\text{com}} &= \frac{V_T^2 + Q^{\text{com}} L_T \omega}{V_T \cos(\delta^{\text{com}} - \delta_T)} \end{aligned} \quad (2.20)$$

where $V_T \angle \delta_T$ is the voltage on the MG side of the coupling inductor (see Fig. 2.8b), and ω is the angular frequency of the MG. Note that Q^{com} is usually zero. Then, the three phase reference voltages for v_c can be calculated as

$$\begin{aligned} v_{ca}^{\text{com}} &= \sqrt{2} V^{\text{com}} \sin(\omega t + \delta^{\text{com}}) \\ v_{cb}^{\text{com}} &= \sqrt{2} V^{\text{com}} \sin\left(\omega t + \delta^{\text{com}} - \frac{2\pi}{3}\right) \\ v_{cc}^{\text{com}} &= \sqrt{2} V^{\text{com}} \sin\left(\omega t + \delta^{\text{com}} + \frac{2\pi}{3}\right) \end{aligned} \quad (2.21)$$

The switching signals of the inverter are generated utilizing the switching controller such that the converter tracks the reference voltage waveforms.

2.6 Switching controllers

As has been mentioned before, once the voltage references are obtained, a switching controller should be employed in order to generate the corresponding switching signals for the VSCs. Two switching techniques, namely “single-step prediction horizon” and “state feedback control” are explained in this section that will be used for switching control [119].

2.6.1 Single-step prediction horizon

The single-step prediction horizon technique is utilized to track the desired voltage across the capacitor, v_c^{com} [118]. Defining the state vector $x(t) = [v_c \ i_f]^T$ for

each phase of the VSC of Fig. 2.6, the state-space model of this system can be represented as

$$\dot{x}(t) = Ax(t) + Bw(t) \quad (2.22)$$

where

$$A = \begin{bmatrix} 0 & \frac{1}{C_f} \\ -\frac{1}{L_f} & -\frac{R_f}{L_f} \end{bmatrix}, \quad B = \begin{bmatrix} 0 & -\frac{1}{C_f} \\ \frac{V_{DC}}{L_f} & 0 \end{bmatrix} \quad \text{and} \quad w = \begin{bmatrix} u_c(t) \\ i_T(t) \end{bmatrix}.$$

In (2.22), where u_c is the continuous-time approximation of the switching function u , which is equal to ± 1 . Note that the above realization is based on $L_f - C_f$ part of the filter only. Discretization of (2.22), for a sampling time of T_s , yields

$$x(k+1) = Fx(k) + Gw(k) \quad (2.23)$$

where $F = e^{AT_s}$, $G = \int_0^{T_s} e^{At} B dt$

Let us consider the elements of F and G as f_{ij} and g_{ij} respectively. Therefore, v_c can be written as

$$v_c(k+1) = f_{11}v_c(k) + f_{12}i_f(k) + g_{11}u(k) + g_{12}i_T(k) \quad (2.24)$$

The quadratic cost function, which is chosen to regulate v_c for a single-step prediction horizon, is

$$J(k) = \{v_c^{\text{com}}(k+1) - v_c(k+1)\}^2 \quad (2.25)$$

Minimizing (2.25) with respect to u_c , and then applying the result on (2.24) yields

$$u_c(k) = \lambda_1 v_c^{\text{com}}(k+1) - \lambda_2 v_c(k) - \lambda_3 i_f(k) - \lambda_4 i_T(k) \quad (2.26)$$

where

$$\lambda_1 = 1/g_{11}, \lambda_2 = f_{11}/g_{11}, \lambda_3 = f_{12}/g_{11}, \lambda_4 = g_{12}/g_{11} \quad (2.27)$$

Now by assuming h as a small hysteresis band (e.g., $h = 10^{-4}$), the voltage output of the inverter should alter to $+V_{DC}$ or $-V_{DC}$ if u_c becomes larger or smaller than h respectively. This can be written mathematically as (see also Fig. 2.9)

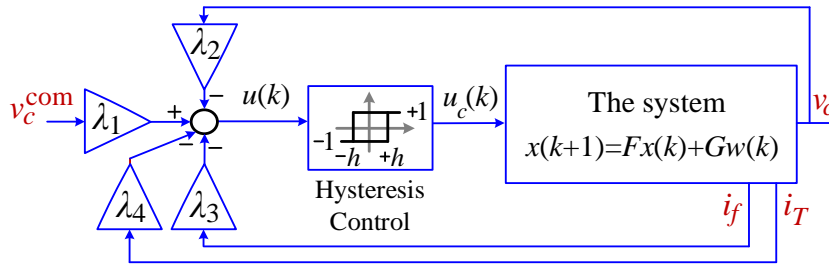


Fig. 2.9: Diagram of the switching technique based on single-step prediction horizon method.

$$\begin{aligned}
 & \text{if} \quad +h < u_c(k) \quad \text{then} \\
 & \quad \quad u = +1 \\
 & \text{elseif} \quad -h \leq u_c(k) \leq +h \quad \text{then} \\
 & \quad \quad u = \text{previous } u \\
 & \text{elseif} \quad u_c(k) < -h \quad \text{then} \\
 & \quad \quad u = -1 \\
 & \text{end}
 \end{aligned} \tag{2.28}$$

2.6.2 State feedback control

By defining the state vector $z(t) = [i_T(t) \ i_c(t) \ v_c(t)]^T$ for each phase of the VSC shown in Fig. 2.6, the state-space description of this system can be represented as [117]

$$\dot{z}(t) = A_z z(t) + B_z u_c(t) + C_z v_T(t) \tag{2.29}$$

where

$$A_z = \begin{bmatrix} 0 & 0 & \frac{1}{L_T} \\ -\frac{R_f}{L_f} & -\frac{R_f}{L_f} & -\left(\frac{1}{L_f} + \frac{1}{L_T}\right) \\ 0 & \frac{1}{C_f} & 0 \end{bmatrix}, \quad B_z = \begin{bmatrix} 0 \\ \frac{V_{DC}}{L_f} \\ 0 \end{bmatrix} \quad \text{and} \quad C_z = \begin{bmatrix} -\frac{1}{L_T} \\ \frac{1}{L_T} \\ 0 \end{bmatrix}$$

Discretization of (2.29) yields

$$z(k+1) = F_z z(k) + G_z u_c(k) + H_z v_T(k) \tag{2.30}$$

where $F_z = e^{A_z T_s}$, $G_z = \int_0^{T_s} e^{A_z t} B_z dt$ and $H_z = \int_0^{T_s} e^{A_z t} C_z dt$ for a sampling time of T_s . Let us consider $[k_1 \ k_2 \ k_3]$ as the gain vector of a state feedback control law and

$z^{\text{com}}(k)$ as the desired state vector in discrete-time domain. Then, $u_c(k)$ can be expressed as

$$u_c(k) = -[k_1 \quad k_2 \quad k_3][z(k) - z^{\text{com}}(k)]^T \quad (2.31)$$

Assuming a full control over $u_c(k)$, an infinite-time linear quadratic regulator (LQR) is employed to compute the feedback gains. The objective function chosen for this problem is

$$J(k) = \sum_{k=0}^{\infty} (z(k) - z^{\text{com}}(k))^T Q (z(k) - z^{\text{com}}(k)) + u_c(k)^T R u_c(k) \quad (2.32)$$

where Q is the state weighting matrix and R is the control cost matrix. Then, the desired values for $[k_1 \quad k_2 \quad k_3]$ can be attained by minimizing (2.32) with respect to u_c via solving the corresponding discrete time algebraic Riccati equation.

Eventually, a hysteresis control is applied to limit the tracking error $u_c(k)$ within the specified bonds, as can be seen from Fig. 2.10. It is to be noted that once v_c^{com} is calculated by the local controller, i.e., (2.19), the corresponding i_T^{com} and i_c^{com} can be easily computed as well.

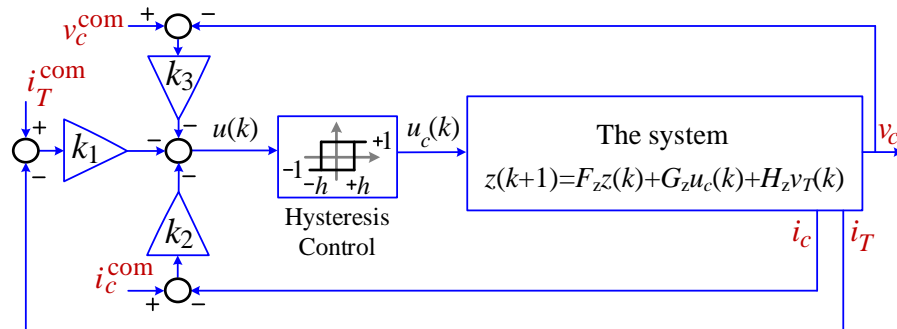


Fig. 2.10: Diagram of the switching technique based on the LQR state feedback control.

2.7 Conclusion

In this section, structure and control configuration of AC MGs are discussed. Different control modes usually applied in MGs are reviewed. Also, architecture of the hierarchical control systems is explained for the MGs. Then, the notion of MG clusters along with some main objectives of forming such clusters is presented. The configurations adopted to model dispatchable as well as non-dispatchable DGs are discussed. Typically, droop regulators are employed to perform the control on the DERs at the primary level. Derivation of the droop equations along with the associated power sharing methods is also explained. Further, the switching techniques used in this thesis to force the converters to track the reference signals are described and relevant formulations are presented for each of them.

Chapter 3. ENHANCING OVERLOADING RESILIENCE OF ISOLATED MICROGRIDS

Tackling the power deficiency issue is one of the main operational challenges with isolated MGs, specifically in the remote areas. Usually, such MGs have limited power generation capacities. Various strategies such as utilizing oversized diesel generators as well as employing energy storage systems have been suggested in the literature to provide frequency support for an overloaded MG [78, 120, 118]. The installation and operating costs of energy storage systems nevertheless are considerable. Also, fuel transport cost is one of the serious concerns with diesel generators that may expose isolated MGs to high electricity prices or even, put them at a risk of supply interruption.

The technique of coupling neighbouring MGs can be considered as an economically promising alternative since it imposes almost no extra capital investment. In this chapter, a self-healing agent is developed to facilitate interconnection as well as isolation of the neighbouring MGs [121]. This agent can implement using either centralized or decentralized methods. When the communication system is available to transmit the power generation data of the DERs in real-time (centralized approach), the self-healing agent appears as a module of the tertiary controller. Alternatively, when data communication system does not exist or is temporarily unavailable (decentralized approach), the self-healing agent appears as a local controller.

Firstly, the MGs coupling conditions are developed. Then, the conditions under which interconnected MGs need to be isolated are defined. Small signal stability (SSS) analysis is also carried out in this section for the CMGs [122, 117]. The results of this analysis are utilized as a decision-making criterion for interconnecting neighbouring MGs. Alternatively, if instability is observed, the

SSS analysis needs to define a range of droop control coefficients for the DERs to enable the interconnection.

The system of an isolated MG with the developed self-healing strategy offers more resilience and flexibility of operation when experiencing overloading and power deficiency conditions. It is expected that, by the help of the developed criteria and coupling the MGs, all or a portion of the required demand of an MG is imported from a neighbouring MG, leading to a reduced/minimized necessity and rate of load-shedding.

3.1 The network under consideration

Consider the network of Fig. 3.1 consisting two MGs, namely MG-1 and MG-2. MG-1 has N_1 DERs (i.e. DER₁₁, DER₁₂, ..., DER_{1N₁}), while MG-2 has N_2 DERs (i.e. DER₂₁, DER₂₂, ..., DER_{2N₂}). In both MGs, all DERs are assumed to be converter-interfaced. In normal conditions, each MG operates in islanded mode and the voltage magnitude and frequency at the output of each DER is regulated by droop control as in (2.16).

Interconnection of the MGs can be realized via back-to-back power converters that can control the active power flow [45, 97, 123], as shown in Fig. 3.2a. However, the disadvantage of applying such a scheme is that the converters introduce additional losses in the system arising due to the conduction and switching losses of the semiconductor valves [124, 125]. It is to be noted that the switching losses in back-to-back converters are present even during a zero power flow condition, since the DC voltage across the DC capacitor connecting these two converters needs to be sustained.

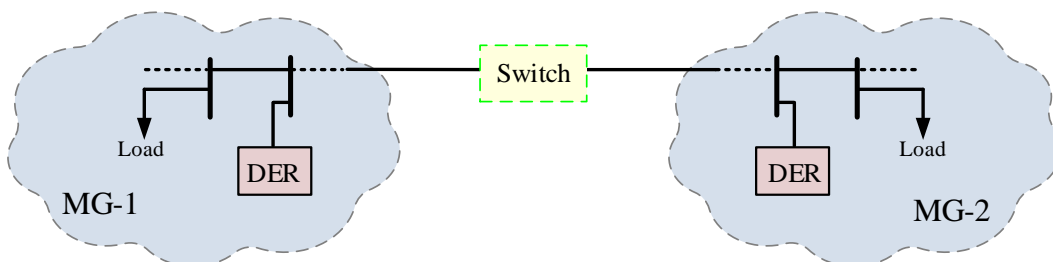


Fig. 3.1: Single line diagram of the network of two isolated MGs with an interconnecting line.

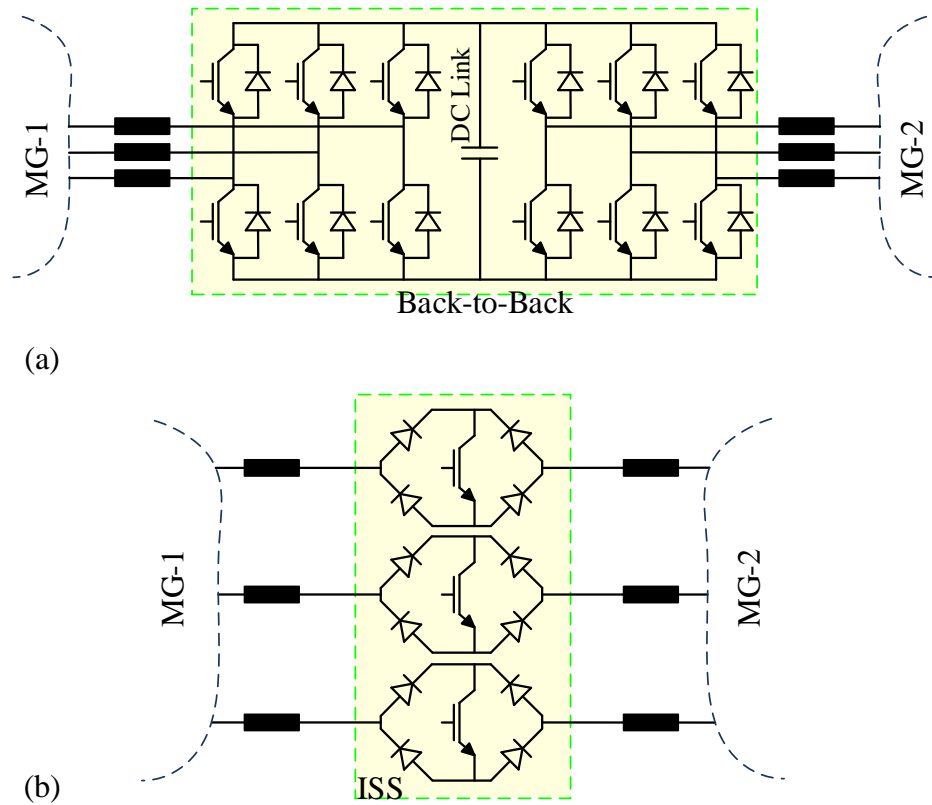


Fig. 3.2 The schematic of the MG interconnecting devices: (a) a back-to-back converter and (b) the adopted structure for the ISS.

Alternatively, a CMG can be formed by closing a normally-open ISS mounted on the tie-line between the MGs. The ISS is a bidirectional switch that facilitates power flow towards an overloaded MG. The schematic of the adopted structure is shown in Fig. 3.2b. This bidirectional device is formed by embedding an IGBT in a diode bridge. Once the IGBT is turned on, i.e., the ISS closes, the supporting power can flow in either direction in accordance with the droop coefficients of the DGs of the MGs. After closing, the ISS maintains this status as long as the coupling is required. Once the controller decides that the interconnection is not required anymore, it sends an OFF command to the ISS to open. It is to be noted that the ISS closing consists of a synchronization process. Further explanations can be found in Appendix A.

A comparison between the ISS and B2B converters utilized for coupling the MGs is presented in Table 3.1.

Table 3.1. Comparison between the ISS and B2B converters used for coupling the MGs.

| | B2B converter | ISS |
|----------------------|---|---|
| Advantages | <ul style="list-style-type: none"> 1- Provides bidirectional power flow control. 2- Provides frequency and voltage isolation between the MGs. 3- Controls the load sharing between the interconnected MGs. | <ul style="list-style-type: none"> 1- Has a simple structure. 2- Almost zero switching losses 3- Requires less number of active switches 4- Its control mechanism is straightforward. |
| Disadvantages | <ul style="list-style-type: none"> 1- Introduces high switching and conduction losses to the system. 2- Imposes switching losses even during a zero power flow condition. 3- Requires higher number of active switches. 4- Its control mechanism is not simple and includes various stages. | <ul style="list-style-type: none"> 1- Has no control on load sharing between the interconnected MGs. 2- The ISS is not able to isolate the MGs' frequencies. |

3.2 The centralized self-healing strategy

In normal conditions, the DERs in each MG operate based on the droop equations of (2.16) independently. Now, let us assume a scenario in which one of MGs in Fig. 3.1 is overloaded (i.e., its power generation is less than its current demand), while another neighbouring MG has surplus power (i.e., its power generation capacity is higher than its current demand). To provide a self-healing capability, the ISS between these MGs should interconnect them so that the DERs in the second MG can share a portion of the load of the first MG to mitigate its overloading. In this regard, the overloaded MG should be first detected and then, any interconnection after which the CMG may suffer from power deficiency should be avoided. This can be achieved under a centralized approach, which is discussed in this section. The conditions and constraints required for the interconnection are explicitly defined. Once the interconnection condition and constraint are satisfied, a command is sent by the self-healing agent to the ISS to close. After synchronization is achieved, the ISS closes and a CMG is formed. It is to be noted that, the self-healing agent discussed and developed in this section is an entity that is responsible for detecting the system conditions and providing the on/off command to the ISS. The network tertiary controller that accommodates the developed self-healing agent communicates with the secondary

controllers in each MG, as can be seen from Fig. 3.3. The operation flowchart of the self-healing strategy is shown in Fig. 3.4 and is discussed in detail below.

3.2.1. Interconnection of the MGs

Consider the network of Fig. 3.3 where MG-1 is overloaded while MG-2 has surplus power. Let the unused power capacity (UPC) in MG- i (ΔS_{MG-i}) for $i \in \{1,2\}$ be

$$\Delta S_{MG-i} = S_{MG-i}^{\text{cap}} - |S_{MG-i}| = \sum_{j=1}^{N_i} S_{\text{DER-}ij}^{\text{cap}} - \left| \sum_{j=1}^{N_i} S_{\text{DER-}ij} \right| \quad (3.1)$$

where S_{MG-i}^{cap} and $|S_{MG-i}|$ are respectively the sum of the maximum capacities and the sum of the apparent powers of all the DERs in MG- i . After the interconnection, the total load of the CMG will be shared by all DERs based on their droop ratios as already discussed in Section 2. 4.

It is desired to interconnect these MGs if UPC in MG-1 falls below a threshold such as $\alpha_1 S_{MG-1}^{\text{cap}}$ where $0 < \alpha_1 < 1$ (e.g., $\alpha_1 = 0.1$). Hence, the MGs are coupled if

$$\Delta S_{MG-1} < \alpha_1 S_{MG-1}^{\text{cap}} \quad (3.2)$$

However, the interconnection should be avoided if it causes MG-2 to fall below power deficiency boundary. Therefore, (3.2) is subject to satisfying a minimum level for UPC of MG-2, as the interconnection constraint. In this regard, the UPC of CMG should fulfil the pre-specified criterion of

$$S_{\text{CMG}}^{\text{cap}} - |S_{MG-1} + S_{MG-2}| > \alpha_1 (S_{MG-1}^{\text{cap}} + S_{MG-2}^{\text{cap}}) \quad (3.3)$$

From complex number rules, we can write

$$|S_{MG-1} + S_{MG-2}| \leq |S_{MG-1}| + |S_{MG-2}| \quad (3.4)$$

Considering (3.4), (3.3) is definitely satisfied if (3.5) is true.

$$S_{\text{CMG}}^{\text{cap}} - (|S_{MG-1}| + |S_{MG-2}|) > \alpha_1 (S_{MG-1}^{\text{cap}} + S_{MG-2}^{\text{cap}}) \quad (3.5)$$

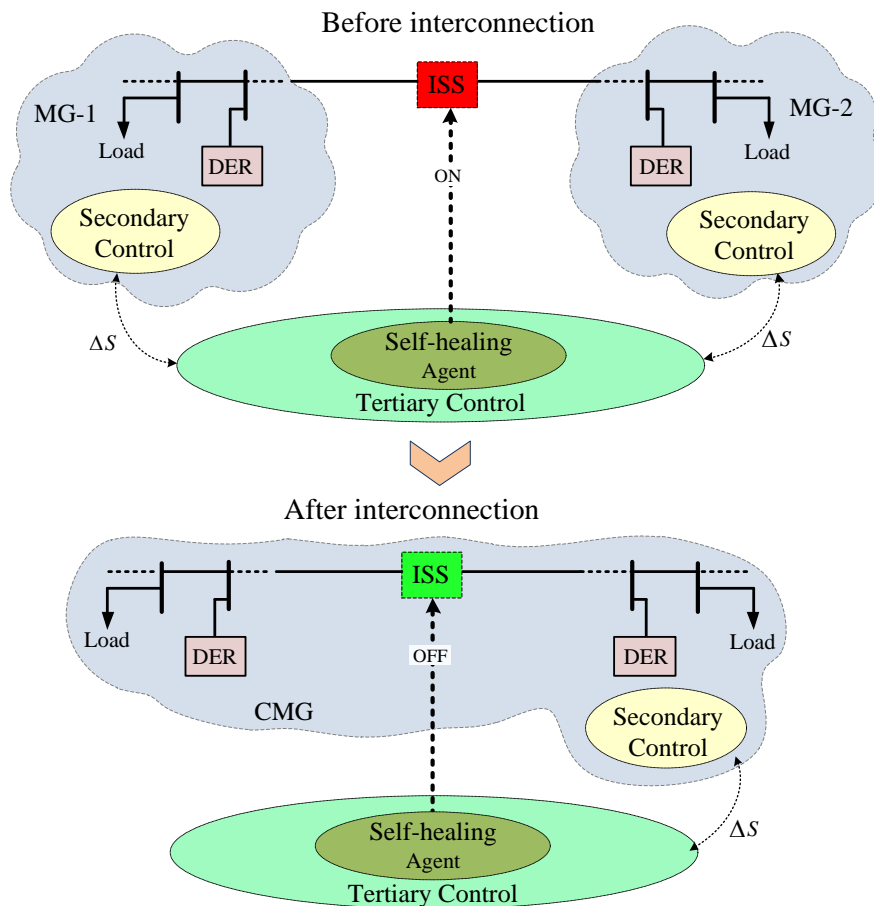


Fig. 3.3: The centralized self-healing agent for interconnecting two neighbouring MGs.

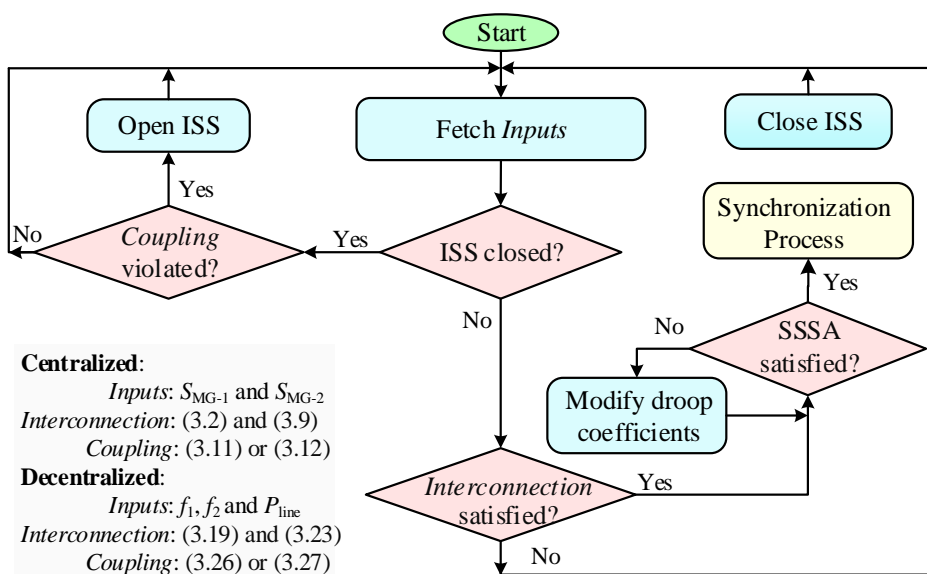


Fig. 3.4: Operation flowchart for the developed self-healing strategy.

Equation (3.5) is rewritten as

$$\Delta S_{MG-1} + \Delta S_{MG-2} > \alpha_1 S_{MG-1}^{\text{cap}} + \alpha_1 S_{MG-2}^{\text{cap}} \quad (3.6)$$

The above equation yields

$$\Delta S_{MG-2} > -\alpha_1 \psi S_{MG-1}^{\text{cap}} + \alpha_1 S_{MG-1}^{\text{cap}} + \alpha_1 S_{MG-2}^{\text{cap}} \quad (3.7)$$

where $0 < \psi < 1$ is derived as

$$\psi = \Delta S_{MG-1} / (\alpha_1 S_{MG-1}^{\text{cap}}) \quad (3.8)$$

Thus, UPC of MG-2 is considered as the interconnection constraint in the form of

$$\Delta S_{MG-2} > \alpha_1 [(1 - \psi) S_{MG-1}^{\text{cap}} + S_{MG-2}^{\text{cap}}] \quad (3.9)$$

Once condition (3.2) and constraint (3.9) are satisfied, the network tertiary controller sends a command to the ISS to close.

3.2.2. Isolation of the interconnected MGs

When a CMG is formed, an apparent power of $S_{\text{Tie-line}}$ flows from MG-2 to MG-1. In this condition, the ISS should open to isolate these MGs if

$$S_{MG-1}^{\text{cap}} - \left| \sum_{j=1}^{N_1} S_{\text{DER-1}j} + S_{\text{Tie-line}} \right| > \alpha_1 (1 + \beta_1) S_{MG-1}^{\text{cap}} \quad (3.10)$$

Interconnection is maintained as long as $S_{\text{Tie-line}}$ is above a threshold. This threshold can be defined from (3.10) considering the inequality (3.4) as

$$\left| S_{\text{Tie-line}} \right| > [1 - \alpha_1 (1 + \beta_1)] S_{MG-1}^{\text{cap}} - \left| \sum_{j=1}^{N_1} S_{\text{DER-1}j} \right| \quad (3.11)$$

In addition, the ISS should remain closed as far as the UPC of CMG satisfies, as per

$$\Delta S_{\text{CMG}} > \alpha_1 (1 - \beta_2) S_{\text{CMG}}^{\text{cap}} \quad (3.12)$$

Once either of (3.11) or (3.12) is violated, the ISS opens to divide the CMG into two isolated MGs. Note that the dead band boundaries of β_1 and β_2 are applied to

prevent chattering of the ISS where $0 < \beta_2 < 1$ and $0 < \beta_1 < \min((1/\alpha_1 - 1), 1)$ where $\min(\cdot)$ is the minimum function.

3.3 The decentralized self-healing strategy

The centralized approach needs the instantaneous apparent power of the DERs in both MGs for interconnection/isolation decision making. If a data communication system does exist or is temporarily unavailable, a decentralized approach is invoked. For this, the self-healing agent is located within the local controller of the ISS and measures the frequency in both sides of the ISS to distinguish and help the overloaded MG.

Note that the centralized approach considers the apparent power (both active and reactive powers) of the DERs whereas the decentralized approach uses the frequency (and thus the active power only) for interconnection decision making and does not consider the voltage (and thus the reactive power).

3.3.1 Interconnection of the MGs

Let us consider the network of Fig. 3.5 where MG-1 is overloaded while MG-2 has surplus power. It is desired to interconnect these MGs if the unused active power capacity (UAPC) in MG-1 is less than a threshold defined as α_2 times of the total maximum active power capacity of all the DERs of that MG,

P_{MG-1}^{cap} , given by

$$P_{MG-1}^{cap} - \sum_{j=1}^{N_1} P_{DER-1,j} < \alpha_2 P_{MG-1}^{cap} \quad (3.13)$$

Since all DERs have the same $\Delta f = f_{max} - f_{min}$, from (2.16) it can be concluded that (3.13) is satisfied if the UAPC of each DER of MG-1 is less than α_2 times of the maximum capacity of that DER, which is expressed as

$$P_{DER-1,j}^{cap} - P_{DER-1,j} < \alpha_2 P_{DER-1,j}^{cap} \quad (3.14)$$

Hence, the interconnection criterion can be simplified to

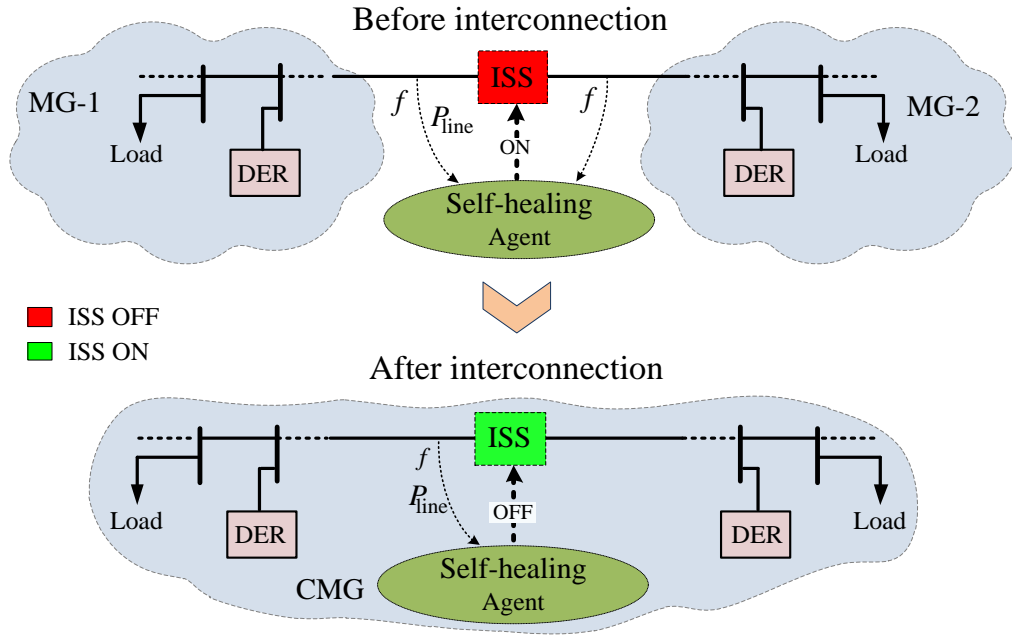


Fig. 3.5: The decentralized self-healing agent for interconnecting two neighbouring MGs.

$$P_{\text{DER-1}j} > (1 - \alpha_2) P_{\text{DER-1}j}^{\text{cap}} \quad (3.15)$$

Thereby, the necessity of interconnecting MGs can be concluded by only looking into the loading of one of the DERs instead of all the DERs in the MG.

From droop equation (2.16), the frequency of DER-1j is

$$f = f_{\text{max}} - m_{\text{DER-1}j} P_{\text{DER-1}j} \quad (3.16)$$

Applying (3.15) in (3.16), the frequency of this DER should be

$$f < f_{\text{max}} - m_{\text{DER-1}j} (1 - \alpha_2) P_{\text{DER-1}j}^{\text{cap}} \quad (3.17)$$

Replacing (2.17) in (3.17) yields

$$f < f_{\text{max}} - \frac{f_{\text{max}} - f_{\text{min}}}{P_{\text{DER-1}j}^{\text{cap}}} (1 - \alpha_2) P_{\text{DER-1}j}^{\text{cap}} \quad (3.18)$$

Hence, MG-1 overloading is determined if the frequency measured at MG-1 side of the ISS ($f_{\text{MG-1}}$) satisfies

$$f_{\text{MG-1}} < f_{\text{min}} + \alpha_2 (f_{\text{max}} - f_{\text{min}}) \quad (3.19)$$

An interconnection constraint is defined to avoid CMG from overloading. After interconnection, thus, it is desired to have

$$\sum_{i=1}^2 P_{MG-i}^{\text{cap}} - \sum_{i=1}^2 \sum_{j=1}^{N_i} P_{\text{DER-}ij} > \alpha_2 \sum_{i=1}^2 P_{MG-i}^{\text{cap}} \quad (3.20)$$

Applying (3.16) in (3.20) yields

$$\sum_{i=1}^2 P_{MG-i}^{\text{cap}} - \sum_{i=1}^2 \sum_{j=1}^{N_i} (f_{\text{max}} - f_{MG-i})/m_{ij} > \alpha_2 \sum_{i=1}^2 P_{MG-i}^{\text{cap}} \quad (3.21)$$

which can be rewritten as

$$(1 - \alpha_2) \sum_{i=1}^2 P_{MG-i}^{\text{cap}} - \sum_{j=1}^{N_1} (f_{\text{max}} - f_{MG-1})/m_{1j} > \sum_{j=1}^{N_2} (f_{\text{max}} - f_{MG-2})/m_{2j} \quad (3.22)$$

Considering the fact that $(f_{\text{max}} - f_{MG-1})$ is same for all DERs in MG-1 and $(f_{\text{max}} - f_{MG-2})$ is same for all DERs in MG-2, (3.22) can be simplified as

$$f_{MG-2} > f_{\text{max}} - \frac{(1 - \alpha_2) \sum_{i=1}^2 P_{MG-i}^{\text{cap}} - (f_{\text{max}} - f_{MG-1}) \sum_{j=1}^{N_1} 1/m_{1j}}{\sum_{j=1}^{N_2} 1/m_{2j}} \quad (3.23)$$

which is used as the interconnection constraint. Thus, the MGs will be interconnected if both (3.19) and (3.23) are satisfied.

3.3.2 Isolation of the interconnected MGs

Once the MGs are interconnected, the CMG will operate at a new frequency of f_{CMG} and an average active power of $P_{\text{Tie-line}}$ will flow from MG-2 to MG-1. In this condition, the power consumption of MG-1 (P_{MG1}) is

$$P_{MG1} = \sum_{j=1}^{N_1} P_{\text{DER-}1j} + P_{\text{Tie-line}} \quad (3.24)$$

The CMG is divided into two isolated MGs if $P_{\text{Tie-line}}$ drops below a threshold. Therefore, replacing (3.24) in (3.13) for the CMG yields

$$P_{MG1}^{\text{cap}} - \left(\sum_{j=1}^{N_1} (f_{\text{max}} - f_{\text{CMG}})/m_{1j} + P_{\text{Tie-line}} \right) < \alpha_2 (1 + \beta_3) P_{MG1}^{\text{cap}} \quad (3.25)$$

which can be rewritten as

$$P_{\text{Tie-line}} > [1 - \alpha_2 (1 + \beta_3)] P_{MG1}^{\text{cap}} - (f_{\text{max}} - f_{\text{CMG}}) \sum_{j=1}^{N_1} 1/m_{1j} \quad (3.26)$$

Equation (3.26) defines the threshold for P_{line} . It is to be noted that this threshold is not fixed and depends on f_{CMG} .

The ISS should also not open as far as f_{CMG} is above a threshold. Using (3.19), this threshold is defined as

$$f_{\text{CMG}} > f_{\text{min}} + \alpha_2(1 - \beta_4)(f_{\text{max}} - f_{\text{min}}) \quad (3.27)$$

Once either of (3.26) or (3.27) is violated, the CMG is divided into two isolated MGs. It is to be noted that they both include a dead-band boundary of β_3 and β_4 where $0 < \beta_4 < 1$ and $0 < \beta_3 < \min((1/\alpha_2 - 1), 1)$ to prevent chattering of the ISS. It is to be noted that $f_{\text{MG-1}}$, $f_{\text{MG-2}}$ and P_{line} are the only measurements used in these two equations.

3.4 Discussion on the Self-Healing Parameters

The proposed methods are general enough to be applied for any MG/CMG system. Actually, their performance does not depend on the MG, CMG and DER parameters. However, the performance can be affected by the selected (assumed) values of the self-healing parameters α_1 , β_1 , β_2 , α_2 , β_3 and β_4 that are used in MGs interconnection/isolation conditions and constraints. These parameters define the UPC and chattering thresholds (margins) within the proposed method and can be used (set) by the network tertiary controller to achieve the desired operating points in the system. The proposed method will operate successfully as far as the values of these parameters are within their defined maximum and minimum boundaries.

As an example, for variables β_1 and β_2 , used in (3.11)-(3.12), it can be mentioned that

- smaller values of β_1 may cause chattering problems, while its larger values will result in the change of the UPC margin of MG-1; hence the owner of MG-1 will be disadvantaged by paying more for some imported power from MG-2, which is undesirable.
- smaller values of β_2 may cause chattering problems while its larger values can jeopardize the supply security of MG-2 even when its local load is not considerable.

From (3.11)-(3.12), the UPC thresholds of an isolated MG and the CMG are shown as a function of α_1 , β_1 and β_2 parameters in Fig. 3.6. The same discussions are also valid for the parameters used in the decentralized method. An optimization technique can be utilized to define the optimal set-points for these parameters, which has not been addressed in this thesis.

3.5 Required Time for MGs Interconnection

Before the MGs interconnection, each MG may have a different voltage and frequency. Hence, a synchronization process is required prior to the interconnection. Synchronization becomes active when the self-healing agent

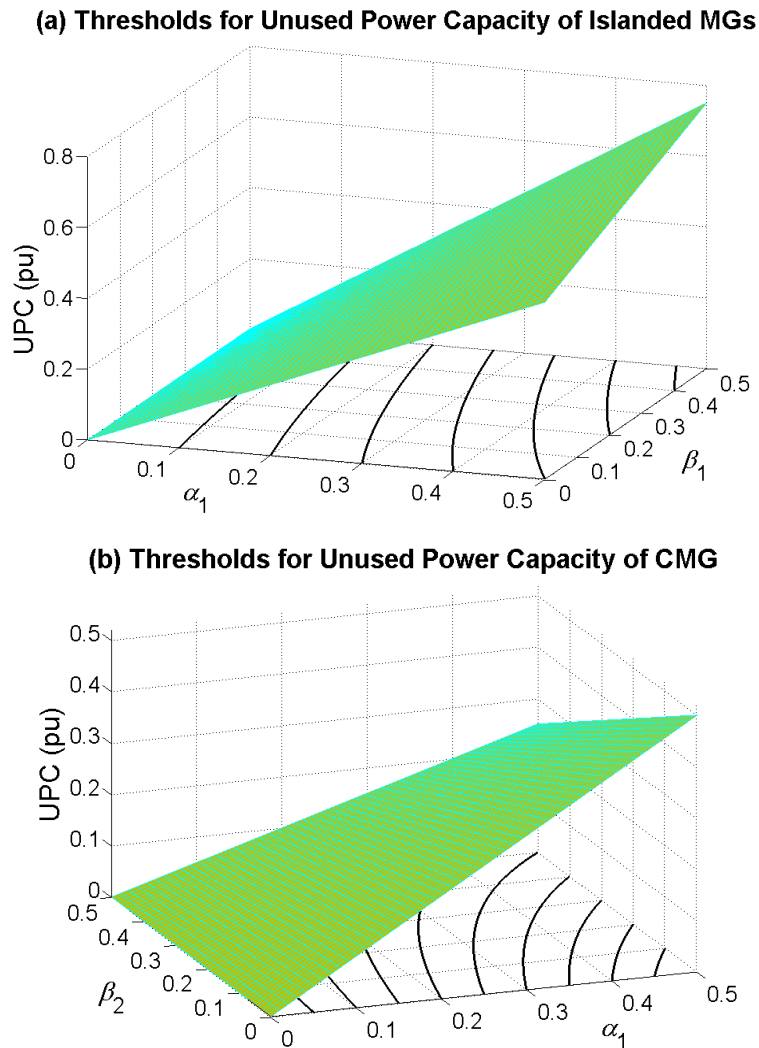


Fig. 3.6: UPC margins of (a) isolated MGs, (b) CMG depending on the variations of the self-healing parameters.

sends a command to the ISS. The ISS closes once the difference of voltage angles and the difference of voltage magnitudes on both sides of the ISS are lower than predefined very small values of ε_δ and ε_v [126]. This prevents significant distortions in the voltage, current and power waveforms in the MGs.

The utilized synchronization technique is discussed in details in Appendix A. The required time for the interconnection of two MGs under such a scheme can be expressed as a function of voltage angle difference across ISS ($\Delta\theta$) and frequency difference of two MGs (Δf) at the initiation time of the self-healing command.

As an example, for a given system, the required interconnection time is shown as a function of $\Delta\theta$ for $0.25 \leq \Delta f \leq 1$ Hz in Fig. 3.7a. It can be seen that for each Δf , the interconnection time increases linearly as $\Delta\theta$ increases. Fig. 3.7b shows the required interconnection time as a function of Δf for $\pi/6 \leq \Delta\theta \leq \pi$. It shows that for each $\Delta\theta$, the required time increases as Δf decreases. Fig. 3.7c illustrates the 4-quadrant plot of time versus Δf and $\Delta\theta$. This is further discussed in Appendix A.

3.6 Reduced load-shedding level

As discussed before, it is expected that by the help of the developed criteria and coupling the MGs, all or a portion of the required demand of an MG is imported from the neighbouring MG, leading to a reduced/minimized necessity and rate of load-shedding.

3.6.1. Under the centralized approach

Let us consider the network of Fig. 3.3 which shows the coupling of two neighbouring MGs under the centralized approach. If the MGs are isolated, assuming that MG-1 is overloaded, the required load-shedding level from MG-1, S_{MG-1}^{shed} , can be expressed from (3.2) as

$$S_{MG-1}^{shed} = |S_{MG-1}| - (1 - \alpha_1) S_{MG-1}^{cap} \quad (3.28)$$

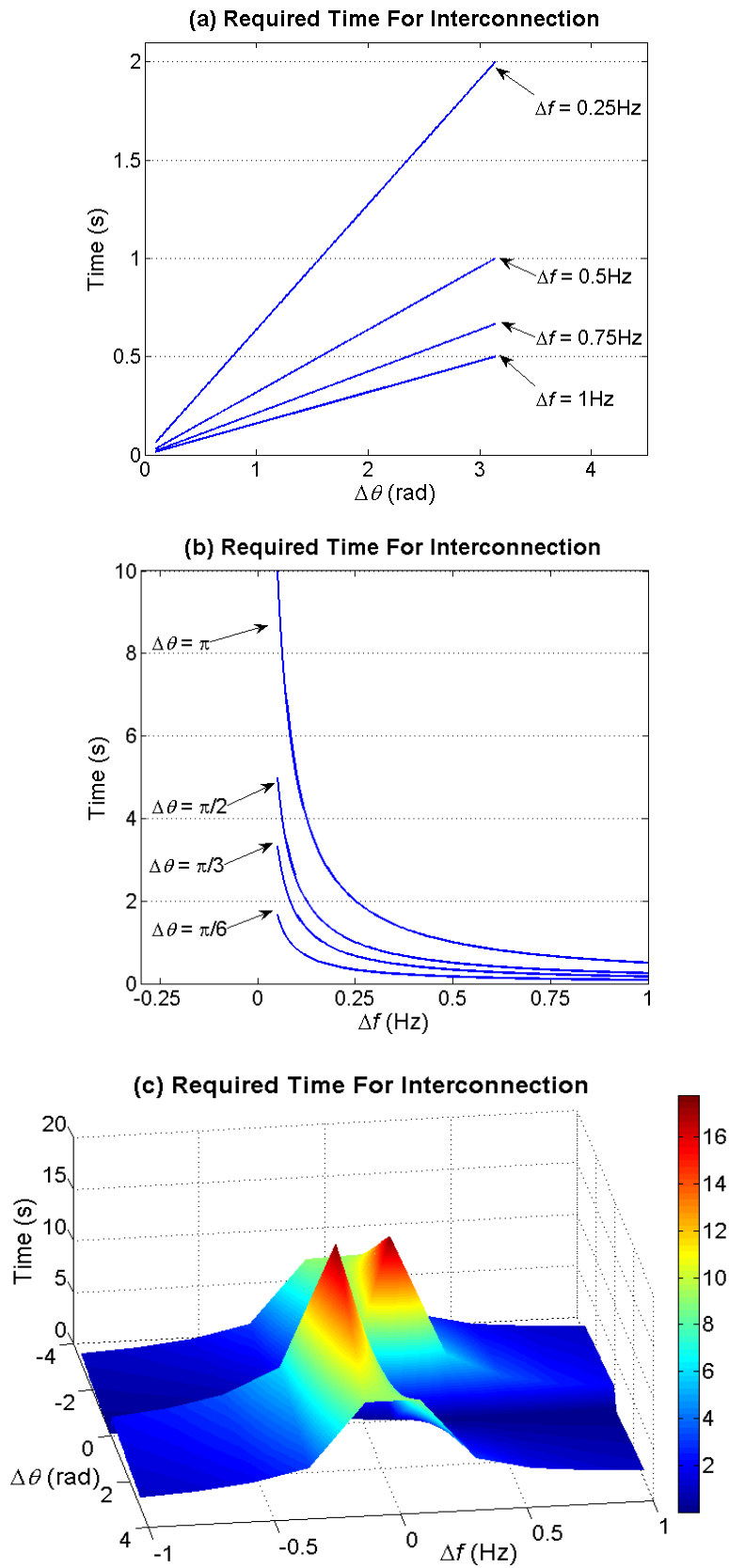


Fig. 3.7: Required time for interconnection of MGs for different $\Delta\theta$ and Δf .

However, if the MGs are interconnected and a CMG is formed, the load-shedding level is not only a function of the instantaneous power and capacity of the DERs of MG-1 but also depends on the instantaneous power and capacity of the DERs in MG-2. Thus, for a CMG, S_{MG-1}^{shed} can be defined from (3.5) as

$$S_{MG-1}^{shed} = \sum_{i=1}^2 |S_{MG-i}| - (1 - \alpha_1) \sum_{i=1}^2 S_{MG-i}^{cap} \quad (3.29)$$

Considering the self-healing parameters provided in Table 3.2, Fig. 3.8 illustrates the required load-shedding level for MG-1 when operating in islanded mode and when interconnected to MG-2 under the centralized approach. For example, Fig. 3.8a shows that when the loading of MG-1 is 110% (i.e., 1.1 pu), 20% (i.e., 0.2 pu) of the load of MG-1 needs to be shed. However, Fig. 3.8b shows that under such a condition if a CMG is formed, no load-shedding is required as far as MG-2 is loaded by 70% before the interconnection, where 70% is the maximum loading of MG-2 for zero load-shedding (ML_{ZLS}^{MG-2}) in the neighbouring MG. This figure also shows that MG-1 load needs to be shed by 5% and 10% if MG-2 is loaded by 75% and 80%, respectively.

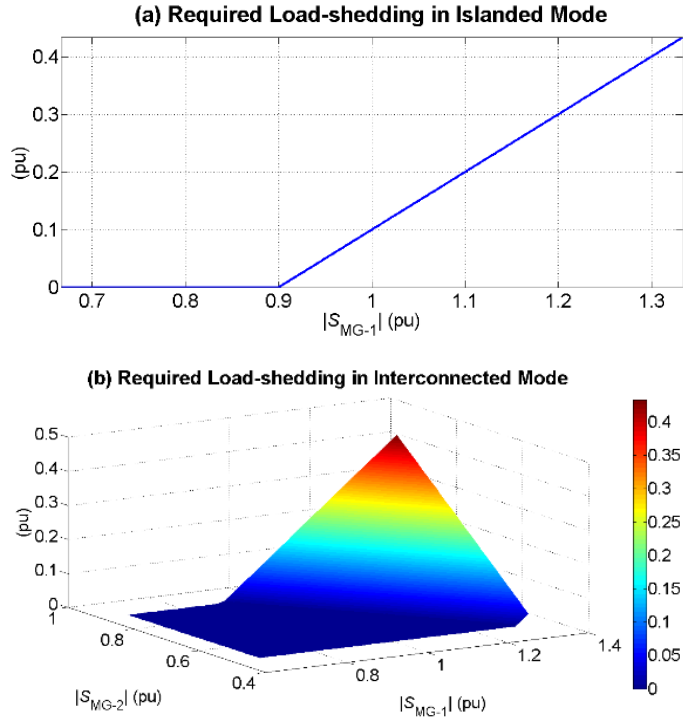


Fig. 3.8: Required load-shedding level for MG-1 in: (a) islanded mode, (b) interconnected mode under the centralized approach.

3.6.2. Under the decentralized approach

Now, let us consider the network of Fig. 3.5 which shows the coupling of two neighbouring MGs under the decentralized approach. If the MGs are isolated, assuming that MG-1 is overloaded, the required load-shedding level from MG-1, P_{MG-1}^{shed} , can be expressed from (3.19) as

$$P_{MG-1}^{shed} = \sum_{j=1}^{N_1} (f_{max} - f_{MG-1}) / m_{1j} - (1 - \alpha_2) P_{MG-1}^{cap} \quad (3.30)$$

while if a CMG is formed, P_{MG-1}^{shed} can be defined from (3.21) as

$$P_{MG-1}^{shed} = \sum_{i=1}^2 \sum_{j=1}^{N_i} (f_{max} - f_{MG-i}) / m_{ij} - (1 - \alpha_2) \sum_{i=1}^2 P_{MG-i}^{cap} \quad (3.31)$$

Considering the self-healing parameters provided in Table 3.2, Fig. 3.9 illustrates P_{MG-1}^{shed} when MG-1 is operating in islanded mode and when interconnected to MG-2 under the decentralized approach. For example, Fig. 3.9a

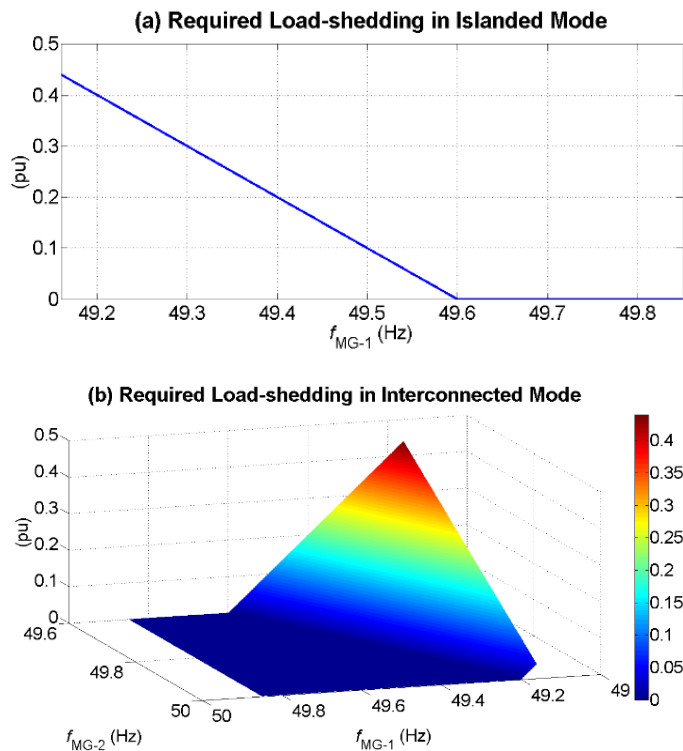


Fig. 3.9: Required load-shedding level for MG-1 in: (a) islanded mode, (b) interconnected mode under the decentralized approach.

shows if the frequency of MG-1 drops to 49.4Hz, 20% (i.e., 0.2 pu) of the load of MG-1 needs to be shed. However, Fig. 3.9b shows that under such a condition if a CMG is formed, no load-shedding is required as far as the frequency of MG-2 is above 49.8Hz before the interconnection, where 49.8Hz is the minimum frequency of MG-2 for zero load-shedding (mF_{ZLS}^{MG-2}) in the neighbouring MG. This figure also shows that MG-1 needs to be shed by 5% and 10% if the frequency of MG-2 drops to 49.75Hz and 49.7Hz, respectively.

3.7 Small signal stability analysis of CMG

SSS analysis is required to assess the stability of the CMG before the interconnection to prevent any instability problems. The results of this analysis are used as a decision-making criterion for interconnection (see Fig. 3.4). If SSS analysis demonstrates the CMG instability, droop control parameters need to be updated accordingly to enable interconnection. This is beyond the scope of this research and is not addressed here.

3.7.1. Model derivation

Consider an MG consisting of N_c converter-interfaced DERs, N_d loads, N_e lines and N_b buses. Let us assume that switching of the DERs is controlled through applying the state feedback technique explained in Section 2.6.2. Thus, the state-space description of the i^{th} DER, with the converter and filter structure of Fig. 2.6, is represented in direct-quadrature domain as [45, 117, 122]

$$\Delta \dot{x}_{\text{conv}}^i = A_i \Delta x_{\text{conv}}^i + B_i \Delta u_{\text{conv}}^i + C_i \Delta v_{\text{conv}}^i \quad (3.32)$$

as expanded in

$$\begin{aligned}
\Delta \begin{bmatrix} i_{fd} \\ i_{fq} \\ i_{Td} \\ i_{Tq} \\ v_{cd} \\ v_{cq} \end{bmatrix} &= \begin{bmatrix} -R_f/L_f & \omega & 0 & 0 & -1/L_f & 0 \\ -\omega & -R_f/L_f & 0 & 0 & 0 & -1/L_f \\ 0 & 0 & 0 & \omega & 1/L_T & 0 \\ 0 & 0 & -\omega & 0 & 0 & 1/L_T \\ 1/C_f & 0 & -1/C_f & 0 & 0 & \omega \\ 0 & 1/C_f & 0 & -1/C_f & -\omega & 0 \end{bmatrix} \Delta \begin{bmatrix} i_{fd} \\ i_{fq} \\ i_{Td} \\ i_{Tq} \\ v_{cd} \\ v_{cq} \end{bmatrix} \\
&+ \frac{aV_{dc}}{L_f} \begin{bmatrix} 1 & 0 \\ 0 & 1 \\ 0 & 0 \\ 0 & 0 \\ 0 & 0 \\ 0 & 0 \end{bmatrix} \Delta \begin{bmatrix} u_d \\ u_q \end{bmatrix} - \frac{1}{L_T} \begin{bmatrix} 0 & 0 \\ 0 & 0 \\ 1 & 0 \\ 0 & 1 \\ 0 & 0 \\ 0 & 0 \end{bmatrix} \Delta \begin{bmatrix} v_{Td} \\ v_{Tq} \end{bmatrix}_{\text{conv}}
\end{aligned} \tag{3.33}$$

It is to be noted that, assuming a perfect tracking, u can be represented by u_c .

Hence, considering a state-feedback control in the form of

$$\Delta u_{\text{conv}}^i = -K_i [\Delta z_{\text{conv}}^i - (\Delta z_{\text{conv}}^i)^{\text{ref}}] = G_i \Delta x_{\text{conv}}^i + H_i (\Delta z_{\text{conv}}^i)^{\text{ref}} \tag{3.34}$$

where

$$G_i = \begin{bmatrix} -k_1 & 0 & k_1 - k_2 & 0 & -k_3 & 0 \\ 0 & -k_1 & 0 & k_1 - k_2 & 0 & -k_3 \end{bmatrix}$$

$$H_i = \begin{bmatrix} k_1 & 0 & k_2 & 0 & k_3 & 0 \\ 0 & k_1 & 0 & k_2 & 0 & k_3 \end{bmatrix}$$

and $\Delta z_{\text{conv}} = \Delta [i_{Td} \ i_{Tq} \ i_{cd} \ i_{cq} \ v_{cd} \ v_{cq}]^T$, the state-space equation of converter- i becomes

$$\Delta \dot{x}_{\text{conv}}^i = A_{\text{conv}}^i \Delta x_{\text{conv}}^i + B_{\text{conv}}^i (\Delta z_{\text{conv}}^i)^{\text{ref}} + C_{\text{conv}}^i \Delta v_{\text{conv}}^i \tag{3.35}$$

where $A_{\text{conv}}^i = A_i + B_i G_i$ and $B_{\text{conv}}^i = B_i H_i$.

The state-space equation of load- j connected to bus- jj and line- k between adjacent buses kk and ll in the MG can be represented in direct-quadrature frame as

$$\begin{aligned}
\Delta \dot{x}_{\text{load}}^j &= A_{\text{load}}^j \Delta x_{\text{load}}^j + C_{\text{load}}^j \Delta v_{\text{load}}^{jj} \\
\Delta \dot{x}_{\text{line}}^k &= A_{\text{line}}^k \Delta x_{\text{line}}^k + C_{\text{line}}^k \Delta v_{\text{MG}}
\end{aligned} \tag{3.36}$$

This is expanded as

$$\begin{aligned}
\Delta \begin{bmatrix} i_d \\ i_q \end{bmatrix}_{\text{load}} &= \begin{bmatrix} -\frac{R_{\text{load}}}{L_{\text{load}}} & \omega \\ \omega & -\frac{R_{\text{load}}}{L_{\text{load}}} \end{bmatrix} \Delta \begin{bmatrix} i_d \\ i_q \end{bmatrix}_{\text{load}} + \frac{1}{L_{\text{load}}} \begin{bmatrix} 1 & 0 \\ 0 & 1 \end{bmatrix} \Delta \begin{bmatrix} v_{Td} \\ v_{Tq} \end{bmatrix}_{\text{load}} \\
\Delta \begin{bmatrix} i_d \\ i_q \end{bmatrix}_{\text{line}} &= \begin{bmatrix} -\frac{R_{\text{line}}}{L_{\text{line}}} & \omega \\ \omega & -\frac{R_{\text{line}}}{L_{\text{line}}} \end{bmatrix} \Delta \begin{bmatrix} i_d \\ i_q \end{bmatrix}_{\text{line}} + \frac{1}{L_{\text{line}}} \begin{bmatrix} 0 & 0 & \dots & 1 & 0 & \dots & -1 & 0 & \dots & 0 & 0 \\ 0 & 0 & \dots & 0 & 1 & \dots & 0 & -1 & \dots & 0 & 0 \end{bmatrix} \\
&\quad \times \Delta \begin{bmatrix} v_{Td}^1 & v_{Tq}^1 & \dots & v_{Td}^{kk} & v_{Tq}^{kk} & \dots & v_{Td}^{ll} & v_{Tq}^{ll} & \dots & v_{Td}^{N_b} & v_{Tq}^{N_b} \end{bmatrix}^T
\end{aligned} \tag{3.37}$$

Hence, the equivalent state-space equation of the MG is

$$\Delta \dot{x}_{\text{MG}} = A_{\text{MG}} \Delta x_{\text{MG}} + B_{\text{MG}} (\Delta z_{\text{MG}})^{\text{ref}} + C_{\text{MG}} \Delta v_{\text{MG}} \tag{3.38}$$

where

$$\begin{aligned}
x_{\text{MG}} &= [x_{\text{conv}}^1 \dots x_{\text{conv}}^{N_c} \ x_{\text{load}}^1 \dots x_{\text{load}}^{N_d} \ x_{\text{line}}^1 \dots x_{\text{line}}^{N_e}]^T \\
z_{\text{MG}} &= [z_{\text{conv}}^1 \dots z_{\text{conv}}^{N_c}]^T \\
A_{\text{MG}} &= \text{diag}(A_{\text{conv}}^1 \dots A_{\text{conv}}^{N_c} \ A_{\text{load}}^1 \dots A_{\text{load}}^{N_d} \ A_{\text{line}}^1 \dots A_{\text{line}}^{N_e}) \\
B_{\text{MG}} &= \text{diag}(B_{\text{conv}}^1 \dots B_{\text{conv}}^{N_c} \ \overbrace{O_2 \dots O_2}^{N_d+N_e}) \\
C_{\text{MG}} &= \begin{bmatrix} \text{diag}(C_{\text{conv}}^1 \dots C_{\text{conv}}^{N_c} \ C_{\text{load}}^1 \dots C_{\text{load}}^{N_d}) \\ C_{\text{line}}^1 \\ \vdots \\ C_{\text{line}}^{N_e} \end{bmatrix}
\end{aligned}$$

while O_2 is a zeros matrix of order 2 and $\text{diag}(\cdot)$ is a diagonal matrix.

On the other hand, the instantaneous output active/reactive power of each converter and filter in direct-quadrature frame is expressed based on its output voltage and current as

$$\begin{bmatrix} p \\ q \end{bmatrix} = \frac{3}{2} \begin{bmatrix} i_{2d} & i_{2q} \\ -i_{2q} & i_{2d} \end{bmatrix} \begin{bmatrix} v_{cd} \\ v_{cq} \end{bmatrix} \tag{3.39}$$

The average active/reactive powers can then be calculated by passing the instantaneous values through a low pass filter with a cut-off frequency of ω_c and a Laplace domain transfer function of $\omega_c/(s+\omega_c)$. In addition, assuming a frequency droop, the angle of the capacitor voltage at the output of each converter can be

calculated from the angular frequency of the converter ($\omega = 2\pi f$) with respect to a common angular frequency ω_{com} (i.e., the angular frequency of one of the converters, e.g., $\omega_{\text{com}} = \omega$) as [127]

$$\delta = \int (\omega - \omega_{\text{com}}) dt \quad (3.40)$$

It is to be noted that all parameters are expressed in the common direct-quadrature reference frame.

Linearizing (3.39)-(3.40) around the operating point for each converter yields

$$\Delta \dot{x}_{\text{PQ}\delta}^i = A_{\text{PQ}\delta}^i \Delta x_{\text{PQ}\delta}^i + B_{\text{PQ}\delta}^i \Delta x_{\text{conv}}^i + M_m^i \Delta P_{\text{com}} \quad (3.41)$$

i.e.,

$$\begin{aligned} \Delta \begin{bmatrix} P \\ Q \\ \delta \end{bmatrix} &= \begin{bmatrix} -\omega_c & 0 & 0 \\ 0 & -\omega_c & 0 \\ -m & 0 & 0 \end{bmatrix} \Delta \begin{bmatrix} P \\ Q \\ \delta \end{bmatrix} \\ &+ \begin{bmatrix} 0 & 0 & v_{cd0} & v_{cq0} & i_{Td0} & i_{Tq0} \\ 0 & 0 & v_{cq0} & -v_{cd0} & -i_{Tq0} & i_{Td0} \\ 0 & 0 & 0 & 0 & 0 & 0 \end{bmatrix} \Delta \begin{bmatrix} i_{fd} \\ i_{fq} \\ i_{Td} \\ i_{Tq} \\ v_{cd} \\ v_{cq} \end{bmatrix} + [0 \quad 0 \quad m_{\text{com}}]^T \Delta P_{\text{com}} \end{aligned} \quad (3.42)$$

Hence, for an MG with N_c converter-interfaced DERs, the total equivalent state-space equation representing the power and voltage angles in the MG is

$$\Delta \dot{x}_{\text{PQ}\delta}^{\text{MG}} = A_{\text{PQ}\delta}^{\text{MG}} \Delta x_{\text{PQ}\delta}^{\text{MG}} + B_{\text{PQ}\delta}^{\text{MG}} \Delta x_{\text{MG}} \quad (3.43)$$

where

$$\begin{aligned} x_{\text{PQ}\delta}^{\text{MG}} &= [x_{\text{PQ}\delta}^1 \dots x_{\text{PQ}\delta}^{N_c}]^T \\ A_{\text{PQ}\delta}^{\text{MG}} &= A'_{\text{PQ}\delta}{}^{\text{MG}} + M_m \\ A'_{\text{PQ}\delta}{}^{\text{MG}} &= \text{diag}(A_{\text{PQ}\delta}^1 \dots A_{\text{PQ}\delta}^{N_c}) \\ B_{\text{PQ}\delta}^{\text{MG}} &= \text{diag}(B_{\text{PQ}\delta}^1 \dots B_{\text{PQ}\delta}^{N_c} \overbrace{O_2 \dots O_2}^{N_d + N_e}) \end{aligned}$$

and M_m is a matrix with the same size of $A'_{\text{PQ}\delta}{}^{\text{MG}}$ in which the column corresponding

to the active power of the reference converter is equal to $[M_m^1 \dots M_m^{N_c}]^T$ while all other elements are zero. For converter- i , $(\Delta z_{\text{conv}}^i)^{\text{ref}}$ can be expressed as a function of $\Delta x_{\text{PQ}\delta}^i$ at the operating point as

$$(\Delta z_{\text{conv}}^i)^{\text{ref}} = M_c^i \Delta x_{\text{PQ}\delta}^i \quad (3.44)$$

where

$$M_c^i = -\frac{2}{3V_{\text{cmo}}^2} \begin{bmatrix} \gamma_{11} & \gamma_{12} & \gamma_{13} \\ \gamma_{21} & \gamma_{22} & \gamma_{23} \\ 0 & \beta_1 \cos \delta_o & \beta_2 \sin \delta_o \\ 0 & \beta_1 \sin \delta_o & \beta_2 \cos \delta_o \\ 0 & -n \sin \delta_o & V_{\text{cmo}} \cos \delta_o \\ 0 & n \sin \delta_o & V_{\text{cmo}} \sin \delta_o \end{bmatrix}$$

in which

$$\begin{aligned} \gamma_{11} &= -V_{\text{cmo}} \sin \delta_o, & \gamma_{12} &= V_{\text{cmo}} \cos \delta_o + n(Q_o \cos \delta_o - P_o \sin \delta_o) \\ \gamma_{21} &= V_{\text{cmo}} \cos \delta_o, & \gamma_{13} &= -V_{\text{cmo}}(Q_o \sin \delta_o + P_o \cos \delta_o) \\ \beta_1 &= -C_f n \omega, & \gamma_{22} &= V_{\text{cmo}} \sin \delta_o + n(Q_o \sin \delta_o + P_o \cos \delta_o) \\ \beta_2 &= -C_f V_{\text{cmo}}, & \gamma_{23} &= V_{\text{cmo}}(Q_o \cos \delta_o - P_o \sin \delta_o) \end{aligned}$$

Thus, $(\Delta z_{\text{MG}})^{\text{ref}}$ can be written as a function of $\Delta x_{\text{PQ}\delta}^{\text{MG}}$ as

$$(\Delta z_{\text{MG}})^{\text{ref}} = M_c \cdot \Delta x_{\text{PQ}\delta}^{\text{MG}} \quad (3.45)$$

Where $M_c = \text{diag}(M_c^1 \dots M_c^{N_c})$. In the above relations, the subscript 0 denotes the operating point values for each state.

For one MG, combining (3.38), (3.43) and (3.45) yields

$$\Delta \dot{x}_{\text{MG}}^{\text{Final}} = A_{\text{MG}}^{\text{Final}} \Delta x_{\text{MG}}^{\text{Final}} + C_{\text{MG}}^{\text{Final}} \Delta v_{\text{MG}} \quad (3.46)$$

which can be expanded as

$$\Delta \begin{bmatrix} x_{\text{MG}}^{\text{MG}} \\ x_{\text{PQ}\delta}^{\text{MG}} \end{bmatrix}^{\bullet} = \begin{bmatrix} A_{\text{MG}}^{\text{MG}} & B_{\text{MG}} M_c \\ B_{\text{PQ}\delta}^{\text{MG}} & A_{\text{PQ}\delta}^{\text{MG}} \end{bmatrix} \cdot \Delta \begin{bmatrix} x_{\text{MG}}^{\text{MG}} \\ x_{\text{PQ}\delta}^{\text{MG}} \end{bmatrix} + \begin{bmatrix} C_{\text{MG}} \\ O_{3N_c \times 2N_b} \end{bmatrix} \cdot \Delta v_{\text{MG}} \quad (3.47)$$

For a CMG composed of two MGs that are interconnected through a tie-line,

the linearized state-space equation can be expressed as

$$\Delta \dot{x}_{\text{CMG}} = A_{\text{CMG}} \Delta x_{\text{CMG}} + C_{\text{CMG}} \Delta v_{\text{CMG}} \quad (3.48)$$

as expanded in

$$\Delta \begin{bmatrix} x_{\text{MG-1}}^{\text{Final}} \\ x_{\text{MG-2}}^{\text{Final}} \\ x_{\text{Tie-line}} \end{bmatrix} = \begin{bmatrix} A_{\text{MG-1}}^{\text{Final}} & O & O \\ O & A_{\text{MG-2}}^{\text{Final}} & O \\ O & O & A_{\text{Tie-line}} \end{bmatrix} \cdot \Delta \begin{bmatrix} x_{\text{MG-1}}^{\text{Final}} \\ x_{\text{MG-2}}^{\text{Final}} \\ x_{\text{Tie-line}} \end{bmatrix} + \begin{bmatrix} C_{\text{MG-1}}^{\text{Final}} & O \\ O & C_{\text{MG-2}}^{\text{Final}} \\ C_{\text{Tie-line}} \end{bmatrix} \cdot \Delta \begin{bmatrix} v_{\text{MG-1}} \\ v_{\text{MG-2}} \end{bmatrix} \quad (3.49)$$

Assuming a large virtual resistor (e.g., $R_v = 10^4$) between each bus and ground, voltage of bus- j can be written as

$$v^j = R_v (i_2^j + \sum \mu^k i_{\text{line}}^k - i_{\text{load}}^j) \quad (3.50)$$

where $\mu^k = +1$ and -1 respectively represent the entering and exiting lines to bus j . Thus, Δv^j can be represented as a function of Δx_{CMG} as

$$\Delta v^j = M_v^j \Delta x_{\text{CMG}} \quad (3.51)$$

Hence, the voltage of all buses in CMG is expressed as

$$\Delta v_{\text{CMG}} = M_v \Delta x_{\text{CMG}} \quad (3.52)$$

where $M_v = (M_v^1 \dots M_v^{N_{\text{b, MG-1}} + N_{\text{b, MG-2}}})^T$. Assuming $A_{\text{CMG}}^{\text{H}} = A_{\text{CMG}} + C_{\text{CMG}} M_v$,

(3.48) is expressed in the homogeneous form of

$$\Delta \dot{x}_{\text{CMG}} = A_{\text{CMG}}^{\text{H}} \Delta x_{\text{CMG}} \quad (3.53)$$

3.7.2. Modal analysis

Modes (eigenvalues) of CMG (λ) are defined as roots of

$$\left| \lambda I - A_{\text{CMG}}^{\text{H}} \right| = 0 \quad (3.54)$$

where I is the identity matrix. The closest modes to the imaginary axis in s-plane are the dominant modes. Any change in the rated capacities and droop coefficients of DERs, as well as the load and line parameters, may result in CMG instability. Hence, their effect should be carefully investigated on the dominant modes

The contribution of each of the states of x_{CMG} on each mode of CMG is calculated from [128]

$$PF = (\Gamma^{-1})^T \otimes \Gamma \quad (3.55)$$

where Γ is the matrix of right eigenvectors of A_{CMG}^h , \otimes indicates the element by element production and PF is the participation factor matrix where $PF(u,w)$ represents the contribution of state u on mode w . By normalizing PF for each mode from

$$\|pf(u, w)\| = |pf(u, w)| / \sum_{\mu} |pf(\mu, w)| \quad (3.56)$$

the normalized weightings of each effective state on each mode are extracted.

The damping ratio of the modes illustrates how the oscillations decay in the system and is calculated as [129]

$$\zeta = \frac{1}{\sqrt{1 + (\kappa/\sigma)^2}} \quad (3.57)$$

where $\lambda = \sigma + j\kappa$. The undamped natural frequency of the modes is calculated from

$$\omega_n = -\sigma/\zeta \quad (3.58)$$

while the period of each mode is

$$T = \frac{2\pi}{\omega_n \sqrt{1 - \zeta^2}} \quad (3.59)$$

and the number of cycles for a mode to damp by 50% is

$$NoC_{50\%} = \ln 2 \frac{\sqrt{1 - \zeta^2}}{2\pi\zeta} \quad (3.60)$$

3.8 Performance evaluation

Performance of the developed strategies is investigated in this section in terms of their impacts on both dynamic response and stability of the system. The network of Fig. 3.1 is considered where each MG has 2 converter-interfaced DERs. Considering the fact that the performance of the strategies does not depend on the internal parameters of the DERs but on the selected self-healing parameters (as discussed in Section 3.4), all DERs are assumed to have the same internal parameters and power capacities of the DERs are assumed to be constant throughout the studies.

Single-line diagram of DERs along with their controllers is shown in Fig. 3.10. Also, technical parameters of the simulation cases are provided in Table 3.2. It is to be noted that Chapter 3 is developed based on the results that are already published in [121]. This paper reports the outcomes of our preliminary work on a small scale isolated MG. Although 6kVA can be considered as a small value for the base power of a regular MG, this value is not modified here in order to maintain the consistency between the already published materials and the content of this thesis. It is to be noted that the developed strategy is not sensitive to the power rating of MGs.

Table 3.2: Parameters of MGs, Self-healing agent and VSCs of DERs.

| |
|---|
| MG network parameters: $V_{\text{base}} = 230 \text{ V}$, $f_{\text{nominal}} = 50 \text{ Hz}$, $S_{\text{base}} = 6 \text{ kVA}$, $Z_{\text{line}} = 0.1 + j 0.1 \Omega$ |
| CMG network parameters: $Z_{\text{tie-line}} = 0.2 + j 0.2$ |
| Self-healing parameters: $\alpha_1 = \alpha_2 = 0.1$, $\beta_1 = \beta_2 = \beta_3 = \beta_4 = 0.2$, $V_{\text{max}} = 230 \text{ V}$, $V_{\text{min}} = 210 \text{ V}$, $f_{\text{max}} = 50.5 \text{ Hz}$, $f_{\text{min}} = 49.5 \text{ Hz}$ |
| VSC Structure and control parameters: $V_{\text{dc}} = 350 \text{ V}$, $a = 2$, $R_f = 0.1 \Omega$, $L_f = 0.37 \text{ mH}$, $C_f = 50 \mu\text{F}$, $K = [6.1802 \ 2.2968 \ 22.968]$, $h = 10^{-4}$ |
| Droop parameters and coupling inductance of the DERs: $m = 0.33 \text{ Hz/kW}$, $n = 8 \text{ V/kVAr}$, $L_T = 27.2 \text{ mH}$ |

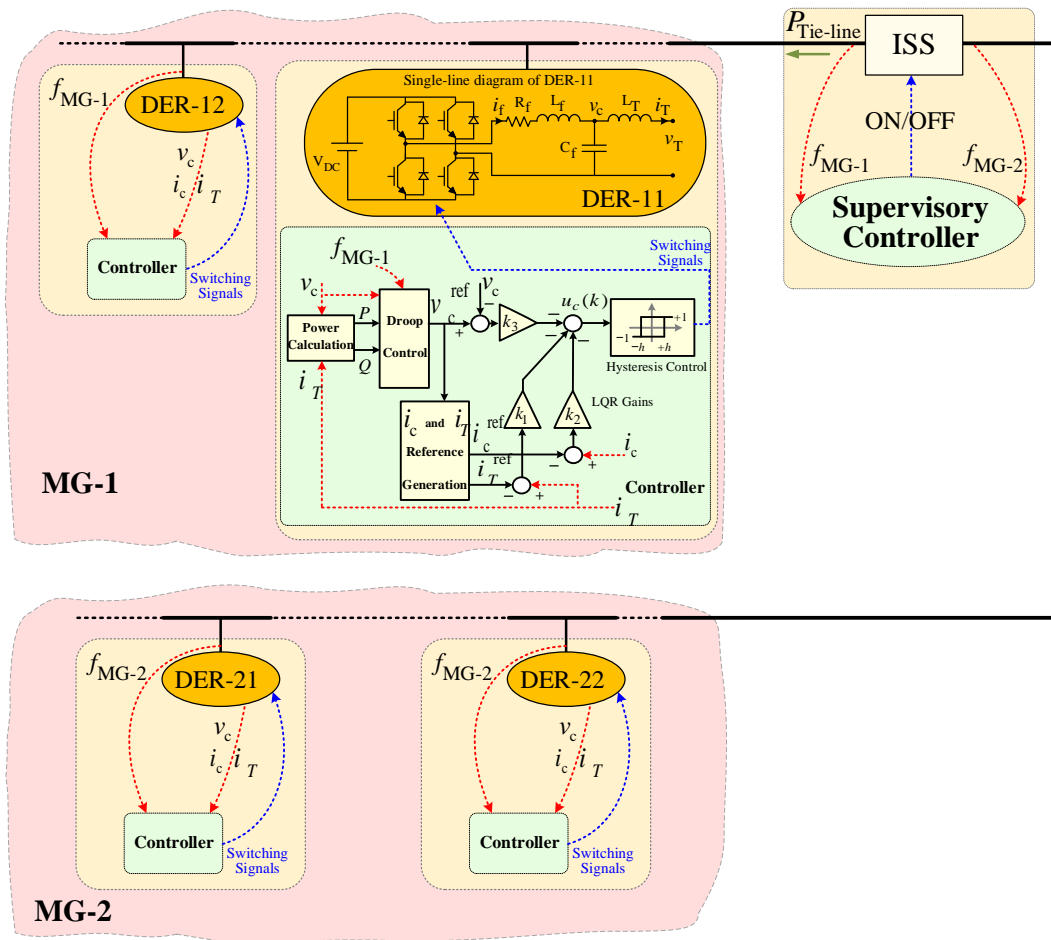


Fig. 3.10: Single-line diagram of the CMG including its DERs along with their controllers.

3.8.1. Dynamic response

To investigate the dynamic performance of the MGs with the proposed self-healing strategy, several simulation study cases are carried out in PSCAD. The developed self-healing agent is realized in FORTRAN language as an embedded self-created block in PSCAD. Alternatively, it can be developed in MATLAB and linked to PSCAD [59].

1) PERFORMANCE OF THE CENTRALIZED SCHEME

Three cases are considered for the self-healing agent operating under the centralized approach. For a simpler presentation, the events of each simulation case are listed in time sequence in Table 3.3. In each case, the load of MG-1 increases such that MG-1 becomes overloaded. The self-healing agent detects the

overloaded MG and then, initiates ISS activation command. After proper synchronization between the MGs, the ISS closes and a CMG is formed. Afterward, further loads changes are applied and the self-healing agent decides whether the CMG should be divided into two isolated MGs.

The dynamic simulation results for the three cases of the centralized approach are shown in Fig. 3.11 to Fig. 3.13. According to these results, the MGs controlled by the proposed strategy can successfully handle the overloading events following the algorithm designed for different scenarios.

It is to be noted that the load changes are applied by arbitrary values in order to verify insensitivity of the approaches to different conditions.

1) Case 1

Initially, the MGs are operating at steady state and the ISS is open. The simulation results are shown in Fig. 3.11. At $t = 1$ s, the output power of the DERs in MG-1 starts increasing due to an increase of about 83% in load demand of MG-1. Consequently, the interconnection condition (3.2) is satisfied at $t = 1.2$ s since UPC of MG-1 has dropped to a value below 0.1 (i.e., 0.03pu). This leads to the initiation of the ISS activation signal as the interconnection constraint (3.9) is satisfied as well. The coupling procedure begins by performing the synchronization. This is done at $t = 2.16$ s at which the CMG is formed by closing the ISS. As a result, MG-2 provides MG-1 with a supporting power of about 0.23pu. Accordingly, the UPC rises to 0.56pu and the shortfall is handled.

Following a 60% increase in MG-2 load at $t = 3.2$ s, all DERs of the MGs raise their power outputs to meet the new load. Although this causes the UPC of the CMG to drop to 0.3pu at $t = 3.5$ s, the interconnection is maintained since it does not violate (3.12). Likewise, the supporting power decreases to a value of about 0.11pu that can satisfy (3.11).

2) Case 2

Let us consider the isolated MGs of Fig. 3.10 operating at the steady state when UPC of MG-1 and MG-2 are 0.28pu and 0.18pu, respectively. Following a load increase of about 32% in MG-1 at $t = 1$ s, the DERs raise the power outputs to

meet the load. As a result, the UPC of MG-1 drops to 0.05pu at $t = 1.2$ s, satisfying the interconnection condition of (3.2). Since the interconnection constraint of (3.9) is satisfied as well, the synchronization process begins to form the CMG. The simulation results are demonstrated in Fig. 3.12. At $t = 1.75$, the CMG forming is accomplished by closing the ISS since the synchronization is achieved. Consequently, a supporting power of about 0.05pu flows towards MG-1 in order to cope with the deficiency successfully through increasing the UPC to 0.23pu.

At $t = 3.3$ s, the MG-1 load drops by 44%. Consequently, the interconnection is not required to be maintained anymore since the condition (3.11) is violated. Thus, the ISS opens at $t = 3.5$ s after which the MG-1 and MG-2 carry out their operation independently with UPC of 0.47pu and 0.18pu, respectively.

3) Case 3

Initially, the MGs are operating at steady state and the ISS is open. The simulation results are shown in Fig. 3.13. At $t = 1$ s, total load of MG-1 increases by 102%. Then, the UPC of MG-1 drops to 0.05pu at $t = 1.2$ s, satisfying the interconnection condition of (3.2). Consequently, the synchronization process is initiated since the interconnection constraint of (3.9) is met as well. The ISS closes when the voltage synchronization is achieved at $t = 2.95$ s. Then, MG-2 provides MG-1 with a supporting power of about 0.04pu, raising UPC of the system to 0.21pu.

Following a further load increase of about 5% in MG-1 at $t = 3.5$ s, the power output of the DERs increases to meet the total demand; however, this drops the UPC of CMG below the threshold of (3.12). Consequently, the ISS opens at $t = 3.6$ s in order to prevent the overloading condition in MG-2. In such a case, load-shedding in MG-1 is inevitable.

Table 3.3: Time sequence of the events in a network controlled with the centralized approach.

| t (s) | Event | Consequence | Numerical Values [pu] |
|---------|--|--|--|
| Case-1 | | | |
| 0 | The MGs are isolated and operating at steady-state. | | $\Delta S_{MG-1} = 0.47, \Delta S_{MG-2} = 0.53$ |
| 1 | MG-1 load increases by 83%. | S_{MG-1} increases to supply the load. | |
| 1.2 | Interconnection condition (3.2) and constraint (3.9) are satisfied | ISS activation command is initiated. | $\Delta S_{MG-1} = 0.03, \Delta S_{MG-2} = 0.53$ |
| 2.16 | Synchronization between the MGs is achieved. | ISS closes and a CMG is formed. | $\Delta S_{CMG} = 0.56, S_{Tie-line} = 0.23$ |
| 3.2 | MG-2 load increases by 60%. | S_{CMG} increases to supply the load. | |
| 3.5 | Conditions (3.11) and (3.12) are not violated. | No changes required. | $\Delta S_{CMG} = 0.30, S_{Tie-line} = 0.11$ |
| Case-2 | | | |
| 0 | The MGs are isolated and operating at steady-state. | | $\Delta S_{MG-1} = 0.28, \Delta S_{MG-2} = 0.18$ |
| 1 | MG-1 load increases by 32%. | S_{MG-1} increases to supply the load. | |
| 1.2 | Interconnection condition (3.2) and constraint (3.9) are satisfied | ISS activation command is initiated. | $\Delta S_{MG-1} = 0.05, \Delta S_{MG-2} = 0.18$ |
| 1.75 | Synchronization between the MGs is achieved. | ISS closes and a CMG is formed. | $\Delta S_{CMG} = 0.23, S_{Tie-line} = 0.05$ |
| 3.3 | MG-1 load reduces by 44%. | S_{CMG} decreases to supply the load. | |
| 3.5 | Condition (3.11) is violated. | ISS opens and CMG divides into 2 MGs. | $\Delta S_{MG-1} = 0.47, \Delta S_{MG-2} = 0.18$ |
| Case-3 | | | |
| 0 | The MGs are isolated and operating at steady-state. | | $\Delta S_{MG-1} = 0.54, \Delta S_{MG-2} = 0.15$ |
| 1 | MG-1 load increases by 102%. | S_{MG-1} increases to supply the load. | |
| 1.2 | Interconnection condition (3.2) and constraint (3.9) are satisfied | ISS activation command is initiated. | $\Delta S_{MG-1} = 0.05, \Delta S_{MG-2} = 0.15$ |
| 2.95 | Synchronization between the MGs is achieved. | ISS closes and a CMG is formed. | $\Delta S_{CMG} = 0.21, S_{Tie-line} = 0.04$ |
| 3.5 | MG-1 load increases by 5%. | S_{CMG} increases to supply the load. | |
| 3.6 | Condition (3.12) is violated. | ISS opens and CMG divides into 2 MGs. | $\Delta S_{MG-1} = 0.01, \Delta S_{MG-2} = 0.15$ |

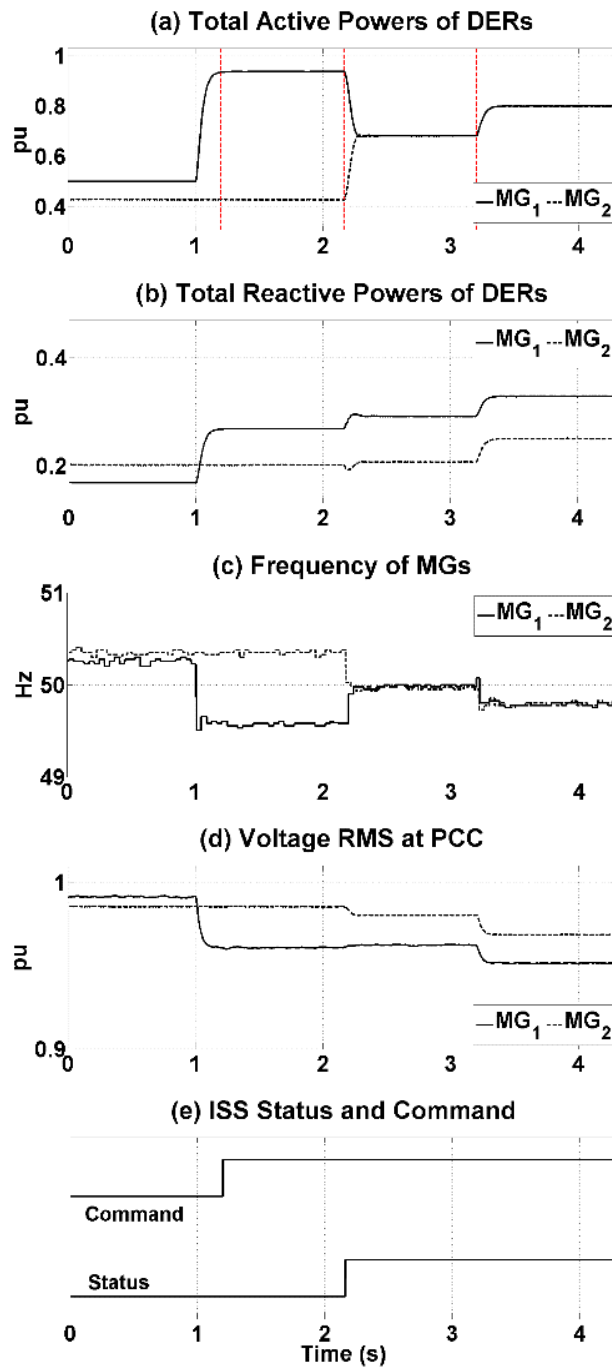


Fig. 3.11: Simulation results for the developed self-healing agent under the centralized approach: Case-1.

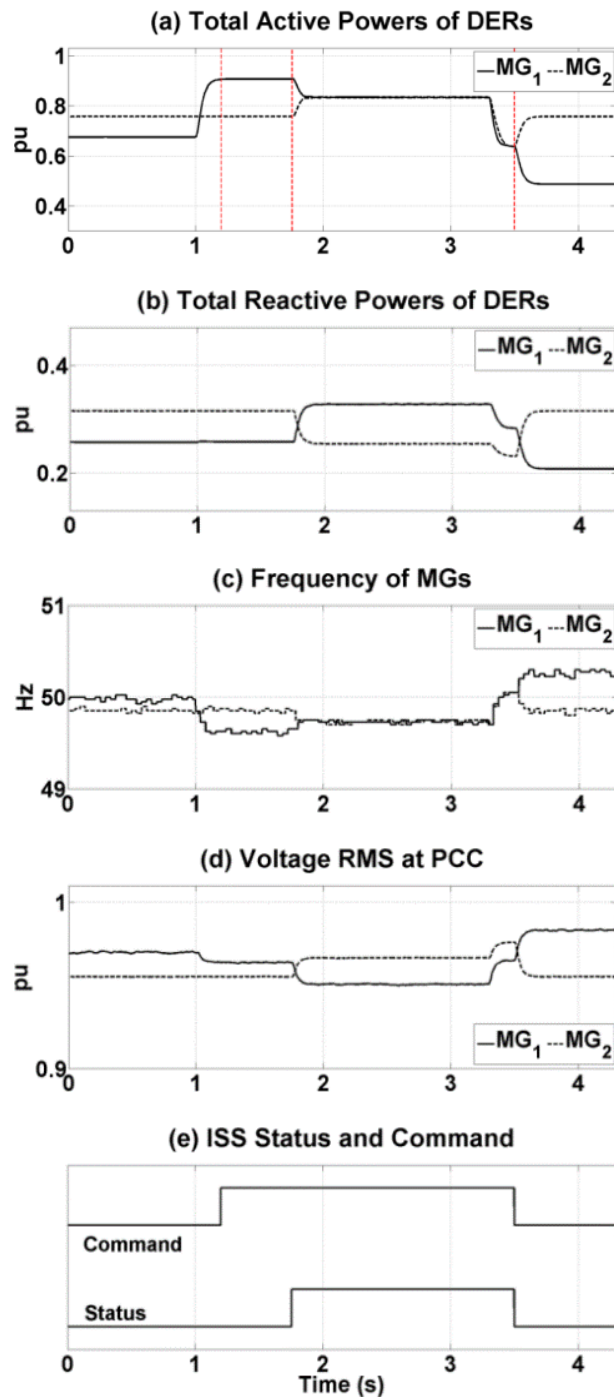


Fig. 3.12: Simulation results for the developed self-healing agent under the centralized approach: Case-2.

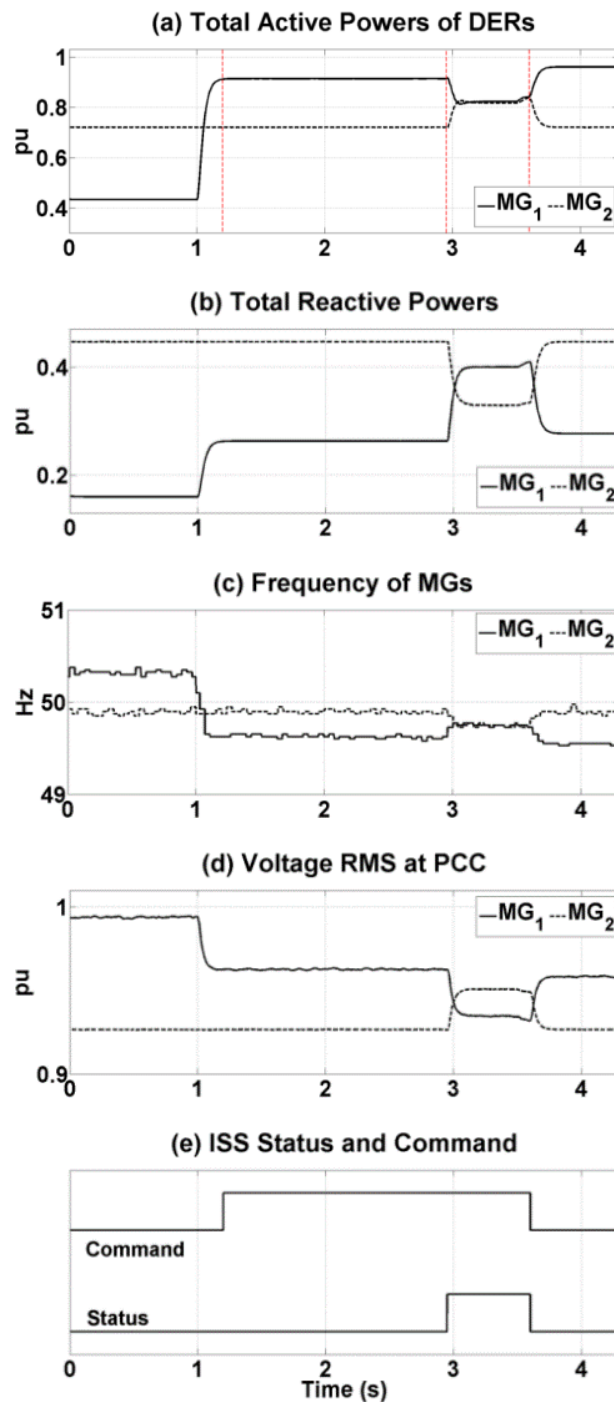


Fig. 3.13: Simulation results for the developed self-healing agent under the centralized approach: Case-3.

2) PERFORMANCE OF THE DECENTRALIZED SCHEME

Likewise, three cases are evaluated for the system operating under the decentralized approach. The events of each simulation case are listed in time sequence in Table 3.4. Similar to the previous cases, MG-1 loading increases in each case such that MG-1 becomes overloaded. The self-healing agent initiates ISS activation command after detecting the overloaded MG. Then, the ISS closes when the proper synchronization between the MGs is achieved in order to form the CMG. Following further loads changes applied in the MGs, the self-healing agent decides whether the interconnection should carry on or the CMG should be divided into two isolated MGs.

The dynamic simulation results for the three cases of the decentralized approach are shown in Fig. 3.14 to Fig. 3.16. The simulation outcomes prove that the proposed strategy can successfully handle the overloading events within the MGs under different scenarios.

1) Case 1

Let us consider the isolated MGs of Fig. 3.10. MG-1 and MG-2 are operating at steady state at a frequency of about 50.08Hz and 50.15Hz, respectively. At $t = 1s$, the DERs of MG-1 raise their power output to meet the demand due to a load increase of about 115%. This drops the frequency of MG-1 to 49.54Hz that satisfies the interconnection condition of (3.19). Consequently, the ISS activation command initiates the synchronization action at $t=1.2s$ since the interconnection constraint of (3.23) is satisfied as well. The CMG formation is done when the synchronization is accomplished at $t = 2.49s$. Then, MG-1 receives a supporting power of about 0.3pu from MG-2, alleviating the overloading condition by increasing the frequency to 49.86Hz. The simulation results are shown in Fig. 3.14.

MG-2 experiences a load increase by 40% at $t = 3.3s$. Although the frequency of the CMG and the tie-line power drop to respectively 49.78Hz and 0.3pu, none of the isolation conditions (i.e., (3.26) and (3.27)) are violated. Therefore, the interconnection is maintained.

2) Case 2

Initially, MG-1 and MG-2 are operating at the steady state and the frequencies are respectively 50.08Hz and 50.15Hz. Following a load increase of about 86% in MG-1 at $t = 1$ s, f_{MG-1} drops to 49.54Hz. Consequently, the synchronization action for forming the CMG is initiated at $t = 1.2$ s since both the interconnection condition and constraint (i.e., (3.19) and (3.23), respectively) are satisfied. The simulation results are shown in Fig. 3.14. After achieving the synchronization at $t = 2.39$ s, the ISS is closed to make the interconnection between the MGs. Then, MG-2 provides MG-1 with a supporting power of about 0.3pu, successfully raising the frequency of the MG to 49.85Hz.

At $t = 3.3$ s, total load of MG-1 reduces by 54%, thereby removing the overloading condition from MG-1. Consequently, the ISS is opened at $t = 3.5$ s to isolate the MGs since (3.26) is violated. From this point onwards, MG-1 and MG-2 operate independently at frequencies of 50.05Hz and 50.15Hz, respectively.

3) Case 3

Consider MG-1 and MG-2 of the network shown in Fig. 3.10 which are operating at steady state at a frequency of about 50Hz and 50.15Hz, respectively. The simulation results are shown in Fig. 3.16. At $t = 1$ s, the total load of MG-1 increases by 94%, dropping f_{MG-1} to 49.51Hz. Consequently, the synchronization is initiated at $t = 1.2$ s. Then, the CMG is formed at $t = 2.28$ s when the synchronization action is accomplished. Due to flowing a supporting power of about 0.31pu through the tie-line, the frequency of MG-1 is increased successfully to 49.82Hz.

At $t = 3.3$ s, total load of MG-2 increased by 150%. This resulted in dropping the frequency to a value below the threshold of (3.27). Consequently, the MGs are isolated at $t = 3.5$ s in order to in order to prevent the overloading condition in MG-2. In such a case, load-shedding in MG-1 is inevitable.

Table 3.4: Time sequence of the events in a network controlled with the decentralized approach.

| t (s) | Event | Consequence | Numerical Values: P [pu], f [Hz] |
|---------|---|--|---|
| Case-1 | | | |
| 0 | The MGs are isolated and operating at steady-state. | | $f_{MG-1} = 50.08$, $f_{MG-2} = 50.15$ |
| 1 | MG-1 load increases by 115%. | P_{MG-1} increases to supply the load. | |
| 1.2 | Interconnection condition (3.19) and constraint (3.23) are satisfied | ISS activation command is initiated. | $f_{MG-1} = 49.54$, $f_{MG-2} = 50.15$ |
| 2.49 | Synchronization between the MGs is achieved. | ISS closes and a CMG is formed. | $f_{CMG} = 49.86$, $P_{line} = 0.3$ |
| 3.3 | MG-2 load increases by 40%. | P_{CMG} increases to supply the load. | |
| 3.5 | Conditions (3.26) and (3.27) are not violated. | No changes required. | $f_{CMG} = 49.78$, $P_{line} = 0.2$ |
| Case-2 | | | |
| 0 | The MGs are isolated and operating at steady-state. | | $f_{MG-1} = 50.00$, $f_{MG-2} = 50.15$ |
| 1 | MG-1 load increases by 86%. | P_{MG-1} increases to supply the load. | |
| 1.2 | Interconnection condition (3.19) and constraint (3.23) are satisfied. | ISS activation command is initiated. | $f_{MG-1} = 49.54$, $f_{MG-2} = 50.15$ |
| 2.39 | Synchronization between the MGs is achieved. | ISS closes and a CMG is formed. | $f_{CMG} = 49.85$, $P_{line} = 0.3$ |
| 3.3 | MG-1 load reduces by 54%. | P_{CMG} decreases to supply the load. | |
| 3.5 | Condition (3.26) is violated. | ISS opens and CMG divides into 2 MGs. | $f_{MG-1} = 50.05$, $f_{MG-2} = 50.15$ |
| Case-3 | | | |
| 0 | The MGs are isolated and operating at steady-state. | | $f_{MG-1} = 50.00$, $f_{MG-2} = 50.15$ |
| 1 | MG-1 load increases by 94%. | P_{MG-1} increases to supply the load. | |
| 1.2 | Interconnection condition (3.19) and constraint (3.23) are satisfied | ISS activation command is initiated. | $f_{MG-1} = 49.51$, $f_{MG-2} = 50.15$ |
| 2.28 | Synchronization between the MGs is achieved. | ISS closes and a CMG is formed. | $f_{CMG} = 49.82$, $P_{line} = 0.31$ |
| 3.3 | MG-2 load increases by 150%. | P_{CMG} increases to supply the load. | |
| 3.5 | Condition (3.27) is violated. | ISS opens and CMG divides into 2 MGs. | $f_{MG-1} = 49.51$, $f_{MG-2} = 49.62$ |

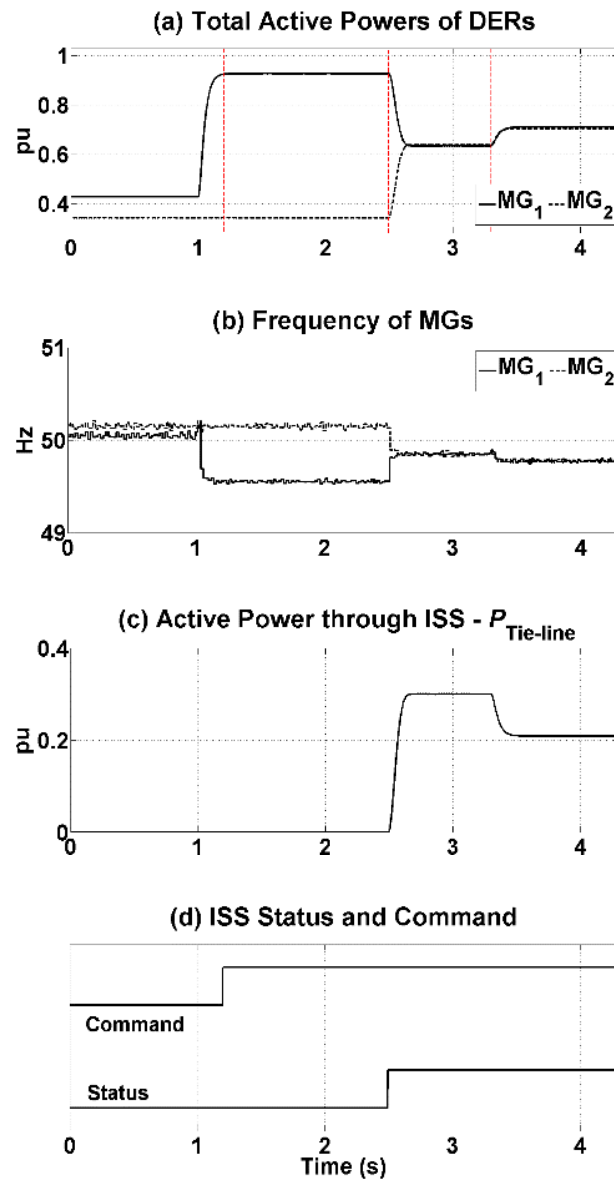


Fig. 3.14: Simulation results for the developed self-healing agent under the decentralized approach: Case-1.

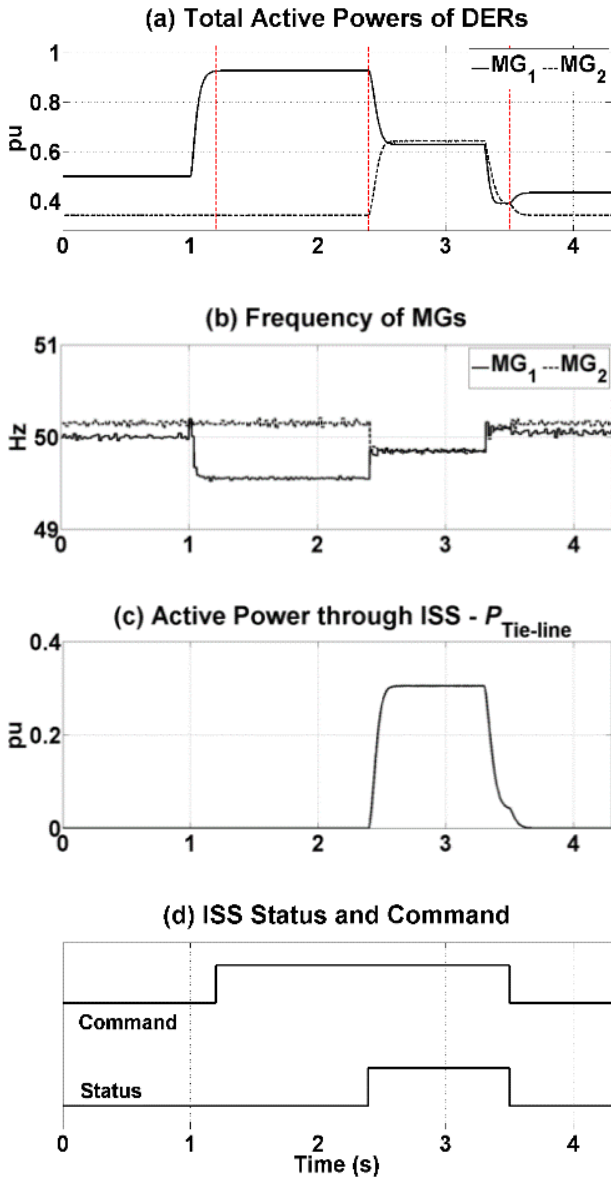


Fig. 3.15: Simulation results for the developed self-healing agent under the decentralized approach: Case-2.

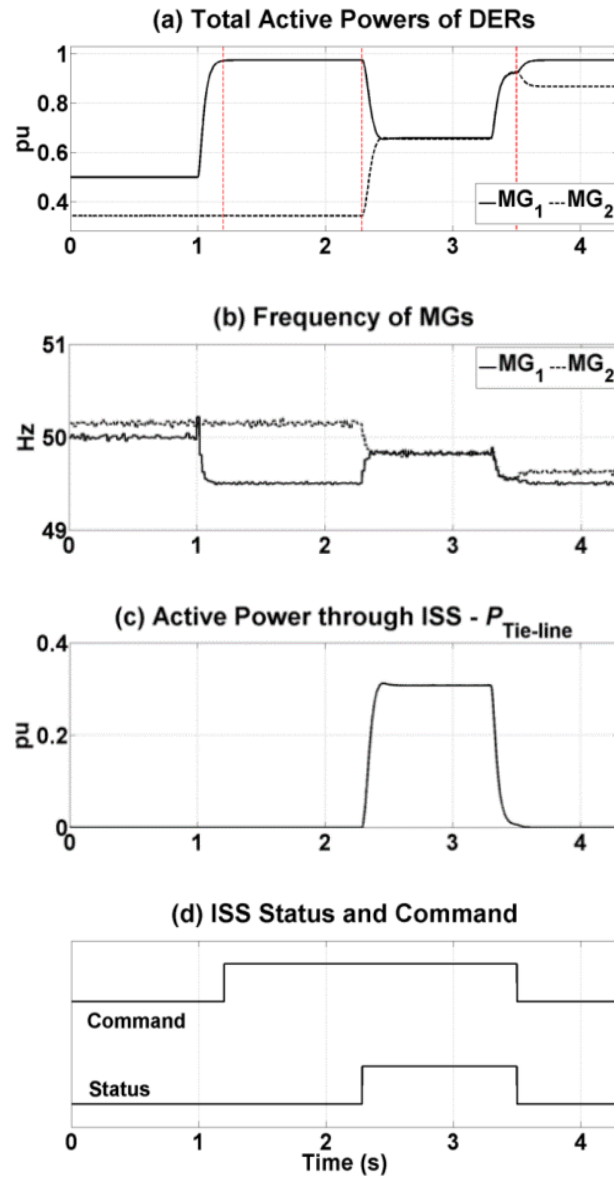


Fig. 3.16: Simulation results for the developed self-healing agent under the decentralized approach: Case-3.

3) REDUCTION IN THE LEVEL OF LOAD SHEDDING

Table 3.5 and Table 3.6 present the required load-shedding level in MG-1 in the considered cases, before and after applying the developed self-healing methods. Table 3.5 presents S_{MG-1}^{shed} for MG-1 before the interconnection as well as the instantaneous loading and ML_{ZLS}^{MG-2} of MG-2. As discussed in Section 3.6, since the instantaneous loading is equal or less than ML_{ZLS}^{MG-2} in the simulation study cases of Fig. 3.11 to Fig. 3.13, the MGs interconnection results in reducing the level of load-shedding in MG-1 to zero. Similarly, Table 3.6 presents P_{MG-1}^{shed} for MG-1 before the interconnection as well as the frequency and mF_{ZLS}^{MG-2} of MG-2. Since the frequency of MG-2 is above mF_{ZLS}^{MG-2} in the simulation study cases of Fig. 3.14 - Fig. 3.16, the MGs interconnection results in reducing the level of load-shedding to zero.

Table 3.5: Required level of load-shedding [pu] in MG-1 in simulation studies cases 1-3 of the centralized approach.

| | Case-1 | Case-2 | Case-3 |
|--|--------|--------|--------|
| S_{MG-1}^{shed} before interconnection | 0.07 | 0.05 | 0.05 |
| $ S_{MG-2} $ | 0.47 | 0.82 | 0.85 |
| ML_{ZLS}^{MG-2} | 0.83 | 0.85 | 0.85 |
| S_{MG-1}^{shed} after interconnection | 0 | 0 | 0 |

Table 3.6: Required level of load-shedding [pu] in MG-1 in simulation studies cases 1-3 of the decentralized approach.

| | Case-1 | Case-2 | Case-3 |
|--|--------|--------|--------|
| P_{MG-1}^{shed} before interconnection | 0.06 | 0.06 | 0.09 |
| f_{MG-2} | 50.15 | 50.15 | 50.15 |
| mF_{ZLS}^{MG-2} | 49.66 | 49.66 | 49.69 |
| P_{MG-1}^{shed} after interconnection | 0 | 0 | 0 |

3.8.2. Stability analysis

The stability of the considered CMG is also analysed based on the developed SSS model in MATLAB. This analysis shows that the stability of CMG depends mainly on the droop coefficients (m and n) of the DERs and the ratio of the capacities between the DERs (*Ratio*). Fig. 3.17 illustrates the eigenvalues for the considered CMG when m varies between 0.00023 and 0.023 around the operating point of 0.0023. From this figure, it can be seen that CMG with $m = 0.0218$ is marginally stable. Note that in the considered CMG, there are 4 similar DERs (2 in each MG); hence, m is the droop coefficient of all the DERs.

To validate the accuracy of the mathematical modelling in MATLAB, three points (i.e., point **a**, **b** and **c**) are specified on the eigenvalue trajectory plot of Fig. 3.17 that respectively represent a stable focus, stable limit cycle and unstable focus operating points of the CMG system. The time-domain responses corresponding to these three points are then captured from PSCAD. From these captured data, the phase plane and time domain plots are obtained for each point separately, as shown in Fig. 3.17. These results closely associate with the system performance expected from eigenvalue trajectory (captured from MATLAB).

The SSS analysis is repeated for different values of n (Fig. 3.18a) as well as *Ratio* (Fig. 3.18b). From these figures, it can be seen that the considered CMG is marginally stable for $n = 0.0112$ and *Ratio* = 5.7. The dominant modes for the considered CMG which push the CMG into instability region, when m , n and *Ratio* are varied, are listed in Table 3.7. The characteristics of each dominant mode including its damping ratio, ζ , undamped natural frequency, ω_n , oscillation period, T , and number of cycles for its oscillations to damp by 50%, $NoC_{50\%}$, are also listed in this table. In addition, this table highlights the states which have the highest impact on dominant modes with their relevant weightings.

The SSS analysis is repeated for the tie-line impedance, assuming the impedance of the tie-line as $l_Z \times z_{\text{tie-line}}$, l_Z is varied between 1 and 10. The analysis is carried out assuming $X_{\text{tie-line}}$ is constant and equal to 0.2Ω (based on [130]) at

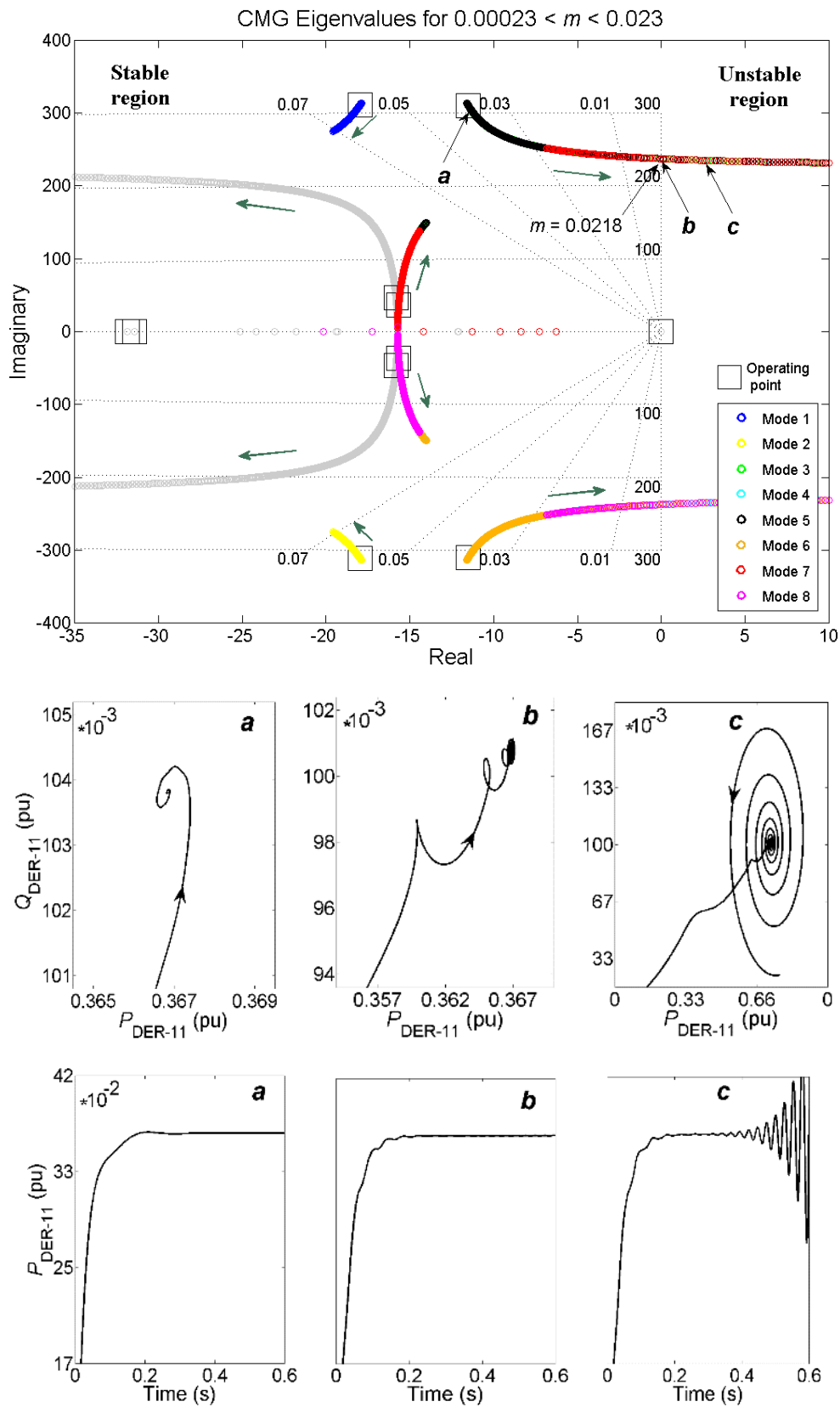


Fig. 3.17: Eigenvalues of the considered system of CMG, with the dynamic performance investigated in Section 3.8.1.

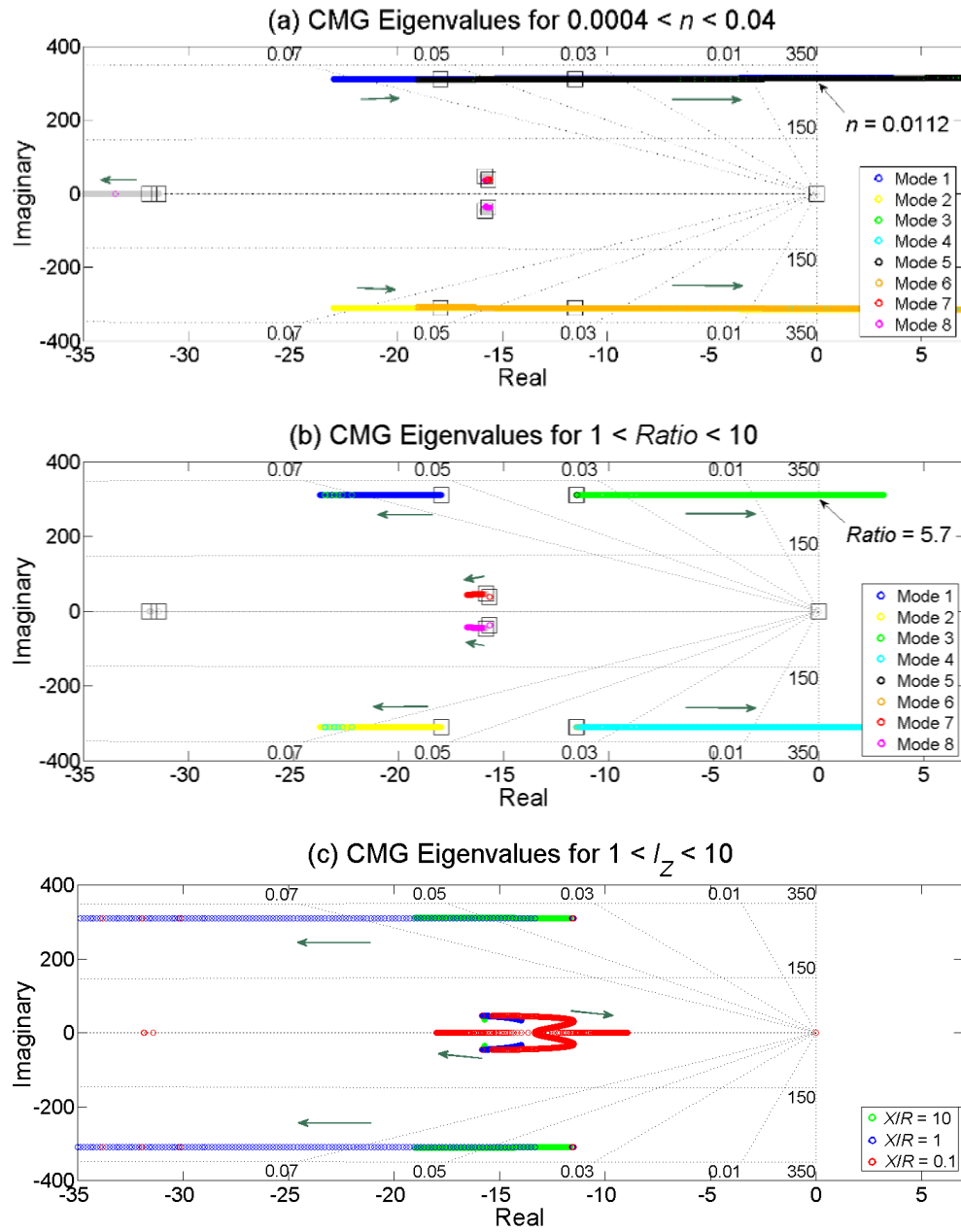


Fig. 3.18: Eigenvalues of the considered CMG.

the operating point while the X/R of the tie-line is either 0.1, 1 or 10. The eigenvalues of the CMG when the impedance of the tie-line is varied in all three scenarios are shown in Fig. 3.18c. This figure illustrates that variations in the tie-line impedance of the considered CMG do not lead to its instability.

Table 3.7: Dominant modes of CMG and their characteristics.

| Modes | Critical for | ζ | ω_n (rad/s) | T (s) | $NoC_{50\%}$ | Effective states (weightings %) |
|-------|---------------|---------|--------------------|---------|--------------|---|
| 1, 2 | $n, Ratio$ | 0.0576 | 311.81 | 0.0202 | 1.91 | $i_{TDER-11}, i_{TDER-12}, i_{TDER-21}, i_{TDER-22}$ (16.4) – $i_{Tie-line}$ (30.82) |
| 3, 4 | $m, n, Ratio$ | 0.0371 | 310.32 | 0.0203 | 2.97 | $i_{TDER-11}, i_{TDER-12}$ (47.5) |
| 5, 6 | m, n | 0.0371 | 310.32 | 0.0203 | 2.97 | $i_{TDER-21}, i_{TDER-22}$ (47.5) |
| 7, 8 | m | 0.3908 | 40.09 | 0.1703 | 0.26 | $P_{DER-11}, P_{DER-12}, P_{DER-21}, P_{DER-22}$ (12.25) – $\delta_{DER-21}, \delta_{DER-22}$ (24.5) |

According to the results of the SSS analysis, coupling two droop-regulated stable MGs which are operating with the same range of frequency variation will result in a stable CMG system. Consequently, variations of the droop gains prior and subsequent to the coupling of the two MGs are not required.

In order to evaluate the effect of the number of DERs in each MG on the CMG stability, the SSS analysis is repeated for the network of Fig. 3.10, assuming the number of DERs in one MG is 2 while the number of DERs in the other MG is either 2, 3 or 4. For each case, the voltage and frequency deviation which pushes each MG and CMG into marginal stability are given in Table 3.8. To be able to derive a common reference for all systems, the marginal stability in this table is represented by two new parameters of marginal frequency deviation (f_{Δ}) and marginal voltage deviation (V_{Δ}) instead of m and n . From this table, it can be seen that smaller marginal frequency deviation and smaller marginal voltage deviations are observed as the number of DERs in an MG or a CMG increases, assuming that the maximum generation capacity in each MG is kept constant. Moreover, the marginal frequency deviation of the CMG is between the marginal frequency deviations of the MGs. However, the marginal voltage deviation of the CMG is equal to the minimum of the marginal voltage deviations.

Table 3.8: Marginal voltage and frequency deviations of MGs and CMG.

| Scenario | | f_{Δ} (pu) | | | V_{Δ} (pu) | | |
|----------|-------|-------------------|--------|--------|-------------------|--------|--------|
| N_1 | N_2 | MG-1 | MG-2 | CMG | MG-1 | MG-2 | CMG |
| 2 | 2 | 0.2100 | 0.2076 | 0.2084 | 0.1215 | 0.1213 | 0.1213 |
| 2 | 3 | 0.2100 | 0.1244 | 0.1586 | 0.1215 | 0.0800 | 0.0798 |
| 2 | 4 | 0.2100 | 0.0666 | 0.0804 | 0.1215 | 0.0594 | 0.0592 |
| 3 | 2 | 0.1260 | 0.2076 | 0.1590 | 0.0800 | 0.1213 | 0.0798 |
| 4 | 2 | 0.0670 | 0.2076 | 0.0806 | 0.0594 | 0.1213 | 0.0592 |

3.9 Conclusion

In this section, a self-healing agent is developed to couple two isolated MGs, when one of them is overloaded. This agent operates under centralized and decentralized approaches, based on the availability of the communication system. Different interconnection and isolation conditions are derived for each approach. Through PSCAD simulation studies, it can be seen that the developed self-healing agent can successfully detect the overloaded MG and couple them after evaluating the interconnection conditions. It also divides the CMG into two isolated MGs when coupling conditions are violated.

It is to be noted that the use of DER units for reactive power exchange and voltage support is an expensive option and should be kept to minimum. This means the DER units should be operated with the unity power factor as much as possible, while much cheaper capacitor banks are used for reactive power support. Consequently, the decentralized self-healing strategy is preferred over its centralized counterpart since it only uses active power measurements for its decision making process, not to mention its minimal need for communications.

For the considered network, composed of two MGs, the SSS analysis demonstrates that the stability of CMG is highly dependent on the droop curve coefficients of the DERs as well as the ratio of their capacities. In addition, the

sensitivity of the CMG stability to the number of DERs within each MG is evaluated and it reveals that the systems are pushed towards instability with smaller voltage and frequency deviations as the number of DERs are increased, assuming the maximum generation capacity in each MG is kept constant. Moreover, the marginal frequency deviation of the CMG is between the marginal frequency deviations of the MGs; however, the voltage deviation of the CMG is equal to the minimum of the marginal voltage deviations. The tie-line interconnecting the MGs does not affect the stability of the considered CMG. This can be mainly due to the larger inductances considered for coupling the DERs to the MGs.

Chapter 4. INTERNAL/EXTERNAL POWER EXCHANGE FOR SUPPORTING ISOLATED MGs

Remote and rural areas usually have stand-alone power systems which operate autonomously due to the lack of utility grid connections. Thus, their power systems can be considered as isolated and self-sufficient MGs [131]. Conventionally, these MGs are supplied by diesel/gas-based generators; however, the fuel cost and transportation difficulties are motivating the owners of the MGs towards renewable-energy-based DERs, if the areas are rich in renewable sources. The ultimate goal of such systems is a sustainable MG in which all electricity demand is generated by renewables [132]. From another standpoint, a remote area/town can be supplied by several sustainable MGs, each with a different operator and supplying loads of a particular region. Therefore, the distribution network of such areas can resemble the system of Fig. 4.1.

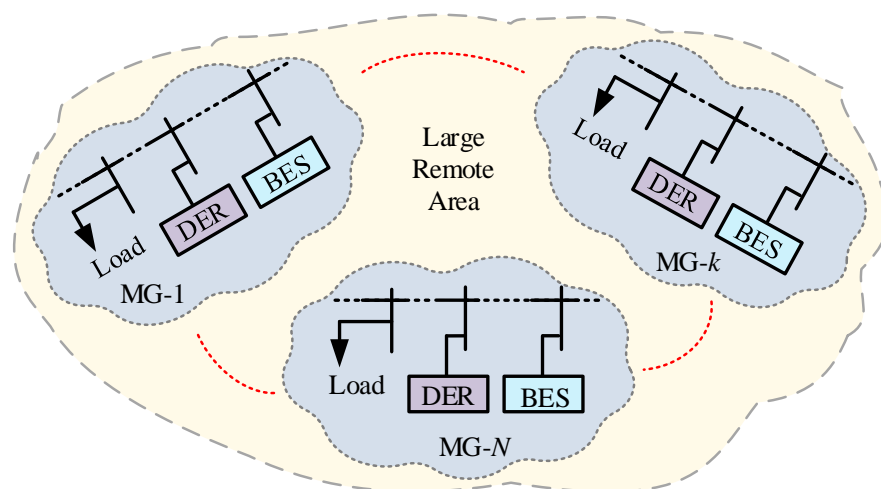


Fig. 4.1: A large remote area supplied by multiple isolated MGs.

Any deficiency in the generation capability versus the existing load demand leads to an overloading condition. To address the overloading in MGs, a variety of operational solutions have been presented in the literature. In Chapter 3, a self-healing strategy is developed to manage power shortfalls in isolated MGs. In this regard, an overloaded MG can get a supporting power from its neighbouring MG to overcome the shortfall. However, the lighter power deficiencies can be addressed by small-scale BESes locally while CMG formation can be limited to severe deficiencies only [133]. In other words, the formation of a CMG is not required for minor power shortfalls if locally installed BESes are properly coordinated. Thus, the cooperative performance of an internal power support from BESes and external support from a neighbouring MG seems a superior strategy.

This chapter proposes a two-level power exchange strategy (PExS) to support an overloaded isolated sustainable MG [134]. The PExS is a synergy of local support from the BES in the MG and external support from a coupled neighbouring MG. It can operate under either a decentralized approach or a centralized approach, depending on the availability of a data communication system. An agent, referred to as the PExS agent in this chapter, is an entity responsible for applying the developed strategy. The conditions and constraints (C&Cs) for BES connection or the coupling of two neighbouring MGs are formulated. Likewise, the C&Cs under which a BES should be disconnected or the interconnected MGs need to be isolated are established. An isolated sustainable MG with the developed strategy offers more resilience and flexibility when overloaded, since all, or a portion of the demand of the MG is supported by the local BES or is imported from the neighbouring MG, leading to a reduced necessity and rate of load-shedding.

The SSS analysis is also performed, and its results are used as a decision-making criterion for connecting the BESes and coupling the MGs. Alternatively, if instability is observed, the SSS analysis defines a range of droop control coefficients for the DERs to enable power exchanges.

4.1 Network under consideration

Consider the system of Fig. 4.2 with two sustainable MGs. MG-1 has N_1 DERs and one BES (DER₁₁, ..., DER_{1M1}, and BES₁) while MG-2 has N_2 DERs and one BES (DER₂₁, ..., DER_{2N2}, and BES₂). Each DER is thought to have local energy storages to smoothen their output power such that it can be represented as a dispatchable DER. These storages are different and independent from BES-1 and BES-2 that only support the network during power deficiencies. Each BES is connected to the MG via a BES static switch (BSS) while the MGs are interconnected through an ISS and a tie-line.

In normal conditions, each MG operates in islanded mode and the voltage magnitude and frequency at the output of each dispatchable DER is regulated by droop control of (2.16). Moreover, the ratio of power generated by any two DERs in an MG is desired to be equal to the proportion of their capacities, which is controlled by their droop coefficients as in (2.17).

As the state of charge (SoC) of a BES reduces when it discharges, it is desired the BES generates less power when its SoC level is low compared to that of high SoC level. Thus, the P - f droop coefficient of the BES is controlled as [135]

$$m_{\text{BES}} = \frac{\Delta f}{\text{SoC}^{\text{d}} \times P_{\text{BES}}^{\text{cap}}} \quad (4.1)$$

where $P_{\text{BES}}^{\text{cap}}$ is the active power capacity of the BES and SoC^{d} represents the SoC in discrete steps of 0.1. Note that the discharge control of the BESes is discussed in details in this chapter as they operate in this mode for the PExS, while their charging control is briefly explained in Appendix B.

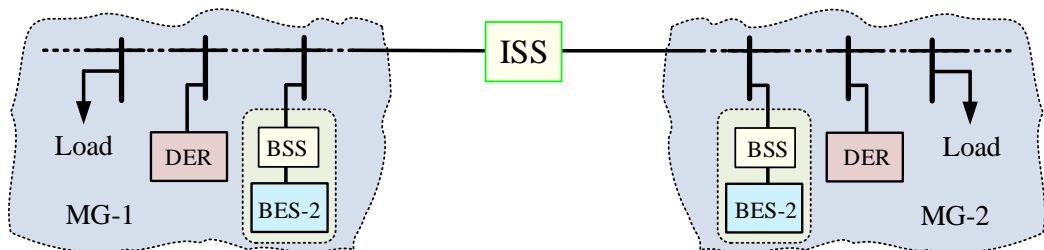


Fig. 4.2: Single line diagram of the network of two isolated MGs.

4.2 Power exchange strategy

Assume a scenario in which MG-1 in Fig. 4.2 experiences a power deficiency (i.e., MG total demand approaches to the total generation capacity of its DERs or rises above that). Lighter power deficiencies will be managed internally by power exchange with BES-1 while larger power deficiencies will be addressed externally by power exchange with MG-2. Four general overloading situations are considered for MG-1. Table 4.1 lists these situations, their reasons, the actions that will be undertaken by the PExS in each situation, the constraints of these actions, the notation of the newly generated system if the constraints are met, as well as the activity that will be taken if the constraints are not met. During each step, if MG-1’s overloading is eliminated (following a generation capacity increase or demand decrease), the steps will be processed backward. Fig. 4.3 illustrates these steps schematically and is referred appropriately within Table 4.1.

Table 4.1: Summary of the different steps of the proposed PExS.

| | | |
|--------|--------------------------------|--|
| Step 1 | Situation | Overloaded MG-1 |
| | Reason 1 | Demand increase, and/or generation decrease |
| | Operation of the PExS agent | Internal Support: BES-1 connects to MG-1 and injects power (Fig. 4.3b) |
| | Constraint of the operation | BES-1’s SoC is above SoC_{min} System is stable |
| | System notation | BMG-1 |
| | Activity if constraint not met | Step-2 |
| Step 2 | Situation | Overloaded MG-1 or BMG-1 |
| | Reason 2 | Reason1, and/or BES-1’s SoC becomes SoC_{min} |
| | Operation of the PExS agent | External Support: ISS between MG-1 and MG-2 closes (Fig. 4.3c) |
| | Constraint of the operation | Available capacity in MG-2 System is stable |
| | System notation | CMG |
| | Activity if constraint not met | Load-shedding |
| Step 3 | Situation | Overloaded CMG |
| | Reason | Reason 2 |
| | Operation of the PExS agent | Internal Support: BES-2 connects to support CMG (Fig. 4.3d) |
| | Constraint of the operation | BES-2’s SoC is above SoC_{min} System is stable |
| | System notation | BCMG |
| | Activity if constraint not met | Isolation of MGs and load-shedding |
| Step 4 | Situation | Overloaded BCMG |
| | Reason | Reason 2, and/or BES-2’s SoC becomes SoC_{min} |
| | Operation of the PExS agent | Nil |
| | Constraint of the operation | |
| | System notation | |
| | Activity if constraint not met | Isolation of MGs and load-shedding |

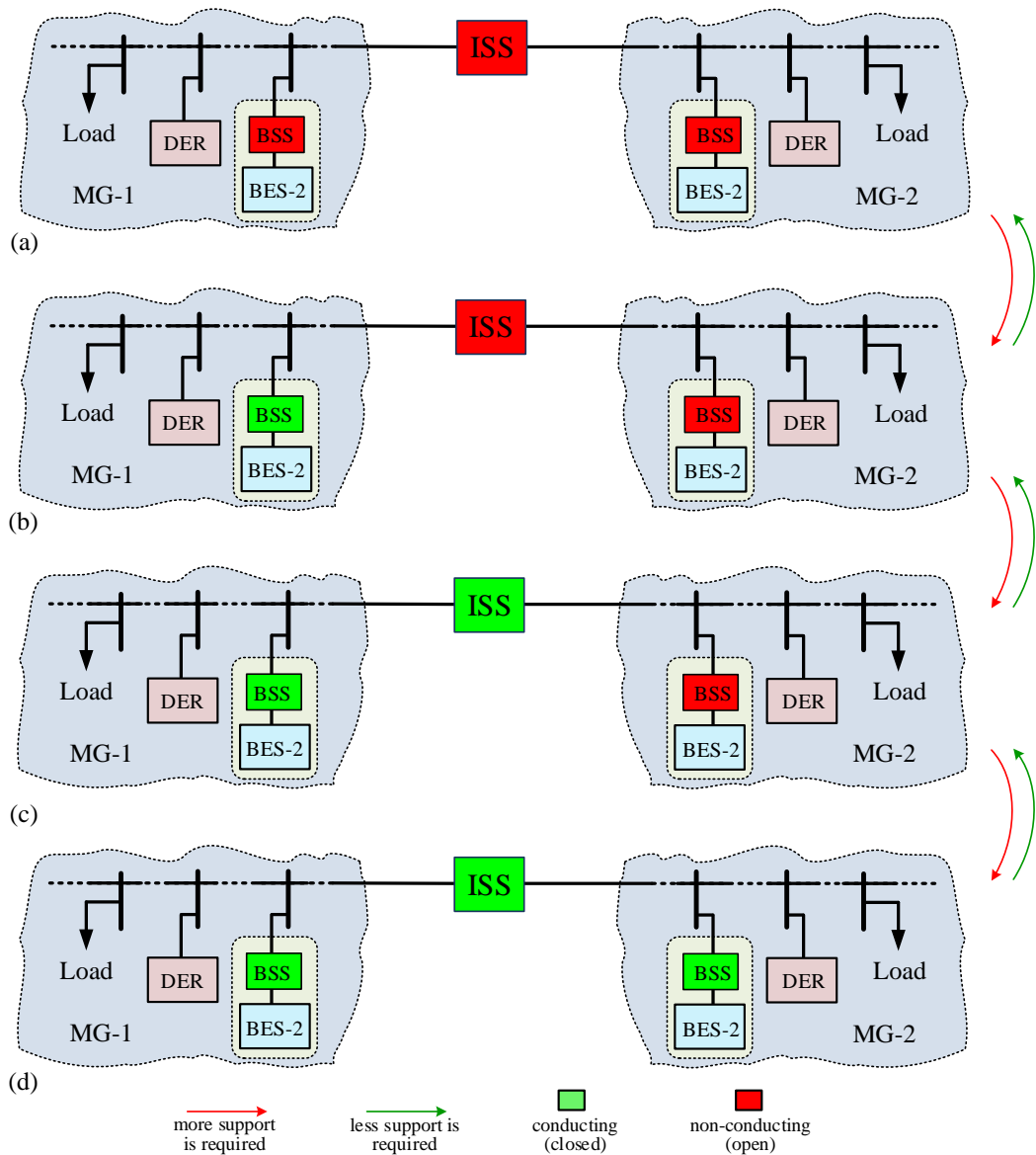


Fig. 4.3: Steps of the operation of the PExS on a two-MG system.

To visualize the steps of the PExS, consider Fig. 4.4a as a representation of MG-1's dispatchable DERs, in which each cell depicts the capacity of a DER. Based on (2.18), the loadings of the DERs (i.e., the ratio of their output power versus their capacity) are equal. This figure depicts a non-overloaded condition in which MG-1's demand is within its maximum capacity (the accumulated capacity of its dispatchable DERs). If due to a demand increase in MG-1, it becomes overloaded (Fig. 4.4b), the PExS agent connects BES-1 to support the MG locally (*Step-1*). We denote MG-1 with BES-1 connected as BMG-1. After BMG-1 formation, MG-1's demand is shared among the DERs and BES-1, reducing the

loading of the DERs (Fig. 4.4c). Fig. 4.4d illustrates a scenario in which MG-1 becomes overloaded significantly. Thus, the PExS agent closes the ISS to couple MG-1 with MG-2 (*Step-2*), forming a CMG. As seen from Fig. 4.4e, MG-2's DERs then share a portion of MG-1's demand. If CMG becomes overloaded (Fig. 4.4f), the PExS agent connects BES-2 to support CMG (*Step-3*). We denote the CMG with BES-2 connected as BCMG. After BCMG formation, MG-1's demand is shared among all DERs and BESEs of both MGs (Fig. 4.4g).

4.2.1. The centralized approach

A centralized approach can be developed if a proper data communication system is available. Under this approach, the agent located at the network tertiary controller is responsible for detecting the system conditions and to provide the on/off commands to the ISS and both BESEs. Consider the network of Fig. 4.5 in which MG-1 is assumed to be overloaded. The suitable C&Cs under which internal and external power exchange is provided to MG-1 are discussed below.

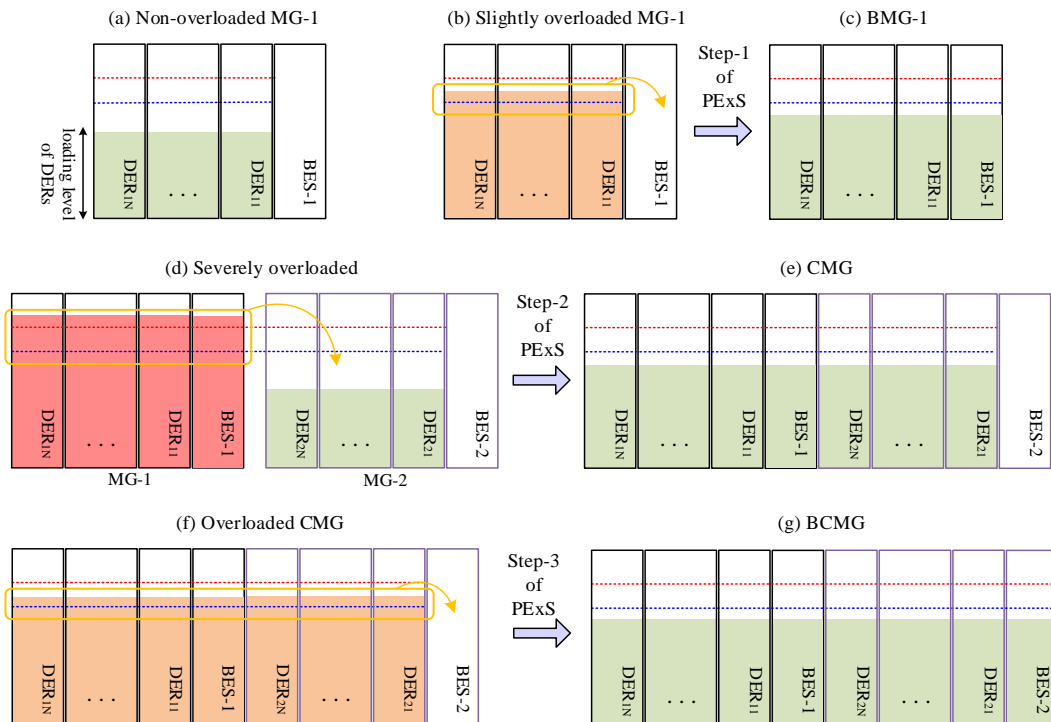


Fig. 4.4: Loading level of the DERs in the MG operating under the proposed PExS.

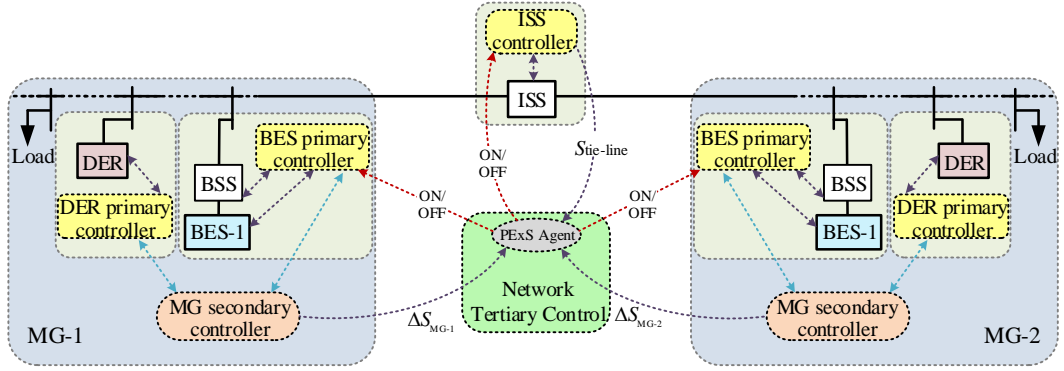


Fig. 4.5: Structure of the centralized approach to realize the PEXs on a two-MG system.

1) CONNECTION OF THE BES OF THE OVERLOADED MG (STEP-1)

Similar to Section 3.2.1, BES-1 starts to inject power to MG-1 if the UPC in MG-1 (ΔS_{MG-1}) becomes less than α_1 times of the total power capacity of all dispatchable DERs of the MG. In other words, BES-1 should connect if its connection condition defined as (3.2) is met ($\Delta S_{MG-1} < \alpha_1 S_{MG-1}^{cap}$). This threshold is illustrated as the bottom dashed line in Fig. 4.4a. It is to be noted that at the connection time, the SoC of BES-1 should be above SoC_{min} . Once condition (3.2) is satisfied, the PEXs agent sends a command to BES-1 to close.

2) DISCONNECTION OF THE BES OF THE OVERLOADED MG

Once the BSS of BES-1 is closed, the BMG-1 system is formed and an apparent power of S_{BES-1} flows from BES-1 to MG-1. Under this situation, the capacity of the BMG-1 system (S_{BMG-1}^{cap}) is $S_{BMG-1}^{cap} = S_{MG-1}^{cap} + \kappa_1 S_{BES-1}^{cap}$ where $\kappa_1 = 1$ if BES-1 is connected and injecting power; otherwise, it is zero. Also, $0 < \beta < 1$ (e.g., $\beta = 0.2$) is used to include a dead-band boundary to prevent a repetitive closing and opening (chattering) of the BSS. Let us assume the UPC of BMG-1 is expressed as

$$S_{BMG-1}^{cap} - |S_{BMG-1}| > \alpha_1 (1 + \beta) S_{BMG-1}^{cap} \quad (4.2)$$

For any two complex numbers z_1 and z_2 , the triangle inequality rule states that

$$|z_1 + z_2| \leq |z_1| + |z_2| \quad (4.3)$$

Considering (4.3), (4.2) is definitely satisfied if

$$S_{\text{BMG-1}}^{\text{cap}} - (|S_{\text{MG-1}}| + |S_{\text{BES-1}}|) > \alpha_1 (1 + \beta) S_{\text{BMG-1}}^{\text{cap}} \quad (4.4)$$

The BES-1 connection is maintained as long as $S_{\text{BES-1}}$ is above a threshold. This threshold can be defined from (4.4) as

$$|S_{\text{BES-1}}| > [1 - \alpha_1 (1 + \beta)] S_{\text{BMG-1}}^{\text{cap}} - |S_{\text{MG-1}}| \quad (4.5)$$

BES-1 should disconnect if the overloading of MG-1 is removed. Therefore, once (4.5) is violated, the PExS agent sends a command to the BSS of BES-1 to open.

3) INTERCONNECTION OF ISOLATED MGs (STEP-2)

If the UPC of MG-1 drops below the threshold in (3.2), BES-1 connects. If the shortfall is severe, however, and the BES is not capable of increasing the UPC, the two neighbouring MGs should be interconnected. Similar to (3.2), this can be conducted if

$$\Delta S_{\text{BMG-1}} < \alpha_2 S_{\text{BMG-1}}^{\text{cap}} \quad (4.6)$$

where $0 < \alpha_2 < \alpha_1$. This is because (3.2) should be satisfied before (4.6) in order to facilitate the internal support by the BES before the external support by coupling the MGs.

The interconnection of two MGs should be avoided if it causes MG-2 to fall below power deficiency boundary. Therefore, condition (4.6) is subject to satisfying a minimum level for UPC of MG-2, as the interconnection constraint. In this regard, the UPC of CMG should fulfil the pre-specified criterion of

$$S_{\text{CMG}}^{\text{cap}} - |S_{\text{CMG}}| > \alpha_2 S_{\text{CMG}}^{\text{cap}} \quad (4.7)$$

where $S_{\text{CMG}}^{\text{cap}} = S_{\text{BMG-1}}^{\text{cap}} + S_{\text{MG-2}}^{\text{cap}}$ and $S_{\text{CMG}} = S_{\text{BMG-1}} + S_{\text{MG-2}}$. Considering (4.3), (4.7) is definitely satisfied if

$$S_{\text{CMG}}^{\text{cap}} - (|S_{\text{BMG-1}}| + |S_{\text{MG-2}}|) > \alpha_2 S_{\text{CMG}}^{\text{cap}} \quad (4.8)$$

Similar to (3.9), (4.8) can be rewritten as

$$\Delta S_{MG-2} > \alpha_2 [(1-\psi) S_{BMG-1}^{cap} + S_{MG-2}^{cap}] \quad (4.9)$$

where $0 < \psi < 1$ is

$$\psi = \Delta S_{BMG-1} / (\alpha_2 S_{BMG-1}^{cap}) \quad (4.10)$$

Once the interconnection condition of (4.6) and constraint of (4.9) are satisfied, the PExS agent, located at the network tertiary controller, sends a command to the ISS to close.

4) ISOLATION OF INTERCONNECTED MGs

When a CMG is formed, an apparent power of $S_{Tie-line}$ flows from MG-2 to MG-1. In this situation, the power consumption in MG-1 is expressed as

$$S_{MG-1} = S_{BMG-1} + S_{Tie-line} \quad (4.11)$$

The ISS should open to isolate the MGs if

$$S_{BMG-1}^{cap} - |S_{BMG-1} + S_{Tie-line}| > \alpha_2 (1 + \beta) S_{BMG-1}^{cap} \quad (4.12)$$

Thus, the interconnection of two MGs is maintained as long as $S_{Tie-line}$ is above a threshold. This threshold can be defined from (4.12), considering the inequality of (4.3), as

$$|S_{Tie-line}| > [1 - \alpha_2 (1 + \beta)] S_{BMG-1}^{cap} - |S_{BMG-1}| \quad (4.13)$$

In addition, the ISS should remain closed as far as the UPC of the CMG is above a threshold given by

$$\Delta S_{CMG} > \alpha_2 (1 - \beta) S_{CMG}^{cap} \quad (4.14)$$

Once either of condition (4.13) or (4.14) is violated, the ISS opens to divide the CMG into two isolated MGs.

5) CONNECTION OF THE BES OF THE NEIGHBOURING MG (STEP-3)

If condition (4.14) is violated, the two interconnected MGs should be isolated. This necessitates conducting a load-shedding process in MG-1. To avoid this undesired scenario, the BES of the neighbouring MG (i.e., BES-2) should

connect to prevent the isolation if the MGs. Let us assume BES-2 should connect if the UPC in the CMG system is less than a threshold defined as

$$\Delta S_{\text{CMG}} < \alpha_1 S_{\text{CMG}}^{\text{cap}} \quad (4.15)$$

Thus, the PExS agent sends a command to the BSS of BES-2 to close if condition (4.15) is satisfied. It is to be noted that the SoC of BES-2 at the connection time should be above SoC_{min} .

6) DISCONNECTION OF THE BES OF THE NEIGHBOURING MG

After formation of the BCMG system, BES-2 delivers an apparent power of $S_{\text{BES-2}}$. In this situation, the power capacity of the BCMG system ($S_{\text{BCMG}}^{\text{cap}}$) is $S_{\text{BCMG}}^{\text{cap}} = S_{\text{CMG}}^{\text{cap}} + \kappa_2 S_{\text{BES-2}}^{\text{cap}}$ where $\kappa_2 = 1$ if BES-2 is connected and injecting active power; otherwise it is zero. Now, let us assume that the UPC of the BCMG system can be expressed as

$$S_{\text{BCMG}}^{\text{cap}} - |S_{\text{CMG}} + S_{\text{BES-2}}| > \alpha_1 (1 + \beta) S_{\text{BCMG}}^{\text{cap}} \quad (4.16)$$

where $S_{\text{CMG}} + S_{\text{BES-2}}$ is the cumulative apparent power consumption of the BCMG system. Under this situation, the connection of BES-2 is maintained as long as $S_{\text{BES-2}}$ is above a threshold. Considering (4.3), this threshold can be defined from (4.16) as

$$|S_{\text{BES-2}}| > [1 - \alpha_1 (1 + \beta)] S_{\text{BCMG}}^{\text{cap}} - |S_{\text{BCMG}}| \quad (4.17)$$

Therefore, the PExS agent sends a command to the BSS of BES-2 to open if condition (4.17) is violated.

4.2.2. The decentralized approach

A decentralized approach is developed for the PExS because the lack of a proper data communication system in remote areas is very likely. Let us assume MG-1 of the network shown in Fig. 4.6 is overloaded. The suitable C&Cs under which internal and external power exchange is provided to MG-1 are discussed in this section.

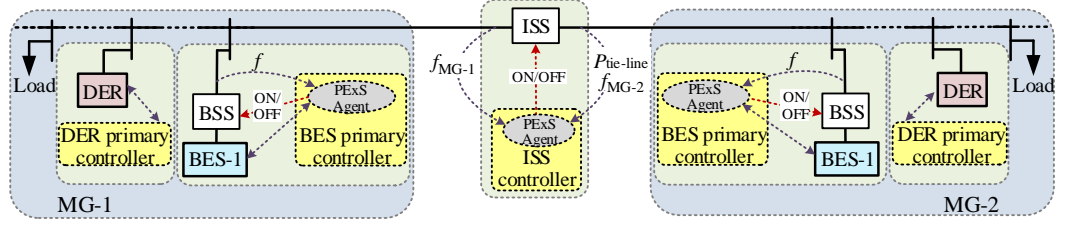


Fig. 4.6: Structure of the decentralized approach to realize the PExS on a two-MG system.

1) CONNECTION OF THE BES OF THE OVERLOADED MG (STEP-1)

BES-1 starts to inject power to MG-1 if the unused active power capacity (UAPC) in MG-1 (ΔP_{MG-1}) can be expressed as

$$\Delta P_{MG-1} = P_{MG-1}^{cap} - \sum_{j=1}^{N_1} P_{DER-1j} < \alpha_1 P_{MG-1}^{cap} \quad (4.18)$$

where $P_{MG-1}^{cap} = \sum_{j=1}^{N_1} P_{DER-1j}^{cap}$. Therefore, from Section 3.3.1, MG-1's overloading is determined if f_{MG-1} satisfies (3.19). Note that (3.19) which is BES-1's connection condition is only based on local monitoring of the MG frequency at the MG side of the BSS. As the constraint, BES-1's SoC should be above SoC_{min} at the connection time.

2) DISCONNECTION OF THE BES OF THE OVERLOADED MG

When BES-1 connects, BMG-1 is formed and operates at a new frequency of f_{BMG-1} . Now, the UAPC in MG-1 is

$$\Delta P_{MG-1} = P_{MG-1}^{cap} - P_{BMG-1} < \alpha_1 (1 + \beta) P_{MG-1}^{cap} \quad (4.19)$$

where $P_{BMG-1} = \kappa_1 P_{BES-1} + \sum_{j=1}^{N_1} P_{DER-1j}$. Replacing (2.17) in (4.19) yields

$$P_{MG-1}^{cap} [1 - \alpha_1 (1 + \beta)] < \frac{f_{max} - f_{BMG-1}}{m_{BES-1}} + \sum_{j=1}^{N_1} \frac{f_{max} - f_{BMG-1}}{m_{1j}} \quad (4.20)$$

which can be simplified as

$$f_{BMG-1} < f_{max} - \frac{P_{MG-1}^{cap} [1 - \alpha_1 (1 + \beta)]}{\frac{1}{m_{BES-1}} + \sum_{j=1}^{N_1} \frac{1}{m_{1j}}} \quad (4.21)$$

BES-1's support is required as far as $f_{\text{BMG-1}}$ is below the threshold of (4.21) and it should be disconnected if $f_{\text{BMG-1}}$ goes above this threshold.

3) INTERCONNECTION OF ISOLATED MGs (STEP-2)

If $f_{\text{MG-1}}$ drops below the threshold of (3.19), BES-1 connects and injects power so that the frequency increases. However, if the BES is not capable of increasing the frequency, or if a further load increase is applied in the MG, or if BES-1's stored energy exhausts, the PExS proceeds to interconnect the overloaded MG with MG-2. Similar to (4.18) this can be conducted if

$$\Delta P_{\text{BMG-1}} = P_{\text{BMG-1}}^{\text{cap}} - P_{\text{BMG-1}} < \alpha_2 P_{\text{BMG-1}}^{\text{cap}} \quad (4.22)$$

where $P_{\text{BMG-1}}^{\text{cap}} = P_{\text{MG-1}}^{\text{cap}} + \kappa_1 P_{\text{BES-1}}^{\text{cap}}$. Similar to (3.19), (4.22) can be expressed as

$$f_{\text{BMG-1}} < f_{\text{min}} + \alpha_2 \Delta f \quad (4.23)$$

Therefore, MG-2 should interconnect to MG-1 when $f_{\text{BMG-1}}$ drops below the threshold of (4.23). Since the newly formed CMG should not be overloaded, it is desired, after the interconnection, to have

$$\Delta P_{\text{CMG}} = P_{\text{CMG}}^{\text{cap}} - P_{\text{CMG}} > \alpha_2 P_{\text{CMG}}^{\text{cap}} \quad (4.24)$$

where $P_{\text{CMG}}^{\text{cap}} = P_{\text{BMG-1}}^{\text{cap}} + P_{\text{MG-2}}^{\text{cap}}$ and $P_{\text{CMG}} = P_{\text{BMG-1}} + P_{\text{MG-2}}$. Applying (2.17) in (4.24) yields

$$(1 - \alpha_2) P_{\text{CMG}}^{\text{cap}} > \frac{f_{\text{max}} - f_{\text{MG-1}}}{m_{\text{BES-1}}} + \sum_{i=1}^2 \sum_{j=1}^{N_i} \frac{f_{\text{max}} - f_{\text{MG-}i}}{m_{ij}} \quad (4.25)$$

which can be rewritten as

$$(1 - \alpha_2) P_{\text{CMG}}^{\text{cap}} > (f_{\text{max}} - f_{\text{MG-1}}) \left(\frac{1}{m_{\text{BES-1}}} + \sum_{j=1}^{N_1} \frac{1}{m_{1j}} \right) + (f_{\text{max}} - f_{\text{MG-2}}) \sum_{j=1}^{N_2} \frac{1}{m_{2j}} \quad (4.26)$$

Hence, the interconnection constraint can be expressed as

$$f_{\text{MG-2}} > f_{\text{max}} - \frac{(1 - \alpha_2)P_{\text{CMG}}^{\text{cap}} - (f_{\text{max}} - f_{\text{MG-1}}) \left(\frac{1}{m_{\text{BES-1}}} + \sum_{j=1}^{N_1} \frac{1}{m_{1j}} \right)}{\sum_{j=1}^{N_2} \frac{1}{m_{2j}}} \quad (4.27)$$

Equation (4.27) illustrates a threshold for MG-2's frequency above which interconnection of the MGs will not overload the CMG. Thus, (4.27) is considered as the closing constraint of the ISS.

4) ISOLATION OF INTERCONNECTED MGs

After closing the ISS, both MGs operate at a new frequency of f_{CMG} and an active power of $P_{\text{Tie-line}}$ flows from MG-2 to MG-1. Under this condition, MG-1's power consumption is

$$P_{\text{MG-1}} = P_{\text{BMG-1}} + P_{\text{Tie-line}} \quad (4.28)$$

Assume the UAPC in BMG-1 can be expressed as

$$\Delta P_{\text{BMG-1}} = P_{\text{BMG-1}}^{\text{cap}} - (P_{\text{BMG-1}} + P_{\text{Tie-line}}) < \alpha_2(1 + \beta)P_{\text{BMG-1}}^{\text{cap}} \quad (4.29)$$

Substituting (2.17) in (4.29) yields

$$P_{\text{Tie-line}} > [1 - \alpha_2(1 + \beta)]P_{\text{BMG-1}}^{\text{cap}} - (f_{\text{max}} - f_{\text{CMG}}) \left(\frac{1}{m_{\text{BES-1}}} + \sum_{j=1}^{N_1} \frac{1}{m_{1j}} \right) \quad (4.30)$$

Equation (4.30) defines an f_{CMG} -dependent threshold for $P_{\text{Tie-line}}$ above which MG-2's support for MG-1 is essential. If $P_{\text{Tie-line}}$ drops below this threshold, the external support becomes superfluous.

The ISS should also open if CMG is overloaded due to a new load increase in the MGs or exhaustion of BES-1's stored energy. This can be identified if f_{CMG} drops below a threshold. Using (4.23), this threshold is defined as

$$f_{\text{CMG}} > f_{\text{min}} + \alpha_2(1 - \beta)\Delta f \quad (4.31)$$

If either (4.30) or (4.31) is violated, CMG has to divide into two isolated MGs. Note that the frequencies of the MGs and $P_{\text{Tie-line}}$ are the only measurements utilized in (4.30) and (4.31).

5) CONNECTION OF THE BES OF THE NEIGHBOURING MG (STEP-3)

The CMG divides into two MGs if (4.31) is violated which results in load-shedding in MG-1. To avoid this, BES-2 connects to MG-2 and injects power to provide extra support. BES-2 should connect if CMG's UAPC becomes less than a threshold as

$$\Delta P_{\text{CMG}} = P_{\text{CMG}}^{\text{cap}} - P_{\text{CMG}} < \alpha_1 P_{\text{CMG}}^{\text{cap}} \quad (4.32)$$

Similar to (3.19), (4.32) can be expressed as

$$f_{\text{CMG}} < f_{\text{min}} + \alpha_1 \Delta f \quad (4.33)$$

BES-2 should connect and inject power if (4.33) is satisfied, subject to its SoC being above SoC_{min} at this time.

6) DISCONNECTION OF THE BES OF THE NEIGHBOURING MG

When BES-2 connects, BCMG is formed and operates at a new frequency of f_{BCMG} . BCMG's capacity ($P_{\text{BCMG}}^{\text{cap}}$) is $P_{\text{BCMG}}^{\text{cap}} = P_{\text{CMG}}^{\text{cap}} + \kappa_2 P_{\text{BES-2}}^{\text{cap}}$. Let us assume that UAPC of the BCMG is less than $\alpha_1(1+\beta)$ times of the total maximum capacity of all the DERs and BESes in the CMG as

$$\Delta P_{\text{BCMG}} = P_{\text{BCMG}}^{\text{cap}} - P_{\text{BCMG}} < \alpha_1(1+\beta)P_{\text{CMG}}^{\text{cap}} \quad (4.34)$$

where $P_{\text{BCMG}} = \sum_{i=1}^2 (P_{\text{BES-}i} + \sum_{j=1}^{N_i} P_{\text{DER-}ij})$. Replacing (2.17) in (4.34) yields

$$P_{\text{CMG}}^{\text{cap}} (1 - \alpha_1(1+\beta)) < \sum_{i=1}^2 \frac{f_{\text{max}} - f_{\text{BCMG}}}{m_{\text{BES-}i}} + \sum_{i=1}^2 \sum_{j=1}^{N_i} \frac{f_{\text{max}} - f_{\text{BCMG}}}{m_{ij}} \quad (4.35)$$

which can be rewritten as

$$f_{\text{BCMG}} < f_{\text{max}} - \frac{P_{\text{CMG}}^{\text{cap}} [1 - \alpha_1(1+\beta)]}{\sum_{i=1}^2 \left(\frac{1}{m_{\text{BES-}i}} + \sum_{j=1}^{N_i} \frac{1}{m_{ij}} \right)} \quad (4.36)$$

Hence, BES-2 supports the CMG as far as f_{BCMG} is below the threshold of (4.36).

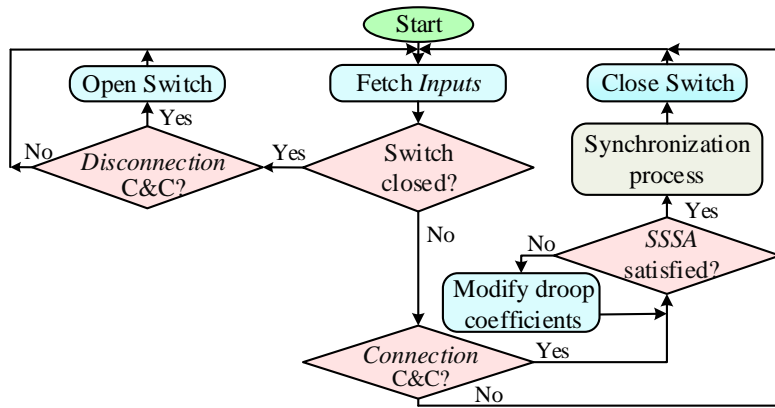
However, BES-2 should be disconnected if the frequency goes above this limit.

4.3 Operation Flowchart of the PExS Agents

Under the decentralized approach, there are three PExS agents, one located within the controller of the ISS and two located within the controllers of each BES. The PExS agent at the ISS fetches the frequencies of the MGs and the active power flow through the tie-line as its inputs, while the PExS agent at BES only fetches the local frequency. When MG-1's frequency drops below the threshold of (3.19), the PExS agent at BES-1 sends a command to its BSS to close; thereby, BES-1 starts to inject power according to its $P - f$ droop coefficient defined in (4.1) if its SoC is above SoC_{\min} . This PExS agent sends a command to the BSS to open and disconnect BES-1 when MG-1's frequency rises above the threshold of (4.21). When MG-1's frequency falls below the threshold of (4.23), the PExS agent at the ISS sends a command to the ISS to close and to couple the MGs if constraint (4.27) is met. This PExS agent sends a command to the ISS to open and divide the MGs when CMG's frequency drops below the threshold of (4.31) or when the power transfer through the tie-line becomes less than the threshold of (4.30). When CMG's frequency drops below the threshold of (4.33), the PExS agent at BES-2 sends a command to its BSS to close and thereby, BES-2 starts to inject power if its SoC is above SoC_{\min} . This PExS agent sends a command to the BSS to open and disconnect BES-2 when CMG's frequency rises above the threshold of (4.36).

Under the centralized approach, there is only one PExS agent that is located at the tertiary controller of the network and fetches the cumulative apparent power of DERs and BESes, as well as the apparent power flowing through the tie-line. This PExS agent uses the same operation strategy as the PExS agents of the centralized approach but with the C&Cs mentioned in Section 4.2.1.

The operational flowchart of the PExS agents under both the approaches is shown in Fig. 4.7. For each BSS, the PExS agent has 4 different operation states based on the open/close status of the BSSes and the ISS. The states are expressed as



| BESes | State | Centralized | | | Decentralized | | |
|-------|-------|---|------------|---------------|---|------------|---------------|
| | | Inputs | Connection | Disconnection | Inputs | Connection | Disconnection |
| BESes | 1 | S_{MG-1}, S_{BES} | (3.2) | (4.5) | f_{MG} | (3.19) | (4.21) |
| | 2,3 | S_{CMG}, S_{BES} | (4.15) | (4.17) | f_{MG} | (4.33) | (4.36) |
| | 4 | S_{CMG}, S_{BES} | - | N/A | f_{MG} | - | N/A |
| ISS | | $S_{MG-1}, S_{MG-2}, S_{Line}$ (4.6) and (4.9) (4.13) or (4.14) | | | $f_{MG-1}, f_{MG-2}, P_{Line}$ (4.23) and (4.27) (4.30) or (4.31) | | |

Fig. 4.7: Operation flowchart of the PEXs agents under centralized and decentralized approaches.

- state-1: the ISS is open.
- state-2: the ISS is closed while the BSS is open.
- state-3: the ISS and the BSS are closed where the ISS was closed earlier.
- state-4: the ISS and the BSS are closed where the BSS was closed earlier.

State-1 is for both BESes whereas state-2 and state-3 are for the BES of the non-overloaded MG while state-4 is for the BES of the overloaded MG. For each state, the PEXs agent fetches different inputs (shown in the table below the flowchart of Fig. 4.7) and depending on the open/close status of BSS/ISS, checks the C&Cs for appropriate opening/closing. For state-1 to 3, the closing and opening of the BSS is evaluated. In state-4, the switch is already closed (i.e., no need to check the connection) and because it is the BES of the overloaded MG, its disconnection is not allowed (N/A).

Before closing the ISS and the BSSes, the stability of the new system will be checked, and the closing is allowed if the new system is determined stable. Also, each closing needs a synchronization, which is discussed in Appendix A.

4. 4 Impact of the Power Exchange Strategy

Consider Fig. 4.2 in which MG-1 is overloaded. Assume that load-shedding in the MG is initiated if the supplied power by its DERs is above $(1 - \alpha_2)$ times the MG capacity. The load-shedding level of MG-1 in the original condition and after applying different stages of the PExS is discussed below:

4.4.1. The centralized approach

The load-shedding level of MG-1 (S_{MG-1}^{shed}) is expressed from (3.2) as

$$S_{MG-1}^{shed} = |S_{MG-1}| - (1 - \alpha_2)S_{MG-1}^{cap} \quad (4.37)$$

If BMG-1 is formed, the load-shedding level depends also on BES-1's capacity.

Thus, S_{MG-1}^{shed} is defined from (4.6) as

$$S_{MG-1}^{shed} = |S_{MG-1}| + |S_{BES-1}| - (1 - \alpha_2)S_{BMG-1}^{cap} \quad (4.38)$$

Likewise, if CMG is formed, S_{MG-1}^{shed} is defined from (4.15) as

$$S_{MG-1}^{shed} = \sum_{i=1}^2 (|S_{MG-i}| + |S_{BES-i}|) - (1 - \alpha_2)S_{CMG}^{cap} \quad (4.39)$$

Considering the parameters provided in Table 4.2, Fig. 4.8 illustrates MG-1's load-shedding level. The left side plots of Fig. 4.8 represent the results when the MG is operating under the centralized approach. Fig. 4.8a shows S_{MG-1}^{shed} without and with BES-1's support. From this figure, it can be seen that no load-shedding is required when MG-1's DERs are loaded below 0.9 pu while a 10% and 20% load-shedding is needed if they are loaded by 1 and 1.1 pu, respectively. When BES-1 is connected, S_{MG-1}^{shed} is related to its SoC. As BES-1's SoC reduces, the support level provided by the BES also decreases and thereby load-shedding increases. As seen from these figures, no load-shedding is required when MG-1's DERs are loaded by 1.2, 1.1 and 1 pu if BES-1's SoC at the connection time is respectively 100%, 67% and 31%.

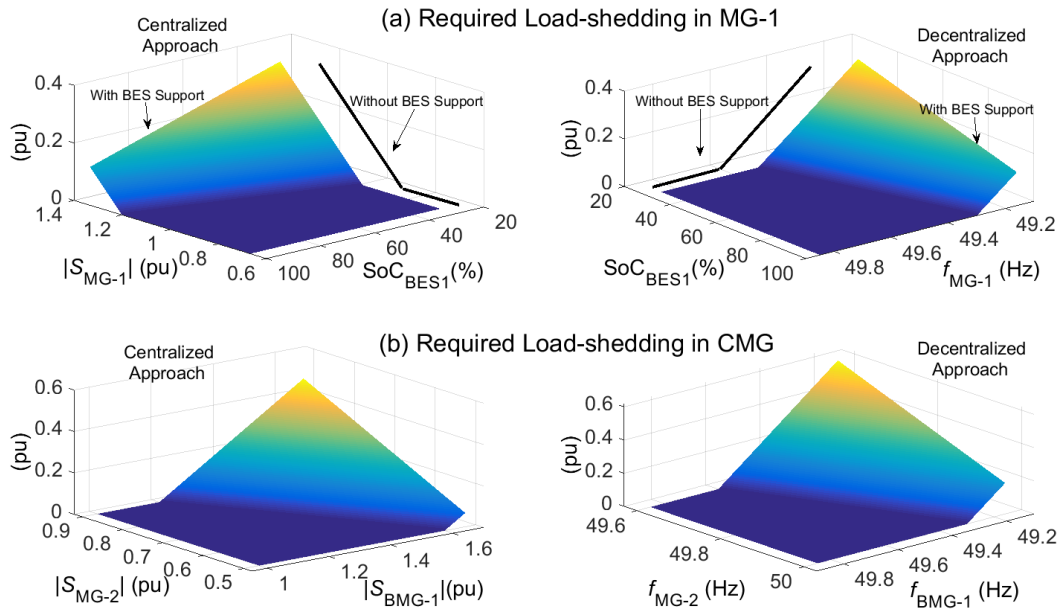


Fig. 4.8: Level of load-shedding for MG-1 under the decentralized and centralized approaches: (a) without and with the BES support, (b) after forming the CMG (SoC = 100%).

Fig. 4.8b shows S_{MG-1}^{shed} after CMG formation. This figure indicates that no load-shedding is required as far as BMG-1 is loaded by 1.6 pu if MG-2 is loaded by 0.5pu before the interconnection. As the UPC of MG-2 decreases (loading level of MG-2 increases), S_{MG-1}^{shed} rises accordingly. As an example, no load-shedding is required when MG-2 is loaded by 0.7 and 0.9 pu if BMG-1's loading is respectively 1.4 and 1.2 pu. The results of Fig. 4.8b are based on the assumption of BES-1 being fully-charged; thus, S_{MG-1}^{shed} increases if BES-1's SoC reduces.

4.4.2. The decentralized approach

Under the decentralized approach, MG-1's load-shedding level (P_{MG-1}^{shed}) is expressed from (4.18) as

$$P_{MG-1}^{shed} = \sum_{j=1}^{N_1} \frac{f_{max} - f_{MG-1}}{m_{1j}} - (1 - \alpha_2) P_{MG-1}^{cap} \quad (4.40)$$

If BES-1 is connected, P_{MG-1}^{shed} can be defined from (4.22) as

$$P_{\text{MG-1}}^{\text{shed}} = (f_{\text{max}} - f_{\text{BMG-1}}) \left(\frac{1}{m_{\text{BES-1}}} + \sum_{j=1}^{N_1} \frac{1}{m_{1j}} \right) - (1 - \alpha_2) P_{\text{BMG-1}}^{\text{cap}} \quad (4.41)$$

Similarly, $P_{\text{MG-1}}^{\text{shed}}$ can be described from (4.32) when CMG is formed as

$$P_{\text{MG-1}}^{\text{shed}} = (f_{\text{max}} - f_{\text{CMG}}) \sum_{i=1}^2 \left(\frac{1}{m_{\text{BES-}i}} + \sum_{j=1}^{N_i} \frac{1}{m_{ij}} \right) - (1 - \alpha_2) P_{\text{CMG}}^{\text{cap}} \quad (4.42)$$

The right figures of Fig. 4.8 illustrate $P_{\text{MG-1}}^{\text{shed}}$ when the MG is operating under the decentralized approach. These figures show that no load-shedding is required when $f_{\text{MG-1}} > 49.6\text{Hz}$ (equivalent to a loading of less than 0.9pu). However, a load-shedding of 10% and 20% is needed if $f_{\text{MG-1}}$ drops to 49.5 and 49.4Hz, respectively. This figure also illustrates that $P_{\text{MG-1}}^{\text{shed}} = 0$ if $f_{\text{MG-1}} > 49.3\text{Hz}$ (equivalent to system loading of below 1.2pu), at the connection time of fully-charged BES-1. It can also be seen from this figure that if CMG is formed, the load-shedding is not required when $f_{\text{MG-2}} > 50\text{Hz}$ (comparable to MG-2's loading of below 0.5pu) if $f_{\text{BMG-1}} = 49.3\text{Hz}$ (equivalent to the 1.6pu loading of BMG-1) before the interconnection.

4.5 Impact of the PExS Parameters

The performance of the PExS relies on the values of α_1 , α_2 and β . The PExS operates successfully as far as the values of these parameters are within their defined boundaries; however, the outcome relies on their numerical values. For example, smaller values of α_1 in (4.18) may jeopardize MG-1's supply security while its larger values may result in the aging of BES-1 which imposes extra costs on the owner of the MG. Similarly, smaller values of β in (4.19) may cause chattering problems while its larger values result in the unnecessary depletion of BES-1's stored energy. Likewise, smaller values of α_2 in (4.22) may endanger the supply security of the MG while its larger values may cause earlier interconnection of the MGs which disadvantages owner of MG-1 financially for importing an unrequired power from MG-2.

From (4.19), MG-1's UAPC threshold can be shown as a function of α_1 and β , as illustrated in Fig. 4.9a. As seen from this figure, the lower and upper boundaries of α_1 are suggested to be 0.1 and 0.3, respectively. From (4.31), similarly, the frequency threshold of CMG under which CMG should be isolated can be expressed as a function of α_2 and β , as depicted in Fig. 4.9b. As seen from this figure, the lower and upper boundaries of β are also suggested to be 0.1 and 0.3, respectively.

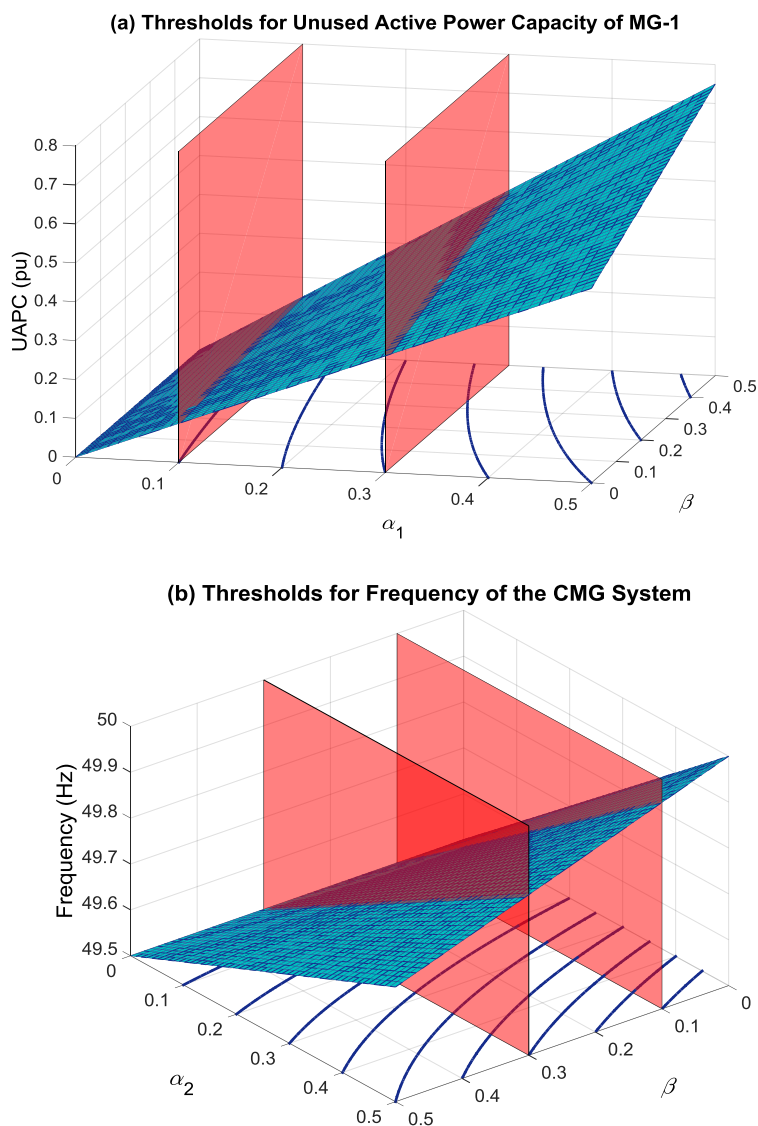


Fig. 4.9: (a) UAPC thresholds of MG-1 as a function of various values for α_1 and β in the C&Cs, (b) Frequency thresholds of CMG as a function of various values for α_2 and β in the C&Cs.

4.6 Performance Evaluation

To investigate the dynamic performance of the PExS, consider the system of Fig. 4.2, composed of two sustainable MGs. Each MG has two converter-interfaced DERs and one BES, with the technical data provided in Table 4.2. The network is modelled in PSCAD/EMTDC while the PExS agents are realized in FORTRAN as embedded self-created blocks.

4.6.1. Dynamic performance of the centralized approach

Five different cases are simulated for the system controlled under the centralized approach. The events of each case along with the associated outcomes are listed in time sequence in Table 4.3 to Table 4.7. Further, the simulation results are depicted in Fig. 4.10 to Fig. 4.14 and each figure is located just below its corresponding table. The aggregated power of the loads and the DERs in each MG, the power supplied by BES-1 and tie-line, the required power to be shed, and the activation signal and the status of ISS and BSSes are separately shown.

Table 4.2: Parameters of MGs, DERs and BESes, Synchronization, and the PExS

MG-1 and MG-2 network parameters:

$$V_{\text{base}} = 230 \text{ V}, f_{\text{nominal}} = 50 \text{ Hz}, Z_{\text{line}} = 0.1 + j 0.1 \Omega$$

CMG network parameters:

$$Z_{\text{tie-line}} = 0.2 + j 0.2 \Omega$$

PExS parameters:

$$\alpha_1 = 0.2, \alpha_2 = 0.1, \alpha_3 = 0.5, \beta = 0.2, V_{\text{max}} = 230 \text{ V}, \Delta V = 10\%, \Delta f = 1 \text{ Hz}, \text{SoC}_{\text{min}} = 30\%$$

Converter structure and control parameters:

$$V_{\text{dc}} = 350 \text{ V}, a = 2, R_f = 0.1 \Omega, L_f = 0.37 \text{ mH}, C_f = 50 \mu\text{F}, h = 10^{-4}, k_1 = 6.180, k_2 = 2.297, k_3 = 22.968$$

Synchronization parameters: $\varepsilon_v = \varepsilon_\delta = 10^{-3}$

| MG No. | BES No. | L_T [mH] | m [rad/kW] for SoC = 100% | n [V/kVAr] |
|--------|-------------------|------------|-----------------------------|--------------|
| 1 | BES ₁ | 40.8 | 3.14 | 12 |
| 2 | BES ₂ | 40.8 | 3.14 | 12 |
| MG No. | DER No. | L_T [mH] | m [rad/kW] | n [V/kVAr] |
| 1 | DER ₁₁ | 27.2 | 2.09 | 8 |
| | DER ₁₂ | 27.2 | 2.09 | 8 |
| 2 | DER ₂₁ | 16.4 | 1.26 | 4.8 |
| | DER ₂₂ | 81.7 | 6.28 | 24 |

In case-1, each MG is initially operating independently. A load increase in MG-1 results in an overloading. Consequently, BES-1 is connected to support MG-1. A further demand increase leads to CMG formation.

In case-2, initially, it is assumed that CMG is formed. A demand decrease in MG-1 eliminates the necessity of extra support from MG-2; thus, CMG divides into two isolated MGs while BES-1 remains connected to supply the required power to MG-1.

In case-3, initially, it is assumed that CMG is formed. A load increase in MG-2 results in BES-2's connection to CMG. A subsequent load decrease in MG-2 eliminates the necessity for support from BES-2; thereby, it disconnects; while CMG is sustained.

In case-4, a demand increase in MG-2 pushes the formed CMG into overloading. Assuming that the SoC of BES-2 is at its minimum, BES-2 cannot connect as its connection constraint is not satisfied. Consequently, the condition for isolation of two MGs is achieved, and CMG divides into two independent MGs. In such a case, load-shedding in MG-1 is inevitable.

In case-5, initially, it is assumed that CMG is formed. A load increase in MG-2 results in connection of BES-2 to CMG. CMG is pushed into overloading by a subsequent load increase in MG-2; and thus, the isolation condition of the system is satisfied. As CMG divides into two independent MGs, a load-shedding in MG-1 is inevitable. Note that both BESEs remain connected to their MGs to support them.

The dynamic performance of the PExS is successfully validated as seen from Fig. 4.10 to Fig. 4.14. The simulation outcomes demonstrate that the proposed approach can effectively cope with the overloading events within the MGs under different scenarios.

Table 4.3: Time sequence of the events in the system with the centralized approach, Case 1.

| t (s) | Event | Outcome | Numerical Values [pu] |
|---------|---|---|--|
| 0 | The MGs and BES-1 are isolated and operating at steady-state. | | $\Delta S_{MG-1} = 0.41$ |
| 0.2 | MG-1 demand increases by 44%. | S_{MG} increases to supply the demand. | |
| 0.3 | BES-1's connection condition (3.2) is satisfied. | BSS activation command is initiated. | $\Delta S_{MG-1} = 0.14$ |
| 0.98 | Synchronization between BES-1 and MG-1 is achieved. | BSS closes, and BMG-1 is formed. | $\Delta S_{BMG-1} = 0.44,$ $ S_{BES-1} = 0.23$ |
| 2 | MG-1 demand increases by 40.5%. | S_{BMG-1} increases to supply the demand. | |
| 2.1 | Interconnection C&C of (4.6) and (4.9) are satisfied. | ISS activation command is initiated. | $\Delta S_{BMG-1} = 0.06,$ $\Delta S_{MG-2} = 0.67$ |
| 2.29 | Synchronization between the MGs is achieved. | ISS closes, and CMG is formed. | $\Delta S_{CMG} = 0.32,$ $ S_{Tie-line} = 0.33$ |

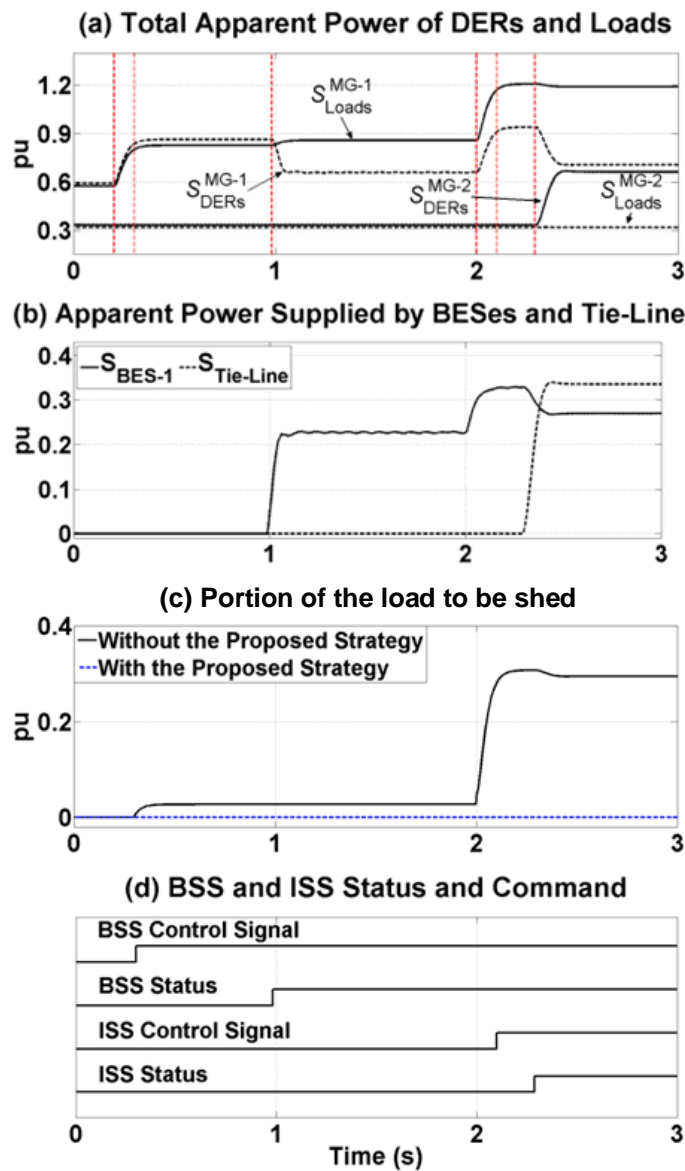


Fig. 4.10: Dynamic performance of the system with the centralized approach, Case 1.

Table 4.4: Time sequence of the events in the system with the centralized approach, Case 2.

| t (s) | Event | Outcome | Numerical Values [pu] |
|---------|-----------------------------------|---|---|
| 0 | CMG is operating at steady-state. | | $\Delta S_{CMG} = 0.32$, $ S_{Tie-line} = 0.33$ |
| 0.3 | MG-1 demand reduces by 13.4%. | S_{CMG} decreases to supply the demand. | |
| 0.5 | Condition (4.13) is violated. | ISS opens, and CMG divides into 2 MGs. | $\Delta S_{BMG-1} = 0.19$, $\Delta S_{MG-2} = 0.67$ |

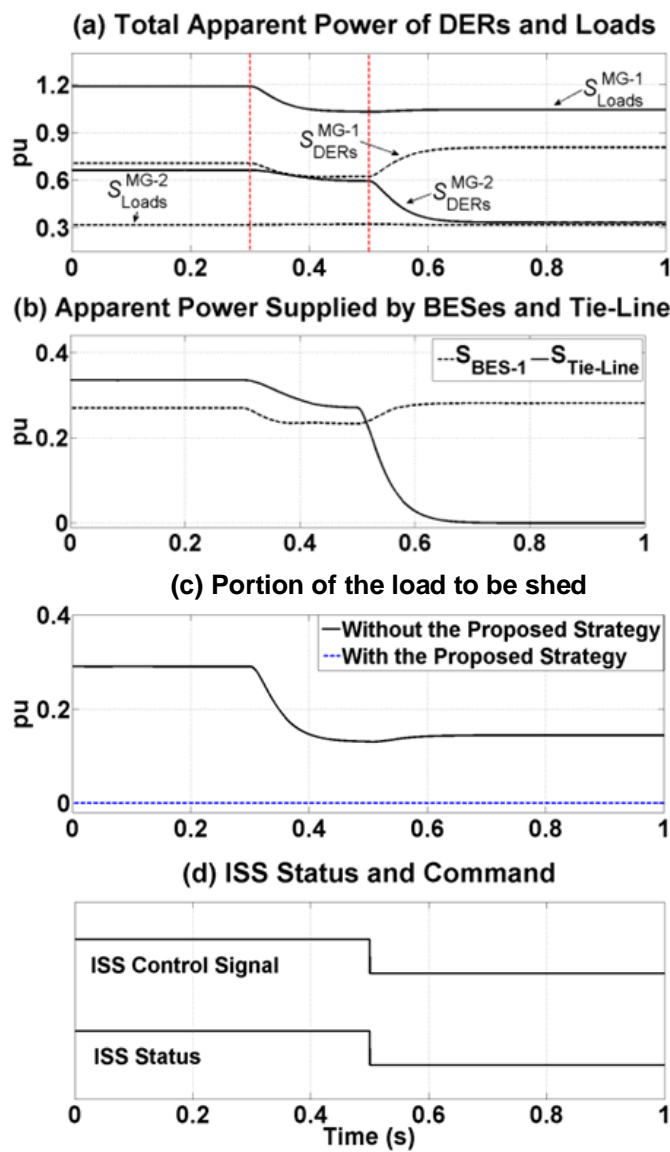


Fig. 4.11: Dynamic performance of the system with the centralized approach, Case 2.

Table 4.5: Time sequence of the events in the system with the centralized approach, Case 3.

| t (s) | Event | Outcome | Numerical Values [pu] |
|---------|---|---|--|
| 0 | CMG is operating at steady-state. | | $\Delta S_{\text{CMG}} = 0.32$, $ S_{\text{Tie-line}} = 0.33$ |
| 0.5 | MG-2 demand increases by 117%. | S_{CMG} increases to supply the demand. | |
| 0.7 | BES-2's connection condition (4.15) is satisfied. | BSS activation command is initiated. | $\Delta S_{\text{CMG}} = 0.15$, $ S_{\text{Tie-line}} = 0.18$ |
| 1.16 | Synchronization between BES-2 and CMG is achieved. | BSS closes, and BCMG is formed. | $\Delta S_{\text{BCMG}} = 0.25$, $ S_{\text{BES-2}} = 0.25$ |
| 2.5 | MG-2 demand reduces by 80%. | S_{BCMG} decreases to supply the demand. | |
| 2.7 | Condition (4.17) is violated ($ S_{\text{BES-2}} = 0.17$). | BSS opens, and BES-2 disconnects. | $\Delta S_{\text{CMG}} = 0.39$, $ S_{\text{Tie-line}} = 0.43$ |

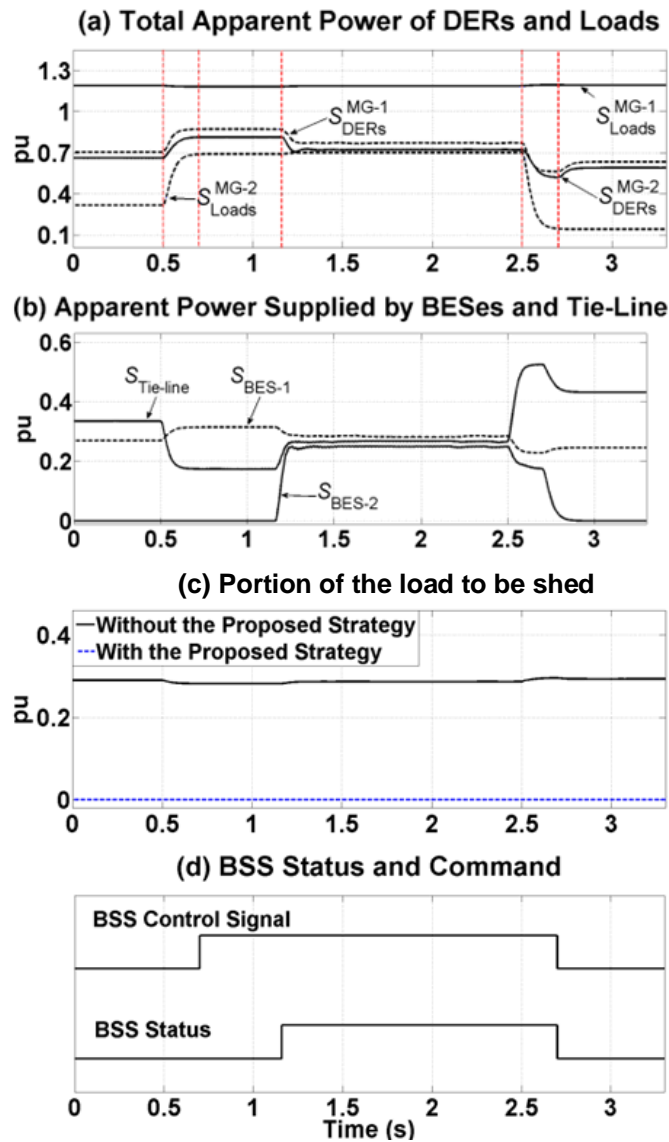


Fig. 4.12: Dynamic performance of the system with the centralized approach, Case 3.

Table 4.6: Time sequence of the events in the system with the centralized approach, Case 4.

| t (s) | Event | Outcome | Numerical Values [pu] |
|---------|--|---|---|
| 0 | CMG is operating at steady-state. | | $\Delta S_{CMG} = 0.32$, $ S_{Tie-line} = 0.33$ |
| 0.2 | MG-2 demand increases by 167%. | S_{CMG} increases to supply the demand. | |
| 0.4 | BES-2 condition (4.15) is satisfied but its constraint is not satisfied. | BSS activation command is not allowed. | $\Delta S_{CMG} = 0.08$, $ S_{Tie-line} = 0.17$ |
| 0.4 | Condition (4.14) is violated. Load-shedding is inevitable. | ISS opens, and CMG divides into 2 MGs. | $\Delta S_{BMG-1} = 0.06$, $\Delta S_{MG-2} = 0.18$ |

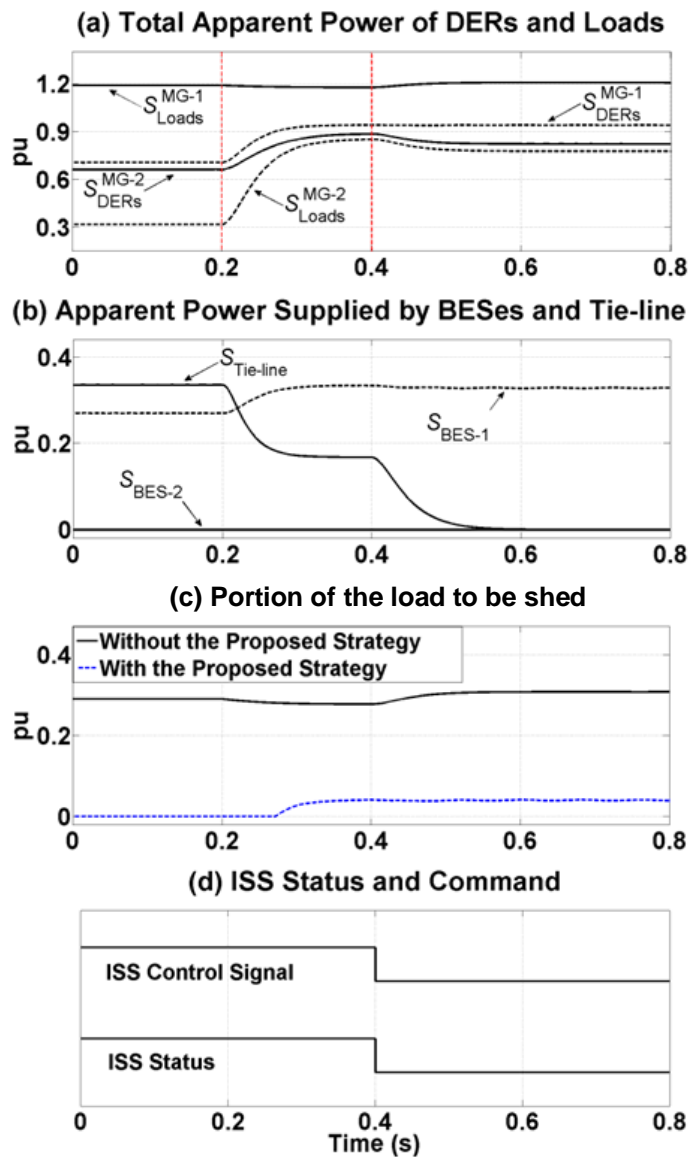


Fig. 4.13: Dynamic performance of the system with the centralized approach, Case 4.

Table 4.7: Time sequence of the events in the system with the centralized approach, Case 5.

| t (s) | Event | Outcome | Numerical Values [pu] |
|---------|--|---|---|
| 0 | CMG is operating at steady-state. | | $\Delta S_{\text{CMG}} = 0.32$, $ S_{\text{Tie-line}} = 0.33$ |
| 0.5 | MG-2 demand increases by 117%. | S_{CMG} increases to supply the demand. | |
| 0.7 | BES-2 connection condition (4.15) is satisfied. | BSS activation command is initiated. | $\Delta S_{\text{CMG}} = 0.15$, $ S_{\text{Tie-line}} = 0.18$ |
| 1.16 | Synchronization between BES and CMG is achieved. | BSS closes, and BCMG is formed. | $\Delta S_{\text{BCMG}} = 0.25$, $ S_{\text{BES-2}} = 0.25$ |
| 2.5 | MG-2 demand increases by 28%. | S_{BCMG} increases to supply the demand. | |
| 2.7 | Condition (4.14) is violated. Load-shedding is inevitable. | ISS opens, and CMG divides into 2 MGs. | $\Delta S_{\text{BMG-1}} = 0.06$, $\Delta S_{\text{MG-2}} = 0.34$ |

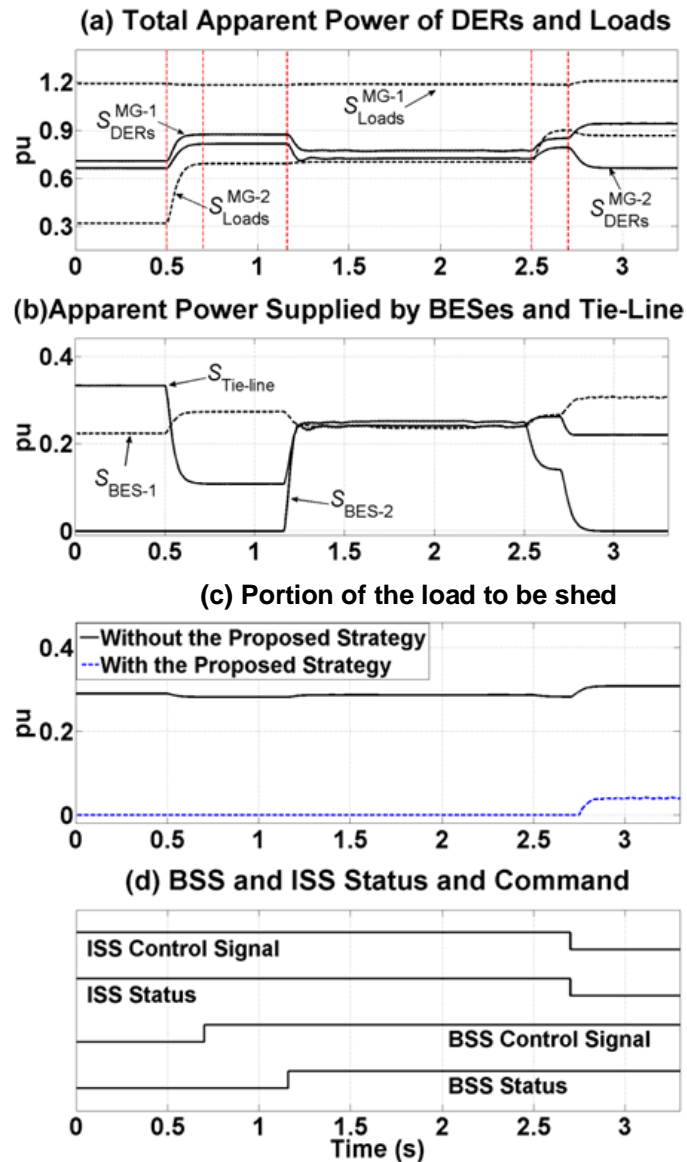


Fig. 4.14: Dynamic performance of the system with the centralized approach, Case 5.

4.6.2. Dynamic performance of the decentralized approach

Similar to the previous section, the same five cases are simulated for the system controlled under the decentralized approach as well. The events of each case along with the associated outcomes are listed in time sequence in Table 4.8 to Table 4.12. Further, the simulation results are depicted in Fig. 4.15 to Fig. 4.19. Note that each figure is located just below its corresponding table. The aggregated active power of the loads and the DERs in each MG, the power supplied by BES-1 and tie-line, the required power to be shed, the frequency of each MG, and the activation signal and the status of ISS and BSSes are separately shown.

According to the simulation results, it is demonstrated that the PExS agents can successfully detect overloading of the MG and can take the appropriate steps after evaluating the formulated conditions and constraints. This is validated through the derived outcomes considering different scenarios, as can be seen from Fig. 4.15 to Fig. 4.19.

Table 4.8: Time sequence of the events in the system with the decentralized approach, Case 1.

| t (s) | Event | Outcome | Numerical Values: f [Hz], P [pu] |
|---------|---|---|--|
| 0 | The MGs and BESEs are isolated and operating at steady-state. | | $f_{MG-1} = 49.90$, $f_{MG-2} = 50.18$ |
| 0.5 | MG-1 demand increases by 44%. | P_{MG-1} increases to supply the demand. | |
| 0.7 | BES-1's connection condition (11) is satisfied. | BSS activation command is initiated. | $f_{MG-1} = 49.65$ |
| 1.07 | Synchronization between BES-1 and MG is achieved. | BSS closes, and BMG-1 is formed. | $f_{BMG-1} = 49.84$, $P_{BES-1} = 0.22$ |
| 2 | MG-1 demand increases by 47.2%. | P_{BMG-1} increases to supply the demand. | |
| 2.2 | Interconnection C&C of (16) and (20) are satisfied. | ISS activation command is initiated. | $f_{BMG-1} = 49.53$, $f_{MG-2} = 50.18$ |
| 2.36 | Synchronization between the MGs is achieved. | ISS closes, and CMG is formed. | $f_{CMG} = 49.80$, $P_{Tie-line} = 0.36$ |

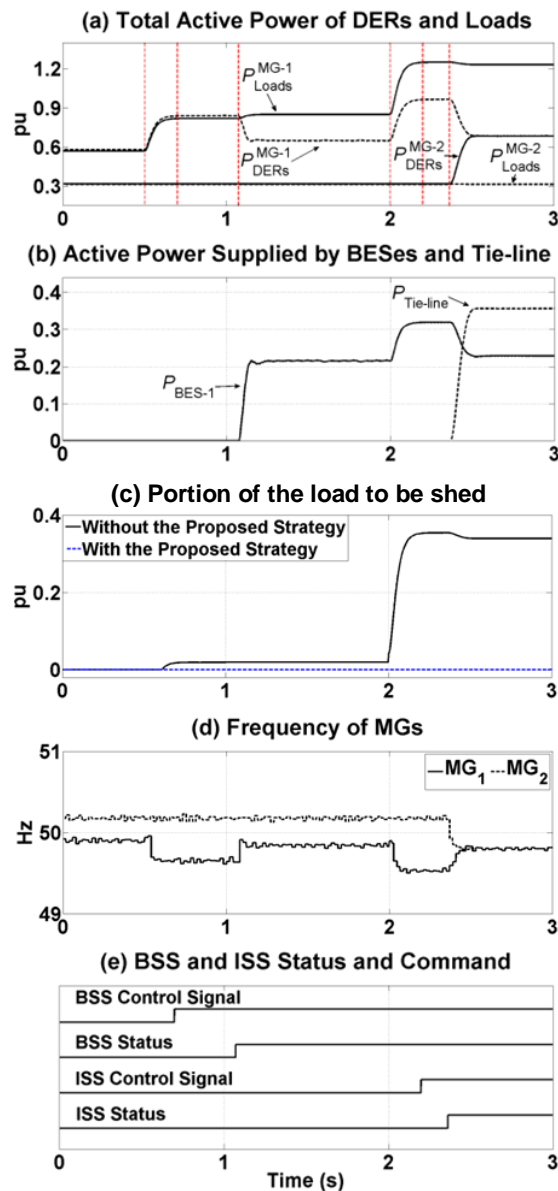


Fig. 4.15: Dynamic performance of the system with the decentralized approach, Case 1.

Table 4.9: Time sequence of the events in the system with the decentralized approach, Case 2.

| t (s) | Event | Outcome | Numerical Values: f [Hz], P [pu] |
|---------|-----------------------------------|--|--|
| 0 | CMG is operating at steady-state. | | $f_{\text{CMG}} = 49.80$, $P_{\text{Tie-line}} = 0.36$ |
| 0.3 | MG-1 demand reduces by 12%. | P_{CMG} decreases to supply the demand. | |
| 0.53 | Condition (23) is violated. | ISS opens, and CMG divides into 2 MGs. | $f_{\text{BMG-1}} = 49.66$, $f_{\text{MG-2}} = 50.18$ |

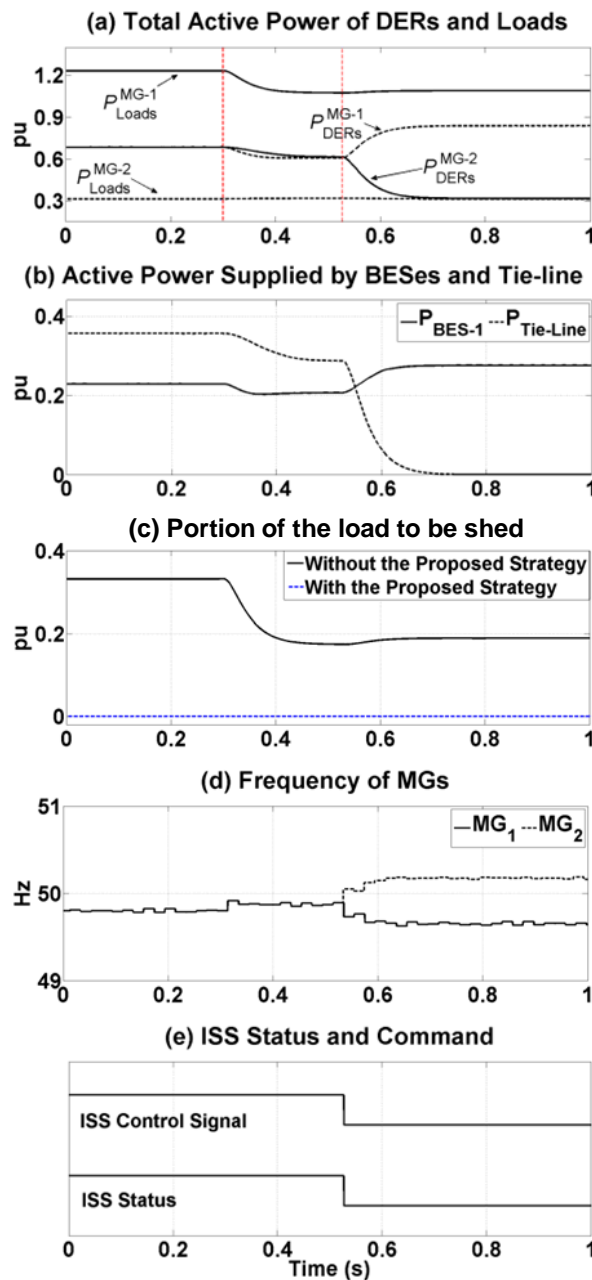


Fig. 4.16: Dynamic performance of the system with the decentralized approach, Case 2.

Table 4.10: Time sequence of the events in the system with the decentralized approach, Case 3.

| t (s) | Event | Outcome | Numerical Values: f [Hz], P [pu] |
|---------|---|---|--|
| 0 | CMG is operating at steady-state. | | $f_{\text{CMG}} = 49.80$, $P_{\text{Tie-line}} = 0.36$ |
| 0.5 | MG-2 demand increases by 116%. | P_{CMG} increases to supply the demand. | |
| 0.7 | BES-2's connection condition (26) is satisfied. | BSS activation command is initiated. | $f_{\text{CMG}} = 49.65$, $P_{\text{Tie-line}} = 0.14$ |
| 1.09 | Synchronization between BES-2 and CMG is achieved. | BSS closes, and BCMG is formed. | $f_{\text{BCMG}} = 49.75$, $P_{\text{BES-2}} = 0.25$ |
| 2.5 | MG-2 demand reduces by 80%. | P_{BCMG} decreases to supply the demand. | |
| 2.7 | Condition (29) is violated ($f_{\text{BCMG}} = 49.95$). | BSS opens, and BES-2 disconnects. | $f_{\text{CMG}} = 49.88$, $P_{\text{Tie-line}} = 0.46$ |

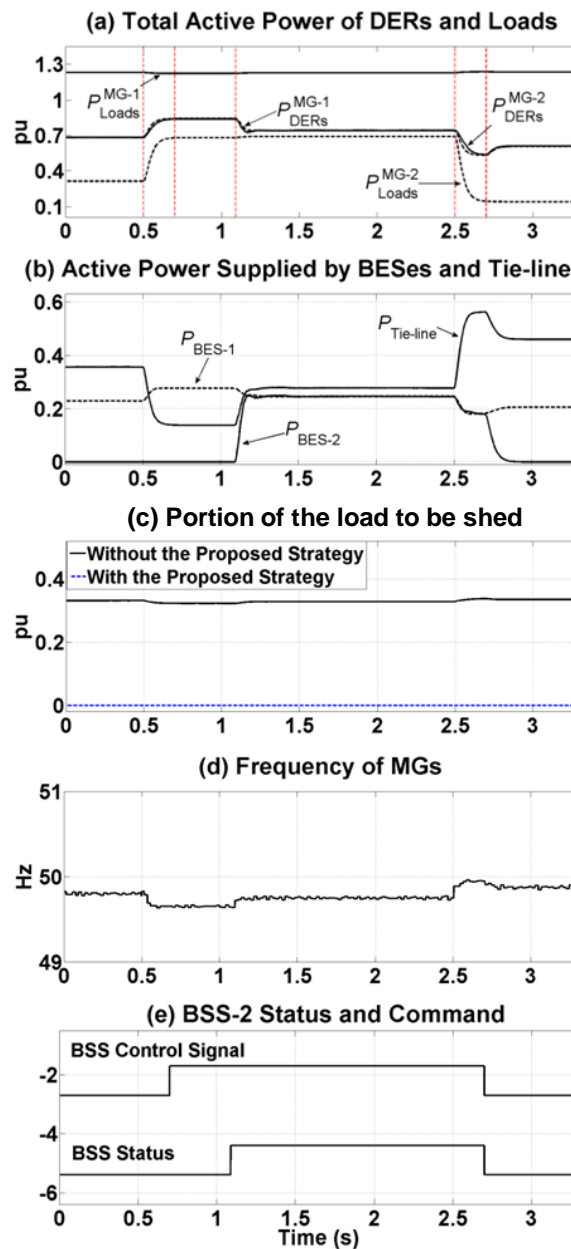


Fig. 4.17: Dynamic performance of the system with the decentralized approach, Case 3.

Table 4.11: Time sequence of the events in the system with the decentralized approach, Case 4.

| t (s) | Event | Outcome | Numerical Values: f [Hz], P [pu] |
|---------|--|--|--|
| 0 | CMG is operating at steady-state. | | $f_{\text{CMG}} = 49.80$, $P_{\text{Tie-line}} = 0.36$ |
| 0.2 | MG-2 demand increases by 167%. | P_{CMG} increases to supply the demand. | |
| 0.5 | BES-2 condition (26) is satisfied but its constraint is not satisfied. | BSS activation command is not allowed. | $f_{\text{CMG}} = 49.58$, $P_{\text{Tie-line}} = 0.04$ |
| 0.5 | Condition (24) is violated. Load-shedding is inevitable. | ISS opens, and CMG divides into 2 MGs. | $f_{\text{BMG-1}} = 49.53$, $f_{\text{MG-2}} = 49.69$ |

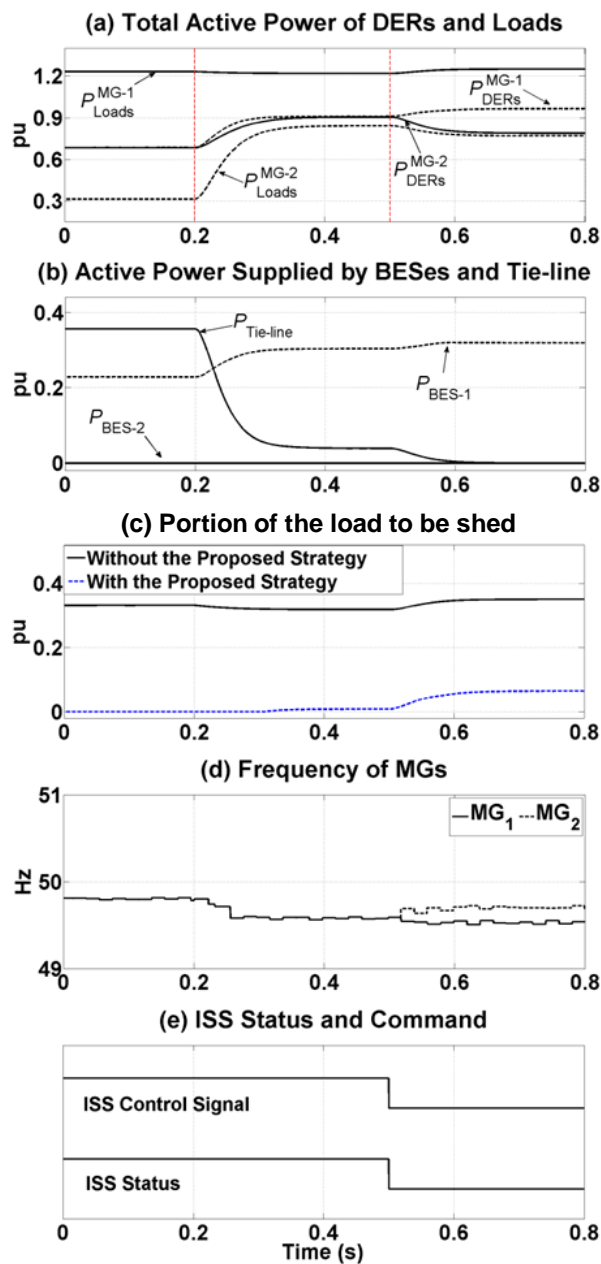


Fig. 4.18: Dynamic performance of the system with the decentralized approach, Case 4.

Table 4.12: Time sequence of the events in the system with the decentralized approach, Case 5.

| t (s) | Event | Outcome | Numerical Values: f [Hz], P [pu] |
|---------|--|---|--|
| 0 | CMG is operating at steady-state. | | $f_{\text{CMG}} = 49.80$, $P_{\text{Tie-line}} = 0.36$ |
| 0.5 | MG-2 demand increases by 116%. | P_{CMG} increases to supply the demand. | |
| 0.7 | BES-2 connection condition (26) is satisfied. | BSS activation command is initiated. | $f_{\text{CMG}} = 49.65$, $P_{\text{Tie-line}} = 0.14$ |
| 1.09 | Synchronization between BES and CMG is achieved. | BSS closes, and BCMG is formed. | $f_{\text{BCMG}} = 49.75$, $P_{\text{BES-2}} = 0.25$ |
| 2.5 | MG-2 demand increases by 27%. | P_{BCMG} increases to supply the demand. | |

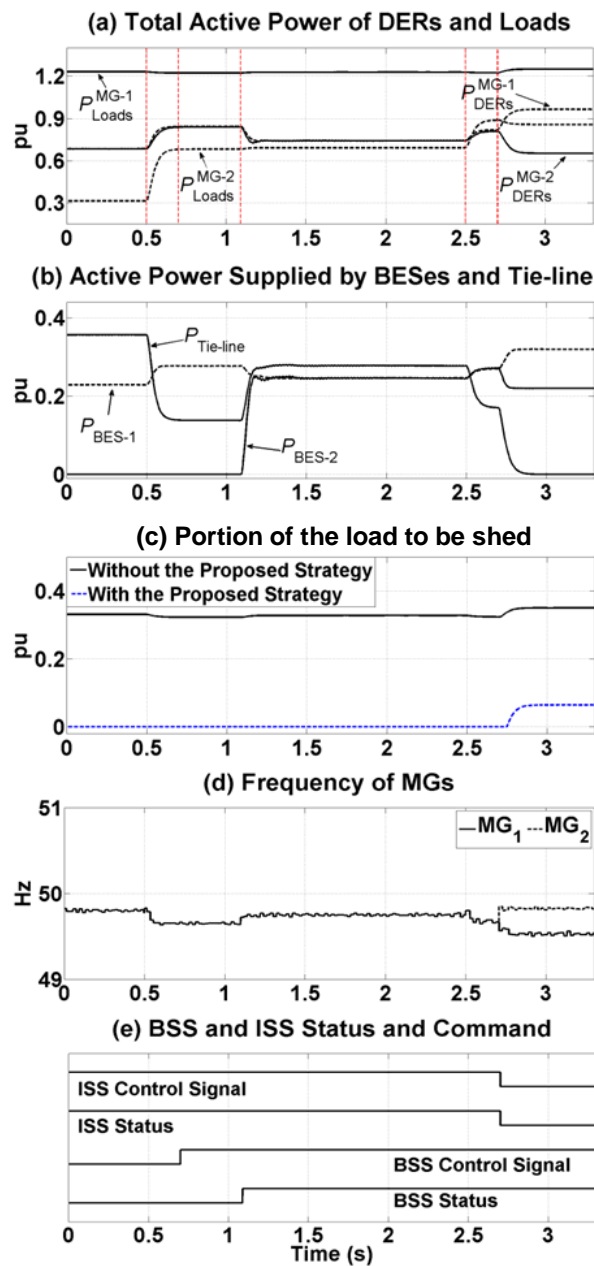


Fig. 4.19: Dynamic performance of the system with the decentralized approach, Case 5.

4.7 Small Signal Stability Analysis

In order to assess the stability of the formed CMG, SSS analysis should be fulfilled before allowing the modifications in each step of the power exchange strategy. The results of this analysis are used as a decision-making criterion for each connection (Fig. 4.3) [122]. If SSS analysis demonstrates instability, droop control parameters need to be updated accordingly to enable the system change.

4.7.1. Model derivation

Let us assume an MG with N_{bes} BESes. The small signal model of the MG consisting of converter interfaced DERs is explained in detail in Section 3.7. Likewise, each BES is connected to the MG through a converter, with the same structure and control method of the DER converters. Thus, the linearized state-space equations repressing the converter and filter output of BES- i is identical to (3.35) and can be expressed as

$$\Delta \dot{x}_{conv}^{BES-i} = A_{conv}^{BES-i} \Delta x_{conv}^{BES-i} + B_{conv}^{BES-i} (\Delta z_{conv}^{BES-i})^{ref} + C_{conv}^{BES-i} \Delta v_{conv}^{BES-i} \quad (4.43)$$

where $\Delta x_{conv}^{BES-i} = \Delta [i_{fd}^{BES-i} \quad i_{fq}^{BES-i} \quad i_{Td}^{BES-i} \quad i_{Tq}^{BES-i} \quad v_{cd}^{BES-i} \quad v_{cq}^{BES-i}]^T$.

Similar to (3.39)-(3.40), the instantaneous output active/reactive power of each BES as well as the angle of its output capacitor voltage can be expressed as

$$\begin{bmatrix} p \\ q \end{bmatrix}^{BES-i} = \frac{3}{2} \begin{bmatrix} i_{2d} & i_{2q} \\ -i_{2q} & i_{2d} \end{bmatrix}^{BES-i} \begin{bmatrix} v_{cd} \\ v_{cq} \end{bmatrix}^{BES-i} \quad (4.44)$$

$$\delta^{BES-i} = \int (\omega^{BES-i} - \omega_{com}) dt \quad (4.45)$$

On the other hand, a BES is characterized by its stored energy, which is calculated as

$$e^{BES-i}(t) = \int p^{BES-i} dt \quad (4.46)$$

where $p^{\text{BES-}i}$ is the output instantaneous active power described in (4.44). Now, linearizing the power and energy state equations of each BES around its operating point yields

$$\Delta \dot{x}_{\text{PQ}\varnothing e}^{\text{BES-}i} = A_{\text{PQ}\varnothing e}^{\text{BES-}i} \Delta x_{\text{PQ}\varnothing e}^{\text{BES-}i} + B_{\text{PQ}\varnothing e}^{\text{BES-}i} \Delta x_{\text{Bconv}}^{\text{BES-}i} + M_{\text{Bm}}^{\text{BES-}i} \Delta P_{\text{com}} \quad (4.47)$$

which can be expanded as

$$\Delta \begin{bmatrix} P \\ Q \\ \delta \\ e \end{bmatrix}^{\text{BES-}i} = \begin{bmatrix} -\omega_c & 0 & 0 & 0 \\ 0 & -\omega_c & 0 & 0 \\ -m_{\text{BES-}i} & 0 & 0 & 0 \\ 0 & 0 & 0 & 0 \end{bmatrix} \Delta \begin{bmatrix} P \\ Q \\ \delta \\ e \end{bmatrix}^{\text{BES-}i} + \frac{3}{2} \begin{bmatrix} 0 & 0 & v_{cd0}\omega_c & v_{cq0}\omega_c & i_{2d0}\omega_c & i_{2q0}\omega_c \\ 0 & 0 & v_{cq0}\omega_c & -v_{cd0}\omega_c & -i_{2q0}\omega_c & i_{2d0}\omega_c \\ 0 & 0 & 0 & 0 & 0 & 0 \\ 0 & 0 & v_{cd0} & v_{cq0} & i_{2d0} & i_{2q0} \end{bmatrix}^{\text{BES}} \Delta \begin{bmatrix} i_{1d} \\ i_{1q} \\ i_{2d} \\ i_{2q} \\ v_{cd} \\ v_{cq} \end{bmatrix}^{\text{BES-}i} + \begin{bmatrix} 0 \\ 0 \\ m_{\text{com}} \\ 0 \end{bmatrix} \Delta P_{\text{com}} \quad (4.48)$$

By modifying (4.47) with the procedure described in (3.43)-(3.45) the final linearized state-space equation for each BES consisting of all current, voltage, power, angle and energy states can be expressed as

$$\Delta \dot{x}_{\text{BES}}^{\text{Final}} = A_{\text{BES}}^{\text{Final}} \Delta x_{\text{BES}}^{\text{Final}} + C_{\text{MG}}^{\text{Final}} \Delta v_{\text{MG}} \quad (4.49)$$

where $x_{\text{BES}}^{\text{Final}} = [x_{\text{Bconv}} \quad x_{\text{PQ}\varnothing e}]^T$.

For a system of coupled MGs with one BES in each MG, which is referred to as BCMG in the rest of this section, the linearized state-space equation can be calculated by combining (3.36), (3.47) and (4.49) as

$$\Delta \dot{x}_{\text{BCMG}} = A_{\text{BCMG}} \Delta x_{\text{BCMG}} + C_{\text{BCMG}} \Delta v_{\text{BCMG}} \quad (4.50)$$

as expanded in

$$\Delta \begin{bmatrix} x_{MG-1}^{Final} \\ x_{BES-1}^{Final} \\ x_{MG-2}^{Final} \\ x_{BES-2}^{Final} \\ x_{Tie-line} \end{bmatrix} = \begin{bmatrix} A_{MG-1}^{Final} & O & O & O & O \\ O & A_{BES-1}^{Final} & O & O & O \\ O & O & A_{MG-2}^{Final} & O & O \\ O & O & O & A_{BES-2}^{Final} & O \\ O & O & O & O & A_{Tie-line} \end{bmatrix} \Delta \begin{bmatrix} x_{MG-1}^{Final} \\ x_{BES-1}^{Final} \\ x_{MG-2}^{Final} \\ x_{BES-2}^{Final} \\ x_{Tie-line} \end{bmatrix} + \begin{bmatrix} C_{MG-1}^{Final} & O \\ C_{BES-1}^{Final} & O \\ O & C_{MG-2}^{Final} \\ O & C_{BES-2}^{Final} \\ \hline C_{Tie-line} \end{bmatrix} \Delta \begin{bmatrix} v_{MG-1} \\ v_{MG-2} \end{bmatrix} \quad (4.51)$$

Assuming a large virtual resistor (e.g., $R_v = 10^4$) between each bus and ground, voltage of bus- j can be written as

$$v^j = R_v (i_2^j + \sum \mu^k i_{line}^k - i_{load}^j) \quad (4.52)$$

where $\mu^k = +1$ and -1 respectively represent the entering and exiting lines to bus j . Thus, Δv^j can be represented as a function of Δx_{BCMG} as

$$\Delta v^j = M_v^j \Delta x_{BCMG} \quad (4.53)$$

Hence, the voltage of all buses in BCMG is expressed as

$$\Delta v_{BCMG} = M_v \Delta x_{BCMG} \quad (4.54)$$

Assuming $A_{BCMG}^H = A_{BCMG} + C_{BCMG} M_v$, (4.50) is expressed in the homogeneous form of

$$\Delta \dot{x}_{BCMG} = A_{BCMG}^H \Delta x_{BCMG} \quad (4.55)$$

Since each BMG has $9N_c + 10N_{bes} + 2N_e + 2N_d$ states, the number of states of BCMG will be the sum of the states of each BMG plus two (for the tie-line interconnection the MGs).

Using (3.54), the eigenvalues of the system (λ) can be derived from (4.55). The impact of different parameters on the dominant modes should be carefully investigated. For this, the participation factor of the involved states, the damping

ratio of the modes, the undamped natural frequency of the modes, the period of each mode, and the number of cycles for a mode to damp by 50% should be computed using (3.55)-(3.60).

4.7.2. Stability evaluation

The stability of the considered BCMG of Fig. 4.2 is analysed based on the small signal model developed in MATLAB. This analysis shows that stability of the system depends mainly on the droop coefficients of the DERs and BESes as well as the SoC of the BESes. Fig. 4.20 illustrates the eigenvalues for the considered BCMG when m of DER₁₁ varies between 0.00023 and 0.023 rad/W, around the operation point of 0.002. From this figure, it can be seen that BCMG with $m=0.0186$ is marginally stable. It is to be noted that Fig. 4.20 is plotted by taking into account the droop coefficient of DER₁₁. Since the DERs in BCMG have different capacities and thus various values for the droop slopes, m of other DERs can be calculated from (2.16).

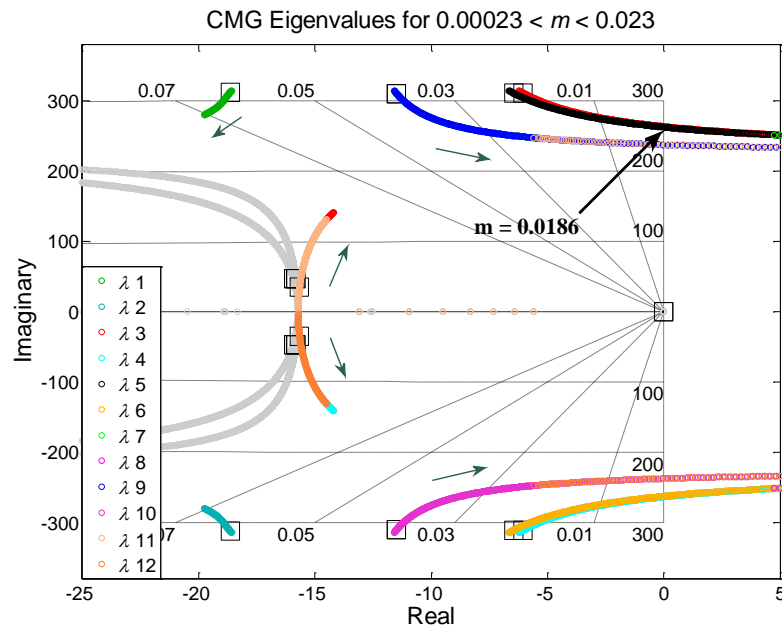


Fig. 4.20: Eigenvalue trajectory for the considered BCMG for variation of m .

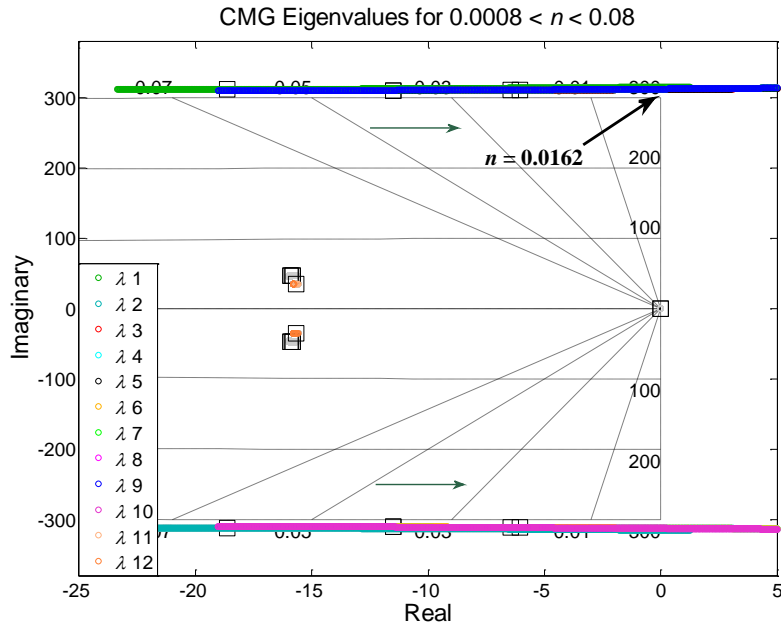


Fig. 4.21: Eigenvalue trajectory for the considered BCMG for variation of n .

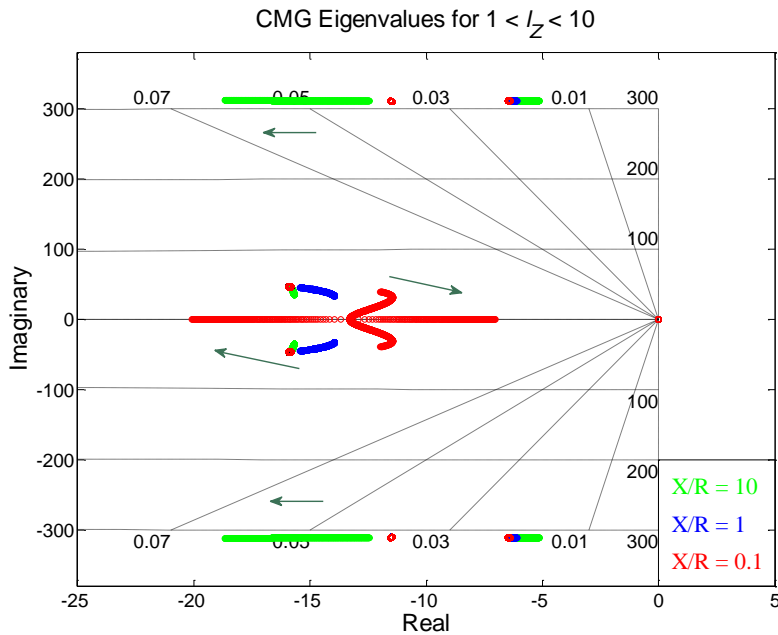


Fig. 4.22: Eigenvalue trajectory for the considered BCMG for variation of the tie-line impedance.

The SSS analysis is repeated for different values of n when it varies between 0.0008 and 0.08V/Var, around the operation point of 0.008. As can be seen from Fig. 4.21, the considered BCMG is marginally stable for $n=0.0162$ for DER₁₁. In such a case, n of other DERs can be calculated from (2.18).

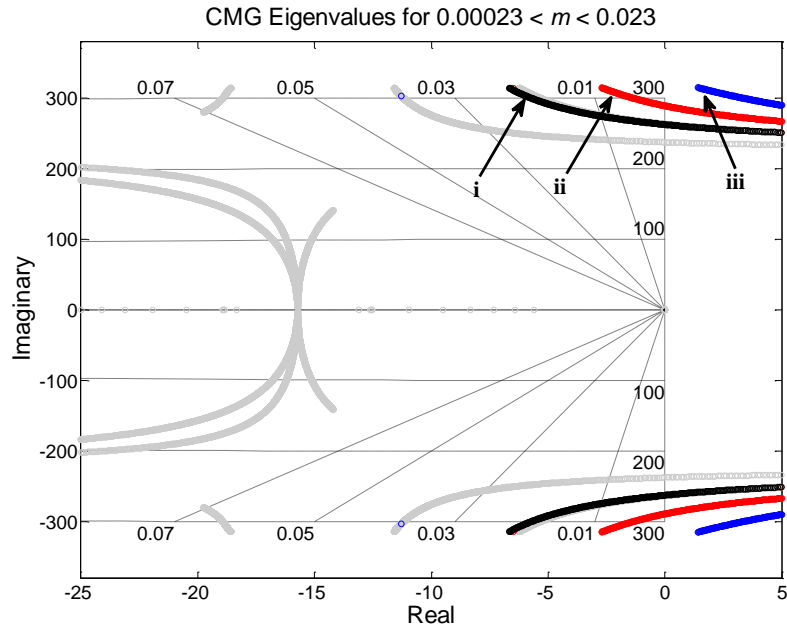


Fig. 4.23: Eigenvalue trajectory for the considered BCMG for SoC variation.

The SSS analysis is reiterated to evaluate the impact of the distance between two MGs. For this, the tie-line impedance is considered as $l_z \times Z_{\text{tie-line}}$, where l_z is varied between 1 and 10. The analysis is carried out assuming $X_{\text{tie-line}}$ is constant and equal to 0.2Ω [130] at the operating point while the tie-line X/R ratio is either 0.1, 1, or 10. The eigenvalues of BCMG when the impedance of the tie-line is varied in all three scenarios are shown in Fig. 4.22. This figure illustrates that the variations in the tie-line impedance of the considered BCMG do not lead to instability due to the comparatively large coupling inductances of the DERs.

The SSS analysis is applied to contemplate the significance of SoC of the BESes on the system stability. In this analysis, the SoC of BES-1 is 100% while SoC of BES-2 is varied from 100% (case-i) to 70% (case-ii), and 40% (case-iii). Fig. 4.23 illustrates the dominant eigenvalue trajectory for variation of the droop coefficient m of this analysis. From this figure, it can be seen that two modes are highly sensitive to the energy states of the BESes and move towards right s -plane as a BES's SoC reduces; thus, the marginal stability value of m decreases.

To examine the effect of the SoC of the BESes of each MG on BCMG's stability, a SSS-based sensitivity analysis is conducted in which m and n are varied as before while the SoC of both BESes is ranging from 30 to 100%. The

values of m and n for the marginally stable condition of BCMG are defined for every combination of SoCs. These two values are expressed as two new parameters of marginal frequency deviation (f_{Δ}) and marginal voltage deviation (V_{Δ}) in pu from (2.17).

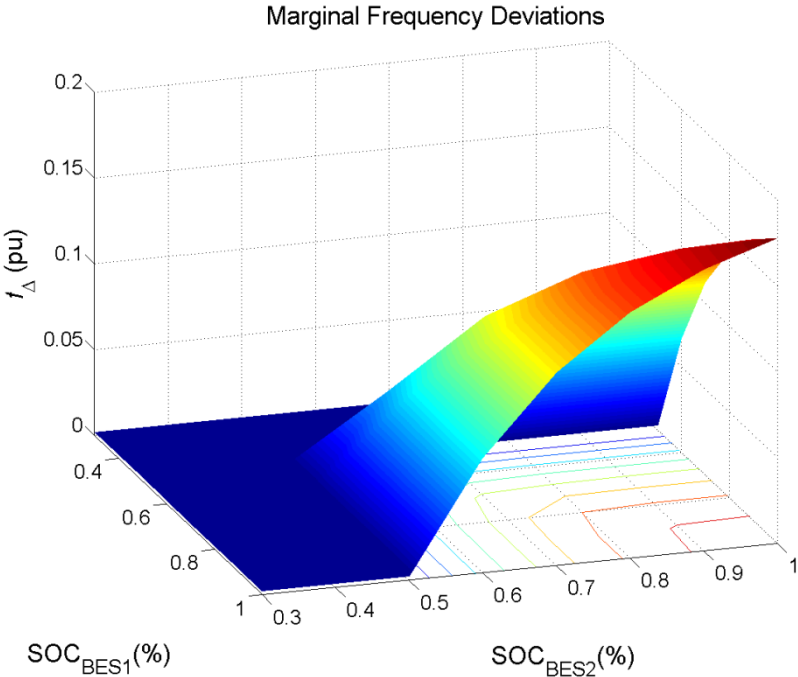


Fig. 4.24: Marginal frequency deviations of the BCMG.

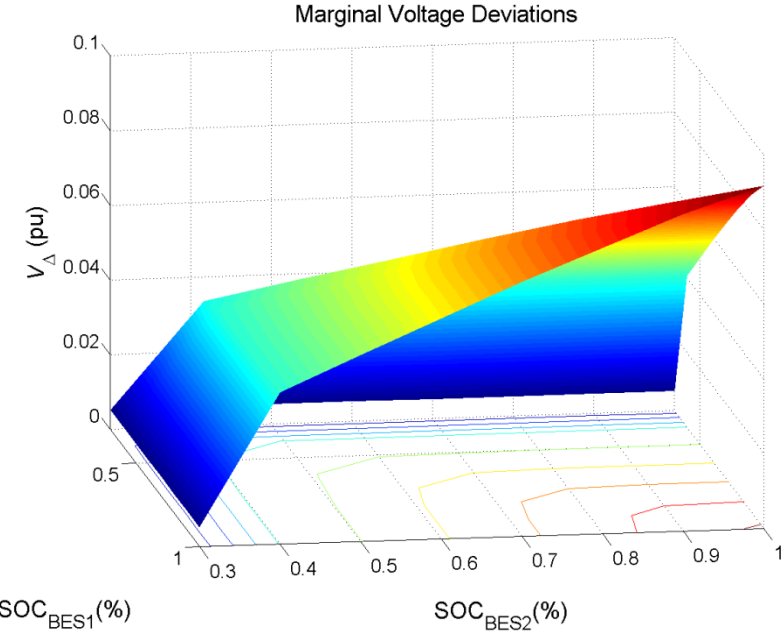


Fig. 4.25: Marginal voltage deviations of the BCMG.

The sensitivity analysis results are shown in Fig. 4.24 and Fig. 4.25. As it can be seen from these figures, the BCMG becomes unstable for smaller deviations in the voltage and frequency from their nominal values, as the SoC of the BESes reduces. However, the marginal values for the voltage and frequency deviations are considerable when the SoC of the BESes are of higher values.

Fig. 4.26 illustrates the values of the participation factor matrix for this system. As it is evident, each mode of the system is influenced by some of the states each with a different weighting. For example, state-73 and 74 which are the energy states of BES-1 and BES-2 (x_e), contribute to mode-1 and 2, respectively with a weighting of 100%. Similarly, mode-57 to 74 are highly influenced by active/reactive power and voltage angle states of DERs and BESes ($x_{PQ\delta}$).

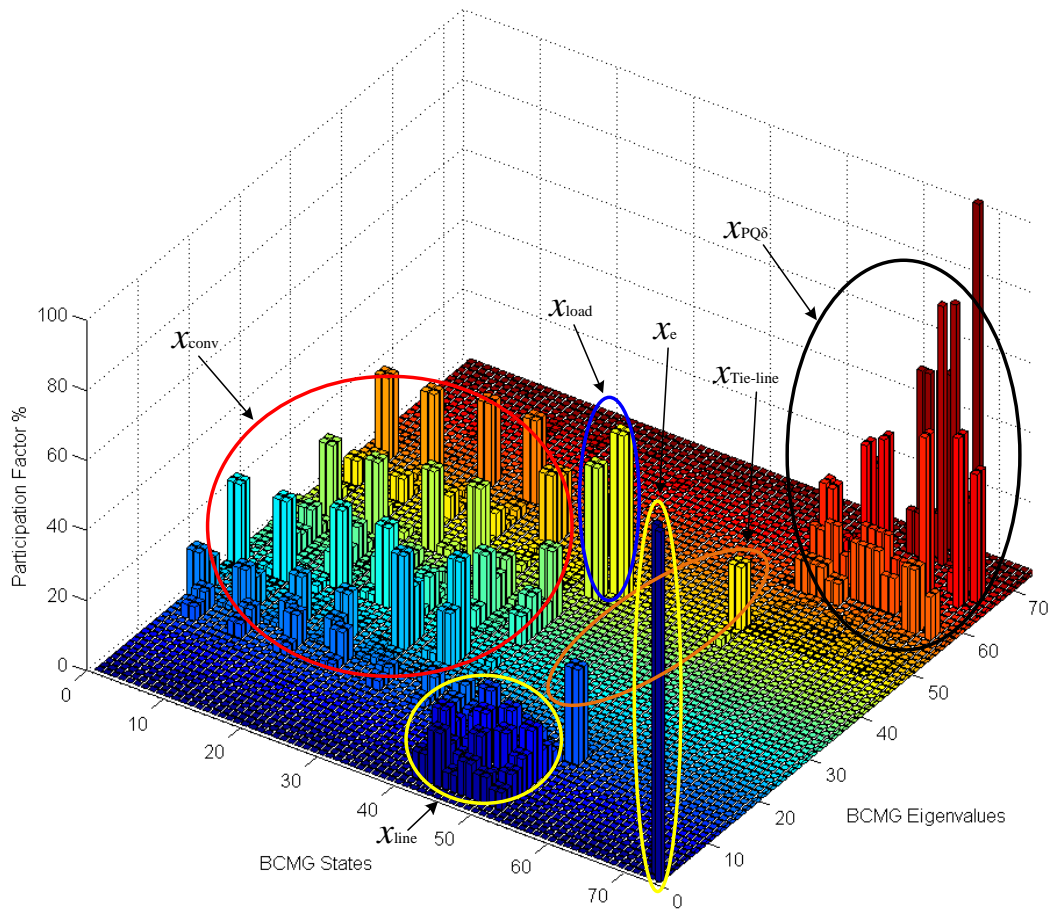


Fig. 4.26: Participation factor of each state on BCMG eigenvalues.

The dominant modes for the considered BCMG which tend to instability, when m and n are varied, are listed in Table 4.13 along with their damping ratio (ζ), undamped natural frequency (ω_n), oscillation period (T), and the number of cycles of its oscillations to damp by 50% ($NoC_{50\%}$) [129]. Also, the states with the highest impact on the dominant modes are shown with their relevant weightings.

Table 4.13: Dominant modes of the considered BCMG and their characteristics.

| Modes | Critical for | ζ | ω_n (rad/s) | T (s) | $NoC_{50\%}$ | Effective states (weightings %) |
|-------|--------------|---------|--------------------|---------|--------------|---|
| 1, 2 | n | 0.0597 | 312.06 | 0.0202 | 1.84 | $i_{TDER-11}, i_{TDER-12}, i_{TDER-21}, i_{TDER-22}$ (14); $i_{Tie-line}$ (36). |
| 3, 4 | m, n | 0.0194 | 310.56 | 0.0202 | 5.67 | i_{TBES-1}, i_{TBES-2} (36). |
| 5, 6 | m, n | 0.0208 | 310.48 | 0.0202 | 5.30 | i_{TBES-1}, i_{TBES-2} (40). |
| 7, 8 | m, n | 0.0371 | 310.29 | 0.0203 | 2.98 | $i_{TDER-11}, i_{TDER-12}$ (48). |
| 9,10 | m, n | 0.0370 | 310.29 | 0.0203 | 2.98 | $i_{TDER-21}, i_{TDER-22}$ (48). |
| 11,12 | m | 0.4084 | 38.32 | 0.1796 | 0.25 | $P_{DER-11}, P_{DER-12}, P_{DER-21}, P_{DER-22}$ (9); P_{BES-1}, P_{BES-2} (6); δ_{BES-2} (12); $\delta_{DER-21}, \delta_{DER-22}$ (18). |

4.8 Conclusion

A two-level power exchange strategy is developed in this chapter in order to decrease the rate and necessity of load-shedding in isolated sustainable MGs during power shortfalls. The PExS coordinates an internal support for an overloaded MG from its local BES and external support from a neighbouring MG, after their temporary interconnection. Based on the availability of the communication system, the PExS operates under decentralized or centralized approaches. Proper conditions and constraints are established for each level and each approach in order to manage both connection and disconnection of the ISS and BSSes. Through PSCAD/EMTDC-based simulation studies, it is demonstrated that the PExS agent can successfully detect overloading of the MG

and can take the appropriate steps after evaluating the formulated conditions and constraints.

A small signal model is formulated in detail for the considered isolated network including the DERs and BESEs. Then, stability of the system is evaluated for variations in various parameters. The SSS analysis demonstrates that stability of the BCMG highly depends on the droop curve coefficients of the DERs as well as the SoC of BESEs. It is revealed that the system is pushed towards instability when the SoC of the BESEs reduces.

Chapter 5. A HIERARCHICAL STRATEGY TO SUPPORT FREQUENCY IN ISOLATED MGS

The transition from oil-based MGS to the systems with significant renewable energy penetration is highly desirable for the remote areas that are rich in renewables [102]. The integration of renewable resources, however, can adversely affect the stability of an MG. Lack of appropriate measures to deal with their intermittency may lead to over-loading conditions, resulting in a frequency decrease in the MG [136]. A number of techniques such as utilizing extra-sized diesel generators along with employing energy storage systems are suggested in the literature in order to provide frequency support for isolated MGS. The installation and operating costs of an energy storage system nevertheless are considerable. Alternatively, the idea of coupling isolated MGS can be an economically preferred approach as it imposes almost no extra capital investment on the owners. In previous chapters, the power exchange strategies are presented to handle the power deficiency problem in isolated MGS assuming that forming a CMG removes the necessity of load shedding actions.

Under any of aforementioned techniques, however, there may be some occasions when the load demand is higher than the total generation capacity of a system, resulting in drastic frequency drops. In such circumstances, implementing an under frequency load shedding (UFLS) procedure is inevitable; otherwise, the MG would experience a black out. UFLS should be the last resort to maintain an MG frequency above the specified limits. Although a variety of UFLS algorithms have been presented for conventional power systems [137], deriving appropriate

techniques for isolated MGs is of great interest. Some significant concerns for an efficient UFLS scheme for isolated MGs are as follows:

- Minimum dependency on any communication system to enhance reliability of the system operation;
- Including a load prioritizing step, since controllable loads (CLs) may have different criticality and importance;
- Properly dispatching the required shed loads among the CLs of different priority types.

The above-mentioned significant aspects of decentralized load shedding actions within isolated MGs are not fully addressed yet. This simply means there is a research gap in terms of implementing a decentralized load shedding approach for isolated MGs. Moreover, although forming a CMG system using decentralized techniques has been reported in the literature, considerable impacts of a load shedding action on the interconnection constraints are neglected.

This chapter proposes a two-level hierarchical cooperative strategy to support frequency of isolated MGs during power shortfalls [118]. The primary level organizes proper dispatch of the required load to be shed among the participating CLs. For this, a multi-layer droop-based algorithm is developed to be embedded in controllers of the CLs. The secondary level of the strategy is responsible for forming a CMG system after evaluating the relevant conditions. A set of frequency-based criteria essential to guarantee the success of interconnection of two neighbouring isolated MGs in coping with the power deficiencies is defined and then, their accurate formulation is derived. The coordination between the two levels of the strategy is fulfilled such that their cooperative operation can facilitate the power deficiency management in remote areas.

5.1 Basic structure of the considered MG

Consider the isolated MG of Fig. 5.1, consisting of N_1 dispatchable DGs (DDGs), N_2 non-dispatchable DGs (NDDGs), N_3 CLs and N_4 uncontrollable loads (UCLs). In this section, the performance characteristics of these components are briefly described and reviewed.

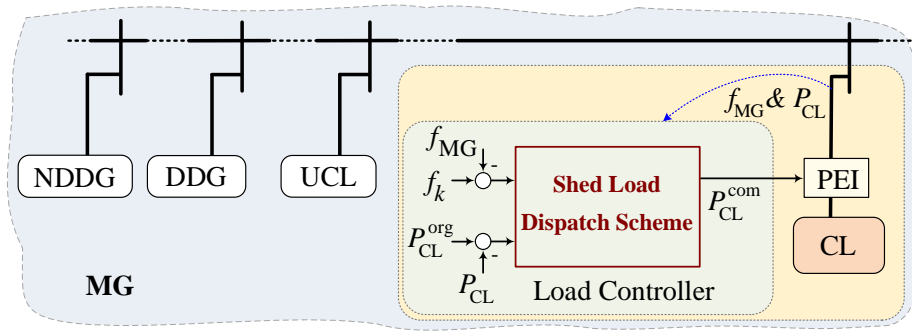


Fig. 5.1: An isolated microgrid consisting of the dispatchable and non-dispatchable DGs along with the controllable and uncontrollable loads.

The DDGs are responsible for adjusting frequency and voltage of this isolated MG. Voltage magnitude and frequency at the output of each DDG are regulated by droop control of (2.16). For each DDG, the droop slopes of the P - f and Q - V regulators, i.e., respectively m and n , are derived from (2.17).

Renewable NDDGs play the key role in the transition to oil-free sustainable MGs. However, frequency of an isolated MG may experience some unpleasant drops due to intermittent nature of these DGs. As an example, wind turbines operate over a limited range of wind speeds. The frequency drop is confronting since the turbine speed can rise above the cut-out speed typically in wind-rich areas [138]. It is assumed that each of NDDGs in Fig. 5.1 has its own maximum power point tracking (MPPT) block to ensure a maximum possible power will be generated. The employed control techniques are described in Section 2. 5.

Nowadays a considerable amount of electric loads of different sizes can be regarded as controllable loads since they include power electronics interface (PEI) that can manage their consuming power. These kinds of loads can usually show fast responses to their controlling signals, making them suitable from the load management point of view. In this chapter, it has been assumed that a CL is a controllable load that is equipped with a power electronics interface (PEI) and the controller of each PEI provides it with a proper power command, P_{CL}^{com} . The controllable loads which do not possess the PEI are considered as UCLs. The clusters of non-critical low-power loads controlled by an aggregator can also be included in the CLs since their aggregated behaviour becomes similar to controllable loads.

Taking into account the dissimilarities among the CLs in terms of criticality and flexibility, they should be given appropriate shedding priorities. Assuming CLs of Fig. 5.1 can be classified into N shedding priority levels, the first priority is assigned to the least significant type of the CLs. In normal conditions, P_{CL}^{com} is equal to the original value of a CL, P_{CL}^{org} , i.e., the power demand of the CL before applying any UFLS action that comes from a pre-specified demand profile. Under a power deficiency condition, however, controller of the CL should alter P_{CL}^{com} with the aim of providing the required support to the frequency. In this case, P_{CL}^{com} can be stated as

$$P_{CL}^{com} = P_{CL}^{org} - P_{CL}^{shd} \quad (5.1)$$

where P_{CL}^{shd} is the resultant shed term. The scheme based on which each controller extracts a proper share of the total required shed load is described in the next section.

5.2 Primary level of the proposed strategy

At the primary level of the strategy, the controllers of the CLs are responsible for shedding a portion of their load demand to prevent any frequency collapse in the MG. This should be done only by using local measurements under a decentralized scheme. Hence, controller of each CL continuously measures its consumed power, P_{CL} , and the MG frequency, f_{MG} . In the case of detecting a power deficiency, the controller should use this information to derive accurate shed load share of the CL such that no over- or under-shedding takes place. This algorithm is elaborated in the following subsections.

5.2.1 Load shedding criteria

Let us consider the MG of Fig. 5.1 wherein the overall demand should be supplied by both DDGs and NDDGs. The NDDGs generate the maximum possible power at each moment according to their MPPT control. Thus, the DDGs

should adjust their generation to maintain the power balance as they are responsible for regulating the MG frequency. For this, the following balance should be always retained

$$\sum_{i=1}^{N_1} P_{\text{DDG}-i} = \sum_{i=1}^{N_3} P_{\text{CL}-i} + \sum_{i=1}^{N_4} P_{\text{UCL}-i} - \sum_{i=1}^{N_2} P_{\text{NDDG}-i} \quad (5.2)$$

where P_{NDDG} and P_{UCL} indicate power output of each NDDG and load demand of each UCL respectively. Fig. 5.2a shows P - f droop curves for power sharing of DDGs, where the frequency decreases to f_{\min} if DDGs reach their rated values. However, it is desired to implement a UFLS action if the unused active power capacity of the DDGs is less than a specified threshold. Let this limit be α_1 times $P_{\text{DDG}}^{\text{cap}}$. Thus, MG is defined to be overloaded if

$$\sum_{i=1}^{N_1} P_{\text{DDG}-i}^{\text{cap}} - \sum_{i=1}^{N_1} P_{\text{DDG}-i} < \alpha_1 \sum_{i=1}^{N_1} P_{\text{DDG}-i}^{\text{cap}} \quad (5.3)$$

where $0 < \alpha_1 < 1$. According to (2.17), all DDGs have the same maximum frequency deviation. Therefore, (5.3) is satisfied if the unused power capacity in each DDG is less than α_1 times of the maximum capacity of that DDG as

$$P_{\text{DDG}-i}^{\text{cap}} - P_{\text{DDG}-i} < \alpha_1 P_{\text{DDG}-i}^{\text{cap}} \rightarrow P_{\text{DDG}-i}^{\text{cap}}(1 - \alpha_1) < P_{\text{DDG}-i}, \quad \forall i \in \{1, \dots, N_1\} \quad (5.4)$$

By substituting (2.17) and (5.4) in (2.16), (5.3) can be easily translated to its corresponding frequency as

$$\begin{aligned} f_{\text{MG}} &< f_{\text{shd}} \\ f_{\text{shd}} &= f_{\min} + \alpha_1(f_{\max} - f_{\min}) \end{aligned} \quad (5.5)$$

where f_{shd} is the frequency below which the MG is considered to be overloaded. Equation (5.5), calculated based only on local monitoring of the MG frequency, is utilized as triggering condition of the UFLS action. As soon as f_{MG} satisfies (5.5), the load controllers should react properly to shift the frequency up to f_{shd} . This guarantees the frequency stability at the cost of $100 \times \alpha_1\%$ less exploitation of the DDGs capacities.

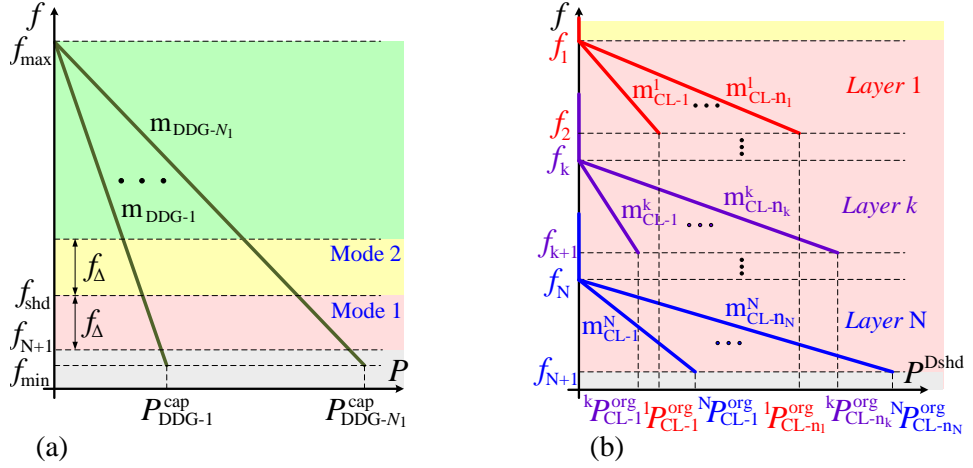


Fig. 5.2: (a) Power sharing droop curves of DDGs, (b) multi-layer shed load sharing curves of CLs

5.2.2 Demand prioritizing

Equation (5.5) is derived assuming all the CLs are of the same type. Now let us consider the CLs of Fig. 5.1 with N different types of shedding priority. Under a centralized strategy, the central controller sends the shedding command of each type of the CLs by using the employed communication infrastructure. Since a decentralized scheme is highly preferred for isolated MGs, the proposed method divides the overloading zone (i.e., the area between f_{shd} and f_{\min} as shown in Fig. 5.2a) to N separate horizontal frequency layers and then, assigns one layer to each type of the CLs, starting from those with the highest shedding priority. This means layer 1, shown in Fig. 5.2b, is dedicated to the least important type of CLs, Type-1, while layer N is allocated to the most significant type of the CLs, Type- N . In this regard, once the frequency falls below the upper limit of each layer, the members of that layer share the required shed load to shift up the frequency to the upper limit. Note that unlike the conventional droop-based load management mechanisms, the proposed scheme is capable of iterative execution to restore the frequency after its deviation (See Fig. 5.3). For instance, when f_{MG} drops below f_k , the top boundary of layer k , the scheme shares a corresponding shed load among n_k loads of Type- k to restore f_{MG} to f_k . By applying this strategy, f_{MG} never drops below f_{\min} even under severe deficiencies.

It is to be noted that the frequency layers may have different sizes depending upon designer's preferences. The height of each layer is desired to have a very small value in order to prevent further frequency drop. However, the minimum size of these layers is limited by the accuracy level of frequency measurement units since the layers should not have any overlaps. Assuming D_H is a minimum threshold to guarantee this, the size constraint for layer k can be described as

$$D_H \leq f_k - f_{k+1} \quad (5.6)$$

Therefore, although f_{shd} should be the upper boundary of layer 1, i.e., $f_1 = f_{\text{shd}}$, the lower limit of layer N can be a value larger than f_{min} , i.e., $f_{N+1} \geq f_{\text{min}}$.

5.2.3 Shed load dispatch

The idea is to define proper droop curves for each frequency layer to proportionally share the required shed load among CLs of the same type. Assume f_{MG} falls below f_k , the upper limit of layer k consisting of n_k loads. In order to achieve the proportional dispatch, the droop gain of the CLs is defined as

$$m_{\text{CL-}i} = \frac{\Delta f_k}{P_{\text{CL-}i}^{\text{org}}} = \frac{f_k - f_{k+1}}{P_{\text{CL-}i}^{\text{org}}} \quad (5.7)$$

where $1 < i < n_k$ and $P_{\text{CL-}i}^{\text{org}}$ indicates the original value of CL- i demanded when no UFLS action is applied. The coefficient $m_{\text{CL-}i}$ is dynamically adjusted in accordance with $P_{\text{CL-}i}^{\text{org}}$. Using (5.7), the shed dispatch of CL- i can be expressed as

$$P_{\text{CL-}i}^{\text{Dshd}} = \frac{f_k - f_{\text{MG}}}{f_k - f_{k+1}} P_{\text{CL-}i}^{\text{org}} \quad (5.8)$$

This means when the frequency decreases from f_k to f_{k+1} , the shed term increases from zero to the maximum level, $P_{\text{CL-}i}^{\text{org}}$. Now the load command sent by the controller is

$$P_{\text{CL-}i}^{\text{com}} = P_{\text{CL-}i} - P_{\text{CL-}i}^{\text{Dshd}} \quad (5.9)$$

where $P_{\text{CL-}i}$ is the power consumed by CL- i during the UFLS action. Iteratively, the frequency deviation from f_k is measured and then, its corresponding power

calculated by (5.8) is decreased from the load demand to maintain the MG frequency at f_k . Thus, the overall shed part of CL- i , P_{CL-i}^{shd} , is the summation of all partially curtailed terms expressed as

$$P_{CL-i}^{\text{shd}} = P_{CL-i}^{\text{org}} - P_{CL-i} \quad (5.10)$$

The power command derived by (5.9) can efficiently fulfil the desired UFLS process. If during the shedding stage, however, P_{CL-i}^{org} decreases to a value smaller than P_{CL-i} , the command should be altered as

$$P_{CL-i}^{\text{com}} = P_{CL-i}^{\text{org}} \quad (5.11)$$

After applying (5.11), if the MG frequency increases above f_k , no more load shedding is required. Otherwise, the shedding action carries on by updating the droop gain in (5.7).

5.2.4 Demand restoration

Let us assume the explained approach restores the MG frequency to f_k . Now, it is desired to not change the demand as long as the frequency satisfies the following criterion

$$f_k \leq f_{\text{MG}} < f_k + \varepsilon_f \quad (5.12)$$

where ε_f is used in order to include a dead-band boundary to protect CLs against chattering. Thus, while the frequency meets (5.12), the command generated by the controller of CL- i is

$$P_{CL-i}^{\text{com}} = P_{CL-i} \quad (5.13)$$

Accordingly, one can say that the load shedding target is to maintain the MG frequency between f_k and $f_k + \varepsilon_f$. If during this period, however, P_{CL-i}^{org} reduces to a value smaller than P_{CL-i} , the power command should switch to (5.11).

However, if for any reason f_{MG} rises above the upper boundary of (5.12), the load shedding necessity is removed and a demand restoration process should be implemented. The restoration is desired to be realized by employing the droop

coefficients defined in (5.7), as is shown in Fig. 5.3. Therefore, the portion of P_{CL-i}^{shd} to be restored can be expressed as

$$P_{CL-i}^{Drest} = \frac{f_{MG} - f_k}{f_k - f_{k+1}} P_{CL-i}^{shd} \quad (5.14)$$

Accordingly, the controller should send a command as

$$P_{CL-i}^{com} = P_{CL-i} + P_{CL-i}^{Drest} \quad (5.15)$$

By applying (5.15), the restoration process fulfils in proportion to the shed terms of the CLs. Now, if during this action f_{MG} falls again to the limits of (5.12), the restoration is accomplished partially and the controller command switches back to (5.13).

Whether the shed term of CL- i restores partially or completely depends upon the available unused power capacity (AUPC) of the MG. In fact, AUPC can be described as a value that if the total generation of DDGs is increased by which, f_{MG} decreases to f_k . In case of a partial restoration, AUPC is smaller than the total shed parts of the CLs of Type- k and can be stated as

$$AUPC = \frac{f_{MG} - f_k}{m_{CL}^{Type-k}} \quad (5.16)$$

where m_{CL}^{Type-k} is the equivalent droop coefficient of all the CLs of Type- k described by

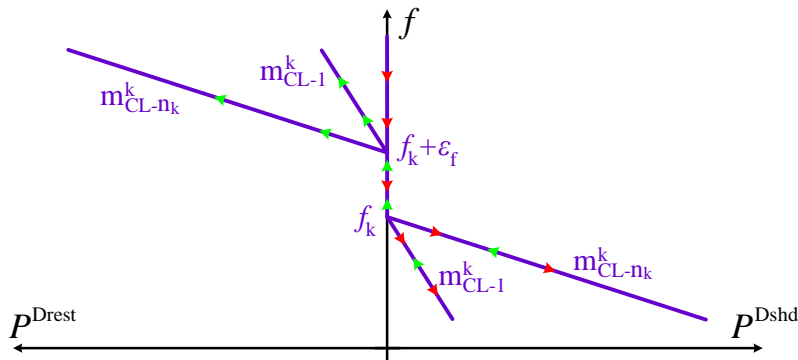


Fig. 5.3: Load shedding and restoring curves of layer k.

$$m_{CL}^{\text{Type-}k} = \frac{1}{\sum_{i=1}^{n_k} \frac{1}{m_{CL-i}}} \quad (5.17)$$

It is to be noted that the UFLS process terminates if P_{CL-i}^{shd} is not positive. This takes place if either the total shed part of CL- i is restored or, during the restoration step, P_{CL-i}^{org} decreases to a value smaller than P_{CL-i} .

5.2.5 Execution of the primary level

The developed scheme has a fully decentralized structure and performs without requiring any communication infrastructure. Fig. 5.4 shows flowchart of the scheme for CL- i of layer k . In normal conditions, this scheme does not interfere the load control process. However, as soon as f_{MG} drops below f_k , it initiates by fetching P_{CL-i}^{org} to derive the droop slope. Then, the frequency deviation, $\Delta f = f_k - f_{MG}$, along with the shed load, P_{CL-i}^{shd} , are calculated. Four different states are possible as stated below

State 1: the MG suffers from power deficiency that drops its frequency below f_k while the present demand of CL- i is not larger than P_{CL-i}^{org} . This means a portion of load specified in (5.8) should be shed. Thus, the controller sends a command as in (5.9).

State 2: the UFLS process has been successful to shift the frequency above f_k . Now the frequency satisfies (5.12) while P_{CL-i}^{org} is still larger than the present demand of CL- i . Since this condition is satisfactory, the controller yields its command signal as in (5.13).

State 3: the frequency rises above the upper limit of (5.12), which means the shortfall is alleviated. Now, the shed term of CL- i should be restored either partially or completely. Hence, the controller employs (5.15) to restore the power specified in (5.14).

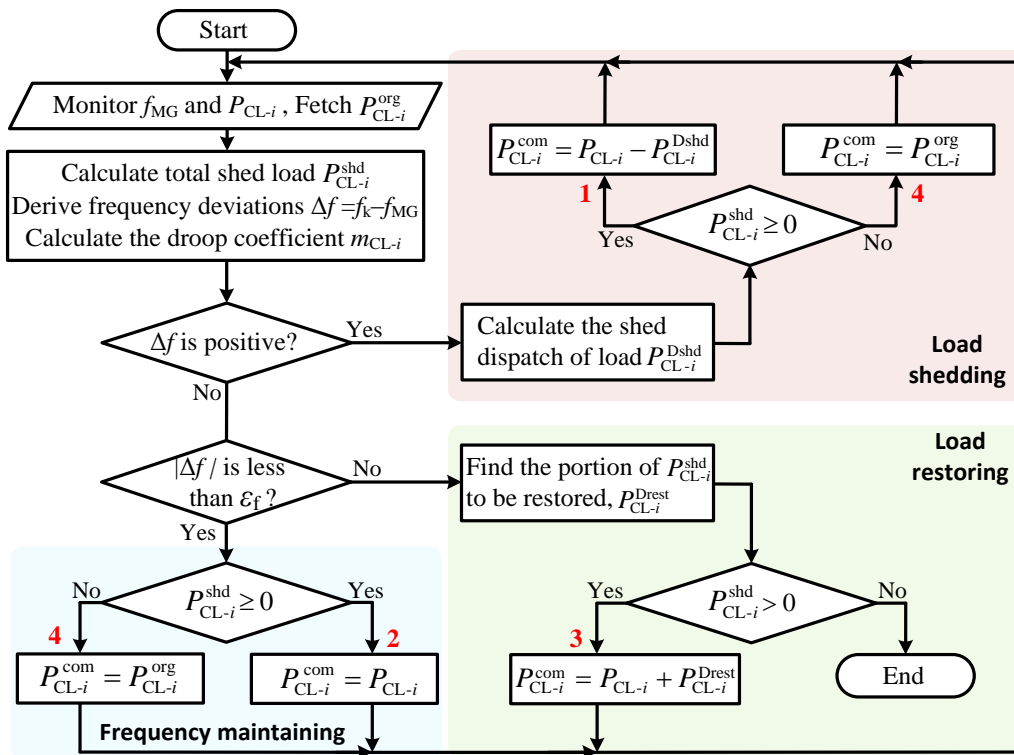


Fig. 5.4: Flowchart of the proposed shed load dispatching scheme.

State 4: the conditions of either state 1 or state 2 are fulfilled. But, P_{CL-i}^{org} decreases to a value smaller than the present demand of CL- i . Thus, the controller sends a command (5.11) to reduce the demand to P_{CL-i}^{org} . This may remove the power deficiency without necessitating a UFLS action.

It is to be noted that the algorithm terminates if the frequency rises above the top threshold of (5.12) while P_{CL-i}^{shd} is not positive anymore. The latter occurs if either the shed term of the load is restored completely or P_{CL-i}^{org} becomes less than P_{CL-i} .

5.3 Secondary level of the proposed strategy

The idea is to interconnect two isolated MGs if one of them suffers from power deficiency while DGs of the other one have surplus generation capacity. Consider the system of two isolated MGs shown in Fig. 5.5. In this system, both MG-1 and MG-2 include the components demonstrated in Fig. 5.1, and DDGs of each MG are regulated by droop control with the same maximum frequency

deviations. The interconnection can be done by closing an ISS sited on the tie-line. By forming a CMG, the total load will be shared by DGs of the both MGs.

In this section, a comprehensive CMG forming technique is developed to operate as the secondary level of the proposed hierarchical strategy. The accurate coordination between the two levels of the strategy is elaborated such that the power shortfalls can be successfully managed by the cooperation of the levels. Note that the ISS controller implements the secondary level merely by local monitoring of frequencies at two sides of the ISS.

5.3.1 Operating modes of the CLs

The shed load dispatching and CMG forming schemes can be employed individually under a communication-free structure. Their cooperative performance, on the other hand, requires a very low-bandwidth communication system as the CLs should alter their working algorithm in accordance with the ISS status. In this sense, three different operating modes are defined for a CL as below

Mode 1: The ISS is open and the MGs are isolated. The CL works complying with the algorithm described in Section 5.2.

Mode 2: A CMG is formed and the neighbouring MG sends a supporting power to the MG of the CL. In this case, as seen in Fig. 5.2a, the CL should shift its assigned layer upward by

$$f_{\Delta} = f_{\text{shd}} - f_{\text{N}} \quad (5.18)$$

For example, the CLs of layer k should apply the following substitutions

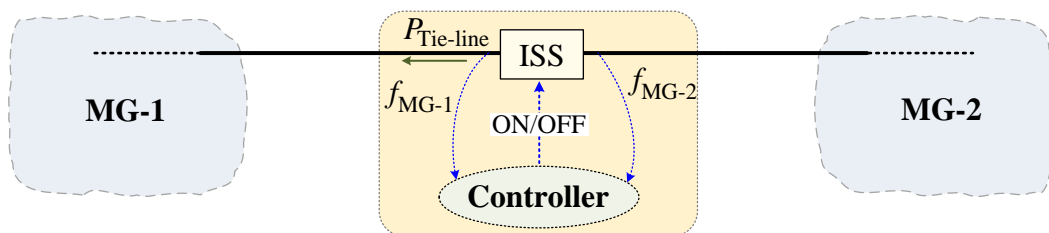


Fig. 5.5: Distribution network of a remote area consisting of two isolated MGs.

$$f_k + f_\Delta \rightarrow f_k \quad \text{and} \quad f_{k+1} + f_\Delta \rightarrow f_{k+1}$$

This enables the CL to fulfill desirably the primary level of the strategy within the CMG.

Mode 3: ISS is closed and the MG of the CL sends a supporting power to the neighbouring MG. Now the primary level scheme should be deactivated for the CL as any power deficiency in the system should be cured only by shedding the CLs of the overloaded MG.

The ISS controller should notify the CLs of both MGs to alter their operating modes accordingly if any change takes place on the status of the ISS. The transition diagram of the operating modes for a CL of layer k is shown in Fig. 5.6.

5.3.2 Coupling algorithm

Let us assume (5.5) defines the overloading threshold for MG-1, initiating the primary level scheme in its CLs. Accordingly, it is desired to launch the MGs coupling procedure if

$$f_{\text{MG-1}} < f_{\text{cpl}} \tag{5.19}$$

where $f_{\text{cpl}} = f_{\text{shd}} + \epsilon_f$. Note that applying the primary level scheme may raise the frequency above f_{shd} (see (5.12)). Thus, selecting the coupling condition as (5.19) ensures proper execution of the interconnection procedure even after the proposed frequency recovery.

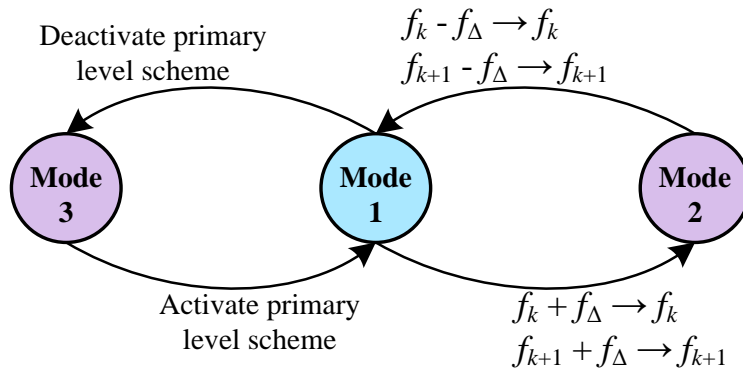


Fig. 5.6: Transition of the operating modes by receiving a notification signal.

Note that fulfilment of (5.19) necessitates coupling of the two neighbouring MGs subject to the fact that after the interconnection, the system of CMG is neither overloaded nor over-shed. In other words, the overloading along with the over-shedding possibilities of the CMG should be evaluated prior to the actual closing of the ISS. For this, let us assume that the CMG is just formed. Now, the following concerns should be taken into account:

- If the CMG frequency, f_{CMG} , still remains below f_{shd} , not only overloading of MG-1 is not relieved but also a power shortfall is imposed on MG-2.
- The CL controllers in MG-1 adopt operating mode 2, thereby shifting their layers upward by f_{Δ} to a position in between f_{shd} and $f_{\text{shd}} + f_{\Delta}$ (see (5.18)). Assume $f_{\text{MG-1}}$ was in layer j at the interconnection moment. Now, if f_{CMG} goes to layer k , $k < j$, forming a CMG results in an over-shedding condition.

In order to address the above challenges, capability of f_{CMG} to satisfy the following constraint should be confirmed before closing the ISS

$$f_{\text{CMG}} > f_{\text{shd}} + f_{\Delta} \quad (5.20)$$

It is to be emphasized that (5.20) describes the system frequency nearly after closing the ISS and before initiating any primary level action. Substituting (5.5) in (5.20) yields

$$f_{\text{CMG}} > f_{\text{min}} + \alpha_1(f_{\text{max}} - f_{\text{min}}) + f_{\Delta} \quad (5.21)$$

which can be rewritten as

$$f_{\text{CMG}} > f_{\text{min}} + \alpha_2(f_{\text{max}} - f_{\text{min}}) \quad (5.22)$$

where

$$\alpha_2 = \alpha_1 + \frac{f_{\Delta}}{f_{\text{max}} - f_{\text{min}}} \quad (5.23)$$

Equation (5.22) introduces a threshold for the frequency of CMG above which a successful interconnection is expected. Note that f_{CMG} is only available after closing the ISS. Thus, (5.24)-(5.32) are formulated to derive a more practical

criterion corresponding to (5.22) which is based on the frequencies of the MGs before the interconnection. Subtracting f_{\max} from both sides of (5.22) and then, simplifying the result yields

$$f_{\max} - f_{\text{CMG}} < (f_{\max} - f_{\min})(1 - \alpha_2) \quad (5.24)$$

Note that DDGs of both MGs are regulated by droop controllers. For each DDG of the CMG, thus, replacing equivalent of $(f_{\max} - f_{\min})$ from (2.17) in (5.24) results in

$$\frac{f_{\max} - f_{\text{CMG}}}{m_{\text{DDG-}i}} < P_{\text{DDG-}i}^{\text{cap}}(1 - \alpha_2) \quad (5.25)$$

where $1 \leq i \leq [(N_1)_{\text{MG-1}} + (N_1)_{\text{MG-2}}]$. The left-hand side of (5.25) can be substituted by (2.16) as

$$P_{\text{DDG-}i} < P_{\text{DDG-}i}^{\text{cap}}(1 - \alpha_2) \quad (5.26)$$

Since (5.26) is valid for all DDGs of the CMG, the following expression can be derived

$$P_{\text{CMG}} < P_{\text{CMG}}^{\text{cap}}(1 - \alpha_2) \quad (5.27)$$

where $P_{\text{CMG}}^{\text{cap}}$ and P_{CMG} are total power capacity and power output of all DDGs. Equation (5.27) considers the CMG before restoring any shed load. Thus, P_{CMG} in (5.27) is equivalent to the summation of total P_{DDGS} of both MG-1 and MG-2 at the closing moment of the ISS as

$$P_{\text{CMG}} = \left(\sum_{i=1}^{N_1} P_{\text{DDG-}i} \right)_{\text{MG-1}} + \left(\sum_{i=1}^{N_1} P_{\text{DDG-}i} \right)_{\text{MG-2}} \quad (5.28)$$

Applying (2.16) in (5.28) yields

$$P_{\text{CMG}} = \left(\sum_{i=1}^{N_1} \frac{f_{\max} - f_{\text{MG-1}}}{m_{\text{DDG-}i}} \right)_{\text{MG-1}} + \left(\sum_{i=1}^{N_1} \frac{f_{\max} - f_{\text{MG-2}}}{m_{\text{DDG-}i}} \right)_{\text{MG-2}} \quad (5.29)$$

By replacing (5.29) in (5.27), the interconnection constraint can be expressed as

$$f_{MG-2} > f_{\max} - \left(m_{DDG}^{MG}\right)_{MG-2} \times \left[(1 - \alpha_2) P_{CMG}^{cap} - f_{\max} - f_{MG-1} / \left(m_{DDG}^{MG}\right)_{MG-1} \right] \quad (5.30)$$

where m_{DDG}^{MG} is the equivalent droop coefficient of all DDGs of an MG which can be explained as

$$m_{DDG}^{MG} = 1 / \sum_{i=1}^{N_1} \frac{1}{m_{DDG-i}} \quad (5.31)$$

and P_{CMG}^{cap} indicates total power capacity of all DDGs of the CMG described as

$$P_{CMG}^{cap} = \left(\sum_{i=1}^{N_1} P_{DDG-i}^{cap} \right)_{MG-1} + \left(\sum_{i=1}^{N_1} P_{DDG-i}^{cap} \right)_{MG-2} \quad (5.32)$$

Now (5.30), as an equivalent to (5.22), defines a threshold for the frequency of MG-2 above which interconnection of the two MGs will cause neither an overloading nor an over-shedding condition in the CMG system. Thereby, the controller sends an activation command to the ISS if both (5.19) and (5.30) are met. Afterward, the ISS closes when voltages at the two sides of the ISS synchronize.

5.3.3 Fulfilling the primary level scheme in the CMG

Since the coupling postpones to the moment at which the synchronization between the voltages at the two sides of the ISS is achieved, the CL controllers of MG-1 implement the primary level scheme under operating mode 1. Once a CMG is formed, both MGs operate at a new frequency of f_{CMG} and an active power of $P_{Tie-line}$ flows from MG-2 to MG-1. The ISS informs its new status to CLs of both MGs; thereby forcing CLs of MG-1 and MG-2 to comply with operating modes 2 and 3 respectively. Two situations are elaborated below for the performance of the primary level scheme within a CMG.

1) REMOVAL OF THE LOAD SHEDDING NECESSITY

Assuming MG-2 can provide MG-1 with the sufficient amount of supporting power, all shed loads of MG-1 will be restored once the CMG is formed. After the restoration phase, the power consumption of MG-1 (P_{MG-1}) can be expressed as

$$P_{MG-1} = \left(\sum_{i=1}^{N_1} P_{DDG-i} \right)_{MG-1} + P_{Tie-line} \quad (5.33)$$

Let us assume the unused power capacity in MG-1 is less than $\alpha_1(1+\varepsilon)$ times of the total maximum capacity of all DDGs. This can be expressed as

$$(P_{DDGs}^{cap})_{MG-1} - P_{MG-1} < \alpha_1(1 + \varepsilon)(P_{DDGs}^{cap})_{MG-1} \quad (5.34)$$

where

$$(P_{DDGs}^{cap})_{MG-1} = \left(\sum_{i=1}^{N_1} P_{DDG-i}^{cap} \right)_{MG-1} \quad (5.35)$$

by applying (2.16) and (5.33), (5.34) can be rearranged as

$$P_{Tie-line} > \left[1 - \alpha_1(1 + \varepsilon) \right] (P_{DDGs}^{cap})_{MG-1} - \frac{(f_{max} - f_{CMG})}{\left(m_{DDG}^{MG} \right)_{MG-1}} \quad (5.36)$$

Equation (5.36) defines a threshold for $P_{Tie-line}$ above which the interconnection should be maintained. However, in case $P_{Tie-line}$ drops below this limit while the frequency satisfies

$$f_{CMG} \geq f_{shd} + f_{\Delta} \quad (5.37)$$

Then the support of MG-2 for MG-1 is not required anymore and the ISS should open.

2) LOAD SHEDDING IN THE CMG

Violation of (5.37) means the overloading condition is severe, requiring a load shedding action within the CMG. Hence, the CLs of MG-1 should utilize the primary level scheme under operating mode 2. In this regard, the cooperation of both levels of the proposed strategy can successfully manage the power deficiency such that the minimum possible portions of the CLs are shed and the frequency is maintained above f_{shd} . For this case, the following scenarios are relevant:

- Forming the CMG may only lead to a partial restoration of the shed loads due to severe power deficiencies before the interconnection.
- After the interconnection, if MG-1 experiences a further power shortfall that results in a frequency drop below $f_{\text{shd}} + f_{\Delta}$, the load shedding is inevitable.
- The supporting power $P_{\text{Tie-line}}$ may reduce because of either a decrease in power generation or an increase in power demand of MG-2. As a result, the CL controllers of MG-1 should apply the shed load dispatch scheme in order to prevent the further drop in the frequency. Note that although $P_{\text{Tie-line}}$ decreases, MG-2 still supports MG-1.

In regards to the above scenarios, the CMG is sustained as long as the frequency is larger than f_{shd} while the supporting power is positive. Otherwise, the ISS controller sends a command to open the ISS as none of the MGs can provide its neighbour with any support. Thus, the CMG divides into two isolated MGs.

5.4 Performance evaluation

In order to appraise the performance of the developed strategy, several simulation case studies are carried out in PSCAD/EMTDC, a few of which are described below. Let us consider the network of Fig. 5.1 with two types of CLs, namely Type-1, consisting of CL-1 and CL-2 as the least important controllable loads of the MG, and Type-2, consisting of CL-3 and CL-4 as the most important controllable loads of the MG. Thus, two layers of droop curves are considered in the primary level scheme of the proposed strategy. A height of 0.02 Hz is selected for each layer assuming this value satisfies (5.6). General structure and control mechanism of the CLs are discussed below. Also, the MG benefits from an NDDG that is simply called the wind generator (WG).

Fig. 5.7a shows control structure of a load controller. As long as there is no need to perform load shedding, a CL is supplied via normally-closed bypass switches whereas the inverter switches are blocked. Once the necessity of the load shedding is detected by the controller, it activates the inverter by opening up the bypass switches. From this point on, the PEI injects $P_{\text{CL}}^{\text{com}}$ and $Q_{\text{CL}}^{\text{com}}$ to the load

where the former is extracted using the algorithm shown in Fig. 5.4 while the latter is the reactive power demand of the CL.

Let us consider single line diagram of the PEI during load shedding actions, as shown in Fig. 5.7. An LCL filter structure is chosen to suppress the switching harmonics. The resistance R_f is included to model the switching losses. In order to deliver the powers to the CL, the reference voltage across the filtering capacitor, $V_c^{com} \angle \delta_c^{com}$, should be computed based on the PQ-based reference generation which can be expressed as (2.20).

Generally, UFLS strategies focus on presenting proper active power managements due to the fact that under frequency challenges are directly related to the generation and consumption levels of active powers. Although the reactive power management is not usually mentioned in such researches, it is certainly performed using one of the already presented appropriate methods. Likewise, under voltage load shedding articles usually focus on the reactive power control only without mentioning the active power flow. In this research, the reactive power flow and bus voltages are satisfactorily controlled by the DDGs based on the voltage droop regulator of (2.16).

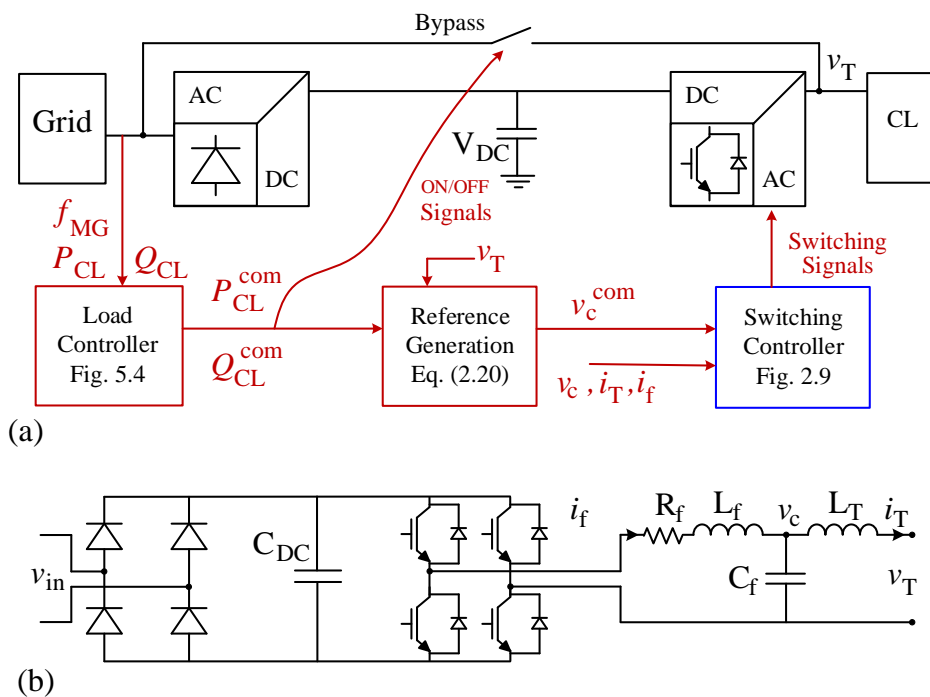


Fig. 5.7: (a) Control scheme, and (b) single-line diagram of a load PEI.

For simplicity, the following assumptions are made:

- In normal conditions, the DGs can easily supply required power demand of the loads.
- Since the considered MGs are sustainable, a DDG here is a combination of wind and battery energy storages (BES).
- The DDGs are modelled as droop-regulated voltage source converters connected to the MG via an LCL filter.
- The NDDGs are modelled as PQ-controlled voltage source converters connected to the MG via an LCL filter.
- All the DGs have identical LCL interfacing filters.
- MPPT blocks of the NDDGs are replaced with pre-specified power generation references.

The detailed technical parameters of the network and the schemes are given in Table 5.1.

Table 5.1: Parameters of the MGs and the proposed strategy.

| | | | | | |
|--|--------|--------|--------|--------|--------|
| Parameters of the strategy: $\alpha_1 = 0.1$, $\varepsilon = 0.2$, $\varepsilon_f = 0.01\text{Hz}$, $V_{\max} = 6.5\text{ kV}$, $V_{\min} = 6\text{ kV}$ $f_{\max} = 50.5\text{ Hz}$, $f_{\min} = 49.5\text{ Hz}$, $f_{\Delta} = 0.04\text{ Hz}$. | | | | | |
| Line impedances: $Z_{\text{line}} = 0.1 + j 0.1\ \Omega$, $Z_{\text{tie-line}} = 0.2 + j 0.2\ \Omega$. | | | | | |
| VSCs: $L_f = 5\text{mH}$, $C_f = 50\mu\text{F}$, $R_f = 0.5\Omega$, $L_T = 15\text{mH}$, $V_{\text{DC}} = 11\text{kV}$, $T_s = 10\mu\text{s}$, $h = 10^{-5}$ $\lambda_1 = 0.4547$, $\lambda_2 = 0.4546$, $\lambda_3 = 0.0909$, $\lambda_4 = -0.0909$. | | | | | |
| | MG-1 | | | MG-2 | |
| DDGs | DDG-1 | DDG-2 | DDG-3 | DDG-1 | DDG-2 |
| m [Hz/kW] | 0.0033 | 0.0067 | 0.0067 | 0.0025 | 0.0050 |
| n [kV/kVAr] | 0.0071 | 0.0143 | 0.0143 | 0.0053 | 0.0106 |

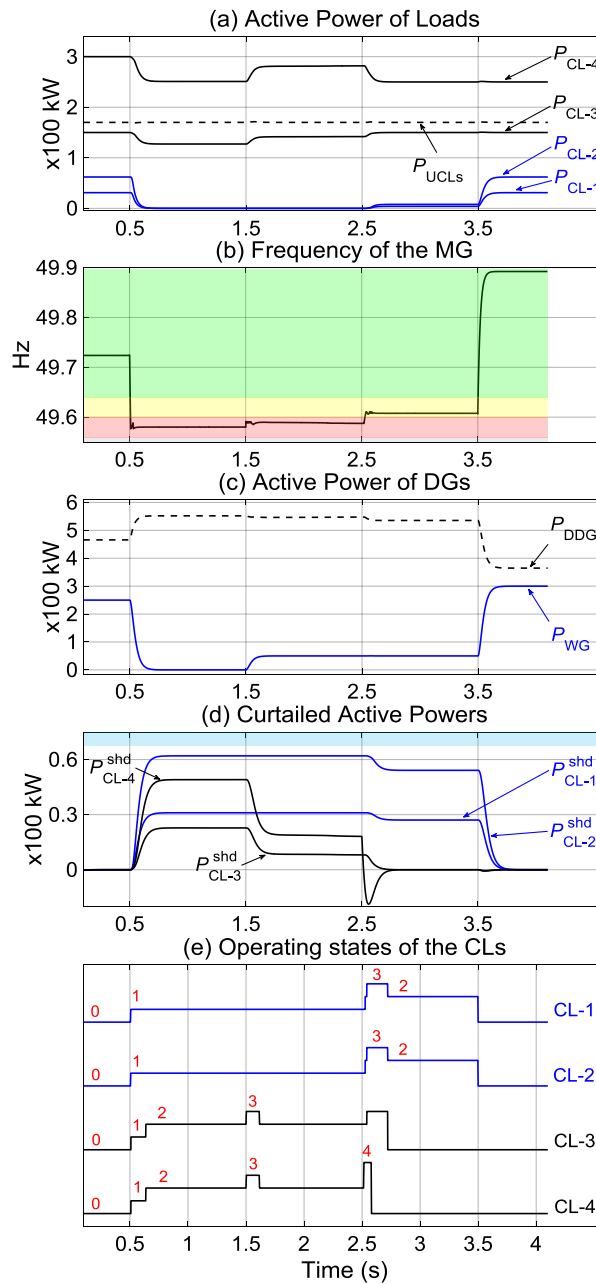


Fig. 5.8: Simulation results of Case 1.

1) Case 1

Different operating states of the primary level scheme are evaluated in this case. Load demands of CL-1 and CL-3 are assumed to be half of CL-2 and CL-4 respectively, as can be seen in Fig. 5.8a. Let us consider the MG of Fig. 5.1 at steady state condition wherein the DDGs have the total power output of 466 kW while the WG delivers 250 kW, resulting in a frequency of 49.72 Hz (see Fig. 5.8b-c).

At $t = 0.5\text{s}$, the output of the WG drops to zero. As f_{MG} at this condition satisfies (5.5), controllers of the CLs initiate algorithm of the primary scheme that successfully raises the frequency to 49.58 Hz at the cost of shedding 100% of the CLs of Type-1 along with 17% of CLs of Type-2, as shown in Fig. 5.8d. All the CLs are in State 1 at the beginning of the procedure since f_{MG} falls below the lower limit of both Layer-1 (i.e., 49.6 Hz), and Layer-2 (i.e., 49.58 Hz), as can be seen from Fig. 5.8e. Once f_{MG} rises above 49.58 Hz, the status of the CLs of Type-2 changes to State 2 to maintain the frequency between limits of (5.12). However, the CLs of Type-1 still should implement the primary level under State 1.

Following an increase of about 50 kW in power output of the WG at $t = 1.5\text{ s}$, the frequency rises above 49.59 Hz. Accordingly, the CLs of Type-2 restore proportionally 63% of their shed terms under State 3.

Since $P_{\text{CL-4}}^{\text{org}}$ decreases to 250 kW at $t = 2.5\text{s}$ and $P_{\text{CL-4}}^{\text{shd}}$ becomes negative, the controller of CL-4 alters its command to (5.11) in order to raise f_{MG} above 49.61 Hz. Consequently, the CLs of Type-1 and Type-2 restore the shed terms by 13% and 100% respectively. This terminates the primary level action in the CLs of Type-2, indicated as zero in Fig. 5.8e.

Finally, the power output of the WG increases to 300 kW at $t = 3.5\text{s}$ that removes the necessity of any load shedding action. After restoring the shed loads, MG operates at $f_{\text{MG}} = 49.89\text{ Hz}$.

2) Case 2

In this case, the cooperative performance of the proposed levels is verified. Let us consider the network of Fig. 5.5 at steady state condition wherein MG-2 has a total demand of 350 kW while the operating condition of MG-1 is identical to the MG studied in case 1, as can be seen from Fig. 5.9a. As ISS is initially open, MG-1 operates at a frequency of about 49.72 Hz while the frequency of MG-2 is about 49.91 Hz, as shown in Fig. 5.9b.

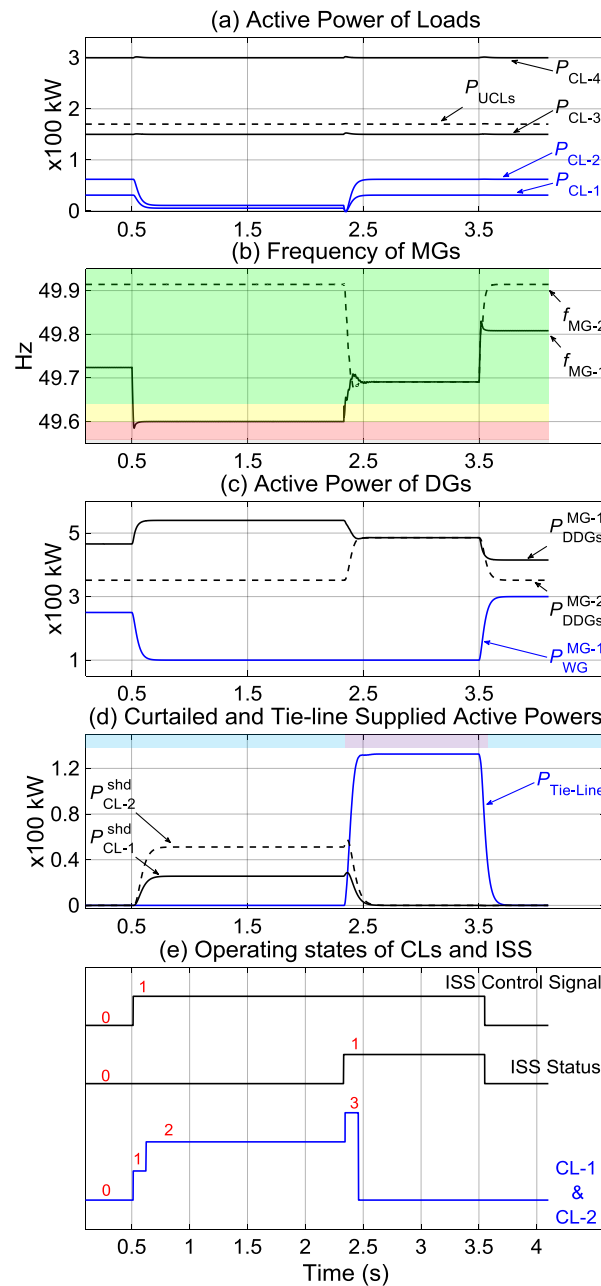


Fig. 5.9: Simulation results of Case 2.

At $t = 0.5s$, the power output of the WG falls to 100 kW, dropping f_{MG-1} below $f_{shd} = 49.6$ Hz. Consequently, the CLs of Type-1 shed proportionally 82.4% of their demand to meet (5.12), as seen from Fig. 5.9d. On the other hand, the ISS controller initiates the secondary level scheme as both (5.19) and (5.30) are satisfied (i.e., $f_{MG-1} < 49.61$ Hz and $f_{MG-2} > 49.68$ Hz). Hence, the controller sends a command to the ISS to close, as shown in Fig. 5.9e.

The ISS postpones the interconnection to $t=2.331s$ at which the voltage synchronization is achieved. By forming the CMG, the CLs of MG-1 and MG-2 are notified to change their operating modes to Mode 2 and Mode 3 respectively. Afterward, the shed terms of the CLs are restored completely as a supporting power of about 133 kW flows toward MG-1, causing the CMG to operate at a new frequency of $f_{CMG} = 49.69Hz$.

At $t = 3.5s$, the power output of the WG increases to 300 kW. Then, once f_{CMG} rises above 49.82Hz, $P_{Tie-line}$ violates the criterion mentioned in (5.36). This means the requirement for the interconnection has been removed. Hence, the ISS opens and the isolated MGs operate at $f_{MG-1}=49.80Hz$ and $f_{MG-2}= 49.91Hz$.

3) Case 3

This case illustrates applying the load shedding action within the CMG due to a further power deficiency in MG-1. The simulation results are shown in Fig. 5.10. Let us consider the system of Case-2 nearly before $t = 3.2 s$. The ISS is already closed and the CLs of MG-1 adopt Mode 2. The frequency of the CMG is about $f_{CMG} = 49.69 Hz$.

Fig. 5.10a shows that load demand of UCLs of MG-1 grows to a high of 250 kW at $t = 3.2s$. Although the supporting power rises for about 23%, f_{CMG} drops below 49.64 Hz, necessitating the primary level action in CLs of Type-1. Therefore, these CLs shed about 25.4% of their demand to increase the f_{CMG} to about 49.642 Hz that satisfies (5.12) (i.e., $49.64 Hz < f_{CMG} < 49.65 Hz$).

At $t = 4s$, the power output of the WG in MG-1 increases to 300kW. The moment f_{CMG} rises above 49.65 Hz, the CL controllers apply (5.15) as the desired command, restoring 100% of the shed terms.

At about $t = 4.1s$, while the frequency is above 49.80 Hz, $P_{Tie-line}$ violates (5.36). Hence, the controller sends a command to isolate the two MGs. Then, MG-1 and MG-2 operate at 49.67 Hz and 49.91 Hz, respectively.

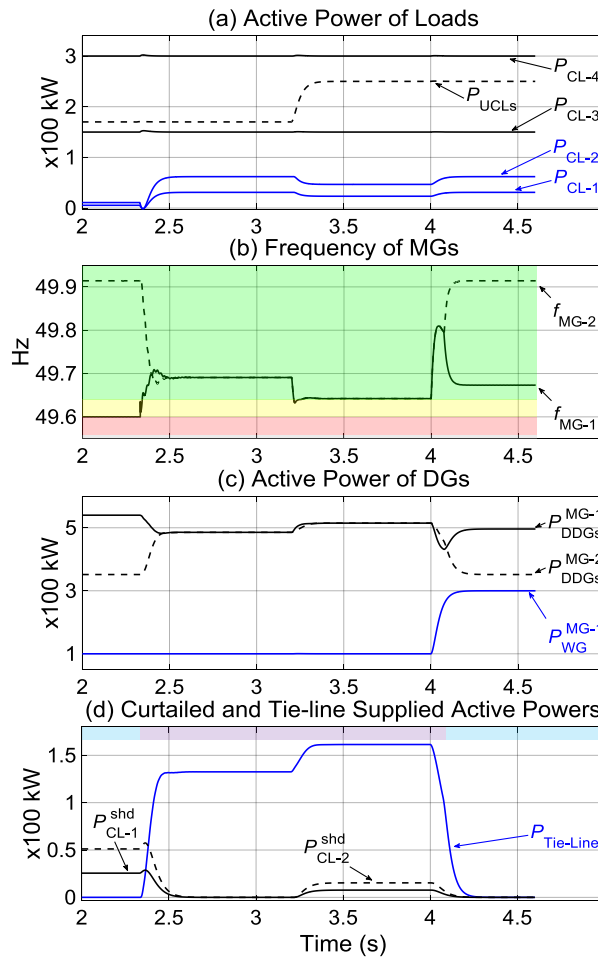


Fig. 5.10: Simulation results of Case 3.

4) Case 4

This case presents performance of the proposed strategy when the level of support provided by the neighbouring MG decreases. The results are shown in Fig. 5.11. Let us consider the system of Case-2 nearly before $t=3.2s$. The CMG is already formed and MG-2 is providing MG-1 with a supporting power of 133 kW.

At $t = 3.2s$, the total demand of MG-2 rises for about 28.5%, resulting in a decrease of about 50% in $P_{Tie-line}$. Once the frequency drops below 49.64Hz, the CLs of Type-1 fulfil the primary scheme in MG-1. The CLs can successfully satisfy (5.12) by shedding 42.6% of their demands.

The WG of MG-1 increases its power output to 300 kW at $t=4s$. Thus, the CL controllers initiate the restoration procedure as the frequency rises above 49.65Hz.

Moreover, the rise in output of the WG reduces the required level of supporting power, violating (5.36). Consequently, the ISS isolates the two MGs since the interconnection is no longer required.

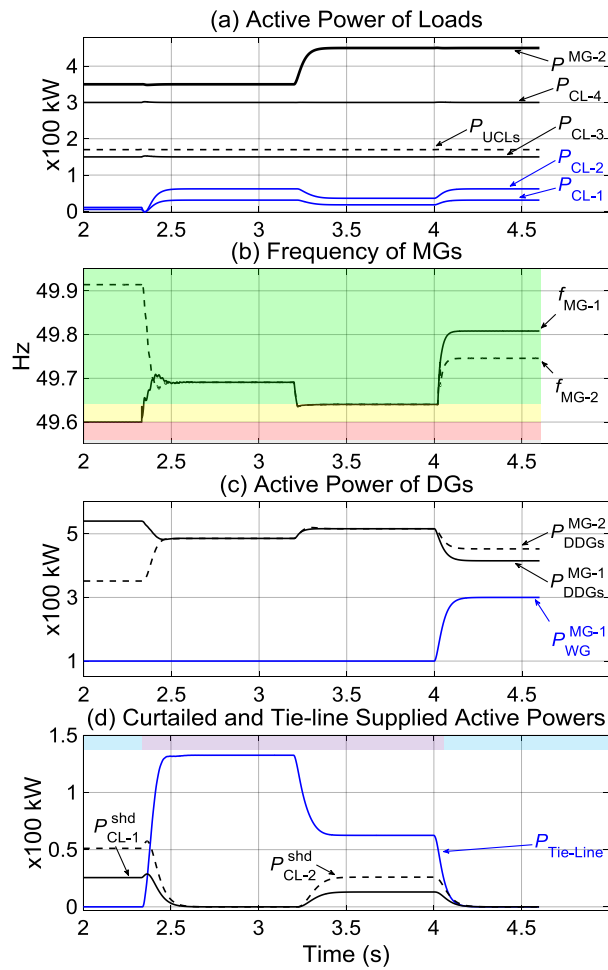


Fig. 5.11: Simulation results of Case 4.

5.5 Conclusion

In this chapter, a two-level control approach is presented to facilitate decentralized management of active power deficiencies in isolated sustainable MGs. The primary level is responsible for fulfilling an under frequency load shedding action based on a developed multilayer droop structure. The droop curves of each layer are assigned to a number of controllable loads of the same priority type. The shedding action is implemented proportionally due to the appropriate adjustment of the related droop coefficients.

The simulation studies show that the system frequency can be successfully increased through the execution of the primary level scheme by the load controllers. Moreover, the secondary level of the proposed approach fulfils a proper coupling between neighbouring MGs. It is validated that the shed terms of the loads can be restored successfully after forming a CMG system based on the developed interconnection/isolation constraints. It is demonstrated that a very low-bandwidth communication system can be adopted to suitably organize the collaboration of the scheme levels.

It is worth mentioning here that although decentralized power management strategies are more beneficial for the uncertain communication infrastructures than the centralized ones, frequency metering methods have substantial impacts on their outcome. In case the frequency measurement is compromised, application of the decentralized schemes would fail to reach the desired targets.

Chapter 6. A SUPERVISORY SCHEME FOR COUPLING ISOLATED MICROGRIDS

Power deficiency issue is one of the main challenges with remote area MGs due to their limited power generation capacities. To address this, coupling neighbouring MGs is considered as an economically promising alternative to traditional methods since it imposes almost no extra capital investment. Instead of a back-to-back power converter, an instantaneous static switch (ISS) is employed in this thesis to form a CMG in order to avoid the disadvantages of power loss introduced by the converters.

The ISS is a normally open switch which is mounted on the tie-line between the MGs. Considering a droop-based decentralized strategy, the required conditions and constraints to perform such interconnection procedures have been presented in previous chapters. Although employing the ISS under a communication-free framework can considerably decrease the total cost, it compromises controllability of the power flowing through the tie-line, and this, in turn, causes two major concerns with the performance of the system as explained below

- 1) By forming a CMG, a supporting power is supplied by the neighbouring MG that relieves the shortfall. Since the DGs of both the MGs share the total load of the system as per their power capacities, the power output of the DGs of the overloaded MG may be less than their maximum allowable limits. In other words, the supporting power is probably larger than the actual requirement of the MG experiencing the power shortfall. This undesirable consequence can impose extra costs on the MG owner. Note that, as a desirable power exchange criterion, the overloaded MG should generate its maximum allowable power while the neighbouring MG should only supply the rest of the load demand.

2) Once the power shortfall is removed, the MGs should isolate to carry on their normal operation independently. Due to the dissimilar configuration of the MGs, however, a non-zero power may still flow through the tie-line. In this case, improper isolation of the MGs can impose considerable voltage spikes on the ISS that may damage the device or decrease its lifetime [139].

This chapter proposes a supervisory control scheme to facilitate ISS-based coupling of the neighbouring MGs, as well as, a proper isolation strategy for the coupled MGs [115]. In order to address the aforementioned challenges, operation of the developed strategy is conducted under three different modes – namely,

- Mode 1: that is initiated by forming the CMG to sustain the power output of the overloaded MG close to its maximum,
- Mode 2: that aims to fulfil a successful isolation when the interconnection is not required anymore and
- Mode 3: that starts by opening the ISS to reset default values of the DG primary controllers.

The ISS controller is responsible for implementing the developed scheme by appropriately modifying the droop coefficients of the DGs located within the overloaded MG.

It is to be noted that the supervisory scheme proposed in this chapter aims at driving the ISS-based CMG system from the current to a desired operating point while maintaining the reliability and simplicity of the network by avoiding complex communication systems.

6.1 The network under consideration

Let us consider the two neighbouring isolated MGs of Fig. 5.5 consisting of N_1 and N_2 droop-controlled DGs. The frequency and voltage at the output of each DG are regulated by droop control of (2.16). Also, the associated P - f and Q - V droop coefficients can be calculated by using (2.17). Note that the DGs of each MG can have different droop coefficients since their power capacities can be dissimilar. The load sharing between any two DGs is performed according to their droop coefficients which are given by (2.18). The MGs can be interconnected by

closing the ISS mounted on the tie-line. The ISS controller manages the interconnection using only the local measurements.

Droop equations of (2.16) should be adopted when the line impedances are inductive. Otherwise, proper decoupling between active and reactive powers cannot be achieved [45]. Therefore, the interfacing inductances of the DGs, L_{DG} , should be chosen large enough in comparison to those of the lines, in order to avoid this negative impact on power sharing. Let us consider the suitable criterion for size selection of L_{DG} as $L_{DG}\omega > (5\sim 10)\times|Z_{line}|$ where ω is the system frequency and Z_{line} represents the line impedances. Note that the maximum output power of each DG sets the upper limit for the size of its L_{DG} .

Due to the reason mentioned above, the active power can be regulated well by (2.16). Accurate sharing of reactive power can, however, be difficult. Since the main focus of this paper is addressing the active power shortfalls in isolated MGs, it is assumed that the reactive term of the loads can be mainly supplied by local reactive power compensators. Thus, adopting (2.16) for DGs of the network is sensible as it can maintain the simplicity of the system while performing the required power regulation. Under extreme situations, however, more complex techniques of droop control should be employed [63].

In [88], the small signal stability performance of a CMG is studied for various selections of different interconnection buses when the coupling inductances of the DGs are in the same range of the lines. The results show that the stability margin of the CMG can be considerably sensitive to the impedances of the lines and tie-line. This, in turn, can lead to strong variations in the performance of the CMG both in terms of stability and transient response. In contrast, eigenvalue analysis of a CMG is performed in Sections 3.7 and 4.7 for different combinations of the tie-line impedance when the DG interfacing inductances are selected adequately high in comparison to those of the lines. The outcomes reveal that variations in the tie-line impedance of the considered CMG do not cause instability under any of the simulated scenarios.

Therefore, another advantage of the proper design of the DGs to meet the aforementioned size constraint on the output inductances is to enhance droop gain

stability margin of the whole system and to extend the range of its insensitivity to various impedance combinations of the CMG lines. Consequently, the performance of the CMG can be satisfactory both in terms of stability and transient response. Further discussions are provided in Section 6.6.3.

6.2 Problem statement

Interconnection of the neighbouring MGs can be a promising alternative to traditional frequency support techniques, mainly in remote areas rich in renewable resources. Let us consider the system of two isolated MGs shown in Fig. 5.5 in which DGs of each MG are regulated by droop control with the same maximum frequency deviations. By forming the CMG system the total load will be shared by DGs of the both MGs. The criteria for the interconnection as well as the isolation procedures are briefly reviewed in this section. Then, the concerns with the communication-free operation of the CMG are fully discussed.

6.2.1 Coupling and isolation conditions

The conditions and constraints under a fully decentralized control scheme to form a CMG are discussed in previous chapters. Let us assume that MG-1 experiences a power shortfall if its frequency, f_{MG-1} , drops below a threshold defined as

$$f_{MG-1} < f_{\min} + \alpha(f_{\max} - f_{\min}) \quad (6.1)$$

where $0 < \alpha < 1$. In Chapter 3, it is shown that if f_{MG-1} meets the above condition, the UPC of MG-1 is less than α times the total power capacity of all DGs of MG-1 $P_{MG-1}^{\text{cap}} = \sum_{i=1}^{N_1} P_{DG-i}^{\text{cap}}$. For example, assuming $\alpha = 0.1$, MG-1 is overloaded if its UPC is less than 10% of its power capacity. In this case, the controller commands the ISS to close provided that the interconnection will not cause power deficiency in MG-2, i.e.,

$$P_{\text{CMG}} < (1 - \alpha)P_{\text{CMG}}^{\text{cap}} \quad (6.2)$$

where $P_{\text{CMG}} = P_{\text{MG-1}} + P_{\text{MG-2}}$ and $P_{\text{CMG}}^{\text{cap}} = P_{\text{MG-1}}^{\text{cap}} + P_{\text{MG-2}}^{\text{cap}}$. Also, it is proved that this constraint is satisfied if the frequency of MG-2, $f_{\text{MG-2}}$, meets the following criterion

$$f_{\text{MG-2}} > f_{\text{max}} - m_{\text{MG-2}} \times \left[(1 - \alpha) \times (P_{\text{MG-1}}^{\text{cap}} + P_{\text{MG-2}}^{\text{cap}}) - \frac{f_{\text{max}} - f_{\text{MG-1}}}{m_{\text{MG-1}}} \right] \quad (6.3)$$

where m_{MG} indicates the equivalent droop coefficient of all DGs of an MG explained as

$$m_{\text{MG}} = 1 / \sum_{i=1}^N \frac{1}{m_{\text{DG-}i}} \quad (6.4)$$

Fig. 6.1 illustrates the equivalent droop curve of an MG containing only two DGs. This figure shows how the two DGs can be aggregated by a single unit representing the droop behaviour of the MG. Similar to (2.17), m_{MG} can also be defined as

$$m_{\text{MG}} = \frac{f_{\text{max}} - f_{\text{min}}}{P_{\text{MG}}^{\text{cap}}} \quad (6.5)$$

The ISS controller initiates the interconnection if both (6.1) and (6.3) are satisfied. Then, the ISS closes when the voltages at its two sides are synchronized.

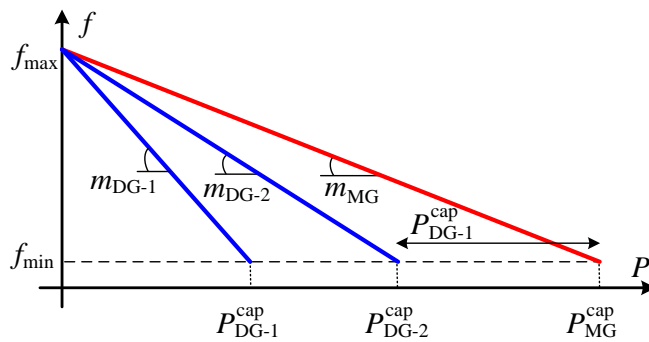


Fig. 6.1: Equivalent droop curve of an MG along with droop curves of its DGs.

After forming the CMG system, a supporting power of $P_{\text{Tie-line}}$ flows through the tie-line towards MG-1. It can be shown that MG-1 requires receiving the support from MG-2 as long as $P_{\text{Tie-line}}$ can be expressed as

$$P_{\text{Tie-line}} > (1 - \alpha) \times P_{\text{MG-1}}^{\text{cap}} - (f_{\text{max}} - f_{\text{CMG}}) / m_{\text{MG-1}} \quad (6.6)$$

where f_{CMG} indicates the frequency of the CMG. However, the interconnection is no longer required in case $P_{\text{Tie-line}}$ drops below the above limit. In other words, the violation of (6.6) means the state of power deficiency in MG-1 is already removed, and hence, the MGs should be isolated.

It is worthwhile to emphasise that (6.1), (6.3) and (6.6) are based only on the local measurements at the ISS.

6.2.2 Challenges with the communication-free CMG

Two undesirable features of forming a CMG system using an ISS under a fully decentralized structure are as follows

1) THE LEVEL OF SUPPORTING POWER

From MG-1 owner's point of view, the power exchange is desirable if $P_{\text{Tie-line}}$ can be expressed as

$$P_{\text{Tie-line}}^{\text{DSR}} = P_{\text{MG-1}}^{\text{Load}} - P_{\text{MG-1}}^{\text{DSR}}, \quad P_{\text{MG-1}}^{\text{DSR}} = (1 - \alpha) P_{\text{MG-1}}^{\text{cap}} \quad (6.7)$$

where $P_{\text{MG-1}}^{\text{Load}}$ is the total load of MG-1 while $P_{\text{MG-1}}^{\text{DSR}}$ indicates the desired power output of MG-1 during the interconnection. Eq. (6.7) implies that the supporting power should be limited to the portion of $P_{\text{MG-1}}^{\text{Load}}$ that cannot be met by the DGs of MG-1. By forming the CMG, however, the total load of the system, $P_{\text{CMG}}^{\text{Load}} = P_{\text{MG-1}}^{\text{Load}} + P_{\text{MG-2}}^{\text{Load}}$, is shared by DGs of the both MGs in accordance with the ratios stated in (2.18). Thus, the total power output of MG-2 can be described as

$$P_{\text{MG-2}} = \frac{P_{\text{MG-2}}^{\text{cap}}}{P_{\text{MG-1}}^{\text{cap}}} P_{\text{MG-1}} \quad (6.8)$$

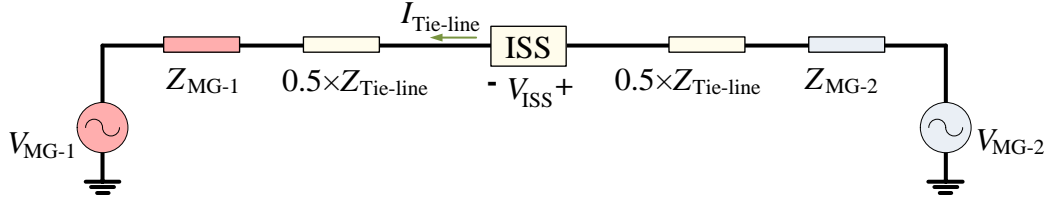


Fig. 6.2: The Thevenin equivalent of the considered CMG.

This is because the CMG is actually a larger MG containing N_1+N_2 droop-regulated DGs. As already mentioned, the satisfaction of (6.3) guarantees that the power output of the CMG can be stated as (6.2). Substitution of (6.8) in (6.2) yields

$$P_{MG-1} + \frac{P_{MG-2}^{cap}}{P_{MG-1}^{cap}} P_{MG-1} < (1-\alpha) P_{CMG}^{cap} \quad (6.9)$$

$$\rightarrow P_{MG-1} < (1-\alpha) P_{MG-1}^{cap}$$

which means the power output of MG-1 is now less than P_{MG-1}^{DSR} , causing the resultant supporting power to be larger than $P_{Tie-line}^{DSR}$.

2) ISOLATION PROCEDURE

According to the Thevenin equivalent of the CMG system shown in Fig. 6.2, the voltage across the ISS can be stated as

$$v_{ISS}(t) = L_{Eq} \frac{di_{Tie-line}(t)}{dt} + R_{Eq} i_{Tie-line}(t) + v_{Eq-MGs}(t) \quad (6.10)$$

where L_{Eq} and R_{Eq} respectively are the equivalent inductance and the resistance of the system seen from the ISS. Also, v_{Eq-MGs} and $i_{Tie-line}$ denote the resultant voltage of the MGs and the tie-line current respectively.

Although the violation of (6.6) indicates the necessity of an isolation action, a considerable power may still pass through the ISS due to the droop-based load sharing of the DGs. Because of the derivative term of (6.10), opening the ISS under this condition may cause destructive transients, damaging the device or decreasing its lifetime. Therefore, a proper mechanism should be developed to

facilitate a successful isolation procedure such that neither the ISS nor the other components of the system are damaged.

6.3 Improved fully decentralized isolation

In this section, a practical communication-free approach is presented to facilitate a successful isolation procedure of the coupled MGs, efficiently mitigating the aforementioned destructive disturbances. The scheme is based on equalizing the load-to-capacity (L2C) ratios of the MGs such that the power flowing through the ISS decreases to zero. Once the necessity of applying an isolation action is detected, the ISS controller commands an auxiliary controllable load (ACL) on the supporting MG side to connect, as can be seen from Fig. 6.3. The reference value of the load that should be demanded by the ACL is accurately derived based on only the local measurements. This section begins with examining the condition under which no supporting power flows through the ISS. Then, the proposed approach to achieve this condition is presented

6.3.1 Load-to-capacity ratio

Let us assume the ISS controller is operating under a fully decentralized structure. By forming a CMG, the total load of the system, $P_{\text{CMG}}^{\text{Load}}$, is shared by DGs of the MGs in accordance with the ratios stated in (2.18). Assuming the power capacity ratio of the MGs can be stated as

$$\frac{P_{\text{MG-1}}^{\text{cap}}}{P_{\text{MG-2}}^{\text{cap}}} = \eta \quad (6.11)$$

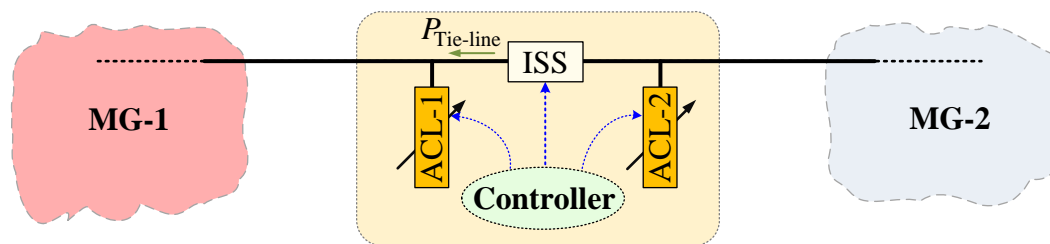


Fig. 6.3: The network of two isolated neighbouring microgrids with ACLs.

the total power output of the MGs can be expressed as

$$\begin{aligned} P_{\text{MG-1}} &= \frac{\eta}{\eta+1} P_{\text{CMG}}^{\text{Load}} \\ P_{\text{MG-2}} &= \frac{1}{\eta+1} P_{\text{CMG}}^{\text{Load}} \end{aligned} \quad (6.12)$$

Using (6.12), $P_{\text{Tie-line}}$ (as shown in Fig. 6.3) can be derived as

$$P_{\text{Tie-line}} = \frac{1}{\eta+1} P_{\text{CMG}}^{\text{Load}} - P_{\text{MG-2}}^{\text{Load}} \quad (6.13)$$

Now, let us define the load-to-capacity (L2C) ratio of an MG as

$$\text{L2C}_{\text{MG}} = \frac{P_{\text{MG}}^{\text{Load}}}{P_{\text{MG}}^{\text{cap}}} \quad (6.14)$$

Assuming the violation of (6.6), the following two scenarios are relevant:

- The L2C ratios of the MGs are identical (i.e., $P_{\text{MG-1}}^{\text{Load}}/P_{\text{MG-2}}^{\text{Load}} = P_{\text{MG-1}}^{\text{cap}}/P_{\text{MG-2}}^{\text{cap}}$). From (6.11), the total load of the system can be described as

$$P_{\text{CMG}}^{\text{Load}} = (\eta+1) \times P_{\text{MG-2}}^{\text{Load}} \quad (6.15)$$

Substituting (6.15) in (6.13), it can be concluded that if the MGs have the same L2C ratios, $P_{\text{Tie-line}}$ becomes zero. Thus, the isolation can be fulfilled without any transient.

- The L2C ratios of the MGs are different. Then, the following cases may occur

$$\begin{cases} 1) \text{ if } \text{L2C}_{\text{MG-1}} \geq \text{L2C}_{\text{MG-2}} \rightarrow P_{\text{CMG}}^{\text{Load}} \geq (\eta+1) \times P_{\text{MG-2}}^{\text{Load}} \\ 2) \text{ if } \text{L2C}_{\text{MG-1}} \leq \text{L2C}_{\text{MG-2}} \rightarrow P_{\text{CMG}}^{\text{Load}} \leq (\eta+1) \times P_{\text{MG-2}}^{\text{Load}} \end{cases} \quad (6.16)$$

Replacing either of the above cases in (6.13) yields a non-zero $P_{\text{Tie-line}}$, causing the undesirable disturbances across the ISS at the isolation moment. Note that this unrequired power flows due to the droop-based power sharing of the DGs.

6.3.2 The proposed method

With the aim of achieving the successful disturbance-free isolation, conduction of an L2C equalization procedure is highly desirable. Assuming $L2C_{MG-1} \geq L2C_{MG-2}$, accordingly, the total load of MG-2 should be temporarily increased to

$$P_{MG-2}^{Temp-Load} = \frac{1}{\eta} \times P_{MG-1}^{Load} \quad (6.17)$$

such that the mentioned desirable performance is achieved. Note that this can force $P_{Tie-line}$ to decrease to zero immediately before the isolation.

The ISS controller is responsible for implementing the isolation action under a decentralized scheme as the system operates based upon a communication-free structure. This means the developed algorithm should be capable of handling the issue by utilizing only the local measurements (i.e., $P_{Tie-line}$ and the frequencies of the MGs). Two ACLs are to be connected at two sides of the ISS in order to temporarily alter the total loads of the MGs. Under normal operation, the load demanded by the ACLs is zero. During the isolation, however, the ACLs should demand a specific amount of power assigned by the controller, balancing the L2Cs of the MGs. With the aim of satisfying (6.17), the ACL at the MG-2 side of the ISS should raise its demand to

$$\begin{aligned} P_{MG-2}^{Temp-Load} &= P_{MG-2}^{Load} + P_{MG-2}^{ACL} \\ \rightarrow P_{ACL-2} &= \frac{1}{\eta} \times P_{MG-1}^{Load} - P_{MG-2}^{Load} \end{aligned} \quad (6.18)$$

The auxiliary demand should be extracted based only on the local measurements. Thus, let us define λ as

$$\lambda = \frac{P_{ACL-2}}{P_{Tie-line}} \quad (6.19)$$

Replacing (6.13) and (6.18) in (6.19) yields

$$\lambda = 1 + \frac{1}{\eta} \quad (6.20)$$

Hence, the derived reference value of the auxiliary demand can be expressed as

$$P_{ACL-2} = \left(1 + \frac{1}{\eta}\right) \times P_{Tie-line} \quad (6.21)$$

Although the controller is unable to directly measure the total loads of the MGs, (6.21) can efficiently consider the dynamic of the loads only through measuring $P_{Tie-line}$.

Equation (6.21) is derived assuming $L2C_{MG-1} \geq L2C_{MG-2}$. Likewise, in case $L2C_{MG-1} \leq L2C_{MG-2}$, $P_{Tie-line}$ which flows toward MG-2 can be stated as

$$P_{Tie-line} = \frac{\eta}{\eta + 1} P_{CMG}^{Load} - P_{MG-1}^{Load} \quad (6.22)$$

Therefore, it can be proved that the reference value of the auxiliary demand can be stated as

$$P_{ACL-1} = (1 + \eta) \times P_{Tie-line} \quad (6.23)$$

Once (6.6) is violated which necessitates an isolation action, the controller utilizes either (6.21) or (6.23), depending upon the L2C ratios of the MGs, to calculate the load to be demanded by the ACL, cancelling the current flowing through the ISS. Then, the opening of the ISS can be accomplished with no destructive spikes.

The flowchart based on which the controller applies the approach is shown in Fig. 6.4. In addition, Fig. 6.5 demonstrates the passing power through the ISS both before and after fulfilling the developed scheme. $P_{Tie-line}$ flows towards MG-1 when $L2C_{MG-1} \geq L2C_{MG-2}$. By this approach, ACL-2 increases its demand to (6.21), forcing the passing current through the tie-line to zero. Fig. 6.5.b shows the procedure when $L2C_{MG-1} \leq L2C_{MG-2}$. Raising the demand of ACL-1 to (6.23) nullifies the ISS current to guarantee a successful isolation.

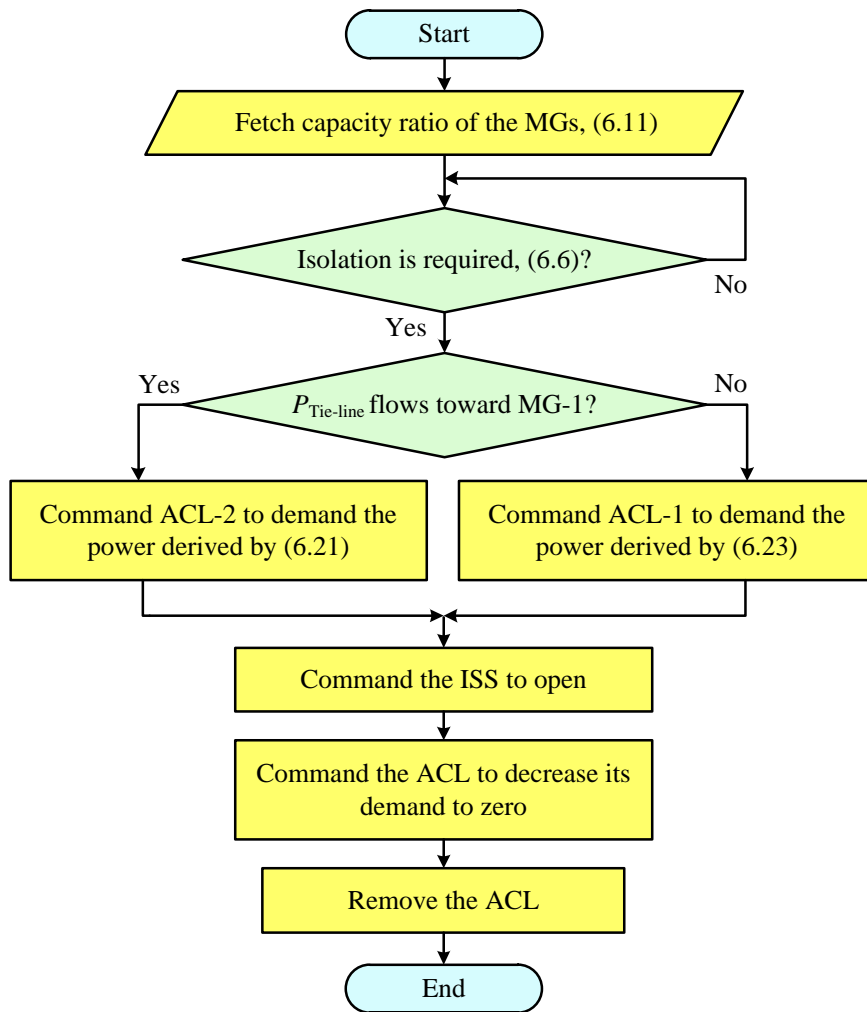


Fig. 6.4: Flowchart of the developed communication-free approach for isolation.

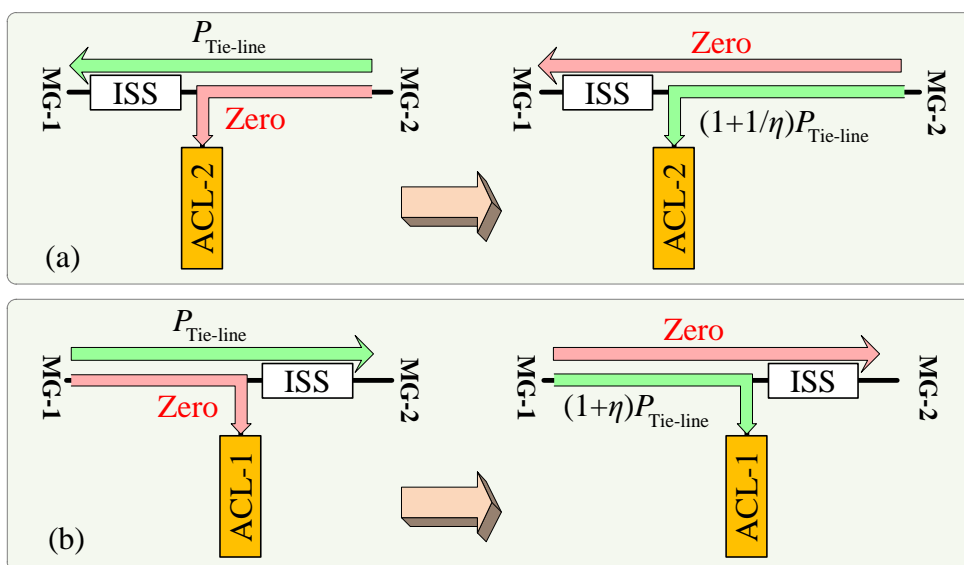


Fig. 6.5: The power transitions at the ISS by applying the developed approach when (a) $L2C_{MG-1} \geq L2C_{MG-2}$ and (b) $L2C_{MG-1} \leq L2C_{MG-2}$

6.4 The proposed supervisory scheme

As explained in Section 6.2.2, the ISS-based CMG forming procedure by adopting pre-specified coefficients of the droop regulators may yield undesirable consequences. Although the method presented in Section 6.3.2 can improve performance of the system during isolation, it can cause extra power losses. Also, the installation and maintenance cost can be considerable.

In this section, the mentioned challenges are addressed by developing a supervisory control scheme that achieves the defined goals by updating the droop coefficients of the overloaded MG during the interconnection. The scheme is embedded in the ISS controller to complement its performance described in Section 6.2.1. The supervisory action is fulfilled based on three operating modes appropriately defined for the scheme as shown in Fig. 6.6. Using only the local measurements, the controller switches to the proper mode and consequently readjusts the droop coefficients of the DGs. Fig. 6.7 shows the flowchart based on which the controller applies the scheme. The defined modes along with the associated transition criteria are discussed in detail in the following sections. From this point on, m_{DG}^{DF} and m_{MG}^{DF} indicate the default droop coefficient of a DG as (2.17) and an MG as (6.5) respectively while m_{DG} and m_{MG} are the ones updated by the controller.

6.4.1 Mode 1: Coupling

The first operating mode is designed to address the concern with the level of supporting power provided by the neighbouring MG, as explained in Section 6.2.2.1. Once the CMG is formed, the DGs of MG-1 should be forced to deliver P_{MG-1}^{DSR} while the rest of its demand can be supported by the neighbouring MG ($P_{Tie-line}^{DSR}$). In order to achieve this goal, from (2.18) and (6.7), the power outputs of the MGs are to satisfy a load sharing ratio as

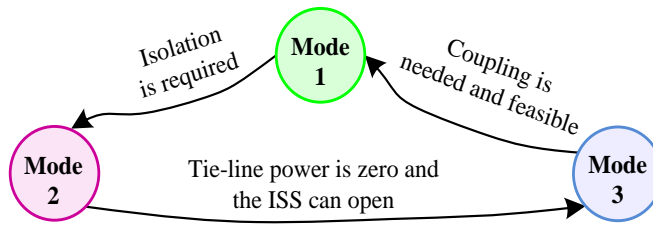


Fig. 6.6: Operating modes of the developed supervisory scheme.

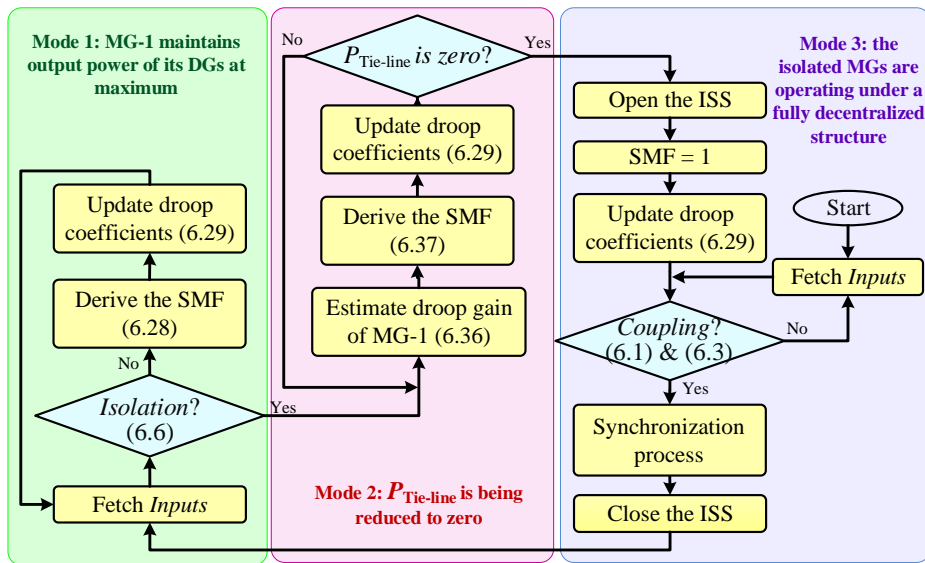


Fig. 6.7: Operation flowchart of the supervisory scheme.

$$\frac{P_{MG-1}^{DSR}}{P_{MG-2}} = \frac{m_{MG-2}^{DF}}{m_{MG-1}} \quad (6.24)$$

Therefore, the equivalent droop coefficient of MG-1 needs to be readjusted as

$$m_{MG-1} = \frac{m_{MG-2}^{DF} \times P_{MG-2}}{(1 - \alpha) P_{MG-1}^{cap}} \quad (6.25)$$

By dynamically applying (6.25), power outputs of the DGs of MG-1 can be always maintained at their maximum. Now, let us define the slope modification factor (SMF) as

$$\gamma = m_{MG} / m_{MG}^{DF} \quad (6.26)$$

which is the supervisory coefficient of the system. The main idea is to extract the

proper SMFs based on which the controller can update droop coefficients of the DGs desirably. Note that the dependency on the communication system should be decreased in order to enhance the CMG reliability. This means the operation of the controller should be mostly based on the local measurements, i.e., f_{CMG} and $P_{\text{Tie-line}}$. To achieve this goal, using (2.16), (6.25) is restated as

$$m_{\text{MG-1}} = \frac{f_{\text{max}} - f_{\text{CMG}}}{(1 - \alpha)P_{\text{MG-1}}^{\text{cap}}} \quad (6.27)$$

Note that m_{MG} is the modified droop coefficient of the MG and $m_{\text{MG}}^{\text{DF}}$ is the default value of the droop coefficient expressed in (6.5). Hence, substituting (6.5) and (6.27) in (6.26) yields the SMF to be sent to MG-1 as

$$\gamma_{\text{MG-1}} = \frac{\frac{f_{\text{max}} - f_{\text{CMG}}}{(1 - \alpha)P_{\text{MG-1}}^{\text{cap}}}}{\frac{f_{\text{max}} - f_{\text{min}}}{P_{\text{MG-1}}^{\text{cap}}}} = \frac{1}{1 - \alpha} \times \frac{f_{\text{max}} - f_{\text{CMG}}}{f_{\text{max}} - f_{\text{min}}} \quad (6.28)$$

Equation (6.28) is capable of yielding the SMF only by measuring the CMG frequency at the ISS. Whenever the SMF is updated by the controller, the DGs of MG-1 should modify their droop coefficients accordingly as

$$m_{\text{DG-}i} = \gamma_{\text{MG-1}} \times m_{\text{DG-}i}^{\text{DF}} \quad (6.29)$$

where $i \in \{1, \dots, N_1\}$. Eventually, the droop regulator of each DG should be altered as

$$f_{\text{CMG}} = f_{\text{max}} - \gamma_{\text{MG-1}} \times m_{\text{DG-}i}^{\text{DF}} P_{\text{DG-}i} \quad (6.30)$$

as shown in Fig. 6.8. By adaptively adjusting the SMF, and thereby the droop coefficients, the controller ensures that the DGs of MG-2 provide MG-1 with

$$P_{\text{Tie-line}}^{\text{DSR}}.$$

In order to provide further insight into the mechanism of the approach, let us consider droop curves of a sample CMG shown in Fig. 6.9 where f_a is the threshold frequency defined in (6.1) and f_1 is the CMG frequency when the supervisory scheme is not included. Without loss of generality, the capacity of

MG-2 is assumed to be larger than that of MG-1. Since the power output of MG-1 at f_1 is definitely less than P_{MG-1}^{DSR} (see (6.9)), extra supporting power is undesirably provided by MG-2. By activating the scheme, the controller calculates regularly the appropriate SMF by using (6.28), which only needs frequency measurement at the ISS. Then, the SMF is sent to the DGs using a very low bandwidth communication system to update the droop coefficients as per (6.29).

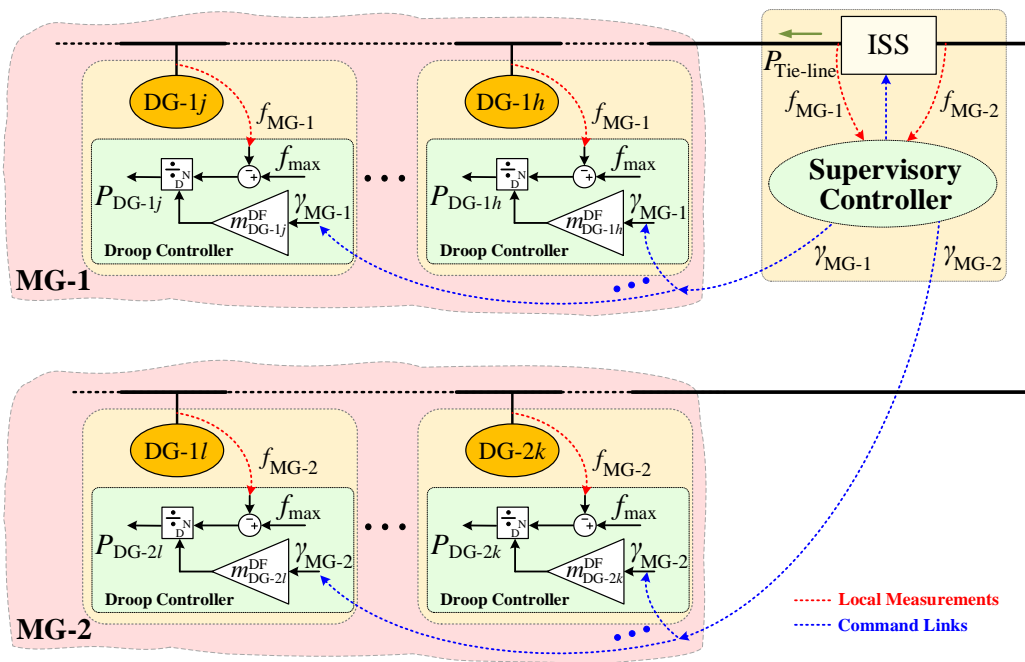


Fig. 6.8: The network of two isolated neighbouring microgrids with the supervisory controller.

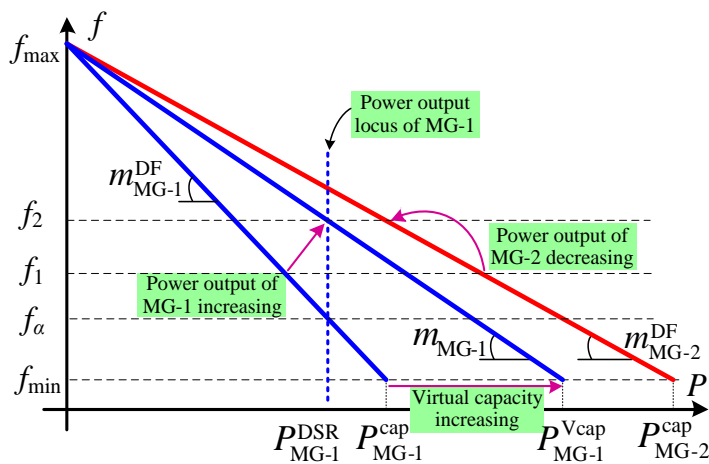


Fig. 6.9: Performance of the developed supervisory scheme under Mode 1.

Consequently, P_{MG-2} can be successfully decreased through increasing P_{MG-1} to P_{MG-1}^{DSR} , as can be seen from Fig. 6.9, reducing the supporting power to $P_{Tie-line}^{DSR}$. From the CMG point of view, the power capacity of MG-1 is virtually increased to

$$P_{MG-1}^{Vcap} = \frac{f_{max} - f_{min}}{f_{max} - f_{CMG}} P_{MG-1}^{DSR} \quad (6.31)$$

This leads to the frequency increase to f_2 as m_{MG}^{DF} is decreased to m_{MG-1} (see (6.5)). As long as Mode 1 of the scheme is active, P_{MG-1}^{DSR} is the power output locus of MG-1, as shown in Fig. 6.9.

6.4.2 Mode 2: Cancelling the tie-line power

The ISS controller is responsible for implementing the isolation action under a quasi-decentralized scheme. This means the developed scheme should be capable of handling the issue raised in Section 6.2.2 by extracting proper SMF values. The target is to decrease $P_{Tie-line}$ to about zero before opening the ISS such that the destructive transients caused by the derivative term of (6.10) can be avoided. The condition under which no supporting power flows through the ISS has been discussed in Section 6.3.1. The supervisory approach to achieve this condition is presented here.

In order to achieve a successful disturbance-free isolation, an L2C equalization procedure should be performed. Due to the fact that the controller has no direct access to the loads, the equalization should be implemented by virtually modifying the power capacity of MG-1. From (6.14), the L2C equalization can be attained if the virtual capacity of MG-1 can be ideally expressed as

$$P_{MG-1}^{Vcap} = \frac{P_{MG-1}^{Load}}{P_{MG-2}^{Load}} P_{MG-2}^{cap} \quad (6.32)$$

According to the direction of $P_{Tie-line}$ shown in Fig. 6.8, the total load demand of the MGs can be described by

$$\begin{aligned} P_{MG-1}^{\text{Load}} &= P_{MG-1} + P_{\text{Tie-line}} \\ P_{MG-2}^{\text{Load}} &= P_{MG-2} - P_{\text{Tie-line}} \end{aligned} \quad (6.33)$$

Substituting (6.33) in (6.32) yields

$$P_{MG-1}^{\text{Vcap}} = \frac{P_{MG-1} + P_{\text{Tie-line}}}{P_{MG-2} - P_{\text{Tie-line}}} P_{MG-2}^{\text{cap}} \quad (6.34)$$

Thus, by redefining the droop coefficient of MG-1 utilizing the virtual capacity of (6.34), the DGs of MG-1 can successfully modify their power outputs to drop the tie-line power to zero. However, (6.34) depends on the simultaneous measurement of power outputs of the DGs of both MGs using appropriate power sensors that necessitates a high bandwidth bidirectional communication system, compromising reliability as well as increasing complexity and the total cost of the system. This issue can be efficiently addressed by restating (6.34) using the droop equations of (2.16) and (6.5) as

$$P_{MG-1}^{\text{Vcap}(k)} = \frac{f_{\max} - f_{\min}}{m_{MG-1}^{(k-1)}} \times \frac{f_{\max} - f_{\text{CMG}} + m_{MG-1}^{(k-1)} \times P_{\text{Tie-line}}}{f_{\max} - f_{\text{CMG}} - m_{MG-2}^{\text{DF}} \times P_{\text{Tie-line}}} \quad (6.35)$$

where $P_{MG-1}^{\text{Vcap}(k)}$ represents the virtual capacity of MG-1 at step k while $m_{MG-1}^{(k-1)}$ is the droop coefficient of MG-1 at step $k-1$. Therefore, m_{MG-1} at step k can be derived as

$$m_{MG-1}^{(k)} = m_{MG-1}^{(k-1)} \times \frac{f_{\max} - f_{\text{CMG}} - m_{MG-2}^{\text{DF}} \times P_{\text{Tie-line}}}{f_{\max} - f_{\text{CMG}} + m_{MG-1}^{(k-1)} \times P_{\text{Tie-line}}} \quad (6.36)$$

Replacing (6.36) in (6.26) yields the SMF command as

$$\gamma_{MG-1}^{(k)} = \frac{m_{MG-1}^{(k-1)}}{m_{MG-1}^{\text{DF}}} \times \frac{f_{\max} - f_{\text{CMG}} - m_{MG-2}^{\text{DF}} \times P_{\text{Tie-line}}}{f_{\max} - f_{\text{CMG}} + m_{MG-1}^{(k-1)} \times P_{\text{Tie-line}}} \quad (6.37)$$

Note that $m_{MG-1}^{(0)}$ is the last value of m_{MG-1} derived by (6.27) during Mode 1. Now employing (6.37), the controller can iteratively update the SMF by only measuring the CMG frequency and the tie-line power at the ISS. Therefore, the DGs of MG-1 are ordered to readjust their droop coefficients accordingly as

(6.29), intending to reduce the passing power through the ISS. Eventually, the controller sends a command to the ISS to open once the tie-line power drops to zero. Note that the step size can be determined in accordance with the dynamic response of the MG as well as the bandwidth of the communication system.

Let the change between droop coefficients of MG-1 at two consecutive steps be expressed as

$$\Delta^{(k)} = m_{\text{MG-1}}^{(k)} - m_{\text{MG-1}}^{(k-1)} \quad (6.38)$$

If the error $\Delta^{(k)}$ tends to zero, then $P_{\text{Tie-line}}$ also approaches the desired value of $P_{\text{Tie-line}}=0$. Let us assume (6.6) is violated following a load change in MG-1; however, Mode 2 is not activated yet. Considering the direction of $P_{\text{Tie-line}}$ in Fig. 6.8, the following scenarios are relevant:

- $P_{\text{Tie-line}}$ is positive which means the total generation of MG-1, $P_{\text{MG-1}}$, is still lower than its total load. In this case, employing (6.36) at each step causes a relative reduction in the droop slope of MG-1, which, in turn, results in increasing $P_{\text{MG-1}}$ (see (2.18)), decreasing $P_{\text{Tie-line}}$. Carrying on this procedure can ultimately drop Δ to zero, cancelling the tie-line power.
- If the total generation of MG-1 is now larger than its load, the violation of (6.6) is followed by a negative $P_{\text{Tie-line}}$. Thus, applying the supervisory scheme of Mode 2 increases the droop slope of MG-1 to decrease $P_{\text{MG-1}}$, reducing the tie-line power step by step. Note that Δ decreases by dropping $P_{\text{Tie-line}}$. This ensures that the scheme can successfully achieve its goal.

6.4.3 Mode 3: Isolation

As soon as $P_{\text{Tie-line}}$ reduces to zero, the ISS can open to isolate the MGs with no destructive transients. By opening the ISS, the droop coefficients of MG-1 should be reset to their default values. This task can be performed through sending an SMF of

$$\gamma_{\text{MG-1}} = 1 \quad (6.39)$$

to the DGs, retrieving their normal droop regulation. Now the supervisory action is not required anymore and the two isolated MGs can carry on their operation independently under a communication-free structure. In other words, as long as the ISS is open and no power shortfall is detected, the supervisory controller stays idle and does not interfere with the normal operation of the MGs.

According to Section 6.2.1, two sets of conditions are defined, namely the coupling conditions formulated as (6.1) and (6.3), and the isolation condition formulated as (6.6). As illustrated in the flowchart of Fig. 6.7, the coupling conditions are included in Mode 3 of the proposed scheme. After opening the ISS and resetting the droop coefficient of the DGs to their default values, the controller should monitor the frequencies regularly to detect the next overloading. This action is implemented via the loop included in the flowchart of Mode 3 shown in Fig. 6.7. In case of a power deficiency in one of the MGs, i.e., when (6.1) is met, the controller initiates the synchronization and interconnection procedures subject to availability of sufficient surplus generation in the neighbouring MG, i.e., if (6.3) is satisfied as well. Afterwards, the controller executes the supervisory actions through activating Mode 1. On the other hand, the algorithm carries on the operation within the mentioned loop if any of the coupling conditions are not satisfied. It is to be noted that the transient-free interconnection procedure of the MGs has already been presented in Chapter 3.

6.4.4 Overall description

This chapter aims at developing a supervisory control scheme to modify the droop coefficients of the DGs within an overloaded MG for regulating the amount of supporting power provided by its neighbouring MG. This target should be attained with lower dependency on the communication systems in order to enhance reliability of the formed CMG. Therefore, a supervisory scheme is proposed based on a single parameter called the SMF, γ , capable of being implemented via a unidirectional low bandwidth communication system to

modify the droop coefficients of the DGs properly for the overloaded MG in accordance with the defined operating modes. In brief, the following steps can express algorithm used by the controller:

- I. Set the operating mode based on the fetched inputs and the ISS status.
- II. Calculate the appropriate SMF using (6.28), (6.37) and (6.39) for Modes 1, 2 and 3, respectively.
- III. Send the SMF to all DGs within the overloaded MG.

Then, each DG should apply the SMF on its own droop regulator as in (6.30) to achieve the desired target. It is to be mentioned again that all DGs within the overloaded MG receive the same SMF. This identical SMF is called γ_{MG-1} when the overloaded MG is MG-1 and γ_{MG-2} if MG-2 is overloaded.

Note that, without loss of generality, the scheme is described assuming MG-1 is overloaded and MG-2 is the supporting MG. However, if MG-2 is overloaded and MG-1 is the supporting one, the extracted formulations can be straightforwardly applied by exchanging the subscripts.

6.5 Small signal stability analysis

The small-signal analysis is carried out by augmenting the model presented in Chapter 3 to consider the effect of the SMF. However, the derivation procedure of Section 3.7 is not repeated here. The angular frequency of each DG (ω) with respect to a common angular frequency (ω_{com}) (i.e., the angular frequency of one of the DGs) can be expressed as

$$\delta = \int (\omega - \omega_{com}) dt \quad (6.40)$$

From (6.30), ω is described as

$$\omega = \omega_{max} - 2\pi \times \gamma \times m_{DG}^{DF} P_{DG} \quad (6.41)$$

Replacing (6.41) in (6.40) and then, linearizing the result yields

$$\Delta \dot{\delta} / 2\pi = m_{com}^{DF} \gamma^o \Delta P_{com} + \left(m_{com}^{DF} P_{com}^o - m_{DG}^{DF} P_{DG}^o \right) \Delta \gamma - m_{DG}^{DF} \gamma^o \Delta P_{DG} \quad (6.42)$$

where P_{com} and m_{com} represent power output and droop slope of the reference DG respectively, and superscript o indicates the value at the operating point. Taking into account (6.42), it can be shown that for a CMG formed by the two interconnected MGs, the linearized state-space equation can be described as (6.43) in which $x_{\text{MG-}i}$ includes the state variables of MG- i and $v_{\text{MG-}i}$ shows the buses voltages of MG- i .

$$\begin{aligned} \begin{bmatrix} \Delta \dot{x}_{\text{MG-1}} \\ \Delta \dot{x}_{\text{MG-2}} \\ \Delta \dot{x}_{\text{Tie-line}} \end{bmatrix} &= \begin{bmatrix} A_{\text{MG-1}} & O_{\text{Ns1} \times \text{Ns2}} & O_{\text{Ns1} \times 2} \\ O_{\text{Ns2} \times \text{Ns1}} & A_{\text{MG-2}} & O_{\text{Ns2} \times 2} \\ O_{2 \times \text{Ns1}} & O_{2 \times \text{Ns2}} & A_{\text{Tie-line}} \end{bmatrix} \begin{bmatrix} \Delta x_{\text{MG-1}} \\ \Delta x_{\text{MG-2}} \\ \Delta x_{\text{Tie-line}} \end{bmatrix} \\ &+ \begin{bmatrix} B_{\text{MG-1}} & O_{\text{Ns1} \times (2 \times \text{Nb2})} \\ O_{\text{Ns2} \times (2 \times \text{Nb1})} & B_{\text{MG-2}} \\ \hline & B_{\text{Tie-line}} \end{bmatrix} \begin{bmatrix} \Delta v_{\text{MG-1}} \\ \Delta v_{\text{MG-2}} \end{bmatrix} \end{aligned} \quad (6.43)$$

All parameters are expressed in the common d-q reference frame. It is to be noted that for MG- i with N_{DG} DGs, N_{d} loads, N_{L} lines and N_{b} buses, the number of states, $\text{Ns-}i$, is $10N_{\text{DG}} + 2N_{\text{L}} + 2N_{\text{d}}$ while the tie-line has two states, i.e., $x_{\text{MG-1}}$, $x_{\text{MG-2}}$ and $x_{\text{Tie-line}}$ are vectors with Ns1 , Ns2 and 2 elements respectively, while $v_{\text{MG-1}}$ and $v_{\text{MG-2}}$ have, respectively, $2N_{\text{b1}}$ and $2N_{\text{b2}}$ elements. In (6.43), $O_{a \times b}$ is a zeros matrix of a rows and b columns, and $A_{\text{MG-1}}$, $A_{\text{MG-2}}$ and $A_{\text{Tie-line}}$ are matrixes of order $\text{Ns1} \times \text{Ns1}$, $\text{Ns2} \times \text{Ns2}$ and 2×2 respectively. Also, $B_{\text{MG-1}}$, $B_{\text{MG-2}}$ and $B_{\text{Tie-line}}$ are matrixes of order $\text{Ns1} \times 2N_{\text{b1}}$, $\text{Ns2} \times 2N_{\text{b2}}$ and $2 \times 2(N_{\text{b1}} + N_{\text{b2}})$, respectively.

In order to obtain the homogeneous form of the state space representation of the CMG, the node voltages have to be eliminated from (6.43). Using (3.52), the voltages can be expressed as $[\Delta v_{\text{MG-1}} \ \Delta v_{\text{MG-2}}]^T = M \cdot \Delta x_{\text{CMG}}$. Then, (6.43) can be restated in the form of

$$\Delta \dot{x}_{\text{CMG}} = A_{\text{CMG}} \Delta x_{\text{CMG}} \quad (6.44)$$

where $x_{\text{CMG}} = [x_{\text{MG-1}} \ x_{\text{MG-2}} \ x_{\text{Tie-line}}]^T$ and A_{CMG} is the state matrix of the CMG. Now, the eigenvalues of the CMG can be calculated from (6.44).

6.6 Performance evaluation

The challenges with the ISS-based communication-free CMG forming procedure is discussed in this chapter and then, two different sets of solutions are presented. In this section, dynamic performance of the developed schemes is evaluated in order to demonstrate their efficacy. These methods are applied to two different sets of the CMGs with the aim of increasing the number of study cases. Further, eigenvalue analysis of the supervisory approach is reported as well.

6.6.1 Improved fully decentralized isolation

In order to appraise the performance of the approach developed in Section 6.3.2, several simulation case studies are carried out in PSCAD/EMTDC. Consider the network of Fig. 6.3. The detailed technical parameters of the MGs can be found in Table 6.1. MG-1 consists of three DGs while MG-2 includes two DGs with different load sharing characteristics. Let us assume the ISS has already been closed after satisfying both (6.1) and (6.3) due to a sudden power deficiency in MG-1. Then, MG-2 started to provide MG-1 with the required supporting power. Now, by a load decrease in MG-1 at $t = 2s$, (6.6) is violated, necessitating an isolation action. The following cases that are based on six different combinations verify the validity of the proposed approach. In the simulation results, the positive and negative signs of $P_{\text{Tie-line}}$ indicate it flows toward MG-1 and MG-2 respectively. For convenience, a three-second time interval is considered between each two consecutive events. In real systems, however, this interval should be adjusted based upon dynamic characteristics of the components.

$$1) \quad \text{Case 1: } P_{\text{MG-1}}^{\text{cap}} > P_{\text{MG-2}}^{\text{cap}} \text{ while } L2C_{\text{MG-1}} > L2C_{\text{MG-2}}$$

In this case, the generation capacities of MG-1 and MG-2 are assumed to be 600kW and 300kW respectively. Initially, the total load of MG-1 is about 570kW. At $t = 2s$, a 30% load decrease in MG-1 removes the overloading condition, as can be seen from Fig. 6.10a.

Table 6.1: Technical parameters of the MGs considered in Section 6.6.1.

| General parameters: | | | | | | |
|--|--------|--------|--------|--------|-------|-------|
| $\alpha = 0.1, V_{\max} = 6.35 \text{ kV}, V_{\min} = 5.75 \text{ kV}, f_{\max} = 50.5 \text{ Hz}, f_{\min} = 49.5 \text{ Hz}$ | | | | | | |
| MGs and CMG line parameters: | | | | | | |
| $Z_{\text{line}} = 0.1 + j 0.1 \Omega, Z_{\text{tie-line}} = 0.2 + j 0.2 \Omega$ | | | | | | |
| Droop coefficients of MG-1 | | | | | | |
| P^{cap} | 600kW | | | 300kW | | |
| DGs | DG-1 | DG-2 | DG-3 | DG-1 | DG-2 | DG-3 |
| m [Hz/kW] | 0.0033 | 0.005 | 0.01 | 0.0067 | 0.01 | 0.02 |
| n [kV/kVAr] | 0.006 | 0.009 | 0.018 | 0.012 | 0.018 | 0.036 |
| Droop coefficients of MG-2 | | | | | | |
| P^{cap} | 600kW | | 300kW | | | |
| DGs | DG-1 | DG-2 | DG-1 | DG-2 | | |
| m [Hz/kW] | 0.0033 | 0.0033 | 0.0067 | 0.0067 | | |
| n [kV/kVAr] | 0.006 | 0.006 | 0.012 | 0.012 | | |

Fig. 6.10b shows the power sharing among the DGs whereas the frequencies of the MGs are demonstrated in Fig. 6.10c. Due to the fact that the L2C ratio of MG-1 is still larger than that of MG-2, a power of about 33kW flows toward MG-1. Employing (6.21), thus, the controller commands ACL-2 to increase its demand to 49.5kW since $k = 2$. As it is shown in Fig. 6.10d, once ACL-2 demands the determined power at $t=5\text{s}$, the L2C ratios of the MGs become identical, successfully dropping the ISS current to almost zero. Then, at $t=8\text{s}$, the controller commands the ISS to open.

By accomplishing the isolation procedure, the controller resets ACL-2 to zero at $t = 11\text{s}$. Fig. 6.11 compares the voltages at the two sides of the ISS with and without applying the proposed scheme. It can be seen that the level of spikes at the opening moment decreases significantly when the scheme cancels the tie-line power prior to the isolation.

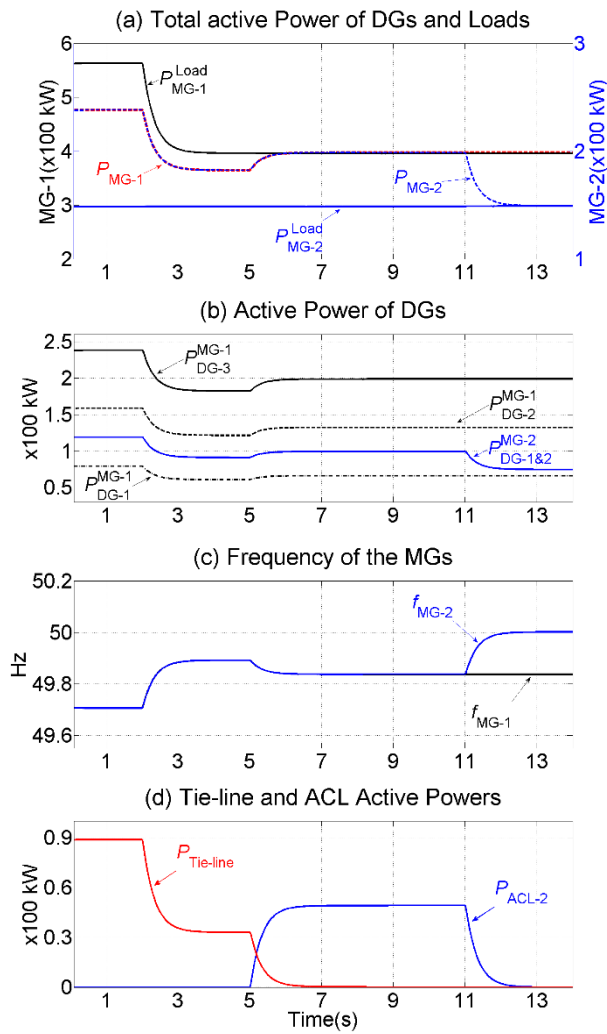


Fig. 6.10: Simulation results of Case 1.

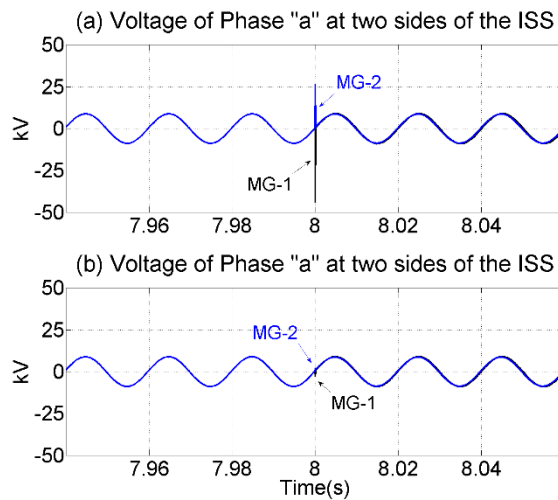


Fig. 6.11: Voltages at two sides of the ISS at the isolation moment (a) without applying the developed approach, (b) with applying the developed approach.

2) Case 2: $P_{MG-1}^{cap} > P_{MG-2}^{cap}$ while $L2C_{MG-1} < L2C_{MG-2}$

Let us assume the generation capacities of the MGs are identical to Case 1. Fig. 6.12a shows that the power deficiency is resolved following a 60% decrease in the load of MG-1 at $t=2s$. This causes $L2C_{MG-2}$ to become larger than $L2C_{MG-1}$, reversing the direction of $P_{Tie-line}$, as can be seen from Fig. 6.12b. Therefore, the controller utilizes (6.23) to calculate a demand reference of about 68.5kW for ACL-1 since $P_{Tie-line}$ is 23 kW. By activating ACL-2 at $t=5s$, the ISS power drops to zero as desired, yielding a successful isolation action with negligible disturbances at $t=8s$. Eventually, the isolation procedure is efficiently completed after decreasing the demand of ACL-1 to zero at $t = 11s$.

3) Case 3: $P_{MG-1}^{cap} = P_{MG-2}^{cap}$ while $L2C_{MG-1} > L2C_{MG-2}$

In this section, the performance of the approach is evaluated assuming the MGs have identical generation capacities of 600kW ($k = 1$). The load sharing ratios of the DGs are given in Table 6.1. Initially, MG-2 supports MG-1 with a power of about 132kW. Fig. 6.13a shows that a load decrease of 30% occurs in MG-1 at $t=2s$, necessitating an isolation action. Since $L2C_{MG-1}$ is still larger than $L2C_{MG-2}$, the controller should command ACL-2 to demand the power derived utilizing (6.21), i.e., 97kW.

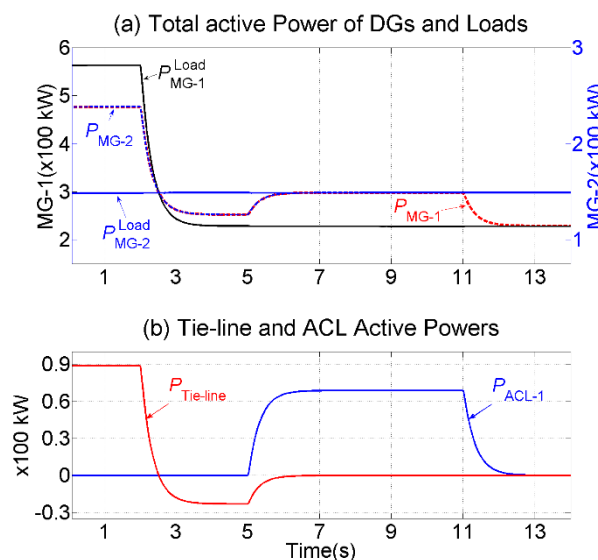


Fig. 6.12: Simulation results of Case 2.

Fig. 6.13b displays that by activating ACL-2 at $t=5s$, $P_{Tie-line}$ is desirably canceled as the L2C ratios of the MGs become the same. Then, the MGs are isolate at $t=8s$. The action is successfully done by removing ACL-2 at $t=11s$.

4) *Case 4:* $P_{MG-1}^{cap} = P_{MG-2}^{cap}$ while $L2C_{MG-1} < L2C_{MG-2}$

This case considers the MGs of Case 3 with the same initial conditions. The power shortfall of MG-1 is relieved due to a 60% decrease in its total load at $t=2s$. Consequently, $L2C_{MG-1}$ becomes smaller than $L2C_{MG-2}$, as shown in Fig. 6.14a.

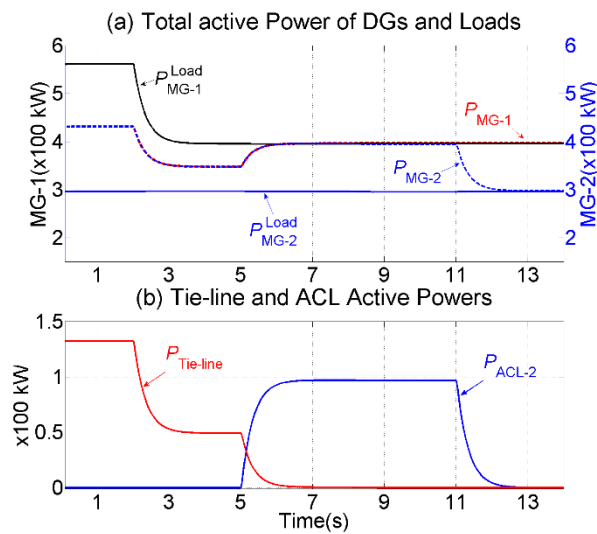


Fig. 6.13: Simulation results of Case 3.

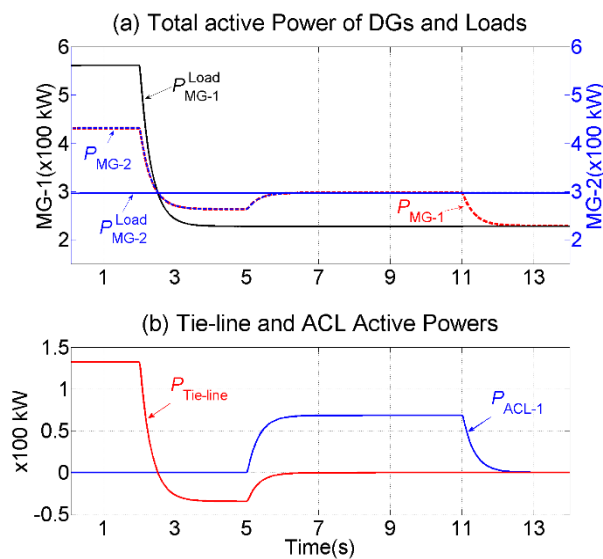


Fig. 6.14: Simulation results of Case 4.

Hence, a power of 35kW flows through the ISS to MG-2. With the aim of nullifying this power, ACL-1 demands a power of about 68kW at $t=5s$, as can be seen from Fig. 6.14b. The isolation is efficiently handled by opening the ISS and removing ACL-1 at $t=8s$ and $t=11s$, respectively.

5) *Case 5: $P_{MG-1}^{cap} < P_{MG-2}^{cap}$ while $L2C_{MG-1} > L2C_{MG-2}$*

Let us assume the generation capacities of MG-1 and MG-2 are 300kW and 600kW, respectively ($k = 0.5$). The simulation results are shown in Fig. 6.15. Initially, the total load demand of MG-1 is 290kW, receiving a supporting power of about 92kW from MG-2. $P_{Tie-line}$ decreases to about 35kW following a 30% decrease in total load of MG-1 at $t=2s$. Thus, ACL-2 is commanded to raise its load to about 103kW at $t=5s$.

Since $P_{Tie-line}$ is successfully dropped to zero, the controller sends a command to the ISS to open at $t=8s$. Afterward, ACL-2 decreases its demand to zero at $t=11s$ to terminate the action.

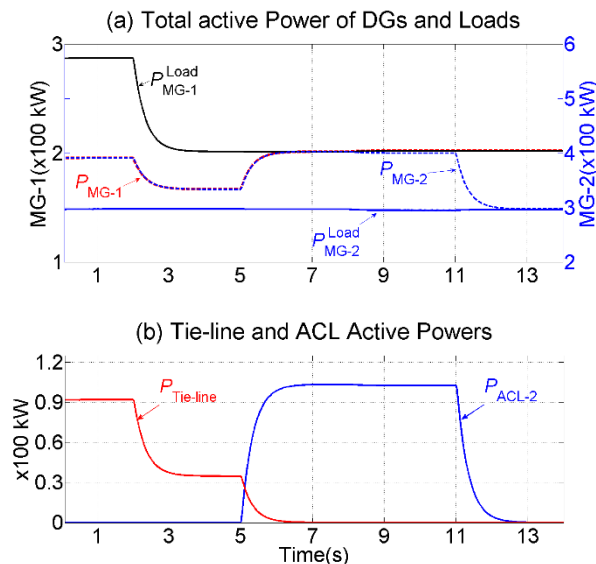


Fig. 6.15: Simulation results of Case 5.

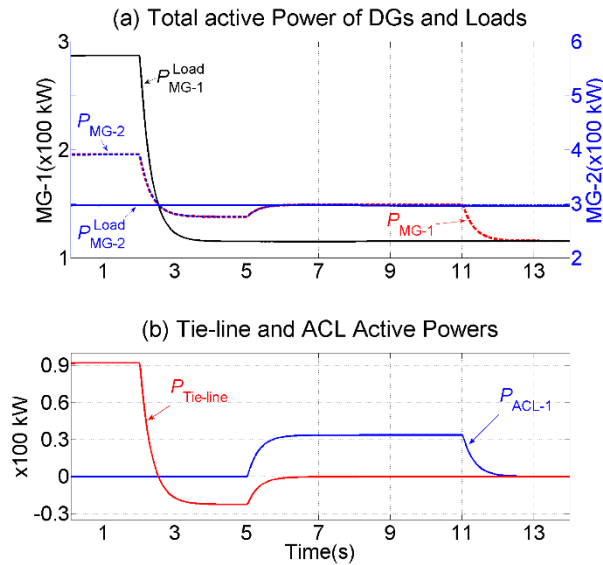


Fig. 6.16: Simulation results of Case 6.

6) Case 6: $P_{MG-1}^{cap} < P_{MG-2}^{cap}$ while $L2C_{MG-1} < L2C_{MG-2}$

Consider the MGs of Case 5 with the same initial conditions. In this case, however, it is assumed that MG-1 experiences a 60% load decrease at $t=2s$, thereby reversing the direction of the passing power through the ISS. The simulation results are presented in Fig. 6.16. According to the developed algorithm, the controller utilizes (6.23) to extract the load should be demanded by ACL-1. Thus, ACL-1 increases its load to a high of about 33.5kW at $t=5s$, canceling tie-line current.

Following the successful act of ACL-1, the ISS opens at $t=8s$, with almost no disturbance. Eventually, the controller deactivates the ACL at $t=11s$ to end the procedure.

6.6.2 The supervisory scheme

In order to appraise the performance of the supervisory scheme, relevant simulation case studies are carried out in PSCAD/EMTDC. Consider the network of Fig. 6.8. The detailed technical parameters of the network and the schemes can be found in Table 6.2. MG-1 consists of three DGs whereas MG-2 includes two

DGs with different ratings. In the simulation results, the positive and negative signs of $P_{\text{Tie-line}}$ indicate it flows towards MG-1 and MG-2, respectively.

1) Case 1

Performance of the supervisory scheme on forming the CMG system is evaluated in this case. The simulation results are shown in Fig. 6.17. Initially, the total load of MG-1 is about 1.3MW. Following a 38% load increase in MG-1 at $t = 1$ s, its frequency drops below 49.6Hz at about $t = 1.33$ s, satisfying the coupling conditions ((6.1) and (6.3)). Once the synchronization condition between the voltages at two sides of the ISS fulfils at about $t = 1.57$ s (See Appendix A), it closes to form the CMG.

Assuming the supervisory scheme is off, a supporting power of about 365kW flows through the tie-line towards MG-1. As a result, the power output of MG-1 decreases to 1.44MW while its desirable value ($P_{\text{MG-1}}^{\text{DSR}}$) is about 1.62MW. This concern can be efficiently addressed by including the proposed approach. The supervisory scheme switches to Mode 1 by closing the ISS. Consequently, the power output of MG-1 is successfully raised to $P_{\text{MG-1}}^{\text{DSR}}$, reducing $P_{\text{Tie-line}}$ to $P_{\text{Tie-line}}^{\text{DSR}}$ (190kW). Based on (6.28), the droop slopes of MG-1 are properly updated in intervals of 100ms using a very low bandwidth communication system, as can be seen from Fig. 6.17d. To achieve this, the SMF decreases from 1 to 0.72. Moreover, by increasing $P_{\text{MG-1}}^{\text{Vcap}}$ by 38% the CMG operates at a higher frequency of about 49.85Hz instead of 49.7Hz, as already demonstrated in Fig. 6.9.

Table 6.2: Technical parameters of the MGs and the CMG

| General parameters: $\alpha = 0.1$, $V_{\text{max}} = 6.35$ kV, $V_{\text{min}} = 6$ kV, $f_{\text{max}} = 50.5$ Hz, $f_{\text{min}} = 49.5$ Hz | | | | | |
|--|--|------|------|--|------|
| MGs and CMG line parameters: $Z_{\text{line}} = 0.1 + j 0.1 \Omega$, $Z_{\text{tie-line}} = 0.2 + j 0.2 \Omega$ | | | | | |
| Droop slopes of the MGs | | | | | |
| P^{cap} | MG-1 ($P^{\text{cap}} = 1.8\text{MW}$) | | | MG-2 ($P^{\text{cap}} = 1.2\text{MW}$) | |
| DGs | DG-1 | DG-2 | DG-3 | DG-1 | DG-2 |
| m [Hz/MW] | 1 | 2.5 | 2.5 | 1.4 | 2 |
| n [kV/MVAr] | 0.3 | 0.75 | 0.75 | 0.42 | 0.6 |
| L_{DG} [mH] | 5 | 12.5 | 12.5 | 7 | 10 |

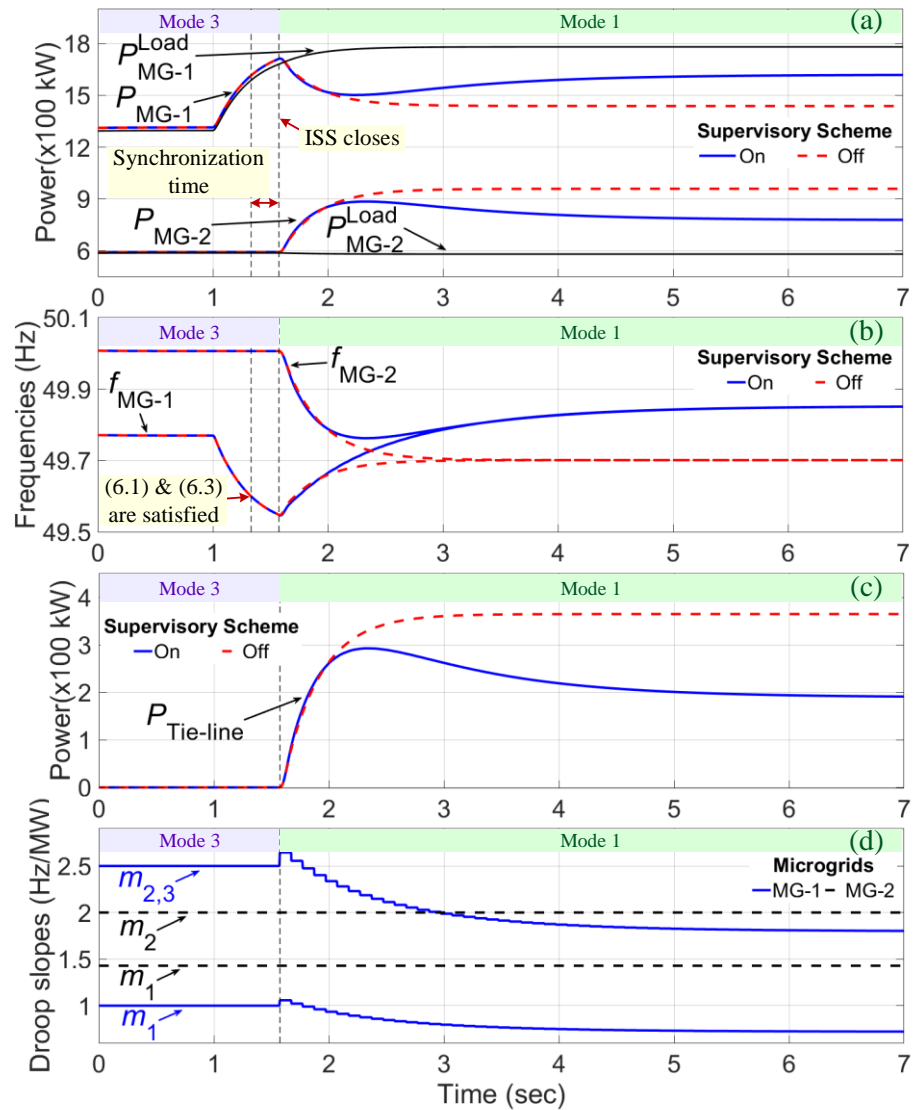


Fig. 6.17: Simulation results of Case 1.

Note that the transition from Mode 3 to Mode 1 causes the SMF to experience two different trends within this case. By rising the load of MG-1 at $t=1$ s, the power output of MG-1 increases to a peak of 1.73MW at $t = 1.57$ s which is about 7% larger than P_{MG-1}^{DSR} . Since from this point onwards the system should be managed under Mode 1, the SMF slightly rises by closing the ISS to reduce the power output of MG-1 to its desired value which is the main target of this mode. At the same time, MG-2 starts supporting MG-1 by providing $P_{Tie-line}$, dropping power output of MG-1 below P_{MG-1}^{DSR} at about $t = 1.71$ s. Afterwards, the SMF keeps

falling in order to shift the power output up to P_{MG-1}^{DSR} again. This goal is reached at about $t = 5.3s$.

2) Case 2

This case validates the efficiency of the scheme in lowering $P_{Tie-line}$ down to zero for a disturbance-free isolation. The simulation results are shown in Fig. 6.18. Let us consider the same CMG system of Case 1 operating at its steady state.

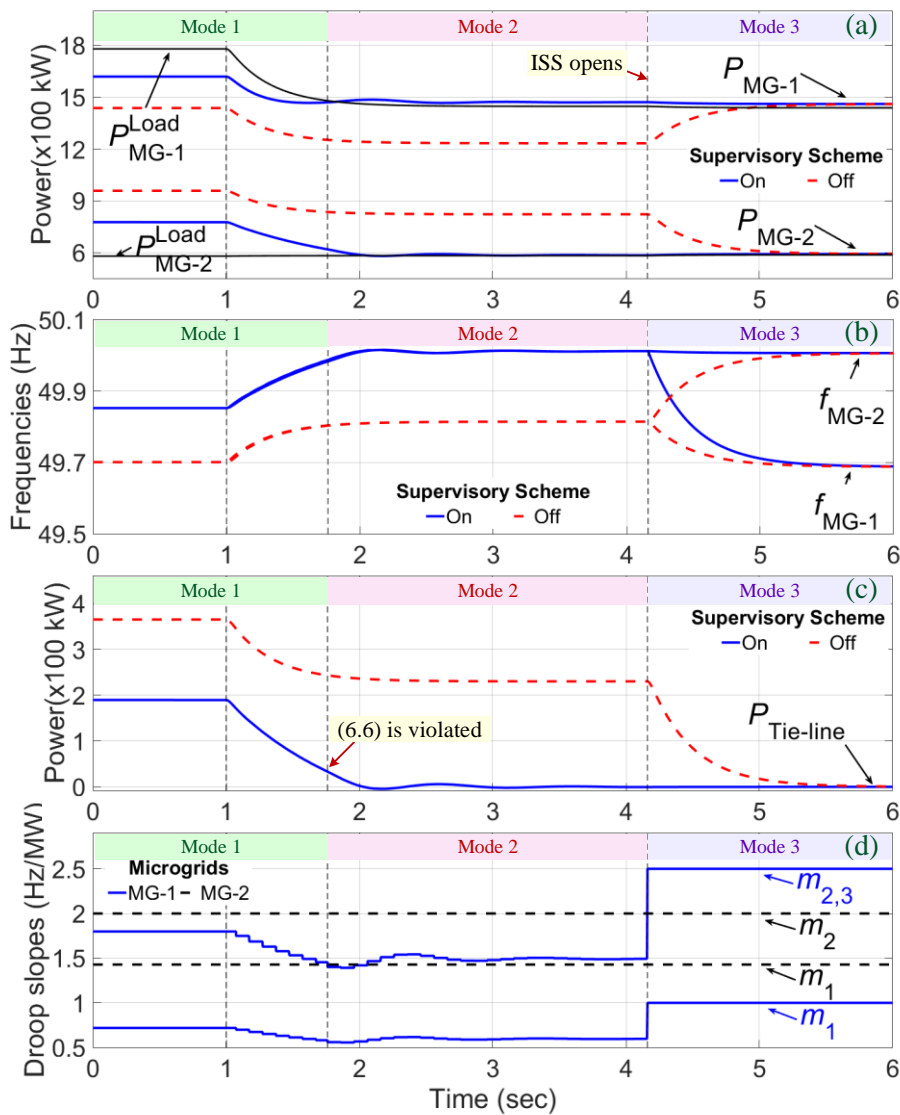


Fig. 6.18: Simulation results of Case 2.

Following an 18% load decrease in MG-1 at $t = 1$ s, $P_{\text{Tie-line}}$ drops below the threshold of (6.6) at $t = 1.76$ s which means the overloading condition of MG-1 is removed and the interconnection is no longer required. Assuming the supervisory scheme is active, its operating mode transits from Mode 1 to Mode 2 to modify the droop coefficients of MG-1 utilizing the SMF of (6.37), as can be seen from Fig. 6.18d. Finally, the controller sends a command to the ISS to open at $t = 4.16$ s when the tie-line power is almost zero.

Once the MGs are isolated, the supervisory scheme switches to Mode 3 based on which the droop coefficients are reset to their default values by (6.39). Also, Fig. 6.18 shows the outcomes when the scheme is off. Since L2C of MG-1 is still larger than that of MG-2, a supporting power of about 230kW flows towards MG-1 even after violation of (6.6). Hence, the ISS should open while $P_{\text{Tie-line}}$ is not zero, causing destructive voltage transients due to the derivative term of (6.10). Note that opening of the ISS is intentionally postponed to $t=4.16$ s to provide a better comparison between on and off states of the scheme.

The transition from Mode 1 to Mode 2 is fulfilled following the load decrease in MG-1. As a result of this reduction, the DGs of MG-1 tend to reduce their output powers as well. Then, the supervisory controller under Mode 1 starts reducing the SMF at $t=1$ s in order to maintain the power output of MG-1 at $P_{\text{MG-1}}^{\text{DSR}}$. This condition carries on till the violation of (6.6) and the subsequent transition to Mode 2 at $t = 1.76$ s, which dictates the new target of reducing $P_{\text{Tie-line}}$ to zero. Since at this moment MG-1 still receives support from MG-2, the controller commands the DGs of MG-1 to increase their power output through decreasing the SMF.

After a few slight variations of the SMF, the ISS can be opened with almost no disturbance at $t = 4.16$ s when the controller is switched to Mode 3. The droop regulators are given back the default values by resetting the SMF to one. As a result, the droop slopes of the DGs in MG-1 are increased, reducing the frequency to about 49.7 Hz.

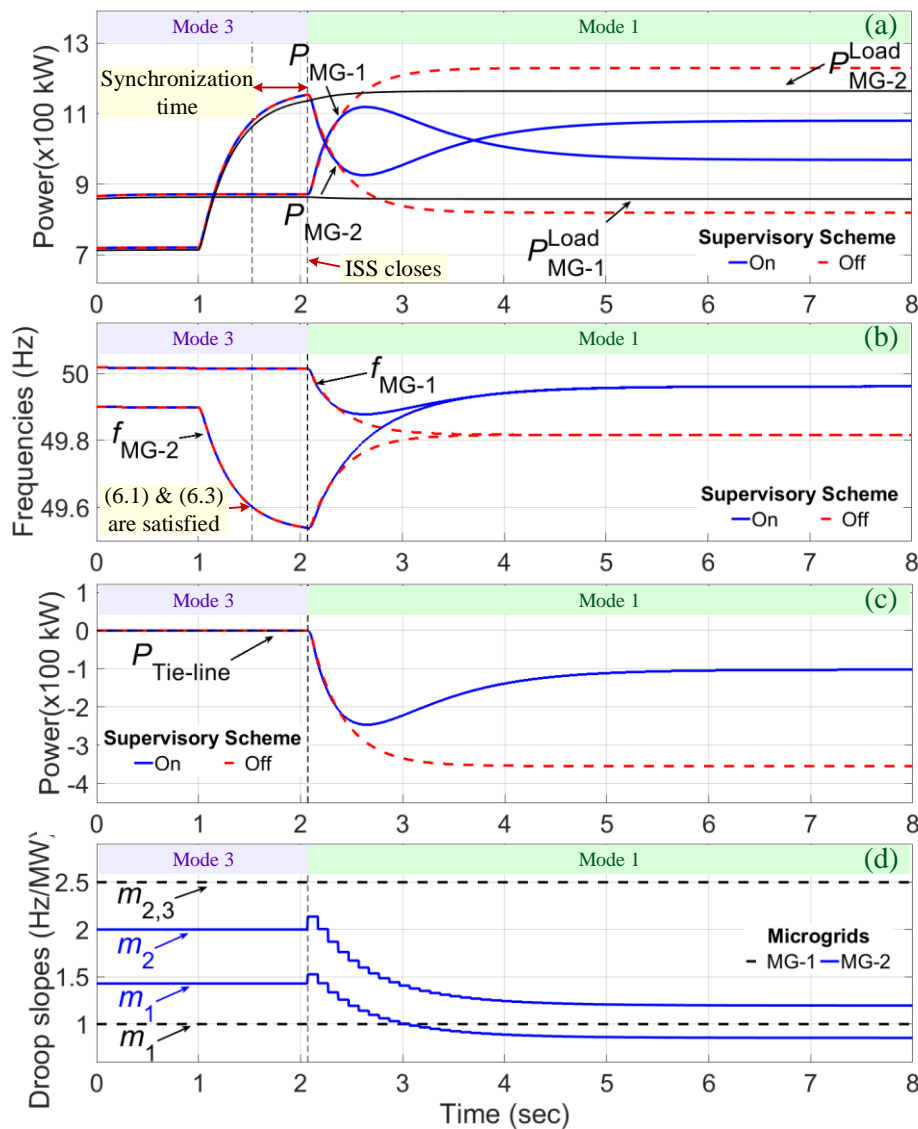


Fig. 6.19: Simulation results of Case 3.

3) Case 3

The operation of the scheme when an overloading occurs in MG-2 is studied in this case. Although the formulation of the scheme is fulfilled assuming a power deficiency in MG-1, similar action can be conducted when the shortfall takes place in MG-2. The simulation results are shown in Fig. 6.19. Following a 62% load increase in MG-2, the coupling conditions are satisfied at about $t = 1.53$ s and the ISS closes at $t = 2.07$ s. Assuming the scheme is off, a supporting power of about 360 kW flows towards MG-2 which is about four times larger than $P_{Tie-line}^{DSR}$, i.e., 100 kW. As can be seen from Fig. 6.19, the supervisory scheme can keep

power output of MG-2 at $P_{MG-2}^{DSR}=1.08\text{MW}$ through properly modifying the droop slopes of MG-2, decreasing the tie-line power to $P_{Tie-line}^{DSR}$ and raising the frequency to about 49.96Hz.

Similar to Case 1, the SMF experiences two different trends in transiting from Mode 3 to Mode 1. By increasing the load of MG-2 at $t = 1\text{s}$, the power output of MG-2 increases to about 1.17MW at $t = 2.07\text{s}$ which is 8.5% larger than P_{MG-2}^{DSR} . At this moment, the operating mode switches to Mode 1 by closing the ISS, raising the SMF slightly to reduce the power output of MG-2 to P_{MG-2}^{DSR} . After a very short time, the output power of MG-2 decreases considerably due to sharing the total load demand among the DGs of both MGs. Hence, the controller reduces the SMF in order to force the DGs of MG-2 to maintain the power output at P_{MG-2}^{DSR} . The system condition settles at about $t=5.6\text{s}$.

4) Case 4

This case considers the same CMG system of Case 3 operating at its steady state to validate the efficiency of the supervisory scheme in implementing a desirable isolation. Following a 30% load decrease in MG-2 at $t = 1\text{s}$, the scheme switches to Mode 2 at about $t = 1.16\text{s}$. Thus, the controller commands the ISS to open at $t=3.78\text{s}$ at which $P_{Tie-line}$ is successfully decreased to about zero with an SMF of 0.68. The waveforms are shown in Fig. 6.20. It is to be noted that without including the supervisory scheme, a supporting power of about 160kW can flow towards MG-2 even after violation of (6.6) which may cause destructive transients during the isolation procedure.

Two transition processes, i.e., Mode 1 to Mode 2 and then, Mode 2 to Mode 3, occur in this case. During the first one, the SMF experiences a number of changes in its trend. From $t = 1\text{s}$ to $t = 1.16\text{s}$, the SMF decreases to maintain the power output of MG-2 at its desired value since the system is operating under Mode 1. From $t = 1.16\text{s}$ to $t = 1.23\text{s}$, the reduction of the SMF continues under Mode 2 in order to cancel the tie-line power through increasing power output of

MG-2. From this point onwards, the SMF experiences a few variations due to the dynamic response of the system.

Eventually, the ISS can open at about $t = 3.78s$ when $P_{Tie-line}$ settles down at zero. At this moment, the second transition takes place through resetting the droop coefficients to their default values. The frequency of MG-2, consequently, decreases to 49.8Hz since the droop coefficients of the DGs are now increased.

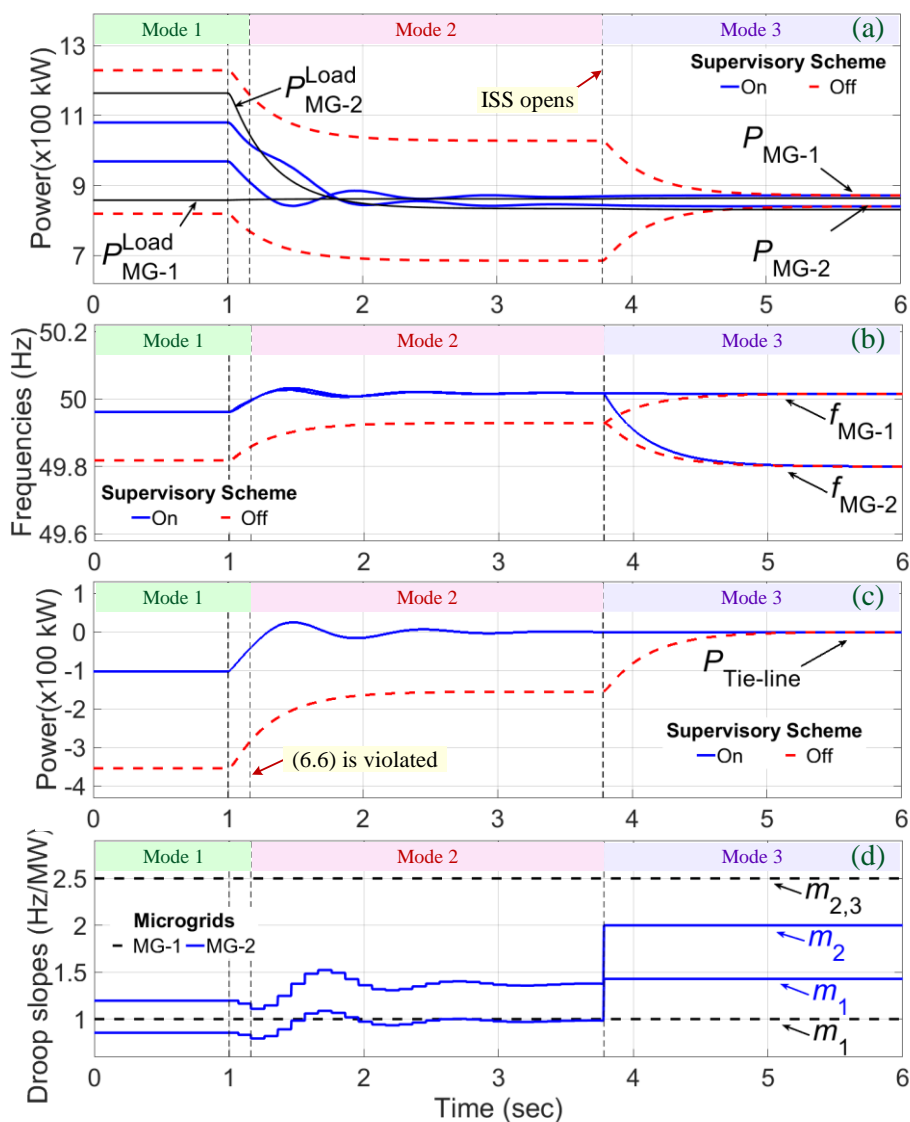


Fig. 6.20: Simulation results of Case 4.

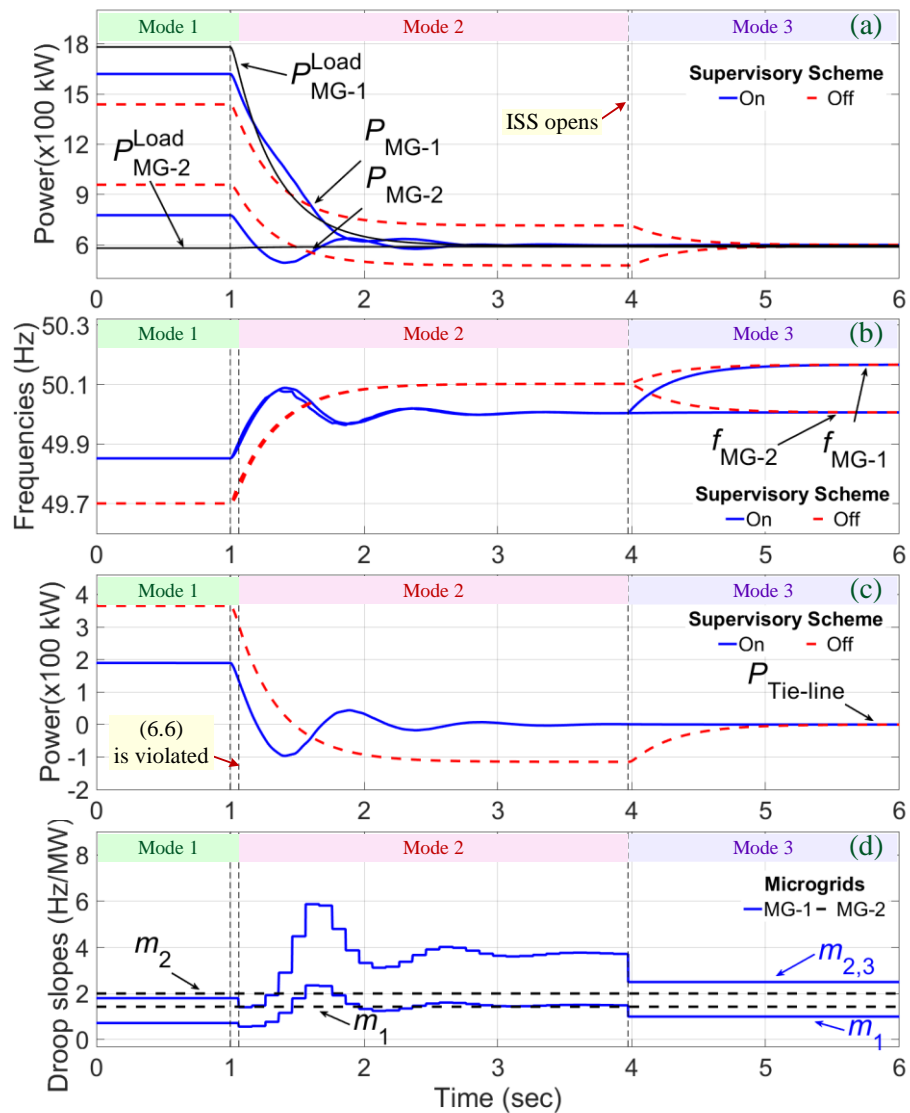


Fig. 6.21: Simulation results of Case 5.

5) Case 5

Fig. 6.21 illustrates the simulation results of the same system of Case 2 when MG-1 experiences a larger load reduction of about 67% at $t = 1$ s. Due to the fact that L2C of MG-1 after the load change is smaller than that of MG-2, $P_{Tie-line}$ changes its direction towards MG-2, as can be seen from Fig. 6.21c. The waveforms prove the capability of the scheme in reducing the tie-line power to zero by transiting to Mode 2 and then, fulfilling a successful isolation at $t = 3.97$ s.

The transition from Mode 1 to Mode 2 takes place in a very short time after the load change at $t = 1$ s. The reduction in the SMF, already started under Mode 1

to maintain the power output of MG-1 at the desired value, carries on till $t = 1.28\text{s}$ under Mode 2 to decrease the tie-line power to zero. Due to the severity of the load change, the power output of the MGs experiences variations, causing some trend changes in the SMF. The main reasons for this type of oscillations can be found in 6.6.3. Finally, the SMF settles down at a comparatively larger value than it had under Mode 1 with the aim of decreasing the power output of MG-1. Otherwise, a non-zero supporting power can flow towards MG-2, resulting in undesirable disturbances during the isolation.

Note that the power curves in Fig. 6.21a are overlapped since both MGs have similar load demands after the load change at $t = 1\text{s}$. By opening the ISS at $t=3.97\text{s}$, the operation transits to Mode 3, resetting the droop coefficients to their defaults. The frequency of MG-1 rises to about 50.17Hz as a result of the reduction in the associated droop coefficients.

6.6.3 Eigenvalue studies

Small signal analysis of the simulated CMG is presented in this section in order to examine the impact of the supervisory coefficient on the stability of the system. Eigenvalues of state matrix of the CMG ($A_{\text{CMG}} \in \mathbb{R}^{70 \times 70}$) are derived by taking into account the variation of SMF. Let us consider the CMG with technical parameters shown in Table 6.2. Fig. 6.22 illustrates traces of the dominant eigenvalues of the CMG when the SMF changes from 1.6 to 0.5 which is the practical range for the considered CMG. In most cases, the SMF should be decreased to a value below one to perform the scheme under both Mode 1 and Mode 2, as already shown by the dynamic simulations.

It is obvious from Fig. 6.22 that decreasing the SMF increases the stability of the system as the eigenvalues move to the left in the s-plane. However, it is possible for the SMF to rise to a value larger than one, especially during isolation procedure of some extreme cases such as Case 5 of the previous section. In such circumstances, although the eigenvalues move towards the right, the system stability can be maintained as the dominant eigenvalues are still on the left half s-

plane. These outcomes fit well with the dynamic response of the system already shown in subsection 6.6.2.

Along with the discussion in Section 6.1, the impact of selecting adequately high coupling inductances of the DGs on the droop gain stability margins is evaluated for the CMG under study. These marginal values indicate the maximum active power droop coefficients of the DGs, before the CMG faces instability. Fig. 6.23 illustrates the marginal droop coefficients of the sample DGs when the ratio $L_{DG}\omega/|Z_{line}|$ varies from 1 to 10. The plots indicate that the sensitivity of the system to different characteristics of the line impedances decreases by increasing the ratio, enhancing droop gain stability margins of the overall system.

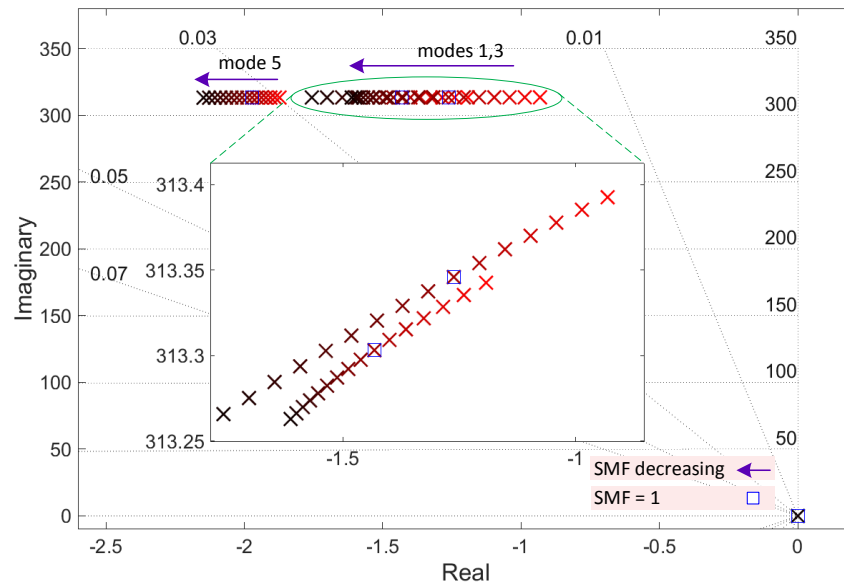


Fig. 6.22: Trace of dominant modes of the CMG when the SMF decreases from 1.6 to 0.5.

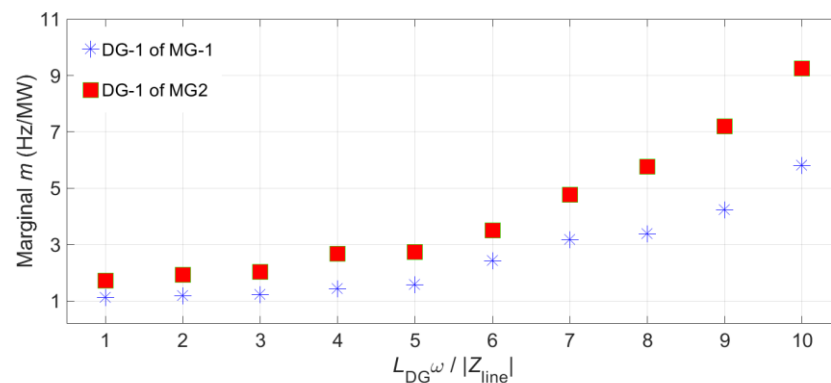


Fig. 6.23: Marginal droop coefficients of the sample DGs when the ratio of the coupling reactance of the DGs to line impedances varies from 1 to 10.

The permitted range of variation for the SMF depends mainly on its impacts on the stability of the CMG. This issue is highly influenced by the operating point of each CMG. Limiting the SMF values from the lower side is not of major concern since decreasing this value has positive impacts on the stability of the system, as can be seen from Fig. 6.22. Note that the SMF should be decreased in most of the cases to achieve the desirable operation of the system. However, the upper boundaries of the SMF should be mainly taken into account due to the fact that increasing the SMF can deteriorate the performance of the system from the stability point of view.

Figure 6.23 shows the upper limits of the droop coefficients of the DGs for different impedance characteristics of the system calculated by taking advantage of the developed small signal model. Similar pattern can be applied to find the upper limits of the SMF considering different operating points of the CMG. For example, this value is about 4.9 for the system studied in Fig. 6.22.

6.7 Conclusion

A supervisory control scheme is presented to address the challenges with the ISS-based coupling of isolated droop-regulated MGs. The strategy is developed to be applied under three modes, namely Mode 1 that is initiated by forming the CMG to keep the power output of the overloaded MG close to its maximum; Mode 2 that aims to fulfil a successful isolation when the interconnection is not required anymore; and Mode 3 that is activated by opening the ISS to reset default values of the DGs controllers.

Several simulation studies are carried out to evaluate performance of the proposed scheme under various conditions. The simulation results illustrate that once the CMG is formed the scheme can desirably control the power output of the MGs by switching to Mode 1. Moreover, success of the scheme in reducing the tie-line power to zero before opening the ISS is shown under various L2C conditions. The obtained results prove that the scheme can effectively achieve the defined goals using a very low bandwidth communication system.

Chapter 7. CONCLUSIONS AND SCOPE OF FUTURE RESEARCH

The key conclusions of this thesis along with the scopes of further research are summarized in this chapter.

7.1 General conclusions

- The overloading condition of an isolated AC MG can be alleviated using the supporting power supplied by a neighbouring MG, thereby considerably reducing the level of load to be shed. Instead of a back-to-back power converter, the associated system of CMG can be established through closing an ISS mounted on the tie-line between the MGs in order to avoid the disadvantages of power loss incurred by the converters.
- The success in implementing a fully decentralized control on the ISS-based CMG systems is highly dependent on the criteria derived for identifying the shortfall in the MG as well as the availability of the surplus power in the neighbouring MG. Operation of the system can be desirably accomplished by accurately defining these criteria; however, any error in correctly detecting them can result in a considerable system malfunction.
- Stability of the system should be evaluated before interconnecting the MGs. This should be done by investigating the impact of the possible interconnection on the eigenvalues of the interconnected system. The coupling should be avoided if it can lead to movement of the dominant modes towards right half s-plane. Sensitivity of these

eigenvalues should be carefully evaluated for variation of various control parameters such as droop coefficients of the local controllers.

- The synergy of local support from BES in an MG and external support from a coupled neighbouring MG can efficiently handle the overloading of different levels. In this case, the formation of the CMG systems is limited to severe shortfalls only, whereas the minor ones can be coped with the local energy storages. However, the operation criteria should be defined carefully since both the number of variables and the possible scenarios increase.
- A decentralized under frequency load-shedding action can be performed in isolated MGs using the multilayer droop-based scheme proposed in this thesis. In this way, the MG frequency can be successfully maintained above a pre-specified minimum. It is demonstrated that the load-shedding action can be desirably coordinated with a CMG formation scheme under a two-level control approach in order to handle the deficiency. A very low-bandwidth communication system can be adopted to suitably organize the collaboration of these control levels.
- As the main challenges with the communication-free ISS-based coupling of isolated droop-regulated MGs, the supporting power is probably larger than the actual requirement of the MG experiencing the power shortfall and the isolation of the coupled MGs can cause destructive transients. The supervisory strategy presented in this thesis can efficiently address these challenges under three operating modes. Consequently, the power output of the overloaded MG is kept close to its maximum by forming the CMG. Also, based on the defined L2C factor, a successful isolation of the MGs is fulfilled when the interconnection is not required anymore.

7. 2 Scope of future research

- The ISS-based interconnection of two MGs is developed in this thesis in order to cope with the overloading problems. Based on the outcomes, the possibility of forming an ISS-based CMG system with larger number of MGs can be taken into account. Also, the MGs can be of different AC and DC types.
- In this thesis, alleviating the overloading conditions through forming ISS-based CMG systems has been the main objective. The required criteria for performing a desirable CMG system should be studied when the other possible targets, such as reliability improvement, are considered. This is because the success of such actions is highly dependent on the accuracy of the derived criteria.
- Stability analysis of the CMG systems is critical and should be done before closing the ISS. In this thesis, small signal models are derived for the MGs based on which the eigenvalue analysis is performed. However, the MG system is actually non-linear. Thus, application of the non-linear stability analysis methods can be investigated for the CMG forming strategies.
- The ISS-based interconnection of the isolated MGs requires a synchronization stage at the CMG forming moment in order to guarantee a disturbance free operation. Stability of the entire system can be endangered if fulfilling the synchronization stage takes a longer time. Therefore, much more suitable and faster synchronization schemes should be developed in order to ensure a desirable CMG forming action.
 - In this thesis, a symmetrical structure is assumed for the MGs. Thus, the proposed strategies as well as the developed models are to be applied to such MGs. The self-healing schemes can be further developed to be efficiently employed for unsymmetrical and hybrid MGs with various types of loads as well.

APPENDIX

Appendix A. Synchronization Process

The ISS closing consists of a synchronization process, after which a CMG is formed. Fig. A1 illustrates the block diagram of the applied synchronization technique, utilized in time-domain analyses of this research. As it can be seen from this figure, the ISS closes once the voltage magnitude difference across ISS, $|\Delta v|$, becomes smaller than ϵ_v and the voltage phase difference across ISS, $|\Delta\delta|$, becomes smaller than ϵ_δ .

Let us assume the controller initiates the ISS closing command at $t=0$. The voltages at the either sides of the ISS are assumed to be synchronized at $t=t_{\text{sync}}$ if

$$(2\pi f_{\text{MG-1}} t_{\text{sync}} + \theta_1) = (2\pi f_{\text{MG-2}} t_{\text{sync}} + \theta_2) + 2k_t\pi \quad (\text{A1})$$

where $f_{\text{MG-1}}$ and $f_{\text{MG-2}}$ are respectively the frequency of MG-1 and MG-2 while θ_1 and θ_2 are the phases of the voltage of MG-1 and MG-2 side of ISS, when the controller command is initiated. Eq. (A1) can be rewritten as

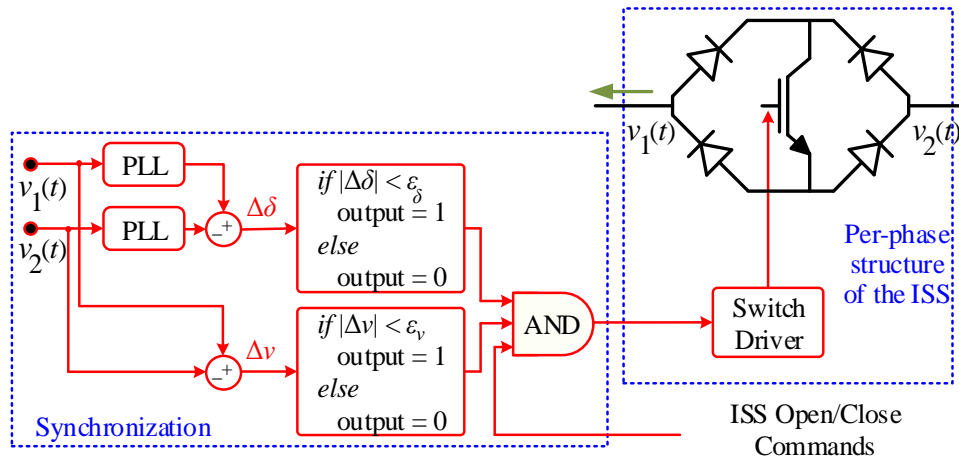


Fig. A1: Diagram of the synchronization process.

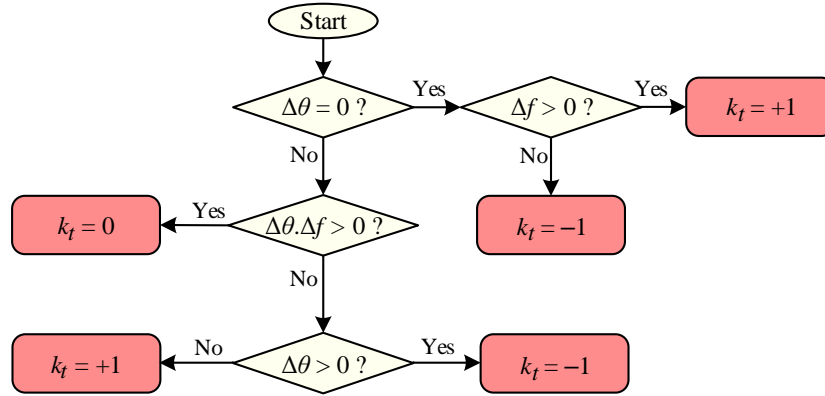


Fig. A2: The employed algorithm to determine the value of k_t .

$$t_{\text{sync}} = \frac{1}{2\pi} \frac{\Delta\theta + 2k\pi}{\Delta f} \quad (\text{A2})$$

where $\Delta\theta = \theta_2 - \theta_1$, $\Delta f = f_{\text{MG-1}} - f_{\text{MG-2}}$. $k_t = 0, \pm 1$ is determined based on the different values of $\Delta\theta$ and Δf , as illustrated in Fig. A2. It is to be noted that the actual synchronization time may be slightly (i.e., less than half a cycle) larger than t_{sync} so that the difference of voltage magnitude at either side of the ISS ($|\Delta v|$) also becomes smaller than ε_v . Fig. 3.7 expresses t_{sync} for different values of $\Delta\theta$ and Δf .

Example: Let us consider simulation study Case-1 of the centralized approach, discussed in Section 3.8.1. In this system, the ISS command is initiated at $t = 1.2\text{s}$ at $f_{\text{MG-1}} = 49.5786\text{Hz}$ and $f_{\text{MG-2}} = 50.3524\text{Hz}$. Fig. A3a shows the instantaneous phase-a voltage at either side of ISS at this time. From this figure, considering the time difference between the command initiation time and the previous zero-crossing of each phase (i.e., $t_1 = 0.0087\text{ s}$ and $t_2 = 0.0138\text{ s}$), one can obtain the voltage phase at either side of ISS as $\theta_1 = 2.7102\text{ rad}$ and $\theta_2 = 4.3660\text{ rad}$. Therefore, the t_{sync} is equal to 0.9518s from (A2). This means the synchronization is expected to occur at $t = 1.2 + 0.9518 = 2.1518\text{ s}$.

Due to the voltage magnitude difference, the synchronization is fulfilled at $t=2.1625\text{ s}$, as seen from Fig. A3b. As it can be seen from Fig. A3c, the ISS closes once the voltage difference across ISS falls below a pre-defined threshold. It is to be noted that some other techniques such as the ones presented in [140, 141] can also be used to speed up the synchronization process.

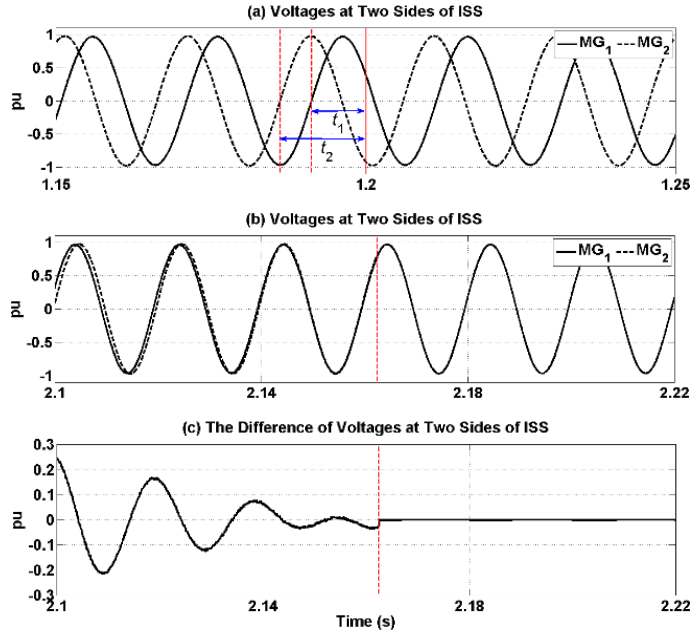


Fig. A3: (a) Voltage at two sides of the ISS when the self-healing command is initiated, (b) voltage at two sides of the ISS when two MGs are synchronized, (c) the difference of voltages at two sides of the ISS at synchronization time.

Appendix B. Charging Control of the BESEs

The charging mechanism of the BESEs is briefly discussed here. The BES is desired to be charged when the MG is lightly loaded. This condition can be described as

$$\Delta P_{MG-1} = P_{MG-1}^{\text{cap}} - \sum_{j=1}^{N_1} P_{\text{DER-}j} > \alpha_3 P_{MG-1}^{\text{cap}} \quad (\text{A3})$$

where $\alpha_1 < \alpha_3 < 1$ (See Section 4.2.2). Eq. (A3) can be rewritten as

$$f > f_{\min} + \alpha_3 (f_{\max} - f_{\min}) \quad (\text{A4})$$

Denote this threshold as f_{α_3} . If the MG's frequency satisfies (A4), the local controller of the BES initiates the charging. The charging droop gain of the BES is defined as

$$m_{\text{BES}}^{\text{chg}} = \frac{f_m - f_{\alpha_3}}{P_{\text{BES}}^{\text{max}}} \quad (\text{A5})$$

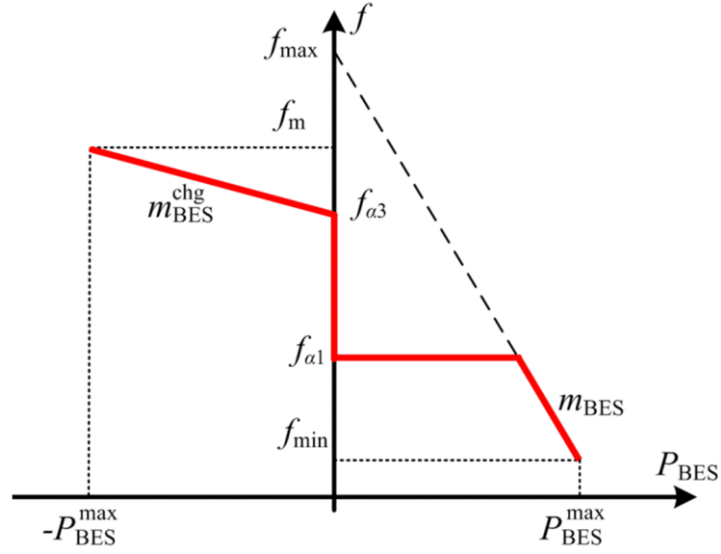


Fig. A4: Droop curve of the BESes.

where f_m is the MG frequency at no-load condition when BES-1 is connected to be charged by its maximum rate. Using (2.16), f_m can be explained as

$$f_m = f_{\max} - \frac{P_{\text{BES-1}}^{\max}}{\sum_{j=1}^{N_1} \frac{1}{m_{1j}}} \quad (\text{A6})$$

Employing (A6), the MG frequency never drops below f_{a3} when the BES is charging. The droop curves for the BESes in the charging and discharging modes are shown in Fig. A4 in which f_{a1} denotes the threshold of (3.19).

REFERENCES

- [1] H. Bevrani and A. L. G. Ghosh, "Renewable energy sources and frequency regulation: survey and new perspectives," *IET Renewable Power Generation*, vol. 4, no. 5, pp. 438-457, 2010.
- [2] A. Prasad, R. Taylor and M. Kay, "Assessment of solar and wind resource synergy in Australia," *Applied Energy*, vol. 190, pp. 354-367, 2017.
- [3] M. Farhadi and O. Mohammad, "Energy storage technologies for high-power applications," *IEEE Trans. Industry Applications*, vol. 52, no. 3, pp. 1953-1961, May 2016.
- [4] A. Hussain, S. Arif and M. Aslam, "Emerging renewable and sustainable energy technologies: State of the art," *Renewable and Sustainable Energy Reviews*, vol. 71, pp. 12-28, 2017.
- [5] A. Davda, B. Azzopardi, B. Parekh and M. Desai, "Dispersed generation enable loss reduction and voltage profile improvement in distribution network—case study, Gujarat, India," *IEEE Trans. Power Systems*, vol. 29, no. 3, pp. 1242-1249, May 2014.
- [6] T. Adefarati and R. Bansal, "Integration of renewable distributed generators into the distribution system: a review," *IET Renewable Power Generation*, vol. 10, no. 7, p. 873–884, 2016.
- [7] A. Keane, L. Ochoa, C. A. G. Borges, A. Alarcon and R. Currie, "State-of-the-art techniques and challenges ahead for distributed generation planning and optimization," *IEEE Trans. Power Systems*, vol. 28, no. 2, pp. 1493-1502, May 2013.
- [8] T. Dragicevic, X. Lu, J. Vasquez and J. Guerrero, "DC microgrids—part I: A review of control strategies and stabilization techniques," *IEEE Trans. Power Electronics*, vol. 31, no. 7, pp. 4876-4891, July 2016.
- [9] B. Muruganatham, R. Gnanadass and N. Padhy, "Challenges with renewable energy sources and storage in practical distribution systems," *Renewable and Sustainable Energy Reviews*, vol. 73, p. 125–134, 2017.
- [10] H. Ghoddami and A. Yazdani, "A mitigation strategy for temporary overvoltages caused by grid-connected photovoltaic systems," *IEEE Trans. Energy Conversion*, vol. 30, no. 2, pp. 413-420, June 2015.
- [11] B. Lasseter, "Microgrids [distributed power generation]," in *IEEE Power Engineering Society Winter Meeting*, Columbus, OH, 2001.
- [12] D. Olivares, A. Mehrizi-Sani, A. C. C. Etemadi, R. Iravani, M. Kazerani, A. Hajimiragha, O. Gomis-Bellmunt, M. Saeedifar, R. Palma-Behnke, G. Jimenez-Estevéz and N. Hatziargyriou, "Trends in microgrid control," *IEEE Trans. Smart Grid*, vol. 5, no. 4, pp. 1905-1919, July 2014.

-
- [13] J. Vasquez, J. Guerrero, A. Luna, P. Rodriguez and R. Teodorescu, "Adaptive droop control applied to voltage-source inverters operating in grid-connected and islanded modes," *IEEE Trans. on Industrial Electronics*, vol. 56, no. 10, pp. 4088-4096, Oct. 2009.
- [14] H. Karimi, H. Nikkhajoei and R. Iravani, "Control of an electronically-coupled distributed resource unit subsequent to an islanding event," *IEEE Trans. Power Delivery*, vol. 23, no. 1, pp. 493-501, Jan 2008.
- [15] Y. Mohamed and A. Radwan, "Hierarchical control system for robust microgrid operation and seamless mode transfer in active distribution systems," *IEEE Trans. on Smart Grid*, vol. 2, no. 2, pp. 352-362, June 2011.
- [16] M. Karimi-Ghartemani, S. Khajehoddin, P. Piya and M. Ebrahimi, "Universal controller for three-phase inverters in a microgrid," *IEEE Journal of Emerging and Selected Topics in Power Electronics*, vol. 4, no. 4, pp. 1342-1353, Dec. 2016.
- [17] S. Golestan, J. Guerrero and J. Vasquez, "Three-phase PLLs: a review of recent advances," *IEEE Trans. Power Electronics*, vol. 32, no. 3, pp. 1894-1907, March 2017.
- [18] B. Eid, N. Rahim, J. Selvaraj and A. ElKhateb, "Control methods and objectives for electronically coupled distributed energy resources in microgrids: a review," *IEEE Systems Journal*, vol. 10, no. 2, pp. 446-458, June 2016.
- [19] S. Parhizi, H. Lotfi, A. Khodaei and S. Bahramirad, "State of the art in research on microgrids: A review," *IEEE Access*, vol. 3, no. pp, pp. 890-925, 2015.
- [20] N. Díaz, A. Luna and J. G. J. Vasquez, "Centralized control architecture for coordination of distributed renewable generation and energy storage in islanded AC microgrids," *IEEE Trans. Power Electronics*, vol. 32, no. 7, pp. 5202-5213, July 2017.
- [21] D. C. T. Brandao, F. Marafão, M. Simões, J. Pomilio and P. Tenti, "Centralized control of distributed single-phase inverters arbitrarily connected to three-phase four-wire microgrids," *IEEE Trans. Smart Grid*, vol. 8, no. 1, pp. 437-446, Jan. 2017.
- [22] M. Yazdani and A. Mehrizi-Sani, "Distributed control techniques in microgrids," *IEEE Trans. Smart Grid*, vol. 5, no. 6, pp. 2901-2909, Nov 2014.
- [23] Q. Xu, J. Xiao, X. Hu, P. Wang and M. Lee, "A decentralized power management strategy for hybrid energy storage system with autonomous bus voltage restoration and state-of-charge recovery," *IEEE Trans. Industrial Electronics*, vol. 64, no. 9, pp. 7098-7108, Sept. 2017.
- [24] A. Etemadi, E. Davison and R. Iravani, "A decentralized robust control strategy for multi-DER microgrids—Part I: fundamental concepts," *IEEE Trans. Power Delivery*, vol. 27, no. 4, pp. 1843-1853, Oct. 2012.
- [25] M. Abdelwahed and E. El-Saadany, "Power sharing control strategy of multiterminal VSC-HVDC transmission systems utilizing adaptive voltage droop," *IEEE Trans. Sustainable Energy*, vol. 8, no. 2, pp. 605-615, April 2017.
- [26] M. Abdelaziz and H. Farag, "An enhanced supervisory control for islanded microgrid systems," *IEEE Trans. Smart Grid*, vol. 7, no. 4, pp. 1941-1943, July 2016.
- [27] T. Dragičević, J. Guerrero, J. Vasquez and D. Škrlec, "Supervisory control of an adaptive-droop regulated DC microgrid with battery management capability," *IEEE trans. Power Electronics*, vol. 29, no. 2, pp. 695-706, Feb. 2014.
- [28] M. Abdelaziz, H. Farag and E. El-Saadany, "Optimum reconfiguration of droop-controlled islanded microgrids," *IEEE Trans. Power Systems*, vol. 31, no. 3, pp.

- 2144-2153, May 2016.
- [29] S. Kotra and M. Mishra, "A supervisory power management system for a hybrid microgrid with HESS," *IEEE Trans. Industrial Electronics*, vol. 64, no. 5, pp. 3640-3649, May 2017.
- [30] J. Guerrero, J. Vasquez, J. Matas, L. Vicuna and M. Castilla, "Hierarchical control of droop-controlled AC and DC microgrids—A general approach toward standardization," *IEEE Trans. Industrial Electronics*, vol. 58, no. 1, pp. 158-172, Jan. 2011.
- [31] J. Vasiljevska, J. Lopes and M. Matos, "Multi-microgrid impact assessment using multi criteria Decision Aid methods," in *IEEE Bucharest PowerTech*, Bucharest, 2009.
- [32] M. Shahidehpour, Z. Li, S. Bahramirad, Z. Li and W. Tian, "Networked microgrids: exploring the possibilities of the IIT-Bronzeville grid," *IEEE Power and Energy Magazine*, vol. 15, no. 4, pp. 63-71, 2017.
- [33] S. Arefifar, M. Ordonez and Y. Mohamed, "Energy management in multi-microgrid systems—development and assessment," *IEEE Trans. Power Systems*, vol. 32, no. 2, pp. 910-922, March 2017.
- [34] R. Lasseter, "Smart distribution: coupled microgrids," *Proceedings of the IEEE*, vol. 99, no. 6, pp. 1074-1082, June 2011.
- [35] S. Arefifar, Y. Mohamed and T. Elfouly, "Supply-adequacy-based optimal construction of microgrids in smart distribution systems," *IEEE Trans. Smart Grid*, vol. 3, no. 3, pp. 1491-1502, Sep 2012.
- [36] Z. Wang, B. Chen, J. Wang and C. Chen, "Networked microgrids for self-healing Power Systems," *IEEE Trans. Smart Grid*, vol. 7, no. 1, pp. 310-319, Jan 2016.
- [37] D. Gregoratti and J. Matamoros, "Distributed energy trading: the multiple-microgrid case," *IEEE Trans. Industrial Electronics*, vol. 62, no. 4, pp. 2551-2559, April 2015.
- [38] H. Wang and J. Huang, "Bargaining-based energy trading market for interconnected microgrids," in *IEEE International Conference on Communications (ICC)*, London, 2015.
- [39] y. Zhang and L. Xie, "Online Dynamic security assessment of microgrid interconnections in smart distribution systems," *IEEE Trans. Power Systems*, vol. 30, no. 6, pp. 3246-3254, Nov 2015.
- [40] Y. Zhang, L. Xie and Q. Ding, "Interactive control of coupled microgrids for guaranteed system-wide small signal stability," *IEEE Trans. Smart Grid*, vol. 7, no. 2, pp. 1088-1096, March 2016.
- [41] C. Abbey, D. Cornforth, N. Hatziargyriou, K. Hirose, A. Kwasinski and E. Kyriakides, "Powering through the storm: microgrids operation for more efficient disaster recovery," *IEEE Power and Energy Magazine*, vol. 12, no. 3, pp. 67-76, 2014.
- [42] H. Farzin, M. Fotuhi-Firuzabad and M. Moeini-Aghaie, "Enhancing power system resilience through hierarchical outage management in multi-microgrids," *IEEE Trans. Smart Grid*, vol. 7, no. 6, pp. 2869-2879, Nov 2016.
- [43] Z. Wang and J. Wang, "Self-healing resilient distribution systems based on sectionalization into microgrids," *IEEE Trans. Power Systems*, vol. 30, no. 6, pp. 3139-3149, Nov. 2015.
- [44] X. Zu, P. yang, Y. Zhang, Z. Zheng, C. Zheng and J. Peng, "Control devices development of mult-imicrogrids based on hierarchical structure," *IET Generation*,

- Transmission and Distribution*, vol. 10, no. 16, p. 4249–4256, 2016.
- [45] R. Majumder, B. Chaudhuri, A. Ghosh, R. Majumder, G. Ledwith and F. Zare, “Improvement of stability and load sharing in an autonomous microgrid using supplementary droop control loop,” *IEEE Trans. Power Systems*, vol. 25, no. 2, pp. 796-808, May 2010.
- [46] M. Goyal and A. Ghosh, “Microgrids interconnection to support mutually during any contingency,” *Sustainable Energy, Grids and Networks*, vol. 6, pp. 100-108, June 2016.
- [47] M. Khederzadeh, H. Maleki and V. Asgharian, “Frequency control improvement of two adjacent microgrids in autonomous mode using back to back voltage-sourced converters,” *International Journal of Electrical Power & Energy Systems*, vol. 74, pp. 126-133, Jan 2016.
- [48] J. Ma, M. Zhu, X. Cai and Y. Li, “Configuration and operation of DC microgrid cluster linked through DC-DC converter,” in *IEEE 11th Conference on Industrial Electronics and Applications (ICIEA)*, Hefei, 2016.
- [49] T. Dragicevic, J. Vasquez, J. Guerrero and D. Skrlec, “Advanced LVDC electrical power architectures and microgrids: a step toward a new generation of power distribution networks,” *IEEE Electrification Magazine*, vol. 2, no. 1, pp. 54-65, March 2014.
- [50] F. Nejabatkhah and Y. Li, “Overview of power management strategies of hybrid AC/DC microgrid,” *IEEE Trans. Power Electronics*, vol. 30, no. 12, pp. 7072-7089, Dec. 2015.
- [51] R. Majumder, “A hybrid microgrid with DC connection at back to back converters,” *IEEE Trans. Smart Grid*, vol. 5, no. 1, pp. 251-259, Jan. 2014.
- [52] N. Nikmehr and S. Ravadanegh, “Optimal power dispatch of multi-microgrids at future smart distribution grids,” *IEEE Trans. Smart Grid*, vol. 6, no. 4, pp. 1648-1657, July 2015.
- [53] H. Dagdougui, A. Oummi and R. Sacile, “Optimal control of a network of power microgrids using the Pontryagin's minimum principle,” *IEEE Trans. Control Systems Technology*, vol. 22, no. 5, pp. 1942-1948, Sep. 2014.
- [54] A. Ouammi, H. Dagdougui, L. Dessaint and R. Sacile, “Coordinated model predictive-based power flows control in a cooperative network of smart microgrids,” *IEEE Trans. Smart Grid*, vol. 6, no. 5, pp. 2233-2244, Sept 2015.
- [55] T. Lu and Z. Wang, “Interactive Model for Energy Management of Clustered Microgrids,” *IEEE Transactions on Industry Applications*, vol. 53, no. 3, pp. 1739-1750, 2017.
- [56] M. Marzban, N. Parhizi, M. Savaghebi and J. Guerrero, “Distributed smart decision-making for a multimicrogrid system based on a hierarchical interactive architecture,” *IEEE Trans. Energy Conversion*, vol. 31, no. 2, pp. 637-648, June 2016.
- [57] P. Tian, X. Xiao, K. Wang and R. Ding, “A hierarchical energy management system based on hierarchical optimization for microgrid community economic operation,” *IEEE Trans. Smart Grid*, vol. 7, no. 5, pp. 2230-2241, Sep 2016.
- [58] R. Minciardi and M. Robba, “A bilevel approach for the stochastic optimal operation of interconnected microgrids,” *IEEE Trans. Automation Science and Engineering*, vol. 14, no. 2, pp. 482-493, April 2017.
- [59] W. Liu, W. Gu, W. Sheng, X. Meng, Z. Wu and W. Chen, “Decentralized multi-agent system-based cooperative frequency control for autonomous microgrids with communication con-straints,” *IEEE Trans. Sustainable Energy*, vol. 5, no. 2, pp.

- 446-456, April 2014.
- [60] S. Moayedi and A. Davoudi, "Distributed tertiary control of DC microgrid clusters," *IEEE Trans. Power Electronics*, vol. 31, no. 2, pp. 1717-1733, Feb. 2016.
- [61] S. Moayedi and A. Davoudi, "Cooperative power management in DC microgrid clusters," in *IEEE First International Conference on DC Microgrids (ICDCM)*, Atlanta, GA, 2015.
- [62] V. Bui and A. Hussain, "A multiagent-based hierarchical energy management strategy for multi-microgrids considering adjustable power and demand response," *IEEE Trans. Smart Grid*, vol. PP, no. 99, pp. 1-1, 2016.
- [63] Y. Han, H. Li, E. Coelho and J. Guerrero, "Review of active and reactive power sharing strategies in hierarchical controlled microgrids," *IEEE Trans. Power Electronics*, vol. 32, no. 3, pp. 2427-2451, March 2017.
- [64] I. L. P. Nutkani, P. Wang, T. Jet and F. Blaabjerg, "Intertied ac-ac microgrids with autonomous power import and export," *International Journal of Electrical Power and Energy Systems*, vol. 65, pp. 385-393, Feb 2015.
- [65] P. Wang, C. Jin, D. Zhu, Y. Tang, P. Loh and F. Choo, "Distributed control for autonomous operation of a three-port AC/DC/DS hybrid microgrid," *IEEE Trans. Industrial Electronics*, vol. 62, no. 2, pp. 1279-1290, Feb 2015.
- [66] P. Loh, D. Li, Y. Chai and F. Blaabjerg, "Autonomous operation of hybrid microgrid with AC and DC subgrids," *IEEE Trans. Power Electronics*, vol. 28, no. 5, p. 2214-2223, May 2013.
- [67] I. L. P. Nutkani and F. Blaabjerg, "Distributed operation of interlinked AC microgrids with dynamic active and reactive power tuning," *IEEE Trans. Industry Applications*, vol. 49, no. 5, pp. 2188-2196, 2013.
- [68] L. Meng, E. Sanseverino, A. Luna, T. Dragicevic and J. M. G. Juan C. Vasquez, "Microgrid supervisory controllers and energy management systems: A literature review," *Renewable and Sustainable Energy Reviews*, vol. 60, pp. 1263-1273, 2016.
- [69] R. Majumder and G. Bag, "Parallel operation of converter interfaced multiple microgrids," *International Journal of Electrical Power & Energy Systems*, vol. 55, pp. 486-496, 2014.
- [70] A. Radwan and Y. Mohamed, "Networked control and power management of AC/DC hybrid microgrids," *IEEE Systems Journal*, vol. PP, no. 99, pp. 1-12, 2014.
- [71] G. Asimakopoulou, A. Dimeas and N. Hatziargyriou, "Leader-follower strategies for energy management of multi-microgrids," *IEEE Trans. Smart Grid*, vol. 4, no. 4, pp. 1909-1916, Dec 2013.
- [72] M. Cintuglu and O. Mohammed, "Behavior modeling and auction architecture of networked microgrids for frequency support," *IEEE Trans. Industrial Informatics*, vol. 13, no. 4, pp. 1772-1782, Aug 2017.
- [73] H. Wang and J. Huang, "Incentivizing energy trading for interconnected microgrids," *IEEE Trans. Smart Grid*, vol. PP, no. 99, pp. 1-1, 2016.
- [74] H. KumarNunna and D. Srinivasan, "Multi-Agent based transactive energy framework for distribution systems with smart microgrids," *IEEE Trans. Industrial Informatics*, vol. PP, no. 99, pp. 1-1, 2017.
- [75] X. Huang, Y. Shen, C. Chen, F. Zeng and Y. Cao, "Reliability evaluation of microgrid cluster based on Monte-Carlo hierarchical dynamic reliability model," in *10th International Conference on Advances in Power System Control, Operation & Management (APSCOM 2015)*, Hong Kong, 2015.

- [76] S. Arefifar, Y. Mohamed and T. El-Fouly, "Optimum microgrid design for enhancing reliability and supply-security," *IEEE Trans. Smart Grid*, vol. 4, no. 3, pp. 1567-1575, Sep 2013.
- [77] S. M. Y. Arefifar and T. El-Fouly, "Comprehensive operational planning framework for self-healing control actions in smart distribution grids," *IEEE Trans. Power Systems*, vol. 28, no. 4, pp. 4192-4200, Nov. 2013.
- [78] S. Arefifar, Y. Mohamed and T. El-fouly, "Optimized multiple microgrid-based clustering of active distribution systems considering communication and control requirements," *IEEE Trans. Industrial Electronics*, vol. 62, no. 2, pp. 711-723, Sep 2015.
- [79] Y. Wang, C. Chen, J. Wang and R. Baldick, "Research on resilience of power systems under natural disasters—a review," *IEEE Trans. Power Systems*, vol. 31, no. 2, pp. 1604-1613, March 2016.
- [80] K. Schneider, F. Tuffner, M. Elizondo, C. X. Y. Liu and D. Ton, "Evaluating the feasibility to use microgrids as a resiliency resource," *IEEE Trans. Smart Grid*, vol. 8, no. 2, pp. 687-696, March 2017.
- [81] M. Khederzadeh, "Resilient distribution system by forming/coupling microgrids in extreme contingencies," in *CIREN Workshop*, Helsinki, 2016.
- [82] M. Khederzadeh, "Distribution grid restoration by forming resiliency-oriented less-vulnerable microgrids," in *CIREN Workshop*, Helsinki, 2016.
- [83] F. Resende, N. Gil and J. Lopes, "Service restoration on distribution systems using Multi-MicroGrids," *Euro. Trans. Electr. Power*, vol. 21, p. 1327–1342, 2011.
- [84] Z. Wang and J. Wang, "Service restoration based on AMI and networked MGs under extreme weather events," *IET Generation, Transmission and Distribution*, vol. 11, no. 2, p. 401–408, 2017.
- [85] J. Li, X. Ma, C. Liu and K. Schneider, "Distribution system restoration with microgrids using spanning tree search," *IEEE Trans. Power Systems*, vol. 29, no. 6, pp. 3021-3029, Nov 2014.
- [86] M. Kabalan, P. Singh and D. Niebur, "Large signal Lyapunov-based stability studies in microgrids: a review," *IEEE Trans. Smart Grid*, vol. 8, no. 5, pp. 2287-2295, Sep 2017.
- [87] R. Majumder, "Some aspects of stability in microgrids," *IEEE Trans. Power Systems*, vol. 28, no. 3, pp. 3243-3252, Aug. 2013.
- [88] I. Nikolakakos, H. Zeineldin, M. El-Moursi and N. Hatziaargyriou, "Stability evaluation of interconnected multi-inverter microgrids through critical clusters," *IEEE Trans. Power Systems*, vol. 31, no. 4, pp. 3060-3072, July 2016.
- [89] Y. Zhang and L. Xie, "A transient stability assessment framework in power electronic-interfaced distribution systems," *IEEE Trans. Power Systems*, vol. 31, no. 6, pp. 5106-5114, Nov 2016.
- [90] "DOE Microgrid Workshop Report," Office of Electricity Delivery and Energy Reliability Smart Grid R&D Program, San Diego, California, 2011.
- [91] C. Marnay, S. Chatzivasileiadis, C. Abbey, R. Iravani, G. Joos, P. Lombardi, P. Mancarella and J. Appen, "Microgrid evolution roadmap," in *International Symposium on Smart Electric Distribution Systems and Technologies (EDST)*, Vienna, 2015.
- [92] L. Xu, X. Ruan, C. Mao, B. Zhang and Y. Luo, "An improved optimal sizing method for wind-solar-battery hybrid power system," *IEEE Trans. Sustainable Energy*, vol. 4, no. 3, pp. 774-785, July 2013.

- [93] M. Bayat, K. Sheshyekani, M. Hamzeh and A. Rezaadeh, "Coordination of distributed energy resources and demand response for voltage and frequency support of MV microgrids," *IEEE Trans. Power Systems*, vol. 31, no. 2, pp. 1506-1516, March 2016.
- [94] A. Marvasti, Y. Fu, S. DorMohammadi and M. Rais-Rohani, "Optimal operation of active distribution grids: A system of systems framework," *IEEE Trans. Smart grid*, vol. 5, no. 3, pp. 1228-1237, May 2014.
- [95] H. Golpîra, H. Seifi, A. Messina and M. Haghifam, "Maximum Penetration level of micro-grids in large-scale power systems: frequency stability viewpoint," *IEEE Trans. Power Systems*, vol. 31, no. 6, pp. 5163-5171, Nov. 2016.
- [96] L. Mariam, M. Basu and M. Conlon, "Microgrid: architecture, policy and future trends," *Renewable and Sustainable Energy Reviews*, vol. 64, pp. 477-489, 2016.
- [97] R. Majumder, A. Ghosh, G. Ledwich and F. Zare, "Power management and power flow control with back-to-back converters in a utility connected microgrid," *IEEE Trans. Power Systems*, vol. 25, no. 2, pp. 821-834, May 2010.
- [98] K. Tan, X. Peng, P. So, Y. Chu and M. Chen, "Centralized control for parallel operation of distributed generation inverters in microgrids," *IEEE Trans. Smart Grid*, vol. 3, no. 4, pp. 1977-1987, Dec. 2012.
- [99] Z. Zhao, P. Yang, J. Guerrero, Z. Xu and T. Green, "Multiple-time-scales hierarchical frequency stability control strategy of medium-voltage isolated microgrid," *IEEE Trans. Power Electronics*, vol. 31, no. 8, pp. 5974-5991, Aug. 2016.
- [100] Q. L. C. Peng, M. Chen, F. Chen, W. Kang, J. Guerrero and D. Abbott, "Networked and distributed control method with optimal power dispatch for islanded microgrids," *IEEE Trans. Industrial Electronics*, vol. 64, no. 1, pp. 493-504, Jan. 2017.
- [101] J. Guerrero, M. Chandorkar and T. L. P. Lee, "Advanced control architectures for intelligent microgrids—part I: decentralized and hierarchical control," *IEEE Trans. Industrial Electronics*, vol. 60, no. 40, pp. 1254-1262, April 2013.
- [102] M. Arriaga, C. Canizares and M. Kazerani, "Northern lights: access to electricity in Canada's northern and remote communities," *IEEE Power and Energy Magazine*, vol. 12, pp. 50-59, 2014.
- [103] J. Lee, J. Guo and J. Z. M. Choi, "Distributed energy erading in eicrogrids: A game-theoretic model and its equilibrium analysis," *IEEE Trans. Industrial Electronics*, vol. 62, no. 6, pp. 3524-3533, June 2015.
- [104] C. Bersani, H. Dagdougui, A. Ouammi and R. Sacile, "Distributed robust control of the power flows in a team of cooperating microgrids," *IEEE Trans. Control Systems Technology*, vol. 25, no. 4, pp. 1473-1479, July 217.
- [105] J. S. F. Matos and L. Ribeiro, "Power control in AC isolated microgrids with renewable energy sources and energy storage systems," *IEEE Trans. Industrial Electronics*, vol. 62, no. 6, pp. 3490-3498, June 2015.
- [106] D. Olivares, C. Canizares and M. Kazerani, "A centralized energy management system for isolated microgrids," *IEEE Trans. Smart Grid*, vol. 5, no. 4, pp. 1864-1875, July 2014.
- [107] Z. Wang, B. Chen, J. Wang and C. Chen, "Networked microgrids for self-healing," *IEEE Trans. Smart Grid*, vol. 7, no. 1, pp. 310-319, Jan 2016.
- [108] Z. Wang, B. Che, J. Wang and J. Kim, "Decentralized energy management system for networked microgrids in grid-connected and islanded modes," *IEEE Trans. Smart Grid*, vol. 7, no. 2, pp. 1097-1105, March 2016.

- [109] Office of the Press Secretary of the White House, "Presidential policy directive -- Critical infrastructure security and resilience," 12 Feb. 2013. [Online]. Available: <https://obamawhitehouse.archives.gov/the-press-office/2013/02/12/presidential-policy-directive-critical-infrastructure-security-and-resil>. [Accessed 3 June 2017].
- [110] C. Chen, J. Wang, F. Qiu and D. Zhao, "Resilient distribution system by microgrids formation after natural disasters," *IEEE Trans. Smart Grid*, vol. 7, no. 2, pp. 958-966, March 2016.
- [111] K. Schneider, F. Tuffner, M. Elizondo, C. Liu, Y. Xu and D. Ton, "Evaluating the feasibility to use microgrids as a resiliency resource," *IEEE Trans. Smart Grid*, vol. 8, no. 2, pp. 687-696, March 2017.
- [112] X. Liu, M. Shahidehpour, Z. Li, X. Liu, Y. Cao and Z. Bie, "Microgrids for enhancing the power grid resilience in extreme conditions," *IEEE Trans. Smart Grid*, vol. 8, no. 2, pp. 589-597, March 2017.
- [113] M. Chandorkar, D. Divan and R. Adapa, "Control of parallel connected inverters in standalone AC supply systems," *IEEE Trans. Industry Applications*, vol. 29, no. 1, pp. 136-143, 1993.
- [114] J. Guerrero, J. Matas, L. de Vicuna, M. Castilla and J. Miret, "Decentralized control for parallel operation of distributed generation inverters using resistive output impedance," *IEEE Trans. Industrial Electronics*, vol. 54, no. 2, pp. 994-1004, April 2007.
- [115] E. Pashajavid, A. Ghosh and F. Zare, "A Multimode Supervisory Control Scheme for Coupling Remote Droop-Regulated Microgrids," *IEEE Trans. Smart Grid*, vol. PP, no. 99, pp. 1-12, 2017.
- [116] K. De Brabandere, B. Bolsens, J. Van den Keybus, A. Woyte, J. Driesen and R. Belmans, "A voltage and frequency droop control method for parallel inverters," *IEEE Trans. Power Electronics*, vol. 22, no. 4, pp. 1107-1115, July 2007.
- [117] R. Majumder, A. Ghosh, G. Ledwich and F. Zare, "Stability analysis and control of multiple converter based autonomous microgrid," in *IEEE International Conference on Control and Automation*, Christchurch, 2009.
- [118] E. Pashajavid and A. Ghosh, "Frequency support for remote microgrid systems with intermittent distributed energy resources—A two-level hierarchical strategy," *IEEE Systems Journal*, vol. PP, no. 99, pp. 1-12, 2017.
- [119] A. Ghosh and G. Ledwich, *Power quality enhancement using custom power devices*, Springer Science & Business Media, 2002.
- [120] J. Xiao, L. Bai, F. Li, H. Liang and C. Wang, "Sizing of energy storage and diesel generators in an isolated microgrid using DFT," *IEEE Trans. Sustainable Energy*, vol. 5, no. 3, pp. 907-916, July 2014.
- [121] E. Pashajavid, F. Shahnia and A. Ghosh, "Development of a self-healing strategy to enhance the overloading resilience of islanded microgrids," *IEEE Trans. Smart Grid*, vol. 8, no. 2, pp. 868-880, March 2017.
- [122] E. Pashajavid, F. Shahnia and A. Ghosh, "Interconnection of two neighboring autonomous microgrids based on small signal analysis," in *9th International Conference on Power Electronics and ECCE Asia (ICPE-ECCE Asia)*, Seoul, 2015.
- [123] M. Hossain, M. Mahmud, F. Milano, S. Bacha and A. Hably, "Design of robust distributed control for interconnected microgrids," *IEEE Trans. Smart Grid*, vol. 7, no. 6, pp. 2724-2735, Nov. 2016.
- [124] T. Friedli, J. Kolar, J. Rodriguez and P. Wheeler, "Comparative evaluation of three-phase ac-ac matrix converter and voltage dc-link back-to-back converter systems,"

- IEEE Trans. Industrial Electronics*, vol. 59, no. 12, pp. 4487-4510, Dec 2012.
- [125] E. Pashajavid, A. Ghosh and F. Zare, "A multimode supervisory control scheme for coupling remote droop-regulated microgrids," *IEEE Trans. Smart Grid*, vol. PP, no. 99, pp. 1-11, 2017.
- [126] IEEE application guide for IEEE Std 1547(TM), "IEEE standard for interconnecting distributed resources with electric power systems," *IEEE Std 1547.2-2008*, pp. 1-217, 15 April 2009.
- [127] N. Pogaku, M. Prodanovic and T. Green, "Modeling, analysis and testing of autonomous operation of an inverter-based microgrid," *IEEE Trans. Power Electronics*, vol. 22, no. 2, pp. 613-625, March 2007.
- [128] W. Hashlamoun, M. Hassouneh and E. Abed, "New results on modal participation factors: Revealing a previously unknown dichotomy," *IEEE Trans. Automatic Control*, vol. 54, no. 7, pp. 1439-1449, 2009.
- [129] P. Kundur, *Power System Stability and Control*, McGraw-Hill, 1994.
- [130] Olex aerial conductors catalogue, "www.olex.com.au," [Online]. Available: http://www.olex.com.au/Australasia/2012/OLC12641_AerialCat.pdf. [Accessed 17 2017].
- [131] Y. Atwa, E. El-Saadany, M. Salama, R. Seethapathy, M. Assam and S. Conti, "Adequacy evaluation of distribution system including wind/solar DG during different modes of operation," *IEEE Trans. Power Systems*, vol. 26, no. 4, pp. 1945-1952, Nov. 2011.
- [132] S. Bae and A. Kwasinski, "Dynamic modeling and operation strategy for a microgrid with wind and photovoltaic resources," *IEEE Trans. Smart Grid*, vol. 3, no. 4, pp. 1867-1876, Dec. 2012.
- [133] E. Pashajavid, F. Shahnia and A. Ghosh, "Overload management of autonomous microgrids," in *IEEE 11th International Conference on Power Electronics and Drive Systems*, Sydney, 2015.
- [134] E. Pashajavid, F. Shahnia and A. Ghosh, "Provisional internal and external power exchange to support remote sustainable microgrids in the course of power deficiency," *IET Generation, Transmission & Distribution*, vol. 11, no. 1, pp. 246-260, 2017.
- [135] T. Hosseinimehr, F. Shahnia and A. Ghosh, "Power sharing control of batteries within autonomous microgrids based on their state of charge," in *Australasian Universities Power Engineering Conference (AUPEC)*, Wollongong, 2015.
- [136] Z. Akhtar, B. Chaudhuri and S. Hui, "Primary frequency control contribution from smart loads using reactive compensation," *IEEE Trans. Smart Grid*, vol. 6, no. 5, pp. 2356-2365, 2015.
- [137] Y. Dai, Y. Xu, Z. Dong, K. Wong and L. Zhuang, "Real-time prediction of event-driven load shedding for frequency stability enhancement of power systems," *IET Generation, Transmission & Distribution*, vol. 6, no. 9, pp. 914-921, Sep. 2012.
- [138] J. Chen, J. Chen and C. Gong, "New overall power control strategy for variable-speed fixed-pitch wind turbines within the whole wind velocity range," *IEEE Trans. Industrial Electronics*, vol. 60, no. 7, pp. 2652-2660, July 2013.
- [139] E. Pashajavid and A. Ghosh, "A fully decentralized approach for mitigating destructive disturbances in isolating process of remote coupled microgrids," in *Australasian Universities Power Engineering Conference (AUPEC)*, Brisbane, QLD, 2016.
- [140] M. Arafat, A. Elrayyah and Y. Sozer, "An effective smooth transition control

- strategy using droop-based synchronization for parallel inverters,” *IEEE Trans. Industry Application*, vol. 51, no. 3, pp. 2443-2454, May 2015.
- [141] C. Lee, R. Jiang and P. Cheng, “A grid synchronization method for droop-controlled distributed energy resource converters,” *IEEE Trans. Industry Applications*, vol. 49, no. 2, pp. 954-962, March 2013.

Every reasonable effort has been made to acknowledge the owners of copyright material. I would be pleased to hear from any copyright owner who has been omitted or incorrectly acknowledged.

PUBLICATIONS FROM THIS THESIS

- [J1] **E. Pashajavid**, A. Ghosh and F. Zare, “A multimode supervisory control scheme for coupling remote droop-regulated microgrids,” *IEEE Trans. Smart Grid*, vol. PP, no. 99, pp. 1-1, doi: 10.1109/TSG.2017.2688475.
- [J2] **E. Pashajavid**, F. Shahnian and A. Ghosh, “Development of a self-healing strategy to enhance the overloading resilience of islanded microgrids,” *IEEE Trans. Smart Grid*, vol. 8, no. 2, pp. 868-880, March 2017.
- [J3] **E. Pashajavid** and A. Ghosh, “Frequency support for remote microgrid systems with intermittent distributed energy resources — A two-level hierarchical strategy,” *IEEE Systems Journal*, vol. PP, no. 99, pp. 1-12, doi: 10.1109/JSYST.2017.2661743.
- [J4] **E. Pashajavid**, F. Shahnian and A. Ghosh, “Provisional internal and external power exchange to support remote sustainable microgrids in the course of power deficiency,” *IET Generation, Transmission & Distribution*, vol. 11, no. 1, pp. 246-260, 2017.
- [C1] **E. Pashajavid** and A. Ghosh, “A fully decentralized approach for mitigating destructive disturbances in isolating process of remote coupled microgrids,” Australasian Universities Power Engineering Conference (AUPEC), Brisbane, QLD, pp. 1-6, 2016.
- [C2] **E. Pashajavid**, F. Shahnian and A. Ghosh, “Interconnection of two neighbouring autonomous microgrids based on small signal analysis,” 9th International Conference on Power Electronics and ECCE Asia (ICPE-ECCE Asia), pp. 213-220, Seoul, 2015.

- [C3] **E. Pashajavid**, F. Shahnian and A. Ghosh, “A decentralized strategy to remedy the power deficiency in remote area microgrids,” 50th International Universities Power Engineering Conference (UPEC), Stoke-on-Trent, 2015.
- [C4] **E. Pashajavid**, F. Shahnian and A. Ghosh, “Overloading conditions management in remote networks by coupling neighbouring microgrids,” 50th International Universities Power Engineering Conference (UPEC), Stoke-on-Trent, 2015.
- [C5] **E. Pashajavid**, F. Shahnian and A. Ghosh, “Overload management of autonomous microgrids,” IEEE 11th International Conference on Power Electronics and Drive Systems (PEDS), Sydney, NSW, pp. 73-78, 2015.